20 November 2009 | $10

# Science

## The Maize Genome

AAAS

# The Maize Genome:

## *Ripe with Promise*

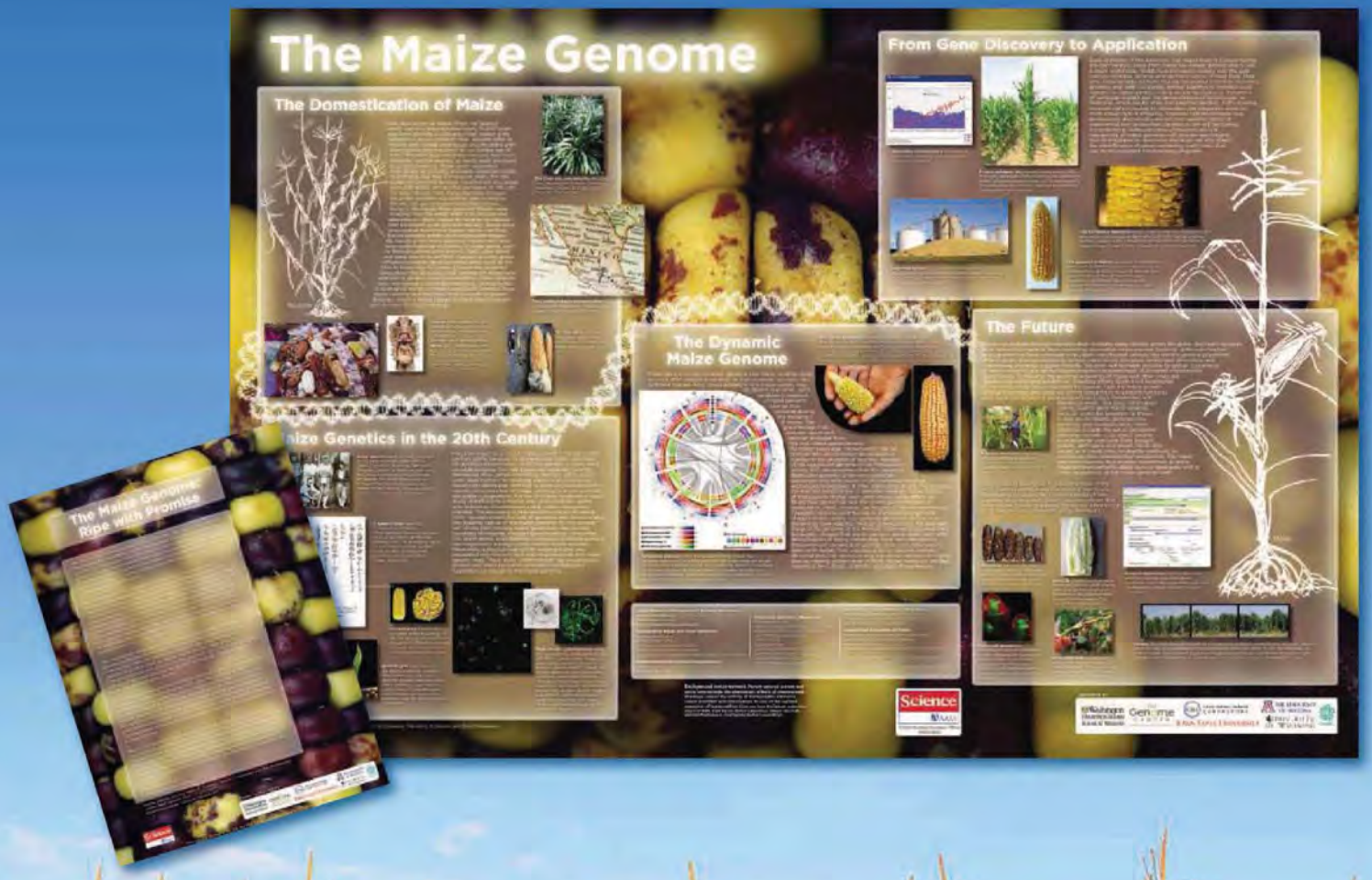


Interest in the genetics of maize began in the early 1900s when geneticists began to document the many varieties and explore the implications of genetic crosses. Understanding the maize genome will enable geneticists to develop new and improved maize varieties that are more nutritious or can withstand harsher environments.

In this special poster, presented in conjunction with the first publication of the full maize genome sequence, we trace the history of modern maize from its beginnings as a wild grass called teosinte, to what is today one of the most productive and widespread crops in the world.

The Maize Genome Poster is available for download at:
**www.sciencemag.org/products/posters/maize_poster.pdf**

Science
AAAS

AAAS/*Science* Business Office Publication

Sponsored By:

Washington University in St. Louis School of Medicine
The Genome Center at Washington University
CSH Cold Spring Harbor Laboratory
Iowa State University
The University of Arizona
University of Wyoming
Cleveland


Geospatial Technologies
Human Rights

Remote, isolated, catastrophic events occur across the globe that affect civilians, the environment, indigenous rights, and more. The AAAS Science and Human Rights Program is the application of geospatial technologies to broaden the ability of non-governmental organizations to rapidly gather, analyze, and disseminate information in these times of crisis. And this is just one of the ways that AAAS is committed to advancing science to support a healthy and prosperous world. Join us. Together we can make a difference. aaas.org/plusyou/humanrights

AAAS + U = Δ

# The SOLiD™ 3 Plus System

**The right answer, the first time.** The SOLiD™ 3 Plus System enables unsurpassed accuracy and throughput to translate your discoveries into biologically relevant information.

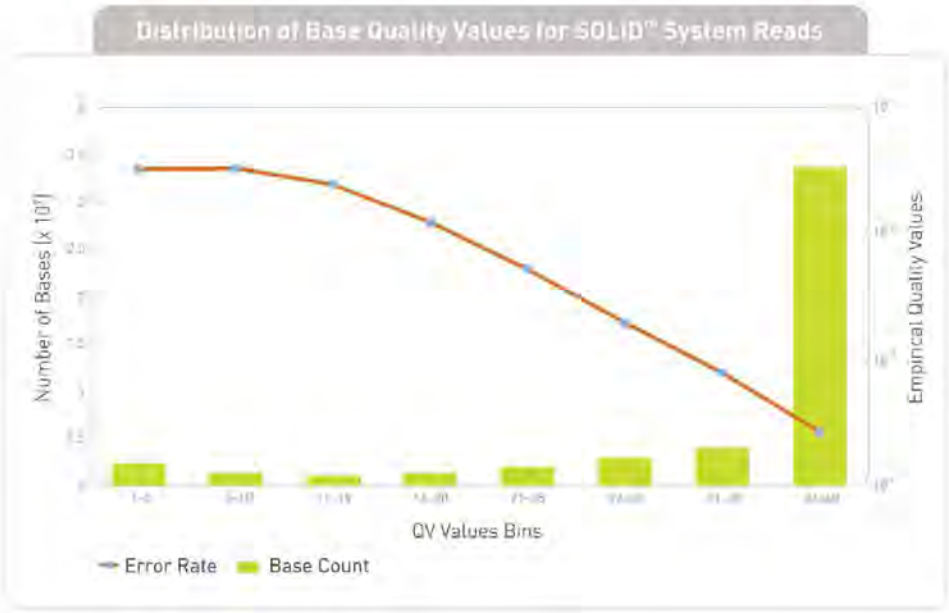


**Figure 1. Distribution of bases and their empirical quality values from SOLiD™ System Sequencing.**

| SOLiD™ 3 Plus System Specifications | |
|---|---|
| Throughput | 60+ GB of mappable sequence or 1 billion reads per run with SOLiD™ 3 Opti reagents |
| Library Type | • Mate-paired libraries (insert sizes between 600 bp to 10 kb)<br>• Fragment libraries |
| Starting Material Type | DNA or cDNA isolated from blood or single cells, RNA, BAC, plasmids, fosmids, tissue (high tumor load), and PCR products |
| Amount of Starting Material | Required input of starting material varies by application<br>• 10 ng to 5 µg for fragment library<br>• 5 µg to 20 µg for mate-paired library |
| Slide Configuration | Individual samples: 1 to 8 per flowcell<br>Multiplexed samples: up to 256 per run |
| Flowcells | 2 independent flowcells |
| System Accuracy | Greater than 99.94% accuracy due to 2 base encoding |
| Consensus Base Accuracy | Greater than 99.999% accuracy at 15x coverage |
| Base Quality | Greater than 80% of bases at >QV30 |
| Multiplexing | 16 barcodes currently available |
| Analysis | • SAM format exports<br>• Powerful computer cluster for large-scale application analysis<br>• Customizable application analysis with new bioinformatics analysis framework for flexible data review |

## System Attributes

### Highest number of bases greater than QV30

The SOLiD™ 3 Plus System enables the superior accuracy and sensitivity to detect biological variation. The innate error-checking capabilities within 2 base encoding result in highly accurate base sequence; a significant number of bases have quality values greater that 30 (Figure 1). This attribute translates to less coverage required for variant detection, yields fewer false positives, and facilitates a corresponding reduction in validation for project time and cost savings.

### Cost-effective research without costly upgrades

The SOLiD™ 3 Plus System generates 60+ GB of mappable sequence or greater than 1 billion reads per run. This level of throughput enables large-scale resequencing and tag-based experiments to be completed more efficiently and rapidly than ever before. The SOLiD™ 3 Plus System's intrinsic open slide format and flexible bead densities facilitate increases in throughput without major system modifications.

### Streamlined analysis and data management

The SOLiD™ 3 Plus System supports standard Sequence Alignment Map (SAM) format with base calls and associated quality values. Experience the benefits of the higher accuracy enabled by 2 base encoding and of the flexibility to export to standard downstream analysis tools. Advanced software solutions reduce analysis time through a 20–40% reduction in data footprint and real-time data export.

# Can Your Next Gen Sequencer Tell The Difference?

**Have confidence in your sequencing results with the new SOLiD™ 3 Plus System.**

- Superior accuracy and sensitivity for variant discovery with less coverage
- Increased throughput and lower running costs
- Standard base sequence format with the quality of color space

The SOLiD™ 3 Plus System. The right answer, the first time.

For data demonstrating the superior accuracy of the SOLiD™ 3 Plus System go to **www.appliedbiosystems.com/solidaccuracy**

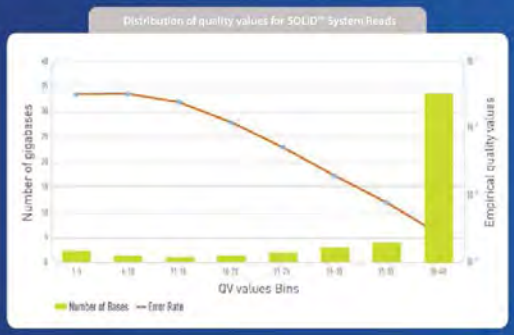


applied biosystems
part of life technologies

GE Healthcare
Life Sciences

# Cell analysis just got easier

The new IN Cell Analyzer 2000 makes previously challenging cell analysis a thing of the past by offering significant throughput gains compared to typical lamp based imaging systems, while still delivering enabling features for your research assays.

From organelles to cells, to tissues and whole organisms – from fixed end-point assays to extended live cell studies – from manual microscopy to automated high-content screening, IN Cell Analyzer 2000 offers you the performance you need for all your screening and research – making your cell analysis faster and easier.

At GE Healthcare Life Sciences, our focus is on helping scientists achieve even more, faster. It's a commitment we have in our genes. And all this is backed by the service, support, and investment for the future that being part of GE can bring.

Cell analysis just got easier. Find out more. **Visit www.gelifesciences.com/incell**

I ÄKTA I Amersham I Biacore I **IN Cell Analysis** I Whatman I GE Service I

## INtroducing the new IN Cell Analyzer 2000

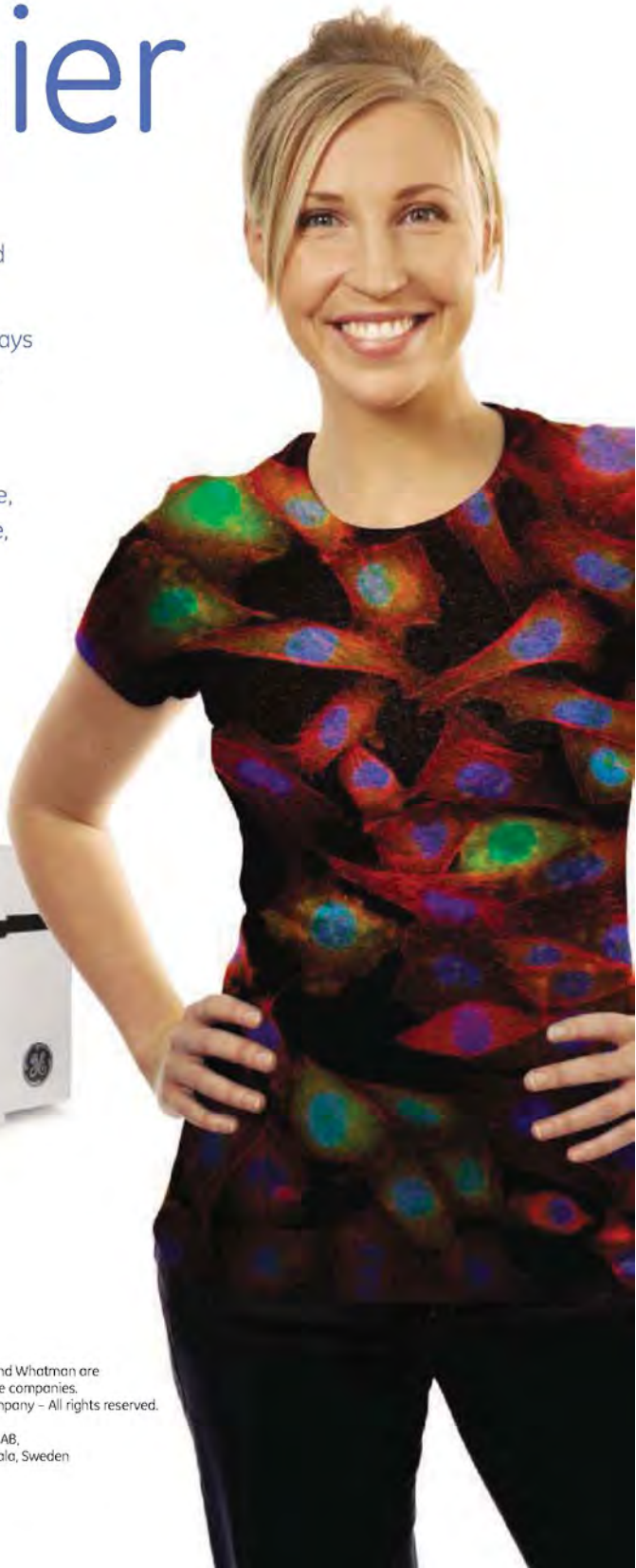

imagination at work


First published May 2009
GE Healthcare Bio-Sciences AB,
Björkgatan 30, 751 84 Uppsala, Sweden
GE09-09

## EDITORIAL



## NEWS OF THE WEEK



## NEWS FOCUS



## LETTERS



## BOOKS *ET AL.*



## POLICY FORUM



## PERSPECTIVES



## REVIEW



CONTENTS continued >>

page 1052

page 1063


## COVER

An ear of *Zea mays* (maize) shows color variation among kernels. Maize is one of the most important crop species worldwide, a vital source of food and fuel, and a valuable model organism for genetic research. Reports starting on pages 1112 and 1115 describe the genome sequences of the B73 and Palomero Toluqueño varieties. See also the related Report (p. 1118), Brevia (p. 1078), and Perspective (p. 1071).

***Photo: Kate Mathis/Getty Images***

## DEPARTMENTS

# Automated sample and assay technologies by QIAGEN

## Free up your time

Automated solutions from sample to result:

- **The widest choice of sample processing protocols**
- **Low-, medium-, and high-throughput automation**
- **Leading solutions for molecular diagnostics**
- **Plug-and-play automated sample preparation**
- **Quantitative, real-time PCR detection**
- **Automated analysis of DNA fragments and RNA**
- **High-resolution sequence-based DNA detection and quantification**
- **HPV testing**

Making improvements in life possible — www.qiagen.com

QIAGEN®

Sample & Assay Technologies

## BREVIA



## REPORTS



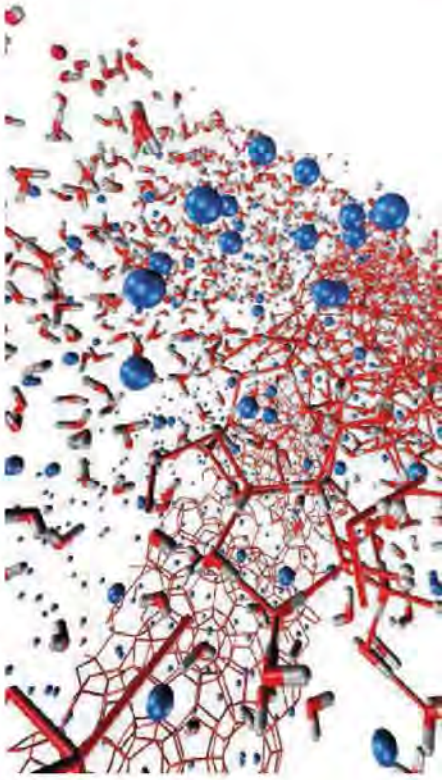

pages 1070 & 1095

page 1103



CONTENTS continued >>

# Eppendorf Consumables – it's Your sample

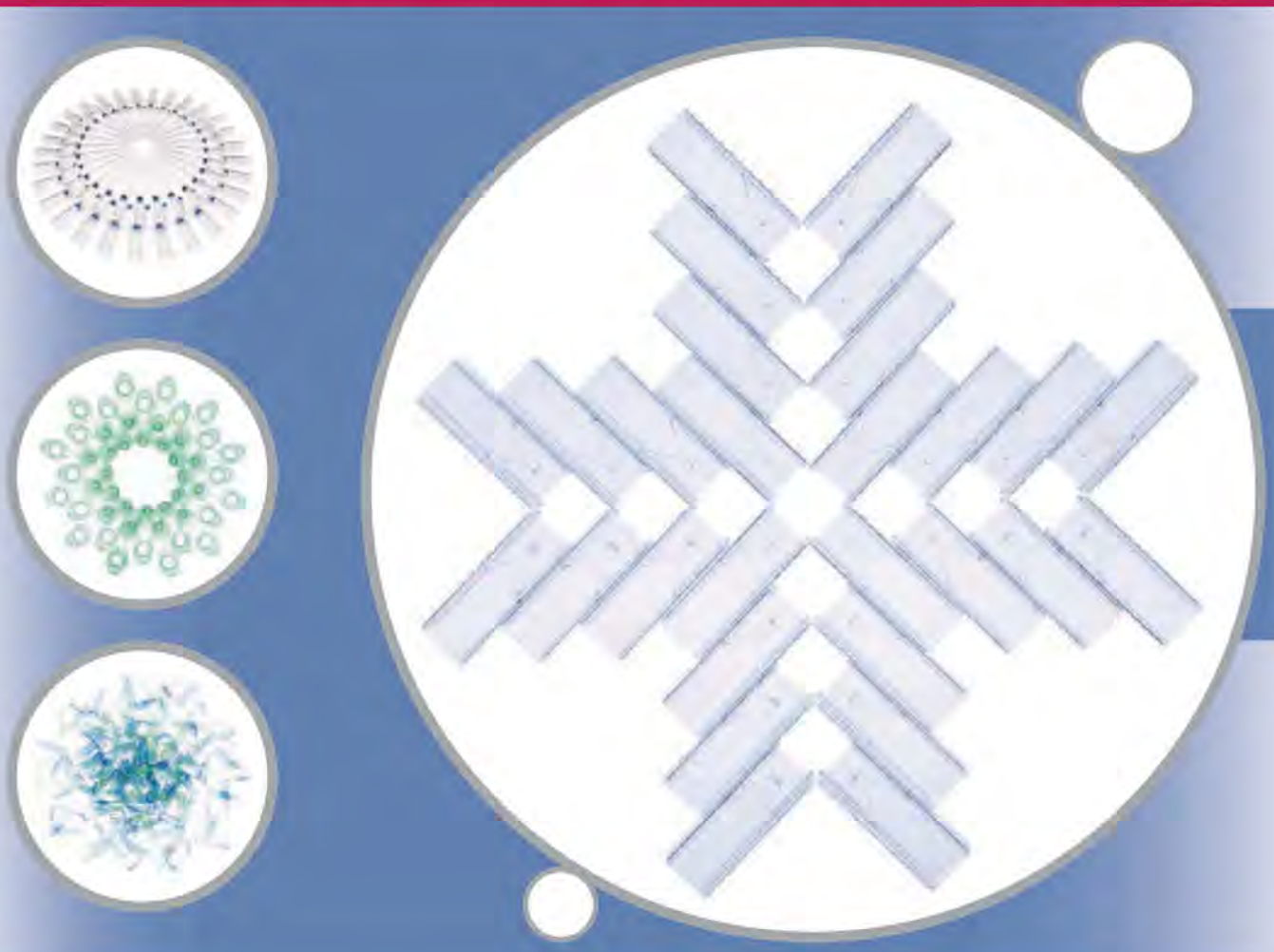



# Make the best of it!

**Top quality for your sample.**

**Each of your valuable samples deserves the best treatment. See for yourself how the Eppendorf disposable cuvette, the UVette®, will save time and reduce costs.**

Imprecise results or sample contamination can be time consuming and expensive. Therefore, the close environment of each sample should be adapted to its specific quality and purity needs. This can involve a specific purity level or the absence of certain substances, but also stability, reliability, or geometry. The patented* Eppendorf UVette® is designed to cover all the specific needs of your samples for photometric measurements!

**Eppendorf disposable UVette®**

- UV- and VIS-transparent between 220 nm and 1,600 nm
- Two optical path lengths (2 mm and 10 mm)
- Tapered cuvette base for accurate filling
- Small sample volume ≥ 50 µl
- Certified PCR-clean and protein-free quality available
- Recovery of samples without the risk of degradation or contamination

**Learn more about Eppendorf consumables:**
**www.eppendorf.com/consumables**

*Covered by US patent 6,249,345

eppendorf

*In touch with life*

**Your local distributor** www.eppendorf.com/worldwide · **Application Support** E-Mail: support@eppendorf.com
Eppendorf AG · Hamburg · Germany · Tel: +49 40 538 01-0 · Eppendorf North America, Inc. · USA · Tel.: +1 800 645 3050

# SCIENCEONLINE

## SCIENCEXPRESS
www.sciencexpress.org

**Phosphorylation of H2A by Bub1 Prevents Chromosomal Instability Through Localizing Shugoshin**
*S. A. Kawashima* et al.
Phosphorylation of the chromatin protein histone H2A plays a critical role in chromosome segregation during cell division.
10.1126/science.1180189

**Overexpression of Alpha2A-Adrenergic Receptors Contributes to Type 2 Diabetes**
*A. H. Rosengren* et al.
Sequence variations in an adrenergic receptor gene cause reduced insulin secretion and contribute to type 2 diabetes.
10.1126/science.1176827

**Gigahertz Dynamics of a Strongly Driven Single Quantum Spin**
*G. D. Fuchs* et al.
Fast spin-flips are observed in the nitrogen vacancy centers in diamond.
10.1126/science.1181193

**Universality in Three- and Four-Body Bound States of Ultracold Atoms**
*S. E. Pollack* et al.
The interactions involved in the formation of few-body bound states can be probed in a cloud of ultracold atoms.
10.1126/science.1182840

**Direct Imaging of Bridged Twin Protoplanetary Disks in a Young Multiple Star**
*S. Mayama* et al.
An infrared image taken with the Subaru Telescope reveals young binary stars and their circumstellar environments.
10.1126/science.1179679

## SCIENCENOW
www.sciencenow.org
Highlights From Our Daily News Coverage

**Meditation Halves Risk of Heart Attack**
A relaxation technique may be as powerful as modern drugs.

**A Silent Killer in Bangladesh Wells**
Researchers discover the cause of arsenic contamination in the country's aquifers.

**Socially Awkward? Check Your Genes**
Researchers link a single genetic difference to the ability to read others' emotions.

## SCIENCESIGNALING
www.sciencesignaling.org
The Signal Transduction Knowledge Environment

**RESEARCH ARTICLE: *Trypanosoma cruzi* Targets Akt in Host Cells as an Intracellular Anti-Apoptotic Strategy**
*M. V. Chuenkova and M. PereiraPerrin*
A surface protein of the intracellular parasite *T. cruzi* directly interacts with Akt to protect infected cells from pro-apoptotic stimuli.

**RESEARCH ARTICLE: Tyrosine Phosphorylation Inhibits PKM2 to Promote the Warburg Effect and Tumor Growth**
*T. Hitosugi* et al.

**PERSPECTIVE: PKM2 Tyrosine Phosphorylation and Glutamine Metabolism Signal a Different View of the Warburg Effect**
*C. V. Dang*
Aerobic glycolysis in cancer cells is associated with tyrosine phosphorylation of a metabolic enzyme.

**PERSPECTIVE: Acetylation Goes Global—The Emergence of Acetylation Biology**
*K. L. Norris* et al.
Proteomic analysis shows protein acetylation to be more prevalent than previously appreciated.

**GLOSSARY**
Discover what TRPA, GJIC, and miR mean in the world of signaling.

## SCIENCECAREERS
www.sciencecareers.org/career_magazine
Free Career Resources for Scientists

**Audacity, Part 3: Funding**
*A. Sasso*
What are the best strategies for funding high-risk, high-reward research?

**Tooling Up: The Project Management Career Track**
*D. Jensen*
Project management, as a career and a skill, requires detail management, good communication, and people skills.

**The New *Science* Careers Communities**
Science *Careers Staff*
Expand your professional network in MySciNet, a community for scientists from diverse backgrounds, and CTSciNet, the Clinical and Translational Science Network.

## SCIENCETRANSLATIONAL MEDICINE
www.sciencetranslationalmedicine.org
Integrating Medicine and Science

**PERSPECTIVE: Researching Genetic Versus Nongenetic Determinants of Disease—A Comparison and Proposed Unification**
*J. Ioannidis* et al.
Studies are needed that concurrently measure genotypes, nongenetic exposures, and outcomes.

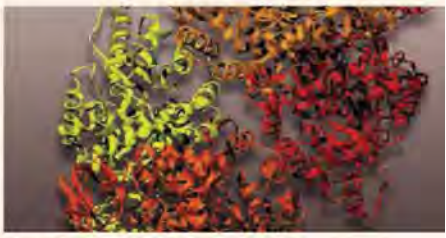

SCIENCESIGNALING
Pyruvate kinase M2 in tumor metabolism.

**RESEARCH ARTICLE: Frequent Release of Low Amounts of Herpes Simplex Virus from Neurons—Results of a Mathematical Model**
*J. T. Schiffer* et al.
A stochastic mathematical model elucidates constitutive herpes simplex virus 2 release in the genital tract in infected individuals.

**RESEARCH ARTICLE: Restoration of Norepinephrine-Modulated Contextual Memory in a Mouse Model of Down Syndrome**
*A. Salehi* et al.

**PERSPECTIVE: Cognitive Enhancement Therapy for a Model of Down Syndrome**
*F. K. Wiseman*
Cognitive deficits in mice can be reversed with precursors to the neurotransmitter norepinephrine.

## SCIENCEPODCAST
www.sciencemag.org/multimedia/podcast
Free Weekly Show
Download the 20 November *Science* Podcast to hear about the demise of Pleistocene megafauna, strengthening memories during sleep, cleaning up tar sands, and more.

## ORIGINSBLOG
blogs.sciencemag.org/origins
A History of Beginnings

## SCIENCEINSIDER
blogs.sciencemag.org/scienceinsider
Science Policy News and Analysis

**SCIENCE (ISSN 0036-8075) is published weekly on Friday, except the last week in December, by the American Association for the Advancement of Science, 1200 New York Avenue, NW, Washington, DC 20005.** Periodicals Mail postage (publication No. 484460) paid at Washington, DC, and additional mailing offices.  Domestic individual membership and subscription (51 issues): $146 ($74 allocated to subscription). Domestic institutional subscription (51 issues): $835; Foreign postage extra: Mexico, Caribbean (surface mail) $55; other countries (air assist delivery) $85. First class, airmail, student, and emeritus rates on request. Canadian rates with GST available upon request, GST #1254 88122. Publications Mail Agreement Number 1069624. **Printed in the U.S.A.**

**Change of address:** Allow 4 weeks, giving old and new addresses and 8-digit account number. **Postmaster:** Send change of address to AAAS, P.O. Box 96178, Washington, DC 20090–6178. **Single-copy sales:** $10.00 current issue, $15.00 back issue prepaid includes surface postage; bulk rates on request. **Authorization to photocopy** material for internal or personal use under circumstances not falling within the fair use provisions of the Copyright Act is granted by AAAS to libraries and other users registered with the Copyright Clearance Center (CCC) Transactional Reporting Service, provided that $20.00 per article is paid directly to CCC, 222 Rosewood Drive, Danvers, MA 01923. The identification code for *Science* is 0036-8075. *Science* is indexed in the *Reader's Guide to Periodical Literature* and in several specialized indexes.

AAAS
ADVANCING SCIENCE, SERVING SOCIETY

CREDIT: CHRIS BICKEL/AAAS

EDITED BY STELLA HURTLEY

## Methane's Path to Captivity

The mutual repulsion of oil and water is well known. It is thus somewhat baffling that in arctic regions and in marine sediments, enormous quantities of methane lie trapped under pressure in surrounding cages of ice. **Walsh *et al.*** (p. 1095, published online 8 October; see the Perspective by **Debenedetti and Sarupria**) undertook extended simulations to probe the steps that guide these two normally incompatible molecules along convergent, rather than divergent, paths. Computed 2- and 5-microsecond trajectories trace the process of methane capture as ice crystals nucleate and ultimately assemble into a cage network.

## Cosmic Acceleration

Cosmic rays are thought to be accelerated in the shock waves produced by supernova explosions and can generate gamma rays when they interact with interstellar particles and radiation. Starburst galaxies, with their increased star formation rates, increased stellar explosion rates, and high densities of gas and radiation fields, are considered to be promising sources of gamma-ray emission. Using the High Energy Stereoscopic System (H.E.S.S) array of telescopes, **Acero *et al.*** (p. 1080, published online 24 September) report the detection of gamma rays from one of the closest starburst galaxies, NGC 253. NGC 253 is a spiral galaxy, similar to our own Galaxy, except that its nucleus is undergoing an episode of intense star formation. The H.E.S.S. findings confirm that cosmic-ray acceleration is indeed efficient in starburst galaxies and open up new ways to understand cosmic-ray acceleration.

## Acidic Ocean

One consequence of the historically unprecedented level of $CO_2$ in the atmosphere that fossil fuel burning has caused, in addition to a warmer climate, is higher concentrations of dissolved $CO_2$ in the oceans. This dissolved $CO_2$ makes the oceans more acidic, and thus less saturated with respect to calcium carbonate. This has important ramifications for organisms that have calcium carbonate skeletons, which depend for their survival on the saturation state of calcium carbonate in the waters where they live. **Yamamoto-Kawai *et al.*** (p. 1098) report that in 2008, surface waters of the Canada Basin became undersaturated with respect to aragonite, a relatively soluble form of calcium carbonate incorporated into the shells or skeletons of many types of marine plankton and invertebrate. This undersaturation occurred much sooner than had been anticipated and has important implications for the composition of the Arctic ecosystem.

## Light in the Slow Lane

The speed of light is constant, reduced by a fraction from its vacuum level as it propagates through a material with a refractive index. In most transparent materials, the refractive index is slightly above unity, making the reduction in speed rather modest. **Boyd and Gauthier** (p. 1074) review the techniques used to reduce the speed of light down to pedestrian speeds, and describe some of the applications that such slow light (and fast light) may find.

## Demise of the Megafauna

**Approximately 10,000 years ago, the Pleistocene-Holocene deglaciation in North America produced widespread biotic and environmental change, including extinctions of megafauna, reorganization of plant communities, and increased wildfire. The causal links and sequences of these changes remain unclear. Gill *et al.* (p. 1100; see the Perspective by Johnson) unravel these connections in an analysis of pollen, charcoal, and the dung fungus *Sporormiella* from the sediments of Appleman Lake, Indiana. The decline in Pleistocene megafaunal population densities (inferred from fungal spore abundances) preceded both the formation of the late-glacial plant communities and a shift to an enhanced fire regime, thus contradicting hypotheses that invoke habitat change or extraterrestrial impact to explain the megafaunal extinction. The data suggest that population collapse and functional extinction of the megafauna preceded their final extinction by several thousand years.**

## Early Ore Formation

Ore deposits contain most of the world's metal resources, from commonly used metals such as iron, to precious and expensive metals such as platinum. Understanding how these ancient deposits form may lead to more efficient metal extraction and give clues about early Earth. **Bekker *et al.*** (p. 1086) studied sulfur and iron isotopes in 2.7-billion-year old Fe-Ni sulfide deposits from Canada and Australia and found that most of the metal-scavenging sulfur was originally atmospheric in origin. Photochemical reactions in the ancient oxygen-free atmosphere produced sulfide that eventually circulated to the sea floor and mixed with newly erupted komatite magmas. Thus, global surface processes in the oceans, atmosphere, and on continents are geochemically linked to ore-forming processes within Earth.

## Periplasmic Redox Regulation

The oxidation state of intracellular and extracellular proteins are carefully managed by cellular redox machineries. **Depuydt *et al.*** (p. 1109) discovered a reducing system that protects single

CREDITS (TOP TO BOTTOM): BARRY ROAL CARLSEN/UNIVERSITY OF WISCONSIN–MADISON; BOYD AND GAUTHIER

cysteine residues from oxidation in the bacterial periplasm. DsbG, a thioredoxin-related protein, appears to be a key player in that system and is the first reductase identified in the periplasm of *Escherichia coli*. Together with DsbC, DsbG controls the global sulfenic acid content of this compartment. Sulfenic acid formation is a major posttranslational modification in the periplasm, and three homologous L,D-transpeptidases are substrates of DsbG. Sulfenic acid formation is not restricted to *E. coli*, but is ubiquitous. Because proteins from the thioredoxin superfamily are widespread, similar thioredoxin-related proteins may control cellular sulfenic acid more widely.

## Anti-HIV Antibody Constraints

Despite significant efforts, an effective vaccine against the HIV-1 virus remains elusive. A site on the HIV-1 gp120 envelope glycoprotein that binds to the CD4 receptor on host cells is vulnerable to antibody, but only rarely are antibodies against this site broadly neutralizing. **L. Chen *et al.*** (p. 1123) have determined crystal structures for two weakly neutralizing antibodies in complex with gp120. The epitopes recognized by these antibodies were similar to those bound by CD4 or a broadly neutralizing antibody. However, small differences in recognition induced conformational shifts in gp120 that were incompatible with formation of a functional viral spike. Thus, the antibody-vulnerable site on HIV-1 is protected by conformational constraints.

## A-Maize-ing

Maize is one of our oldest and most important crops, having been domesticated approximately 9000 years ago in central Mexico. **Schnable *et al.*** (p. 1112; see the cover) present the results of sequencing the B73 inbred maize line. The findings elucidate how maize became diploid after an ancestral doubling of its chromosomes and reveals transposable element movement and activity and recombination. **Vielle-Calzada *et al.*** (p. 1078) have sequenced the *Palomero Toluqueño* (*Palomero*) landrace, a highland popcorn from Mexico, which, when compared to the B73 line, reveals multiple loci impacted by domestication. **Swanson-Wagner *et al.*** (p. 1118) exploit possession of the genome to analyze expression differences occurring between lines. The identification of single nucleotide polymorphisms and copy number variations among lines was used by **Gore *et al.*** (p. 1115) to generate a Haplotype map of maize. While chromosomal diversity in maize is high, it is likely that recombination is the major force affecting the levels of heterozygosity in maize. The availability of the maize genome will help to guide future agricultural and biofuel applications (see the Perspective by **Feuillet and Eversole**).

## Gardening for Ants and Termites

Among the social insects, ants and termites are the most diverse and ecologically dominant. Termites are known to engage in a mutualism with nitrogen-fixing bacteria, and **Pinto-Tomás *et al.*** (p. 1120) have identified similar relationships occurring among leaf-cutter ants, which maintain specialized nitrogen-fixing bacteria in their fungus gardens. Together, these mutualisms are a major source of nitrogen in terrestrial ecosystems. How is the evolutionary stability of such mutualistic cooperation maintained? **Aanen *et al.*** (p. 1103) show that the *Termitomyces* fungus cultured by termites remains highly related because mycelia of the same clone fuse together and grow more efficiently to out-compete rare clones.

## Dysbindin Function in Synaptic Homeostasis

Homeostatic signaling systems are widely believed to stabilize neural function over prolonged periods of time. However, the molecular mechanisms of homeostatic signaling in the nervous system are largely unknown, and direct links between defective homeostatic signaling and disease-causing genes remain obscure. **Dickman and Davis** (p. 1127) performed a large-scale, electrophysiology-based genetic screen for mutations that specifically disrupt synaptic homeostasis. DTNBP1 is one of two genes that are most strongly and consistently associated with schizophrenia susceptibility in humans. The *Drosophila* homolog of DTNBP1 (dysbindin) was identified in the screen and was found to function during synapse development, baseline neurotransmission, and synaptic homeostasis. Dysbindin altered the calcium-dependence of vesicle release and was essential in the presynaptic neuron for both the induction and expression of synaptic homeostasis.

CREDIT: CHEN *ET AL.*

Albert Grimaldi is the Sovereign Prince of Monaco and chairman of the Prince Albert II of Monaco Foundation.

# Governance of Both Poles

AT THE END OF THIS MONTH, THE ANTARCTIC TREATY SUMMIT IN WASHINGTON, DC, WILL CELEBRATE the 50th anniversary of an international agreement that has been centered around science, promoting cooperation to manage nearly 10% of Earth for peaceful purposes since 1 December 1959 (see www.atsummit50.aq). As the world moves toward negotiating effective policies related to climate change, lessons from the Antarctic Treaty experience can be drawn upon, particularly in regard to the future governance of international spaces that are considered to have an amplified response to climate change. Among the most critical are the Arctic regions.

As the most recent country to sign the Antarctic Treaty, the Principality of Monaco, with the 46 other signatory countries, recognizes that multiple nations can indeed maintain sound oversight of a major international region by cooperating on common interests, such as environmental protection and conservation, to avoid issues that would otherwise divide them (such as the exploitation of natural resources). Science has been key to this diplomacy. The treaty emerged at the height of the Cold War. It was designed "with the interests of science and the progress of all mankind," and for five decades has paved the way for other institutions, including the 1980 Convention on the Conservation of Antarctic Marine Living Resources, with its novel ecosystem approach, and the 1991 Protocol on Environmental Protection, with its unified strategies for conservation, pollution prevention, area protection, and moratorium on mineral resource activities.

International spaces (beyond national jurisdictions) exist across nearly 75% of Earth, and the climate interactions with these regions are fundamental on a planetary scale. The Arctic regions are warming twice as rapidly as elsewhere on the planet, so much so that the ice caps may soon disappear, thereby depriving the planet of an essential heat regulator and further accelerating climate change. Despite this awareness, there is still much difficulty in bringing states together, often because there are complex strategic issues, linked in particular to underground treasures. The Arctic is estimated to hold one-fifth of the planet's energy resources, which arouses overt ambitions. In this situation, it is the duty of political officials to catalyze discussions aimed at implementing long-term solutions for responsible oversight of the Arctic, taking into account not only the interests of the coastal countries (Canada, Denmark, Norway, Russia, and the United States) and their populations, but also the international community as a whole, because the future of the Arctic is crucial for all humankind.

This raises the issue of the framework of such action. Whereas a half-century of enforcement of the Antarctic Treaty has clearly led to establishing its effectiveness, there is no international treaty protecting the Arctic. Thus, it is the United Nations Convention on the Law of the Sea of 1982 that applies. It is on that basis that the five coastal countries of the Arctic Council recently agreed to "take steps . . . to ensure the protection and preservation of the fragile marine environment of the Arctic Ocean." But this declaration is unlikely to hold up as interests in the Arctic expand, and a binding agreement may be difficult to achieve in the near future.

Thus, more than ever, scientists must become sentinels and stewards to lead countries in taking concrete action for governing the Arctic. The consequences of climate change are destabilizing to environments, cultures, and economies. Governments should mitigate this instability before they have to react to it. Now is the time to forge policies for the Arctic that are driven by the notion of common interests and based on sound science. Alongside such negotiations, measures for good governance are needed, including the creation of sanctuaries and special zones for the conservation of biodiversity. This has already been done, for example, by France, Italy, and Monaco in the Mediterranean with the Pelagos Sanctuary.

Science has become the conscience of our time. And as the Antarctic Treaty has demonstrated, peaceful solutions can be reached that serve the progress of science and knowledge. Let the success of the Antarctic Treaty inspire political leaders to provide sound guardianship of both poles.

**– Albert Grimaldi**

10.1126/science.1183953

CREDITS: (TOP) PALAIS PRINCIER MONACO; (LEFT) ALAN LESHNER

DEVELOPMENT

## The Digital Divide

Programmed cell death is an important process in development, with mammalian digits being just one such example. The bone morphogenetic proteins (BMPs) and their downstream targets, the *Msx* genes, are known to participate in digit separation. If these components are absent, fingers and toes do not separate, resulting in soft tissue syndactyly. Suzuki *et al.* find that the small GTP-binding protein Rac1, which previously has been shown to function in cell adhesion, migration, and proliferation, also figures in digit development. When Rac1 was inactivated in the mesenchyme of the mouse limb bud, skeletal defects were apparent (such as the malformed sternum shown), yet a striking feature was soft tissue syndactyly due to webbing of the interdigital skin. Epistasis analysis revealed that *BMP* and *Msx* genes were not expressed in the limbs of Rac1-deficient mice; the elimination of Rac1 prevented programmed cell death from removing interdigital limb mesenchymal cells, primarily between the 2nd and 3rd, and the 3rd and 4th digits. — BAP

*Dev. Biol.* **335**, 396 (2009).

MOLECULAR BIOLOGY

## Domestic Tidying-Up

Ciliates, such as *Paramecium* and *Tetrahymena*, are single-celled eukaryotes that deal with the junk DNA infesting their genomes in a truly dramatic manner. They harbor complete copies of their genome within two separate nuclei. The micronucleus (or MIC) gives rise both to future progeny and to the macronucleus (or MAC), wherein the DNA is shredded, rearranged, and amplified, which allows the essential core of the genome—in some cases as little as 5% of it—to be expressed at high levels. The repetitive parasitic sequences that have been derived from transposable elements are trashed in the process.

Baudry *et al.* identify the enzyme (named PiggyMac) responsible for shredding the *Paramecium* MAC genome, and it turns out to have arisen from the very sequences that it so ruthlessly eliminates. PiggyMac is derived from transposases, which are enzymes that normally promote the spread of selfish DNA through the genome that has been "domesticated" during ciliate evolution; although this enzyme can still excise transposon remnants from the host genome, it does not catalyze their reinsertion elsewhere, and instead the junk sequences are safely disposed of. PiggyMac is critical for *Paramecium* development, and the supercharged expression made feasible by abbreviating and amplifying the MAC genome probably facilitates rapid growth and division. Domestication of an enemy of the state has also occurred in our immune system, in which antibody diversification is driven by the recombination-activating gene *RAG*, another erstwhile transposase. — GR

*Genes Dev.* **23**, 2478 (2009).

CHEMISTRY

## Propping Up Cholesterol

Cholesterol is a key component of mammalian cell membranes, but where does it reside? Although it is usually thought to reside "upright" with its hydroxyl group at the water interface, neutron scattering studies have found it lying near the center of the bilayer when the membranes are composed of polyunsaturated fatty acid (PUFA) chains. Kučerka *et al.* used neutron scattering to examine whether the lipid composition of bilayers may play a role in orienting cholesterol. They compared the impacts of adding either monounsaturated or disaturated lipids to PUFA bilayers containing cholesterol. Whereas adding 50% of the monounsaturated lipid moved cholesterol back to the upright position, the same effect occurred on addition of only 5% of the disaturated lipid. — PDS

*J. Am. Chem. Soc.* **131**, 16358 (2009).

BIOTECHNOLOGY

## Paths of Least Resistance

Living cultures of bacteria may seem like unlikely candidates to help generate electricity. Yet microbial fuel cells are indeed intriguing complements to other alternative energy schemes, despite the need for improvements in scalability and power-generation efficiency before they can be used in certain environments (e.g., organic-rich marine sediments or wastewater treatment plants). Advancements in efficiency may be achieved by identifying and then optimizing the important components of well-characterized species, or by identifying new bacteria that are inherently more efficient. On the first front, Newton *et al.* found that despite reducing environmental substrates such as Fe and Mn at a similar rate, two closely related species from the *Shewanella* genus produce very different current profiles over time. As mutants lacking certain proteins exhibited lower current generation, the mechanism of anode reduction—either through the production of mediator compounds or by direct attachment to the anode surface—emerged as a key efficiency determinant. On the second front, Fedorovich *et al.* isolated the dominant current-producing species from a mixed culture of bacteria from natural sediments. The new isolate is from a previously underrepresented class of *Proteobacteria*. — NW


*Appl. Environ. Microbiol.* **75**, 10.1128/AEM.01142-09; 10.1128/AEM.01345-09 (2009).

CREDITS (TOP TO BOTTOM): SUZUKI *ET AL.*, *DEV. BIOL.* **335**, 396 (2009); U.S. DEPARTMENT OF ENERGY

www.sciencemag.org

# Science

**1200 New York Avenue, NW**
**Washington, DC 20005**
Editorial: 202-326-6550, FAX 202-289-7562
News: 202-326-6581, FAX 202-371-9227
**Bateman House, 82-88 Hills Road**
**Cambridge, UK CB2 1LQ**
+44 (0) 1223 326500, FAX +44 (0) 1223 326501

SUBSCRIPTION SERVICES For change of address, missing issues, new orders and renewals, and payment questions: 866-434-AAAS (2227) or 202-326-6417, FAX 202-842-1065. Mailing addresses: AAAS, P.O. Box 96178, Washington, DC 20090-6178 or AAAS Member Services, 1200 New York Avenue, NW, Washington, DC 20005

INSTITUTIONAL SITE LICENSES please call 202-326-6755 for any questions or information

REPRINTS: Author Inquiries 800-635-7181
Commercial Inquiries 803-359-4578

PERMISSIONS 202-326-7074, FAX 202-682-0816

MEMBER BENEFITS AAAS/Barnes&Noble.com bookstore www.aaas.org/bn; AAAS Online Store www.apisource.com/aaas/ code MKB6; AAAS Travels: Betchart Expeditions 800-252-4910; Apple Store www.apple.com/eppstore/aaas; Bank of America MasterCard 1-800-833-6262 priority code FAA3YU; Cold Spring Harbor Laboratory Press Publications www.cshlpress.com/affiliates/aaas.htm; GEICO Auto Insurance www.geico.com/landingpage/go51.htm?logo=17624; Hertz 800-654-2200 CDP#343457; Office Depot https://bsd.officedepot.com/portalLogin.do; Seabury & Smith Life Insurance 800-424-9883; Subaru VIP Program 202-326-6417; VIP Moving Services www.vipmayflower.com/domestic/index.html; Other Benefits: AAAS Member Services 202-326-6417 or www.aaasmember.org.

| | |
|---|---|
| science_editors@aaas.org | (for general editorial queries) |
| science_letters@aaas.org | (for queries about letters) |
| science_reviews@aaas.org | (for returning manuscript reviews) |
| science_bookrevs@aaas.org | (for book review queries) |

Published by the American Association for the Advancement of Science (AAAS), *Science* serves its readers as a forum for the presentation and discussion of important issues related to the advancement of science, including the presentation of minority or conflicting points of view, rather than by publishing only material on which a consensus has been reached. Accordingly, all articles published in *Science*—including editorials, news and comment, and book reviews—are signed and reflect the individual views of the authors and not official points of view adopted by AAAS or the institutions with which the authors are affiliated.

AAAS was founded in 1848 and incorporated in 1874. Its mission is to advance science, engineering, and innovation throughout the world for the benefit of all people. The goals of the association are to: enhance communication among scientists, engineers, and the public; promote and defend the integrity of science and its use; strengthen support for the science and technology enterprise; provide a voice for science on societal issues; promote the responsible use of science in public policy; strengthen and diversify the science and technology workforce; foster education in science and technology for everyone; increase public engagement with science and technology; and advance international cooperation in science.

**INFORMATION FOR AUTHORS**
See pages 807 and 808 of the 6 February 2009 issue or access www.sciencemag.org/about/authors

EDITOR-IN-CHIEF **Bruce Alberts**
EXECUTIVE EDITOR **Monica M. Bradford**
NEWS EDITOR **Colin Norman**
MANAGING EDITOR, RESEARCH JOURNALS **Katrina L. Kelner**
DEPUTY EDITORS **R. Brooks Hanson, Barbara R. Jasny, Andrew M. Sugden**

EDITORIAL SENIOR EDITORS/COMMENTARY Lisa D. Chong, Brad Wible; SENIOR EDITORS Gilbert J. Chin, Pamela J. Hines, Paula A. Kiberstis (Boston), Marc S. Lavine (Toronto), Beverly A. Purnell, L. Bryan Ray, Guy Riddihough, H. Jesse Smith, Phillip D. Szuromi (Tennessee), Valda Vinson, Jake S. Yeston; ASSOCIATE EDITORS Kristen L. Mueller, Jelena Stajic, Nicholas S. Wigginton, Laura M. Zahn; RESEARCH ASSOCIATE Alexis Wynne Mogul; ONLINE EDITOR Stewart Wills; ASSOCIATE ONLINE EDITORS Robert Frederick, Tara S. Marathe; WEB CONTENT DEVELOPER Martyn Green; BOOK REVIEW EDITOR Sherman J. Suter; ASSOCIATE LETTERS EDITOR Jennifer Sills; EDITORIAL MANAGER Cara Tate; SENIOR COPY EDITORS Jeffrey E. Cook, Cynthia Howe, Harry Jach, Barbara P. Ordway, Trista Wagoner; COPY EDITORS Chris Filiatreau, Lauren Kmec; EDITORIAL COORDINATORS Carolyn Kyle, Beverly Shields; PUBLICATIONS ASSISTANTS Ramatoulaye Diop, Joi S. Granger, Jeffrey Hearn, Lisa Johnson, Scott Miller, Jerry Richardson, Jennifer A. Seibert, Brian White, Anita Wynn; EDITORIAL ASSISTANTS Emily Guise, Michael Hicks, Patricia M. Moore; EXECUTIVE ASSISTANT Sylvia S. Kihara; ADMINISTRATIVE SUPPORT Maryrose Madrid; EDITORIAL FELLOW Melissa R. McCartney

NEWS DEPUTY NEWS EDITORS Robert Coontz, Eliot Marshall, Jeffrey Mervis, Leslie Roberts; CONTRIBUTING EDITORS Elizabeth Culotta, Polly Shulman; NEWS WRITERS Yudhijit Bhattacharjee, Adrian Cho, Jennifer Couzin, David Grimm, Constance Holden, Jocelyn Kaiser, Sam Kean, Richard A. Kerr, Eli Kintisch, Andrew Lawler (New England), Greg Miller, Elizabeth Pennisi, Robert F. Service (Pacific NW), Erik Stokstad; INTERNS Michael Torrice, Jue Wang; CONTRIBUTING CORRESPONDENTS Dan Charles, Jon Cohen (San Diego, CA), Daniel Ferber, Ann Gibbons, Robert Koenig, Mitch Leslie, Charles C. Mann, Virginia Morell, Gary Taubes; COPY EDITORS Linda B. Felaco, Melvin Gatling, Melissa Raimondi; ADMINISTRATIVE SUPPORT Scherraine Mack, Fannie Groom; BUREAUS New England: 207-549-7755; San Diego, CA: 760-942-3252, FAX 760-942-4979; Pacific Northwest: 503-963-1940

PRODUCTION DIRECTOR James Landry; SENIOR MANAGER Wendy K. Shank; ASSISTANT MANAGER Rebecca Doshi; SENIOR SPECIALISTS Steve Forrester, Chris Redwood; SPECIALIST Anthony Rosen; PREFLIGHT DIRECTOR David M. Tompkins; MANAGER Marcus Spiegler; SPECIALIST Jason Hillman

ART DIRECTOR Yael Kats; ASSOCIATE ART DIRECTOR Laura Creveling; SENIOR ILLUSTRATORS Chris Bickel, Katharine Sutliff; ILLUSTRATOR Yana Greenman; SENIOR ART ASSOCIATES Holly Bishop, Preston Huey, Nayomi Kevitiyagala; ART ASSOCIATES Jessica Newfield, Matthew Twombly; PHOTO EDITOR Leslie Blizard

*SCIENCE* INTERNATIONAL

EUROPE (science@science-int.co.uk) EDITORIAL: INTERNATIONAL MANAGING EDITOR Andrew M. Sugden; SENIOR EDITOR/COMMENTARY Julia Fahrenkamp-Uppenbrink; SENIOR EDITORS Caroline Ash, Stella M. Hurtley, Ian S. Osborne, Peter Stern; ASSOCIATE EDITOR Maria Cruz; LOCUM EDITOR Helen Pickersgill; EDITORIAL SUPPORT Deborah Dennison, Rachel Roberts, Alice Whaley; ADMINISTRATIVE SUPPORT John Cannell, Janet Clements, Louise Moore; NEWS: EUROPE NEWS EDITOR John Travis; DEPUTY NEWS EDITOR Daniel Clery; CONTRIBUTING CORRESPONDENTS Michael Balter (Paris), John Bohannon (Vienna), Martin Enserink (Amsterdam and Paris), Gretchen Vogel (Berlin)

ASIA Japan Office: Asca Corporation, Tomoko Furusawa, Rustic Bldg. 7F, 77 Tenjin-cho, Shinjuku-ku, Tokyo 162-0808, Japan; +81 3 6802 4616, FAX +81 3 6802 4615, inquiry@sciencemag.jp; ASIA NEWS EDITOR Richard Stone (Beijing: rstone@aaas.org); CONTRIBUTING CORRESPONDENTS Dennis Normile [Japan: +81 (0) 3 3391 0630, FAX +81 (0) 3 5936 3531; dnormile@gol.com]; Hao Xin [China: +86 (0) 10 6307 4439 or 6307 3676, FAX +86 (0) 10 6307 4358; cindyhao@gmail.com]; Pallava Bagla [South Asia: +91 (0) 11 2271 2896; pbagla@vsnl.com]

EXECUTIVE PUBLISHER **Alan I. Leshner**
PUBLISHER **Beth Rosner**

FULFILLMENT SYSTEMS AND OPERATIONS (membership@aaas.org); DIRECTOR Waylon Butler; SENIOR SYSTEMS ANALYST Nomuna Nyamaa; CUSTOMER SERVICE SUPERVISOR Pat Butler; SPECIALISTS Latoya Casteel, LaVonda Crawford, Vicki Linton, April Marshall; DATA ENTRY SUPERVISOR Cynthia Johnson; SPECIALISTS Shirlene Hall, Tarrika Hill, William Jones

BUSINESS OPERATIONS AND ADMINISTRATION DIRECTOR Deborah Rivera-Wienhold; ASSISTANT DIRECTOR, BUSINESS OPERATIONS Randy Yi; MANAGER, BUSINESS ANALYSIS Eric Knott; MANAGER, BUSINESS OPERATIONS Jessica Tierney; FINANCIAL ANALYSTS Priti Pamnani, Celeste Troxler; RIGHTS AND PERMISSIONS: ADMINISTRATOR Emilie David; ASSOCIATE Elizabeth Sandler; MARKETING DIRECTOR Ian King; MARKETING MANAGERS Allison Pritchard, Alison Chandler, Julianne Wielga; MARKETING ASSOCIATES Aimee Aponte, Mary Ellen Crowley, Adrian Parham, Wendy Wise; MARKETING EXECUTIVE Jennifer Reeves; DIRECTOR, SITE LICENSING Tom Ryan; DIRECTOR, CORPORATE RELATIONS Eileen Bernadette Moran; PUBLISHER RELATIONS, ERESOURCES SPECIALIST Kiki Forsythe; SENIOR PUBLISHER RELATIONS SPECIALIST Catherine Holland; PUBLISHER RELATIONS, EAST COAST Phillip Smith; PUBLISHER RELATIONS, WEST COAST Philip Tsolakidis; FULFILLMENT SUPERVISOR Iquo Edim; FULFILLMENT COORDINATOR Carrie MacDonald; MARKETING MANAGER Christina Schlecht; MARKETING ASSOCIATE Mary Lagnaoui; ELECTRONIC MEDIA: MANAGER Lizabeth Harman; PROJECT MANAGER Trista Snyder; ASSISTANT MANAGER Lisa Stanford; SENIOR PRODUCTION SPECIALISTS Ryan Atkins, Christopher Coleman, Walter Jones; PRODUCTION SPECIALISTS Nichele Johnston, Kimberly Oster

ADVERTISING DIRECTOR, WORLDWIDE AD SALES Bill Moran

PRODUCT (science_advertising@aaas.org); MIDWEST/WEST COAST/W. CANADA Rick Bongiovanni: 330-405-7080, FAX 330-405-7081; EAST COAST/E. CANADA Laurie Faraday: 508-747-9395, FAX 617-507-8189; UK/EUROPE/ASIA Roger Goncalves: TEL/FAX +41 43 243 1358; JAPAN ASCA Corporation, Nanako Ide +81 (0) 3 6802 4616, FAX +81 (0) 3 6802 4615; ads@sciencemag.jp; SENIOR TRAFFIC ASSOCIATE Deiandra Simms

COMMERCIAL EDITOR Sean Sanders: 202-326-6430

PROJECT DIRECTOR, OUTREACH Brianna Blaser

CLASSIFIED (advertise@sciencecareers.org); U.S.: SALES MANAGER Daryl Anderson: 202-326-6543; MIDWEST Tina Burks: 202-326-6577; EAST COAST Alexis Fleming: 202-326-6578; WEST/SOUTH CENTRAL Nicholas Hintibidze: 202-326-6533; SALES COORDINATORS Rohan Edmonson, Shirley Young; INTERNATIONAL: SALES MANAGER Tracy Holmes: +44 (0) 1223 326525, FAX +44 (0) 1223 326532; SALES Susanne Kharraz, Dan Pennington, Alex Palmer; SALES ASSISTANT Lisa Patterson; JAPAN ASCA Corporation, Jie Chin +81 (0) 3 6802 4616, FAX +81 (0) 3 6802 4615; careerads@sciencemag.jp; ADVERTISING SUPPORT MANAGER Karen Foote: 202-326-6740; ADVERTISING PRODUCTION OPERATIONS MANAGER Deborah Tompkins; SENIOR PRODUCTION SPECIALIST/GRAPHIC DESIGNER Amy Hardcastle; SENIOR PRODUCTION SPECIALIST Robert Buck; SENIOR TRAFFIC ASSOCIATE Christine Hall

**AAAS** BOARD OF DIRECTORS RETIRING PRESIDENT, CHAIR James J. McCarthy; PRESIDENT Peter C. Agre; PRESIDENT-ELECT Alice Huang; TREASURER David E. Shaw; CHIEF EXECUTIVE OFFICER Alan I. Leshner; BOARD Alice Gast, Linda P. B. Katehi, Nancy Knowlton, Cherry A. Murray, Julia M. Phillips, Thomas D. Pollard, David S. Sabatini, Thomas A. Woolsey

AAAS
ADVANCING SCIENCE, SERVING SOCIETY

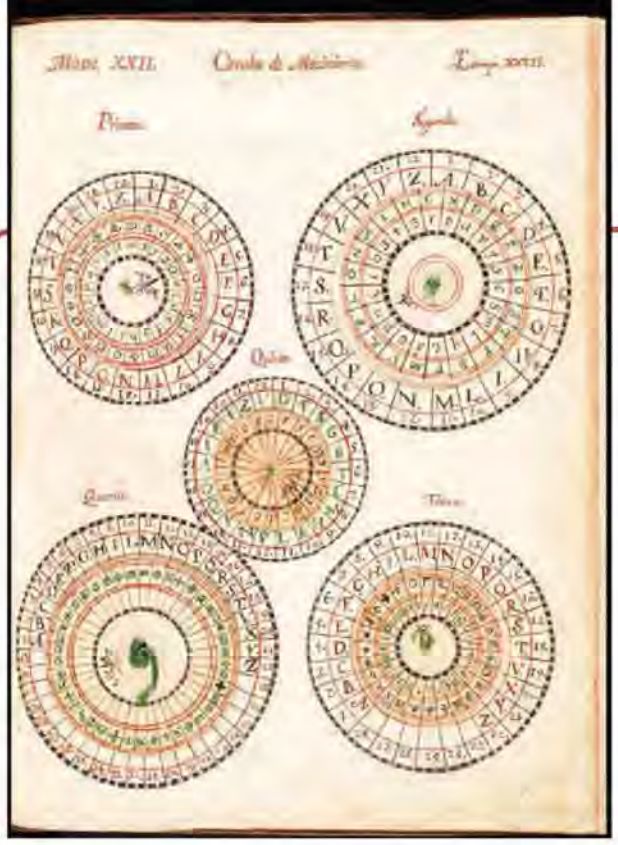

# Medieval Mind Meld

"Migrations of the Mind," an exhibit opening this week at the Getty Research Institute in Los Angeles, California, features more than 50 manuscripts showing how cross-cultural exchanges have fertilized science since medieval times.

At left is "De Zifras," or "On Ciphers," a Spanish primer on cryptography that includes 24 different methods of coding. It's by an anonymous cryptographer responsible for deciphering correspondence between Algeria and the Vatican at the Spanish Court at Navarre in the late 16th century. The manuscript contains coding wheels that the reader can spin to encode and decode. "It's such a beautiful decorated manuscript [that] there's probably no way that they're using it as an 'Enigma machine,' " says curator David Brafman. "But it's clear the author does work in intelligence, and he is showing off his skill."

The oldest manuscript in the show is an early 9th century French translation of Roman philosopher Boethius's commentary on Aristotelian logic. The latest is a Sanskrit document from 1799, linking music and the seasons. The show of manuscripts from the Lawrence J. Schoenberg Collection, which runs through April, "will transform how historians look at the past in the future," predicts Brafman.

## Focus on the Adolescent Brain

Temple University psychologist Laurence Steinberg has been awarded the first Klaus J. Jacobs Research Prize. The new award, worth 1 million Swiss francs ($1 million), comes from the Zurich-based Jacobs Foundation, founded by chocolate magnate Klaus Jacobs. It's designed to further "groundbreaking contributions to the improvement of the living conditions of young people."

Steinberg is well-known for his research on adolescent brain development. He's a former director of the MacArthur Foundation Research Network on Adolescent Development and Juvenile Justice. And he was one of the experts who wrote a U.S. Supreme Court brief arguing that 16- and 17-year-olds are too immature to be executed for capital crimes (*Science*, 30 July 2004, p. 596). In 2005, the court abolished the death penalty for these juveniles.

"It's the only million-dollar prize in the social/behavioral sciences," apart from the Nobel in economics, notes Anne Petersen, former deputy director of the National Science Foundation, who chaired the selection committee. "I believe that it will stimulate more strong research in the field." An award ceremony will take place on 3 December at the University of Zurich.

## Infectious Image

Pollsters know that how they phrase a question can powerfully affect the answers they get. Now researchers have shown that a metaphor people read can influence their opinions in a completely different context.

In a study led by psychologist Mark Landau of the University of Kansas, Lawrence, and colleagues, 69 undergraduates read one of two articles about airborne bacteria. One version stressed bacteria's threats to health.

Then students read an essay about post–Civil War economic growth in the United States. One version was written in neutral language; the other used body-related metaphors, such as "the United States experienced an unprecedented growth spurt and is scurrying to create new laws that will give it a chance to digest" millions of innovations.

Finally, participants were asked whether they agreed with statements about immigration policy. Students who had read the "nation as organism" text were more likely to agree with statements such as "an open immigration policy would have a negative impact on the nation." A control question about the minimum wage showed no difference between the two groups.

The researchers report in the November issue of *Psychological Science* that the body metaphor affected only students who had first read about harmful bacteria. The students' ethnicity did not affect the results. Psychologist Brian Meier of Gettysburg College in Pennsylvania says it's a "pretty tight" study and adds to evidence that "metaphors are more than just communication devices but reflect the way we think."

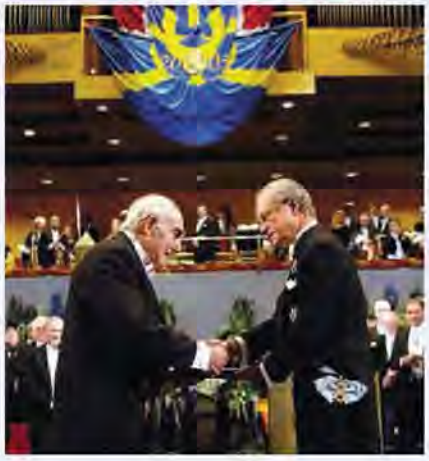

## THANKS ANYWAY

**"If I believed in God, I would start every morning by saying, 'Thank you, My Lord, for making me a theoretical physicist.'"**

—Vitaly Ginzburg, who died this month in Moscow at 93. A contributor to the Soviet H-bomb, Ginzburg survived Stalin's purges and in 2003 shared a Nobel Prize for his work on superconductors.

CREDITS (TOP TO BOTTOM): THE LAWRENCE J. SCHOENBERG COLLECTION/THE J. PAUL GETTY TRUST; AP PHOTOS/JONAS EKSTROMER; AXEL GRIESCH

A middle ground on global oil production 1048

Pigs as islet cell donors 1049

PLANETARY SCIENCE

# Yes, There's Ice on the Moon—But How Much, and What Use Is It?

When a spent rocket booster slammed into the frigid, inky shadow of a lunar crater last month, it sent up a slightly damp plume of dust, NASA scientists reported last week. "We found water, a significant amount of water," Lunar Crater Observation and Sensing Satellite (LCROSS) Principal Investigator Anthony Colaprete of NASA's Ames Research Center in Mountain View, California, said at a press conference.

After several decades of controversy, scientists now know that over billions of years, water can collect as ice in some of the coldest places in the solar system. Whether there's enough lunar water ice for future astronauts to drink or turn into rocket fuel, however, remains to be seen.

The LCROSS mission worked to perfection, except for a disappointing view from Earth. Before the impact, NASA scientists had predicted that ground-based observers, even amateurs, would see the plume in the gap between two mountains. As it turned out, Colaprete said, the impact's plume of debris "was as bright as thought, but it was behind a hill" because the debris did not rise as high as impact modeling had suggested.

The heavily instrumented LCROSS spacecraft, however, had a fine view of the rocket booster's impact and aftermath as it sped to its own impact 4 minutes later. LCROSS spectroscopic instruments delivered a "good, strong detection" of water, Colaprete said. The results show that even on the barren moon, traces of water vapor can freeze into the nooks and crannies of lunar soil in the 40-kelvin cold of permanently shadowed crater floors that never see the sun.

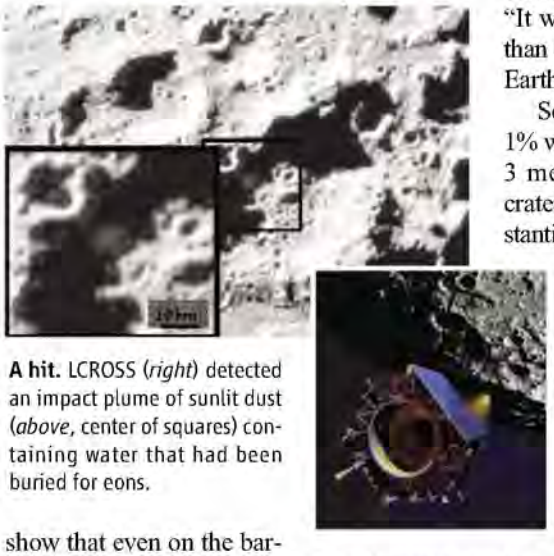

**A hit.** LCROSS (*right*) detected an impact plume of sunlit dust (*above*, center of squares) containing water that had been buried for eons.

LCROSS gives only an inkling of where the water might have come from. Colaprete reported that spectra hint at the presence of other volatile compounds, such as carbon dioxide, methane, and methanol, all found in comets and ice-rich asteroids. So the moon may have retained a tiny bit of the objects that have pummeled it for eons.

Whether anything will ever be made of the moon's stores of ice depends on how much is actually there. All told, LCROSS detected at least 100 kilograms of water, Colaprete said, but he declined to guess how abundant water ice had been beneath the impact site. Team members must still calculate what portion of subsurface ice actually rose into view and could have been measured, Colaprete noted. "It would probably be safe to say it's wetter than the Atacama Desert," the driest place on Earth, he said.

Some remote sensing had suggested about 1% water ice by volume would be in the upper 3 meters within permanently shadowed craters—a figure scientists considered a substantial amount. The 1% estimate "is not inconsistent with what's been observed," says impact modeler and LCROSS team member David Goldstein of the University of Texas, Austin. "I haven't convinced myself yet whether it's 0.1% or 10%. I think we'll work that out."

Both planetary scientists and NASA lunar exploration planners are rooting for the higher number. Scientists see a "treasure-trove of information" locked up in the ice deposits, said Gregory Delory of the University of California, Berkeley. Such deposits could preserve eons of impact history the way ice sheets on Earth preserve climate history. Exploration proponents see a resource for the next round of lunar astronauts to drink and perhaps split into hydrogen and oxygen for rocket fuel, assuming the Obama Administration sticks with NASA's plans to return to the moon (*Science*, 25 September, p. 1606). But both would have to figure out a way to operate at just 40 degrees above absolute zero. Good luck with that.

–RICHARD A. KERR

JAPAN

# Belt-Tightening Could Claim Some Scientific Scalps

**TOKYO**—Attempting to rein in Japan's yawning budget deficit, a government task force last week recommended tens of millions of dollars in cuts in science spending in the fiscal year beginning next April that would hit everything from research grants to big-ticket items such as a next-generation supercomputer. Taking a bite out of one high-profile target—Japan's ocean drilling program—could have international repercussions.

Not surprisingly, "scientists are extremely disappointed," says Masahiro Kami, an internal medicine researcher at the University of Tokyo. But the cuts are not a foregone conclusion: In the coming weeks, the finance ministry will finalize the budget, which must then be approved by Japan's legislature.

The recommendations are the work of the Government Revitalization Unit, set up by the Democratic Party administration to identify wasteful spending in budget requests prepared under the previous government of the Liberal Democratic Party, which governed Japan for most of the past 50 years. In daily reports on its investigations starting 11 November, the task force primarily laid into bloated construction programs. But on 13 November, it also zeroed in on the education ministry's portfolio.

The biggest target in the crosshairs is the $1.3 billion Next-Generation Supercomputer project at RIKEN, a network of national labs headquartered in Wako, near Tokyo. The task force recommended freezing $290 million

CREDITS: NASA, (INSET) NASA/ROGER ARNO

Tar sands' environmental legacy
1052

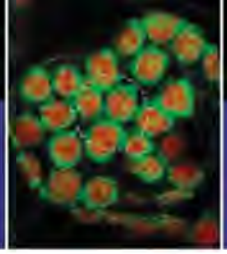

How chloroplasts move
1058

ASTROPHYSICS

# Galactic Glare Reveals Birthplace of Cosmic Rays

Cosmic rays—charged particles that hurtle through space at nearly the speed of light—have long baffled scientists. How do they acquire such tremendous velocities? Two new astronomical results—one in this week's issue of *Science* and the other published online this month in *Nature*—suggest that the physicist Enrico Fermi nailed the answer 60 years ago: They get their oomph from exploding stars. The papers give "pioneering results on a subject that was only explored by theorists" until recently, says Avi Loeb, an astrophysicist at Harvard University who was not involved in either study.

Like a tennis ball being slammed by two opponents running toward the net, Fermi theorized, charged particles inside a supernova bounce back and forth across the powerful blast wave from the explosion. A few of them are accelerated to very high energies and shoot into space as cosmic rays.

If this picture is true, galaxies that harbor many supernova explosions ought to be generating a high concentration of cosmic rays. Because cosmic rays interact with the surrounding gas to produce gamma rays, the most energetic form of light, the hearts of such galaxies should glow brightly in the gamma ray spectrum. And that's exactly what astronomers have found in two galaxies with high supernova activity: NGC 253 and M82.

Fabio Acero and colleagues looked for gamma rays from NGC 253, which lies 10 million light-years away, using the High Energy Stereoscopic System (HESS)—an array of ground-based telescopes in Namibia that can trace gamma radiation from the faint blue light produced when gamma rays strike Earth's atmosphere. On page 1080, the researchers report that they observed a concentration of high-energy gamma rays coming from the nucleus of the galaxy—a relatively small region of intense starburst activity, with a high rate of star formation and supernova explosions. Such a high density of cosmic rays in "a region with an outstanding supernovae explosion rate indicates that the cosmic ray acceleration is connected to supernovae," says co-author Dalibor Nedbal, an astrophysicist at Charles University in Prague.

Another research group, led by Victor Acciari of the Fred Lawrence Whipple Observatory near Amado, Arizona, reported online this month in *Nature* that it had found a similar connection in the M82 galaxy using the observatory's Very Energetic Radiation Imaging Telescope Array System. Both findings are in line with gamma ray observations of M82 and NGC 253 by the Fermi Space Telescope, presented this month at a symposium in Washington, D.C.

The importance of the two papers is that they "identify the 'smoking gun' signature of cosmic rays in a starburst galaxy, which is a much more violent and dense environment than the interstellar medium of the center of the Milky Way," Loeb says. He says the results also signal hope for detecting neutrinos from starburst galaxies using upcoming detectors such as the IceCube telescope, which is being built at the South Pole. That's because cosmic ray particles smashing into the interstellar medium produce subatomic particles known as pions, which decay to produce gamma radiation and neutrinos. Now that the gamma rays have been observed, Loeb says, it's the neutrinos' turn.

–YUDHIJIT BHATTACHARJEE

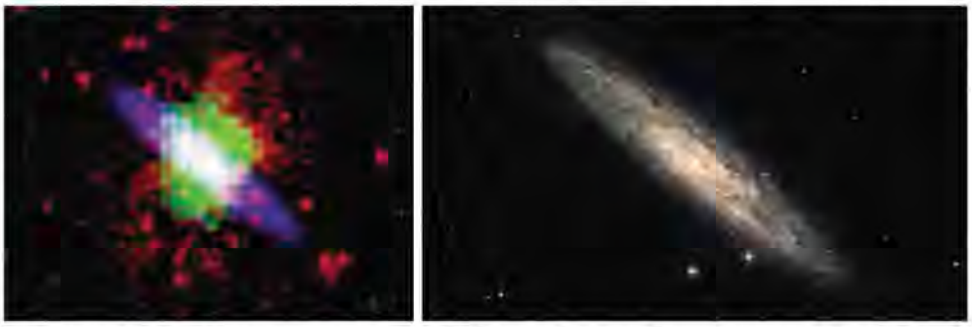

**Cosmic accelerator.** Glowing gamma radiation (*left*) from a "starburst" region in galaxy NGC 253 (*right*) confirms that cosmic rays get boosted to near–light speed inside exploding stars.

CREDITS (LEFT TO RIGHT): F. ACERO *ET AL.*; ESO

budgeted for the project next year pending a review. The government has already spent about $610 million on development and on a center in Kobe to house the computer, which researchers would use to simulate galaxy formation and model Earth's climate, among other things. Any delay would "have a very big impact on the infrastructure for research," says project chief Tadashi Watanabe. "The cuts are very shortsighted."

Another potential casualty is the ocean drilling program. The task force suggests a 10% to 20% reduction in its operating budget. "With a 10% cut, we could drill maybe for 1 month; with a 20% cut, there would be no operations at all," says Asahiko Taira, an executive director of the Japan Agency for Marine-Earth Science and Technology, which operates the drilling ship *Chikyu*—Japan's contribution to the global Integrated Ocean Drilling Program. Idling *Chikyu* would lop off one segment of a worldwide effort to study sub–sea-floor geophysical processes.

Also facing the ax are the education ministry's SPring-8 synchrotron, materials science research, various grant programs, and a major science museum in Tokyo. The task force also suggests abolishing a much-criticized scientific whaling program. More may be in the offing, as the panel will meet through the end of November.

The task force's recommendations give the tightfisted finance ministry a strong hand in upcoming negotiations with other ministries as the government finalizes the fiscal 2010 budget, which is typically sent to the legislature in late December. That leaves affected researchers a window of opportunity to save their necks. But considering the state of the economy and government finances, says Kami, prospects for research funding are grim.

–DENNIS NORMILE

OIL RESOURCES

# Splitting the Difference Between Oil Pessimists and Optimists

World production of conventional oil is likely to peak before 2030 and could reach its limits before 2020, a major report from a new voice in the debate over oil depletion warns. The report from the UK Energy Research Centre (UKERC) steers a middle course between oil pessimists—many of whom think production has already topped out—and optimists, who hold that oil supply will continue to meet demand well beyond 2030. In view of the daunting task of weaning the world's transportation off oil, the risk of a peak before 2030 "needs to be given serious consideration," the report says.

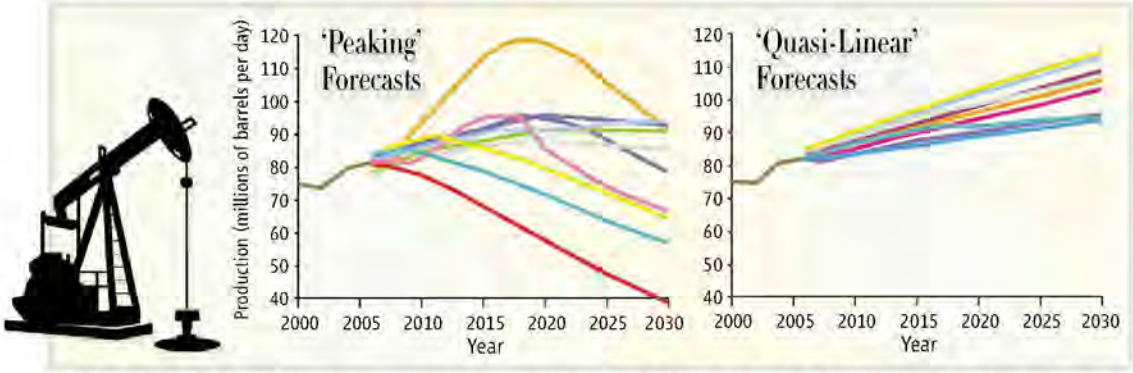


**Not ever upward.** A new report falls midway between pessimistic (*left*) and optimistic (*right*) forecasts of oil production.

Many experts agree, although their reasons vary. The report's prospect of an uncomfortably close peak in easily extracted oil makes sense, says petroleum geologist Lucia van Geuns of the Clingendael International Energy Programme in The Hague, the Netherlands. The report, she says, reinforces the increasingly concerned tone of annual reports from the International Energy Agency (IEA), the most recent of which came out last week with a warning that time is short for action.

The authors of the UKERC report aspired to produce an "independent, thorough, and systematic review of the evidence and arguments in the 'peak oil' debate," as its press release put it. UKERC, an umbrella organization of energy researchers at U.K. universities, was founded 5 years ago and is funded by Research Councils UK. For UKERC's Global Oil Depletion report (http://www.ukerc.ac.uk/support/Global%20Oil%20Depletion) released last month, five researchers headed by energy analyst Steven Sorrell of the University of Sussex commissioned researchers in and out of UKERC to scour the oil depletion literature, both peer-reviewed and not. Synthesizing more than 500 publications, the authors compared 14 forecasts of world production of conventional oil—the sort that will flow up a drill pipe on its own, not the oil locked up in oil sands or shale. After standardizing the forecasts, the authors rated their plausibility in light of the world's past production performance.

In the end, the UKERC report finds fault with both optimistic and pessimistic oil forecasts. Pessimistic forecasts that yield a world production peak today or within a few years often depend upon some estimate of the total amount of oil in the world that will ever be produced, the ultimate recoverable resource (URR). Some forecasters emulate the late geophysicist M. King Hubbert, who in 1956 accurately predicted that production in the continental United States would peak in 1970. They combine their favored URR with Hubbert's rule of thumb that production peaks when half the URR has been consumed. Such "peakists" tend to favor a URR of a little over 2000 billion barrels; the world has consumed 1228 billion barrels, so we're peaking about now, they conclude.

The UKERC report sees a number of problems with the classic Hubbert approach. "We come out quite critical of the pessimists, in part because their methods underestimate the URR," says lead author Sorrell. In 2000, the U.S. Geological Survey (USGS) estimated that URR is 3345 billion barrels—a 47% increase over their previous figure. Peakists pooh-pooh the USGS estimate as wildly optimistic, but the UKERC report finds that "large resources of conventional oil may be available." Among other evidence, it says, the amount of oil still being discovered in and around known fields supports the USGS estimate. The peakists' unwarranted low URRs have "contributed to excessively pessimistic forecasts of future supply," the report concludes.

On the other hand, the UKERC report finds forecasts that have global oil production rising more or less steadily out to 2030 to be overly optimistic. These forecasts from IEA, the U.S. Energy Information Administration, OPEC, and Exxon typically start by predicting how much oil will be required each year, including the expected added demand from growing populations and growing economies. Then forecasters allot the required production to oil-producing countries in proportion to the amount of oil they still hold.

Such demand-driven forecasts, the report says, require world oil production to outperform its already stunning record of doubling every decade for a century. That's unlikely, it finds, because industry is discovering fewer and fewer of the giant, highly productive fields that made such growth possible. "We consider that forecasts that delay the peak until after 2030 rest upon several assumptions that are at best optimistic and at worst implausible," the authors write. The IEA forecast, for example, implies that newly discovered fields will produce oil at rates that "greatly exceed historical experience," says Sorrell. "That may be possible, but the forecasters certainly haven't justified it."

An avowed moderate pessimist—Beijing-based petroleum analyst Michael Rodgers of consulting company PFC Energy—says the UKERC report gets things about right. The report reminds readers that "there are some real subsurface constraints" on production, he says. "You have to find a lot of new fields to offset declining ones and build production, [but] there's no way you can be that optimistic."

Van Geuns agrees that the increasing difficulty in finding and extracting oil will lead to a conventional peak before 2030, but she still sees an optimistic side. As the increasing scarcity of conventional oil pushes up prices, exploitation of more expensive unconventional fuels such as oil sands (see p. 1052) will expand, she says. Higher-cost oil will also make pricey oil in extremely deep waters or in the offshore Arctic more attractive. If unconventional oil can be developed fast enough, she notes, any looming peak in conventional oil could be blunted. The catch, the UKERC report notes, is that the conventional oil peak will not give a clear warning of its approach; studies like this one will likely have to spur early, strong action by themselves. **–RICHARD A. KERR**

SOURCE: UK ENERGY RESEARCH CENTRE (OCTOBER 2009)

CELL THERAPIES

# Clean Pigs Offer Alternative to Stem Cell Transplants

They may be the cleanest pigs on Earth. About 100 swine at the University of Minnesota's Schulze Diabetes Institute in Minneapolis constitute the first herd in the country specially bred to supply insulin-secreting pancreatic islets for people with diabetes.

A scientific team led by surgeon and endocrinologist Bernhard Hering hopes to start clinical trials using these cells within a couple of years. But in addition to immunological challenges, they face the difficulties of gaining U.S. Food and Drug Administration approval for grafting living animal tissues into humans (as opposed to mechanical aids such as cartilage) as well as overcoming public aversion to the idea.

Minnesota immunologist Henk-Jan Schuurman described these special pigs last week at a National Institutes of Health (NIH) meeting on "next-generation beta cell transplantation" to treat type 1 diabetes, in which pancreatic islets containing beta cells are destroyed by a patient's own immune system. Scientists have been working feverishly to develop insulin-producing cells from human embryonic stem (ES) cells and, more recently, induced pluripotent stem cells to substitute for hard-to-get cells from human cadavers. But many believe pigs offer the nearest hope for an abundant source of tissue.

**Immaculate conception.** Second-generation piglets in their sterile nursery.

CREDITS (TOP TO BOTTOM): AUTISM RESEARCH CENTRE/UNIVERSITY OF CAMBRIDGE; SPRING POINT PROJECT

At least two small pig islet transplant trials are already under way, conducted by Living Cell Technologies in Auckland, New Zealand, reported the company's medical director, Robert Elliott. One was begun in Russia in 2007; the other started last month in New Zealand after 14 years of delays and public consultations.

Living Cell uses Auckland Island pigs, billed as "the world's only virus-free pigs." But they now have some serious competitors in the Minnesota porkers. Schuurman says their facility, opened in 2007, features special air and water filtration, autoclaving for all entering materials, sterile garments for workers, and constant medical tests for the inmates, who are strictly vegetarian to avoid importation of alien mammalian proteins. Only second-generation pigs raised in the facility will be used as donors.

"We are now in a position where we can actually think about going forward with a human clinical trial," Hering announced at the meeting. He argues that adult pig islets will be safer and less likely than human cell grafts to induce the autoimmune reaction that causes type 1 diabetes. However, pig tissue still triggers a powerful immune response. The New Zealand team has tackled this by encapsulating the islets in material that will fend off immune attack while allowing insulin out. The Minnesota team is still working on an immunosuppression regimen that will allow the use of "naked islets," says Schuurman, which the scientists think will have better access to nutrients. Further down the road, scientists at the University of Pittsburgh and elsewhere are working on techniques for shuffling pigs' genes or conditioning patients' immune systems to narrow the species gap.

Opinions vary about whether porcine islets are the wave of the future. Immunologist and transplant surgeon Christian Larsen of Emory University in Atlanta bets they are because researchers have still not been able to resolve the main problem with human ES cells: that they can cause teratomas. He says pig islet transplant work with monkeys at Emory and elsewhere has so far shown that the cells can function effectively for up to a year.

But Gordon C. Weir, who studies islets at Harvard's Joslin Diabetes Center in Boston, believes ES cells will be the way to go. He calls the pig work "really intriguing" but fears that the porcine enthusiasts may be too optimistic about prospects for conquering the immune problem. **–CONSTANCE HOLDEN**

## ScienceNOW.org

### From *Science*'s Online Daily News Site

**Meditation Halves Risk of Heart Attack**
Meditation can cut the risk of heart attack, stroke, and death by almost 50% in patients with existing coronary heart disease, according to a new clinical trial. The findings indicate that relaxation and mental focusing can be as effective as powerful new drugs in treating heart disease.
http://bit.ly/transcendentalmeditation

**Socially Awkward? Check Your Genes**
Some people can read your face and know that you've had a bad day. Others seem oblivious. Now researchers have pinpointed a genetic explanation for why some people are better empathizers than others.
http://bit.ly/SociallyAwkward

**A Silent Killer in Bangladesh Wells**
Every day, millions of people in Bangladesh drink poisoned water. Wells all over the country tap into shallow aquifers with high concentrations of arsenic. Now researchers report that they've figured out the cause of this contamination.
http://bit.ly/bangladeshwells

**A Physics Paradox: Holes That Block Light**
The way that light moves, with its fixed speed and its ability to act like either a wave or a particle, often leads to some of the most curious paradoxes of physics. A new one has just been found: Make holes in a film of gold so thin that it's already semitransparent, and *less* light gets through. http://bit.ly/plasmonic

**New Neurons Make Room for New Memories**
The discovery that new neurons are born in the adult brain overturned decades-old dogma in neuroscience. But it also raised a host of questions about what exactly these neurons do. Now the authors of a new study suggest that the newcomers clear away the remnants of old memories to make room for new ones. http://bit.ly/HippocampusMemory

Read the full postings, comments, and more on **sciencenow.sciencemag.org**.

NEWSMAKER INTERVIEW

# University Head Zhu Qingshi Challenges Old Academic Ways

**BEIJING**—Every autumn when Nobel Prize winners are announced and the world's most populous nation misses out—yet again—the mass media and blogs here blame an education system that values rote memorization over creativity. Widespread disaffection is a factor, Chinese state media observed, behind the National People's Congress's decision earlier this month to sack Education Minister Zhou Ji.

But true change may come only from the bottom up. In September, the government of Shenzhen, a city in southern China, appointed physical chemist Zhu Qingshi as president of the planned South University of Science and Technology (SUST). Zhu insisted on also being appointed the university's Communist Party secretary, making it clear he would be calling the shots.

A Sichuan native, Zhu, 63, graduated from the University of Science and Technology of China here in 1968 (USTC later moved to Hefei) and has been a visiting fellow at several top overseas labs, including the University of Oxford, the University of Cambridge, and the Massachusetts Institute of Technology. Zhu's pioneering research in laser spectroscopy won him election to the Chinese Academy of Sciences at the tender age of 45. He became known as a reformer during his tenure as USTC president from 1998 to 2008.

Shenzhen, near Hong Kong, was the cradle of China's market economy 30 years ago. In its bid to become a paragon of education reform, the city paid nearly $1 billion for the land for SUST's campus, expected to open in 2012 with an enrolment of 1500 undergraduates and 500 graduate students in science and engineering—all on scholarships covering tuition and living expenses. (SUST will launch with a small group of students in temporary digs next year.) In an interview with *Science*, Zhu explained how he intends to shake up China's university system—whether the education ministry likes it or not.

**–RICHARD STONE**

**Q: What did you do in Hefei to earn your reputation as a reformer?**

**Z.Q.:** My most important contribution to USTC was not what I did but what I did *not* do. In the past several years, Chinese universities grew very quickly, buying up land and enlarging enrollments. But teaching staffs were not expanded. We wanted to maintain academic standards, so we rejected this approach. Secondly, the Ministry of Education evaluates teaching and research activities at all universities. Evaluation is a good thing. But the ministry's evaluation now is not a real evaluation; it's a formal exercise.

**Q: An exercise in wining and dining?**

**Z.Q.:** Exactly. The evaluators would come to our university, and we didn't prepare anything special; instead we asked them to observe the professors and students.

**Q: Did the education ministry appreciate your approach?**

**Z.Q.:** No, they did not appreciate it. We didn't get perfect marks, but around 70% of China's universities did. Everybody knows the evaluation has no meaning. Of course, it's connected to funding, and our university got less money from the central government. But we kept a very high level of education and research.

**Q: In what way will SUST be different from other Chinese universities?**

**Z.Q.:** We will abolish rank: what we call debureaucratization of the administration.

**Q: How will that help?**

**Z.Q.:** The main problem in higher education is bureaucratic power. Many professors now pursue bureaucratic rank instead of academic excellence. If you attain a high rank, you get money, a car, research funding. This is why Chinese universities have lost vitality.

**Q: How will you persuade people to work for SUST rather than top universities like Tsinghua or Beida [Peking University]?**

**Z.Q.:** First, the Shenzhen government promised that we can hire professors at the same salary as professors at Hong Kong University of Science and Technology. That's higher than Beida, even higher than many U.S. universities. Also, SUST will be the first university in China with a significant budget for research. This is something I'm pursuing very hard. We don't want our professors to have to continuously apply for funding.

**Q: A lot of critics say that China's education system suppresses creativity. At the teaching level, what needs to change?**

**Z.Q.:** We feel that the whole year of grade three of high school [equivalent to senior year in the United States] is wasted just preparing for the *Gao Kao* [the national university entrance exam].

At SUST, we will not enroll students based on *Gao Kao* results. We will enroll them directly from grade two of high school. Next year, we will take 50 students from grade two.

**Q: Does the education ministry see your rebel attitude as a threat to its authority?**

**Z.Q.:** They might not forbid us to carry out our plan, but they also might not encourage us. There is a danger that our students may not get a diploma issued by the education ministry. My goal is to ensure that my students are accepted by society and get good jobs after they graduate. If I accomplish that, this experiment will be a success.

People are looking for a university to challenge the education system and show an effective path for reform. SUST is going to face many problems. I am prepared to be the first to try true education reform, but maybe someone after me will be the first to succeed.

CREDIT: PHOTO COURTESY OF XU WENGE/NDDAILY

**Patent power.** Ashley Stevens, of Boston University, argues that universities must use "socially responsible principles."

INTELLECTUAL PROPERTY

# Research Centers Promise a Break on Medical Patents in Developing Countries

More than a half-dozen major U.S. universities and institutes pledged last week to lean on biotech companies when licensing intellectual property to secure more favorable terms for countries in the developing world.

Harvard, Yale, and Brown universities, the University of Pennsylvania, and the state universities of Oregon and Illinois, as well as the National Institutes of Health and Centers for Disease Control and Prevention, have signed the pledge, which is sponsored by the Association of University Technology Managers (AUTM).

As patent owners, the pledge notes, they can use many strategies to ensure access to new medical technologies. These include filing for but not enforcing patent rights in a poor country, requiring companies not to file for subsequent patents in certain places, and forbidding them to sue manufacturers of generic drugs. Universities can even forgo royalties to give companies an incentive to cooperate. But the pledge includes no specific legal language to use in future licenses.

"It's not clear yet what the best option is," says Ashley Stevens, president-elect of AUTM and executive director of the office of technology transfer at Boston University, a signatory. The impact on therapies such as new drugs and vaccines may be the most important, the pledge says, but it covers all medical technologies. As a practical matter, it will have little effect on the market for 10 to 15 years, roughly the time it takes to commercialize a technology.

Companies usually don't alter licenses already in place, although there are exceptions. In 1988, Yale University licensed an AIDS drug, soon called Zerit, to Bristol-Myers Squibb (BMS). Zerit became part of a "triple cocktail" therapy in the 1990s that made AIDS manageable for the first time. BMS enforced patent rights for Zerit in South Africa, which was hit hard by AIDS and wanted to distribute a cheap generic copy. In 2001, activists and aid organizations asked Yale to press the company to relent. Yale said it had no power to do so.

Only after a prolonged and noisy protest did BMS agree not to sue manufacturers of generic Zerit in South Africa. Stevens says the pledge has its roots in this incident, which helped to convince universities that they often ceded too much control over their technology.

The biotech industry's reaction to the pledge has been mixed. The Biotechnology Industry Organization, a trade group in Washington, D.C., has discussed principles similar to the pledge with universities such as the University of California system, says Tom DiLenge, general counsel at BIO. And he says Gilead and GlaxoSmithKline have already announced that they would not enforce intellectual-property rights for key drugs in developing countries. DiLenge adds that, from an industry perspective, "What's important is that [the pledge] is not a one-size-fits-all approach and that not all agreements contain certain clauses."

**Zerit.** A fight over low-cost copies of this AIDS drug erupted in 2001.

In licensing technologies at his school, Stevens has encountered resistance from companies about giving up some intellectual-property rights: "I wouldn't say the reaction has been, 'What a wonderful idea.' " It has made some negotiations longer and "more difficult," he says, but it hasn't decreased the values of licenses overall. And more biotech companies are coming around. "I think they've realized the developing world is only 3% to 4% of the world drug market." **–SAM KEAN**

CREDITS (TOP TO BOTTOM): BOSTON UNIVERSITY PHOTO SERVICES; NEWSCOM

## *Science*Insider

### From the *Science* Policy Blog

The American Physical Society's governing council has rejected a petition to revise a 2007 **statement on global warming**. That statement said warming was "incontrovertible" and could lead to "significant" ecological or social "disruptions." The council turned back an effort to replace it with one that said, among other things, that recent warming is not "exceptional." http://bit.ly/h3vyT

Brazil has announced a plan to cut carbon emissions from between 36% and 39% by 2020. Meanwhile, negotiators have acknowledged that a comprehensive climate deal won't be reached in **Copenhagen** next month. http://bit.ly/4g1n1c

**Spirit Rover** may be about to die on the surface of Mars. Originally designed for a 90-day mission in early 2004, it has explored the planet for 5 years, but a wheel stuck in sand may prove its undoing. http://bit.ly/3fLWQz

The European Union is lagging behind the United States in terms of total **spending on research and development**, but in 2008 it grew at a rate of 8.1%, two points higher than the United States. By comparison, China and India saw R&D growth of 40% and 27%, respectively. http://bit.ly/3iX6od

Asian scientists speaking at a conference questioned why **cancer**, which is rapidly overtaking AIDS, tuberculosis, and malaria as a cause of premature mortality in the developing world, isn't mentioned in the United Nations Millennium Development Goals. http://bit.ly/4DJSzh

A Florida circuit court ruled in favor of a Stanford University professor of the **history of science** who is trying to keep his unpublished book manuscript out of the hands of R.J. Reynolds. The tobacco company had subpoenaed it as evidence for an upcoming suit, but the judge said Robert Proctor had the right to withhold the manuscript. http://bit.ly/14VqKq

For more science policy news, visit **blogs.sciencemag.org/scienceinsider**.

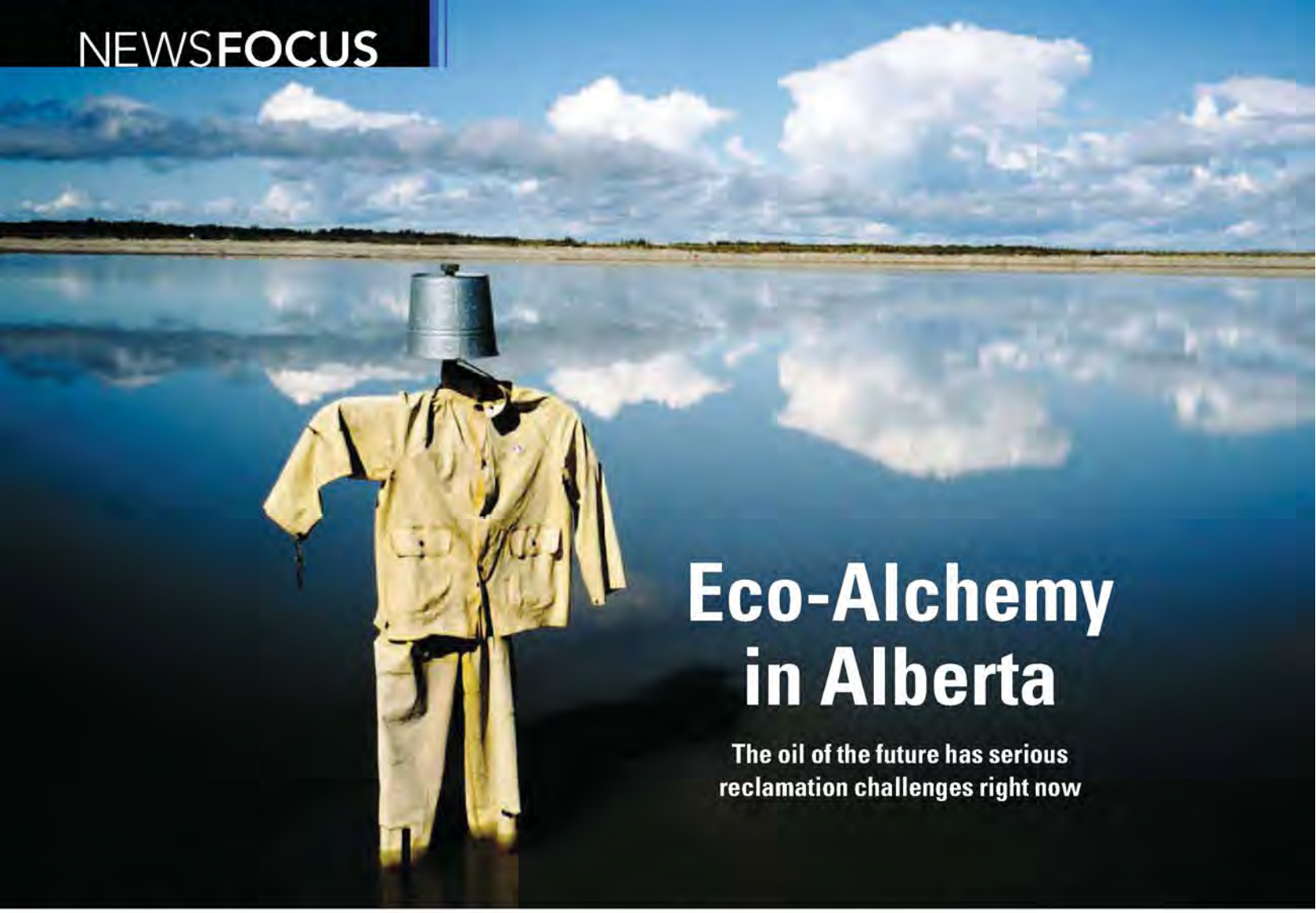

# Eco-Alchemy in Alberta

## The oil of the future has serious reclamation challenges right now

**FORT MCMURRAY, CANADA**—I'd been poking around the oily lake for an hour when security arrived. A white pickup truck labeled Syncrude pulled onto the highway shoulder, near the lake's black dirt beach, and stopped. A short woman with spiky blonde hair, glasses, and an oversized security coat leaned across to the passenger window and demanded to know what I was doing.

"What lake is this?" I called.

"It's a tailings pond," she answered. "And you're trespassing."

Ordering me over, she asked for my name and hometown. With a walkie-talkie, she radioed the information in to Syncrude headquarters. She probably figured me for an activist—environmentalists have staged numerous protests at oil mines, the most visible part of Canada's incredible oil boom. I had gone up in August to visit Alberta's infamous "tar sands," vast and largely untapped reserves of petroleum in the form of tarry deposits a few tens of meters beneath the surface, and I'd been sidetracked looking for a herd of bison that I heard lived nearby. While someone unseen ran my name and decided my fate, I waited near the pickup. In the sudden quiet, cannons fired in the background.

The interaction took a minute. In that time, the oil mines that stretch along Highway 63 in northern Alberta had produced 740,000 liters of wastewater slurry called "tailings," which get dumped into standing pools called "tailings ponds." The "ponds" already cover 130 $km^2$ in Alberta—an area double the size of Manhattan—and are growing. Even oil executives such as Chris Fordham of Suncor Energy, a Canadian company, have said, "Let's be candid: These industrial ponds are not pretty to look at." Different ponds have different colors—some aqua, some rainbow, some gray like skin under a bandage—but all have a sand bottom, a few meters of cloudy water, and a syrupy film of oil on top. Environmentalists swear (though it's hard to see how they know) that the vast pond complexes are visible from space.

There's a roaring debate in Canada about whether tailings ponds, and oil mines in general, are ecologically salvageable—specifically, whether they can ever support the same flora and fauna as undisturbed land. No one knows because oil-mining companies have been reclaiming land for only a few decades, a short time ecologically, and on small scales. But one hint lies a kilometer down the road from the oily lake. There, right off the highway, a gravel road leads up to Wood Bison Viewpoint, a 690-hectare park owned by Syncrude, a conglomerate owned by seven oil companies in Canada. Like the oily lake, the park is artificial, but it supports a real if modest forest. Ducks fly by. Three hundred bison roam about, behind a fence. To all appearances, it's a thriving ecosystem—and it sits atop an exhausted oil-pit mine. Syncrude "reclaimed" this land by covering it with soil, planting trees, and introducing wildlife. It represents dozens of years of effort and millions of dollars of research. Oil companies proudly end tours at Wood Bison Viewpoint to reassure the public that they can indeed rehabilitate disturbed land.

Don Thompson, president of the Oil Sands Developers Group, has no reservations: "I do not believe reclamation is a particular challenge at all." Ecologists don't deny that, as

**Online**
**sciencemag.org**
Podcast interview with author Sam Kean.

CREDIT: MAGNUM PHOTOS

**Bitu-man.** A scarecrow in a "tailings pond" helps keep birds out of toxic mine water.

long as companies commit money, they can recreate green landscapes. But ecologists see shades of green, and not all are equal. Northern Alberta is full of delicate areas such as wetlands, and the oil industry—despite sincere efforts—has a spotty history of recreating fully functioning ecosystems, they say. "There may be some positive outcomes" after oil companies leave, says Jennifer Grant, an analyst at Canada's Pembina Institute in Yellowknife, an environmental think tank. "But there has been no demonstrated long-term reclamation of tailings waste and no willingness by the government to slow down" mining operations until reclamation experts know for sure what's possible.

Twenty years ago, oil companies in northern Alberta spoke with distant hope of producing 1 million barrels of crude oil per day by 2020; they exceeded that in 2004. They currently produce 1.3 million barrels daily, a number that is set to rise to 3 million by 2018, and some projects will last beyond 2060. The four major mining companies—Suncor, Syncrude, Shell Canada (a.k.a. Albian Sands), and Canadian Natural Resources (a.k.a. Horizon Oil Sands)—have already stripped away 530 $km^2$ of forest and wetlands, slicing the top off of the earth and exposing the black gunk. Imperial Oil (with ExxonMobil) will open a fifth major mine in 2012, and other mines are in the works.

Despite ongoing reclamation of the empty pits and lakes of waste, the percentage of reclaimed area—12% of the disturbed land—has shrunk recently. (Seventy percent of the reclaimed land belongs to Syncrude.) And because companies reclaim mines and ponds as they go, new forests and lakes will fight for survival right next to industrial sites.

Ecologists and industry people disagree on a number of scientific points about reclamation. It's not clear what technologies, if any, can reclaim ponds and land on the scale needed. Oil mining also creates unique liquid waste that no one quite knows how to treat. Most contentious is the debate over what degree of ecological restoration is acceptable, and even how to measure that. New government regulations in 2009 put pressure on companies to find answers and solutions quickly. About the only thing industry and ecologists agree on is that this reclamation is unparalleled in ecological history. "The oil sands industry faces unique reclamation challenges for which there are no analogs," Thompson has said. Adds Grant, "It's like one big experiment."

CREDITS: SYNCRUDE CANADA LTD.

## Tar Island

The reclamation challenge is unique because the tar sands industry in the Athabasca region of Canada is unique. Companies there don't pump oil out of the ground; they mine it in vast open pits gouged out of the landscape. Mining oil was long thought unprofitable, and in fact the tar sands had become a standing joke: *It's been the oil of the future for 3 decades*. But at least 1.7 trillion barrels of oil lie beneath the Athabasca region, and as traditional oil sources dry up worldwide, the tar sands have attracted $85 billion in investment in just the past decade. The frenzy centers on Fort McMurray, a boomtown 1000 kilometers north of nowhere, Montana.

From the air, mining pits look flat, but that's only because they are so wide. The pits actually contain many cliffs and mesas, which mark the boundary of where huge mobile diggers (many the size of three-story houses) chew back the edge of the earth. Dump trucks putter up the kilometers of dirt roads that swirl up and out of the deepest ravines. The land looks like different colors, but most are variations of black and gray, a bruise on the formerly green boreal forest. Every day each pit stretches wider and reaches deeper.

**Before and after.** Oil mines chew up vast tracts of land in northern Alberta (*top*). By law, companies must restore these lands to "nature" (*bottom*).

At about 60 meters deep, miners first encounter the bitumen, grains of sand jacketed by oil and water. To shake the oil free, mines spray bitumen with scalding water, creating what looks like Marmite, except stickier. Through various processes, companies skim out 90% of the crude, which they ship to refineries. The leftover slurry of sand, water, oil, and some toxins, such as naphthenic acids, fills tailings ponds.

By Canadian law, oil companies must convert those ponds back to "nature." But before they can do so, the sand, oil, and water must settle into distinct layers in the pond, so engineers can pump the liquid out and build on a solid surface. When oil mining started in the 1960s, companies estimated that it would take ponds a few years to settle. It actually takes decades. And even after pumping off the water and oil, the tailings resemble quicksand, and you can't build an ecosystem on a shifting foundation, says Dave Sego, principal investigator at the Oil Sands Tailings Research Facility, an industry-funded group at the University of Alberta, Edmonton.

Sego says tailings have to be stable enough so that "grandma can walk on it," assuming she'd want to. "Dewatering" the ponds to stabilize them is straightforward in theory, and a few huge and strangely tropical white beaches of partly stabilized sand can be found on some

mines. But with current technologies, this process remains slow and expensive. Nor have companies met stated goals for reducing the volume of waste fluid they produce, notes the government of Alberta's Energy Resources Conservation Board.

Sego's facility is giving oil companies options, and Sego says scientists have seen success with new water-sand separation techniques, some mechanical, like centrifuges, some chemical, like gypsum and other absorbents. Other techniques take advantage of the winters in Fort McMurray, which has an average temperature of about –20°C in January. The mines produce oil 24 hours per day regardless of the conditions, but the seasonal freezing and thawing of water helps squeeze waste out. In addition, engineers at Suncor announced in October a promising new method using "flocculants" to drag particles out of liquid suspension. These technologies could also shorten recovery times for existing tailings ponds. But at least for the techniques at his facility, Sego cautions, "I wouldn't say that any one is field-ready. There are tremendous engineering challenges because of the sheer volumes of material."

The Alberta government estimates that, even with water-recycling and -reduction programs, the largest mines (Syncrude and Suncor, at 350,000 and 300,000 barrels of oil each day, respectively) will have a trillion liters of tailings to deal with by 2020.

In the next few decades, the industry will likely shift more toward "in situ" recovery techniques, which mix bitumen and steam deep underground and produce no tailings. Companies already use in situ technology in Athabasca, but most on a very small scale.

Only one reclamation project for tailings ponds is near completion—at the oldest and most notorious pond, Suncor's Tar Island, which sits next to the Athabasca River, a major water source. To get a better look at Tar Island, I chartered a tour down the river from Andrew Boucher on a drizzly August day. Boucher helped build the first mine in the Athabasca region in the 1960s, when he was 18, and then stayed to work at Syncrude and Suncor for almost 40 years. In the winters, he drove a dogsled down the river to work; in the summer, a motorboat.

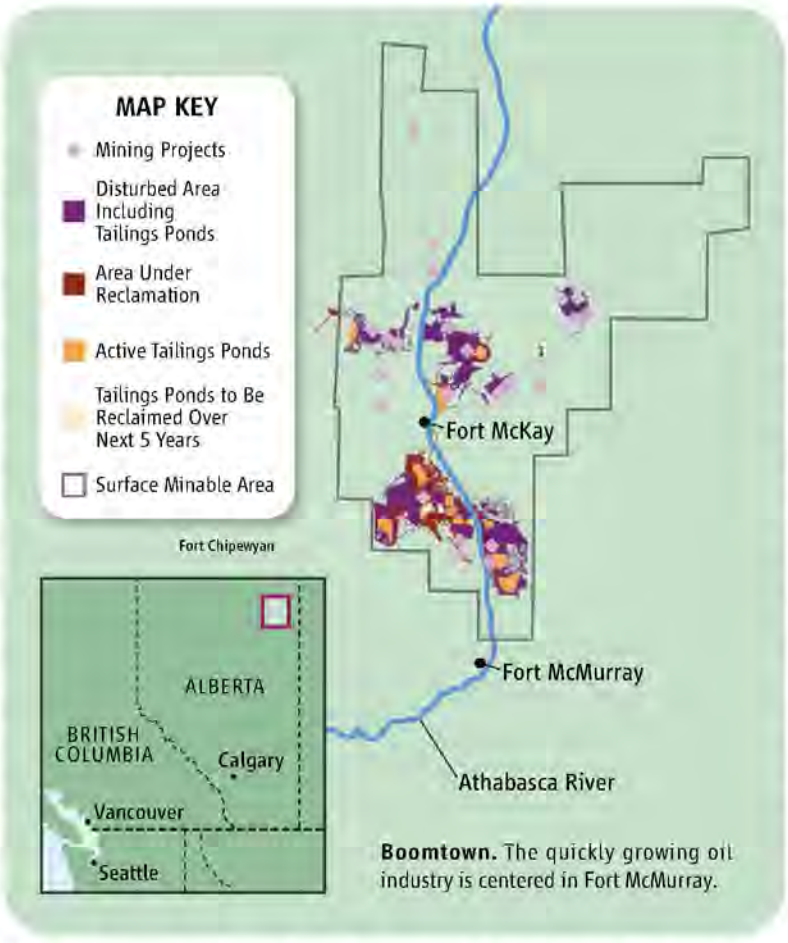


**Boomtown.** The quickly growing oil industry is centered in Fort McMurray.

On our serpentine trip down the river, Boucher pointed out his uncles' cabins for trapping critters, now the property of the mines. Along the way, he identified intake pipes that draw water from the river and explained what various towers and buildings do. When asked the purpose of one alarming tower, crowned by a perpetually roaring fire, he smirked, "To keep reporters out."

After an hour, we arrived at the Tar Island dike, which separates the pond from the river. The pond opened in the 1960s and started leaking through the dike immediately. Earthen dams like the one that surrounds the pond are designed to leak a little: They're made of permeable sand and earth, materials that filter out harmful chemicals as water trickles through. Unfortunately, Tar Island leaked excessively. As a pool of sludgy water formed underground, Suncor scrambled to stanch the leak with more earth. A dike that started a dozen meters tall stands a steep 90 m tall today and stretches 3 km. Despite the continued leakage, Suncor added tailings to the pond until 1997. That year, the company said it hoped to reclaim Tar Island pond by 2002. Engineers now hope they can dewater and stabilize the surface by 2010. After it dewaters the land, Suncor will dump 50 cm or so of soil stripped from a different mine site over the sand, then plant crops like barley to firm up the soil. Soon after come saplings and trees. With luck, Tar Island will become the first reclaimed tailings pond in a few short decades.

Unfortunately, the dike and the soil beneath the old pond have absorbed so much tailings water that they will continue to leak for years, reclaimed or not. And Tar Island is far from the biggest pond and dike system to reclaim. Until the Three Gorges Dam opened in China, one earthen dike on Syncrude land was the largest dam in the world, 18 km around and made of 540 million $m^3$ of material. Hoover Dam is 2.6 million $m^3$.

The reclamation of ponds took on new urgency in February, when new government regulations ordered companies to reduce tailings volume by 50% and dewater existing ponds faster, so that they are ready for planting within 5 years of the last tailings dump. Leaving ponds open for too long threatens wildlife, especially migratory birds, which find the warm tailings ponds attractive during winter. When birds land in ponds, oil either weighs them down and they cannot take off, or it breaks down the insulation in their feathers and they freeze.

One impetus for the regulations was an incident in May 2008, when 1600 ducks landed in a Syncrude pond and drowned. Syncrude said a late spring storm prevented it from installing deterrents—such as scarecrows, nicknamed "bitu-men," that float on oil barrels and wear hazard-orange ponchos, and propane cannons, which fire all day like a Civil War battlefield. It's not clear how well either device works, however. In a May 2003 study, ecologists counted 107 groups of birds landing in tiny experimental tailings ponds in 100 hours, one-quarter of the groups that flew by, despite cannons and bitu-men.

### Eco-alchemy

Environmental law says that tar sands companies must restore tailings ponds and pit mines back to "equivalent land capability," but that phrase is contentious. Ecologists and environmentalists would prefer that every square meter of disturbed boreal forest or wetland be restored to its original state. In

SOURCE: THE OIL SANDS DEVELOPERS GROUP

practice, companies can perform a sort of eco-alchemy: Pit mines can be converted to either new land, like a forest, or a lake, while tailings ponds can become either a lake or new land. Each transformation has its own challenges and controversies.

In creating new land, Alberta allows companies to plant forests that, although similar to existing forests, are geared toward logging and timber. "The forests will be different from what was there," acknowledges Sego. But he says the government wants to ensure economic development when mines leave. Planned forests struggle with one measure of recovery: diversity of native species. A 1998 report, jointly produced by Alberta Environmental Service, a government agency, and oil companies, remains the most comprehensive study of attempts to reclaim tailings waste. The report examined mature test plots of forest (14 to 24 years old) and compared them with untouched natural forest. "In general," it stated, "there was little similarity in terms of species composition between any of the reclaimed areas with the natural stands." In some cases, the sites showed just 10% species overlap.

Thompson acknowledges that the industry has made some mistakes and had some growing pains, partly because early reclamation efforts planted trees on top of hills of stripped soil, instead of contouring them first to mimic the land's natural shape. But he says companies can move massive amounts of soil nowadays (a single dump truck holds 400 tons of material), and once soil is in place, he argues that sites revert to nature with little further management. He dismissed the 1998 report as "10 years out of date." Recent company test sites have grown forests and wetlands just as diverse as any natural site, he says.

Some ecologists agree with Thompson, to a degree. Bill Freedman of Dalhousie University in Halifax, Canada, studies the environmental impact of mines. He says that oil sands ponds are vast but less toxic than ponds at metal or coal mines. And he thinks reclaimed areas can succeed: "They're not pristine ecosystems, but they can provide a habitat, an acceptable degree of restoration."

### The end-pit lakes

Most reclamation studies have focused on new land ecosystems, but oil companies plan to start using a cheaper solution soon: creating new lakes by putting a freshwater cap over tailings ponds and other mine sites. The lake is designed to prevent mixing between toxic materials below and freshwater on top, a stratification known as meromixis. Some two dozen lakes are slated to appear in the next 50 years.

In theory, meromixis is stable because mining water is brackish and dense. If it starts at the bottom, it's apt to stay there, industry experts say. Both natural bodies of water and end-pit lakes at other mines have maintained such layers for years. But some groups question whether the planned lakes in Alberta, which would be shallow and contain chemicals that naturally rise to the surface, will stay stratified. The Cumulative Environmental Management Association (CEMA), a nonprofit organization with representatives from industry, the government, and environmental groups located in Fort McMurray, said in one report that "meromixis will be a temporary solution." A report by CEMA was also ambivalent about how well end-pit lakes could provide habitats for wildlife. Creatures low on the food chain (e.g., plankton and benthos) have trouble establishing themselves in the short term, it said, and "fish stocked in Syncrude's experimental ponds were found to survive but showed sign of chronic stress such as disease and morphological deformities." Many problems can be traced to toxins that seep from tailings sand, especially naphthenic acids—a heterogeneous mix of light and heavy cyclic hydrocarbons.

**Home range.** An exhausted pit mine was ecologically reclaimed by one company and converted into a reserve, complete with bison.

CREDIT: SYNCRUDE CANADA LTD.

Oil companies, says Thompson, are confident that bacteria can break down naphthenic acids at a rate higher than the acids leech out. There is some evidence for this. Phillip Fedorak, a microbiologist at the University of Alberta, Edmonton, says that bacteria degrade naphthenic acids used in commercial applications such as wood preservation "very nicely." Still, heavier molecules in tailings ponds "are not degraded very easily," he adds. "There's been geological amounts of time [for bacteria to work], and they leave these recalcitrant compounds behind." Fedorak's work has shown that ozone bubbled through tailings water can break down recalcitrant bits, but this process is not ready for commercial application. He's not aware of any other process that is, either.

The first experimental end-pit lake will open in 2012—and it happens to be the body of water across from Wood Bison Viewpoint. To be sure, this nascent lake was not a full-fledged tailings pond: It merely contains tailings pumped in from other sites. But the industry is treating it as a full-scale rehearsal for future end-pit lakes to prove the process works.

I had hiked down from the bison park to investigate the soon-to-be-natural lake. At the south end, ducks floated practically in the shade of bitu-men. A huge black pipe was dumping water nearby. Halfway down the lake, a black dirt beach appeared, and the water looked pale green. An immensely long black tube bisected the lake at this point, apparently to catch oil on the surface that was drifting toward the viewpoint. It was anchored, but a meter-wide gap between the tube and shore let oil slither by.

Another kilometer down, at the north tip of the lake, a second black pipe disgorged water. Nearby, the water-oil mixture at the surface was so different from normal water that part of the green hilltop behind it didn't reflect in the lake, like a vampire.

Minutes later, the white Syncrude pickup slowed down and busted me. After negotiations with headquarters—I was harmless, I guess—the security guard drove me back toward Wood Bison Viewpoint. Near the end of the short ride, an all-points bulletin went out for another person snooping around the mine somewhere. The guard took off down Highway 63 before I could even open the door of my rental car parked nearby. There are two worlds along 63, and she'd left me right where I'd started, on the cusp between them—between the reclaimed forest, the hoped-for future, and the oily, unfinished lake, still off-limits to the public, still waiting to be converted.

**–SAM KEAN**

**Light my fire.** Neandertals at Abric Romaní left nearly 200 hearths (*inset*).

ARCHAEOLOGY

# Better Homes and Hearths, Neandertal-Style

**Detailed studies of Neandertal hearths and living quarters suggest that, like modern humans, our extinct cousins had the knack for organization**

**TARRAGONA AND CAPELLADES, SPAIN**—To a passerby, the excited chatter of 100 researchers visiting the Abric Romaní rock shelter must have sounded more like a school trip than a serious scientific expedition. Grown men and women bounded like children up and down the metal steps leading into this huge cliff-side cavern overlooking the village of Capellades, 50 kilometers west of Barcelona. Snapping photos, they darted over wooden planks between blackened hearths looking so fresh that fires might have burned there just yesterday. The hearths had indeed been freshly excavated by archaeologists just 2 weeks before. But the hearthmakers were Neandertals, who visited the cave about 50,000 years ago.

Abric Romaní is a special site: Excavations here have uncovered 14 layers of Neandertal occupation over 20,000 years. Rapid sediment accumulation has led to "near-Pompeii-like" preservation of hearths, stone tools, and other artifacts, permitting "exemplary and unusually high-resolution" research into Neandertal lifeways, says archaeologist Lawrence Guy Straus of the University of New Mexico in Albuquerque.

Last month, Neandertal specialists gathered here to discuss such high-resolution research at a meeting marking the 100th anniversary of Abric Romaní's discovery.* They explored how Neandertals lived and behaved based on detailed studies at individual sites. Although many aspects of Neandertal behavior were discussed, such as their use of stone tools and what they ate—including growing evidence that they sometimes ate each other (see sidebar, p. 1057)—the meeting turned repeatedly to how Neandertals used fire and organized their space as the most fine-grained indicators of what they did every day. Although some archaeologists have argued that Neandertals were less-sophisticated than modern humans in their use of space, that view found little sympathy in Tarragona. "The papers addressing this issue concluded that Neandertal behaviors differed little from those of modern humans," says anthropologist Donald Henry of the University of Tulsa in Oklahoma.

Some researchers see the latest research as a turning point in Neandertal studies. "We are seeing a fundamental change in how archaeologists are approaching hearths," says archaeologist Harold Dibble of the University of Pennsylvania. "Before the 1980s or 1990s, many were simply content to note whether or not there were hearths, but there was no other real interest in them. Now there are many more questions looming about Neandertal use of fire," such as whether it was used for cooking, warmth, light, or other functions; and whether Neandertals, like modern humans, socialized around the hearth.

Many conferences compare the extinct Neandertals and modern humans, but at this meeting modern humans were not much in evidence, except in the audience and on the podium. "We have tended to use the Neandertals as foils," Straus says. "The Neandertals are now coming into their own."

## Around the hearth

In his talk, Dibble pointed out that there were many possible reasons Neandertals might have made fires: to provide warmth and light, roast meat and vegetables, extract grease from bones, protect from predators, heat-treat tools, repel insects, process animal hides, smoke and dry food, and even get rid of accumulated garbage. Although distinguishing among these uses is difficult, archaeologists blessed with well-preserved sites have been trying to generate clues.

At Abric Romaní, a team led by Eudald Carbonell of Rovira i Virgili University

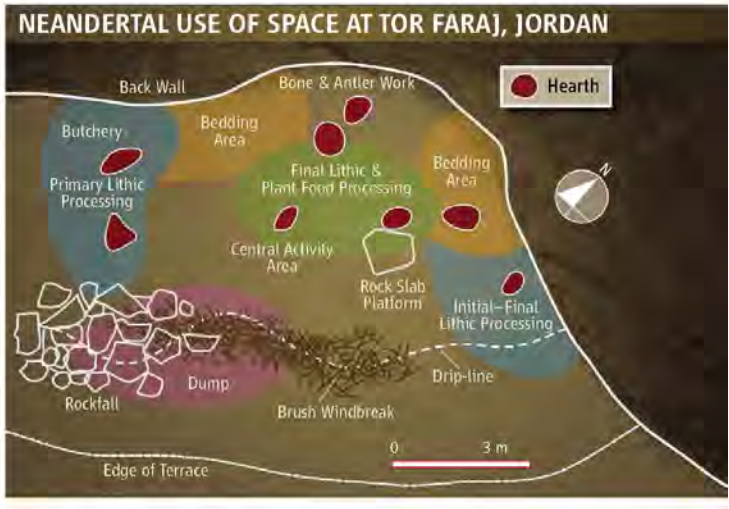


**Getting organized.** Like modern humans, Neandertals divided their living quarters into different task areas, as seen in this cave in Jordan.

CREDITS (TOP TO BOTTOM): GERARD CAMPENY/IPHES (2); SOURCE: DONALD HENRY/UNIVERSITY OF TULSA

*The Neandertal Home: Spatial and Social Behaviors, Tarragona and Capellades, Spain, 6–9 October 2009.

(RiV) in Tarragona has found nearly 200 beautifully preserved hearths since 1983. The hearths are easily identifiable as black, irregularly shaped but sharply outlined ovals on the rock-shelter floor. According to a talk by archaeologist Josep Vallverdú of RiV, the team has identified at least half a dozen hearth types. These include small, flat structures close to the rock shelter wall—which the team interprets as sources of light and warmth near sleeping areas—and larger, more centrally located structures dense with animal bones and lithics, which could represent activity centers for cooking and tool use. Statistical analysis of hearths in six consecutive archaeological levels showed that although their spatial arrangement varied somewhat over thousands of years, they clustered around a constant center point. These findings provide high-resolution evidence that "Neandertal groups established and organized their living space around hearths over and over, in regular fashion," Straus says.

Another high-resolution effort to figure out how Neandertals used fire puts hearths under the microscope both literally and figuratively. At two recently excavated Neandertal sites in southwest France, Roc de Marsal and Pech de l'Azé IV, two archaeologists collaborating with Dibble, Paul Goldberg and Francesco Berna of Boston University, have been thin-sectioning blocks of material taken from well-preserved hearths and using several techniques, including infrared spectroscopy, thermoluminescence, and x-ray diffraction, to determine the composition of the burnt material and the temperatures to which it was heated. At the microscopic level, Goldberg and Berna identified fragments of bone, flint, plant remains, wood, and cave sediments. The work is still in its early days, but some patterns are emerging. In both caves, the thin sections show a significant amount of charred fat, suggesting that meat cut from bone was cooked in the fires. Although many archaeologists have assumed that Neandertals cooked their food, there has been little direct evidence.

Both caves also showed evidence that the hearths were regularly cleaned and raked out. And at Pech de l'Azé IV, some of the bone had been heated to such a high temperature that it, rather than wood, was probably used as fuel to keep the fire going, a pattern not seen at Roc de Marsal. "This kind of fine-grained work provides empirical evidence for human behavior," says Lyn Wadley, an archaeologist at the University of the Witwatersrand in Johannesburg, South Africa. "We can get a huge amount of information" by capturing such "moments in time."

Nevertheless, Wadley adds, echoing a caution raised at the meeting by archaeologist Manuel Vaquero of RiV, it is still unclear how well such "moments in time" capture the big picture of Neandertal behavior over longer periods. In a much-discussed talk about Abric Romaní's stone tools, Vaquero pointed out that too narrow a focus can be misleading. For example, he reassembled stone-tool flakes that had been struck from larger stones to recreate the original cores and was able to establish the detailed tool-making techniques used around hearths in individual occupation levels. But only when he looked at the pattern over several occupation layers did it become clear that the earliest occupants had to search many kilometers away for chert and other stone-tool raw materials, whereas later occupants were able to use stones discarded by their predecessors, thus turning the site into a source of raw materials.

**Modern is as modern does?**

Although modern humans definitely played second fiddle at the meeting, a talk by Henry brought them back to mind. He concluded that when it came to the complex use of space, moderns had little on the Neandertals. Henry and his colleagues have been working at the Tor Faraj rock shelter in Jordan, which harbors typical Neandertal tools but no human fossils and is dated to between about 69,000 and 49,000 years ago. Thanks again to excellent preservation, the team was able to reconstruct activities on two superimposed "living floors."

From the spatial arrangement of lithics and other artifacts found on the floors, Henry and his co-workers conclude that living areas were well-differentiated into dedicated spaces for butchering animals, making stone tools, working with bone and antler, sleeping, and dumping rubbish. For example, fossil plant expert Arlene Rosen of University College London showed that although the remains of date palms and date seed husks clustered around Tor Faraj's central hearths, where they were probably prepared and eaten, the remains of grasses were restricted to areas along the rock shelter wall and were likely used for bedding. Such spatial patterns mirror those found in modern human occupation sites, Henry said. Wadley agrees: "Neandertals were doing pretty much the same things that the so-called moderns were doing; … they used space in an orderly way, although probably not yet in a symbolic way."

That makes them worthy of study "for their own sake," says Dibble. Agrees Antonio Rosas, a paleoanthropologist at the National Museum of Natural Sciences in Madrid: "To be Neandertal is a distinct way of being human. By understanding Neandertals, we enlarge the meaning of humanity."

**–MICHAEL BALTER**


**Eating their own?** Cut marks on a Neandertal jaw might be signs of cannibalism.

CREDIT: ANTONIO ROSAS, PALEOANTHROPOLOGY GROUP MNCN-CSIC

## Did Neandertals Dine In?

Researchers have long debated whether the highly carnivorous Neandertals sometimes ate each other. And although some claims have not held up, in recent years new evidence for this macabre hypothesis has emerged (*Science*, 1 October 1999, p. 18). But few sites have enough complete Neandertal bones to tell for sure.

In Tarragona, paleoanthropologist Antonio Rosas of the National Museum of Natural Sciences in Madrid presented the latest evidence from the cave of El Sidrón in northwest Spain. There, his team has found 1700 Neandertal bones representing at least 11 children and adults dated to about 49,000 years ago. Many of the more complete bones, including those of the arms, legs, and skull, show cut marks, pitting, scarring, deliberate breaking of bones for marrow extraction, and other signs that the bodies were cut up in the same way that hominins butcher animals—the gold standard for signs of cannibalism.

At this point, "there is very compelling evidence for cannibalism" at Neandertal sites, says archaeologist Mary Stiner of the University of Arizona, Tucson.

Why eat each other? Teeth and bones show evidence, such as dental hypoplasia, that the El Sidrón Neandertals were stressed and possibly malnourished. But Rosas thinks there might also have been "a ritualistic side to it," although he declines to give details until his team's ongoing study is published. Until then, the El Sidrón findings are "food for thought," says Lawrence Guy Straus of the University of New Mexico in Albuquerque. **–M.B.**

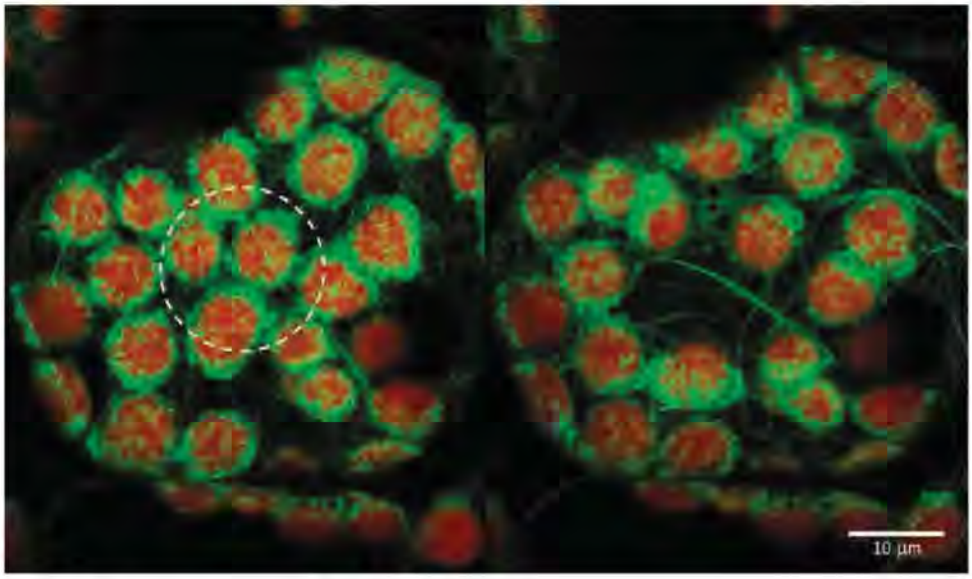


**Dodging light.** (*Left*) The chloroplast's rim of actin (green) disappears in bright light (white circle) and (*right*) reforms just on the leading edge as chloroplasts move away from light.

# Chloroplast Shuffle

For more than a century, researchers have known that chloroplasts move. But it's taken 25 years for Masamitsu Wada to figure out how these photosynthesizing organelles make their way across a cell. His labeling and imaging experiments have revealed that they slide from one place to another, never turning, twisting, or rolling. They seem to rely on the polymerization of protein filaments to pull them along, he reported at the meeting, and they can move quickly—or slowly—depending on the circumstances. The work represents "an outstanding combination of genetics and cutting-edge cell biology," says Eberhard Schäfer, a plant physiologist at the University of Freiburg, Germany.

Chloroplasts have evolved to make the most out of the available light. Photoreceptors on the plant cell surface relay light-intensity information to chloroplasts, which move toward weak light and quickly scatter in strong light that might damage them. "This response is vital to plant survival," says Christian Fankhauser of the University of Lausanne, Switzerland.

Wada, a plant physiologist at Kyushu University in Japan, typically studies chloroplast movements in fern gametophytes, the tiny sexual phase of the plant, which at first grow as a single layer of highly photoreactive cells. He uses a microscope to direct a microbeam of light to specific parts of a cell and records the result with time-lapse videos.

When he shined strong light at one end of a chloroplast, it took less than a minute for it to respond: It slid away from the light at about 1.5 micrometers per minute. When he gave another pulse of light on one side of the advancing chloroplast with another pulse of bright light, the chloroplast stopped and retreated, changing direction without reorienting itself in any way, he reported. "They don't have any head or tail," says Wada. "They can move in any direction."

To get a better handle on what propels the chloroplast, Wada and his colleagues turned to a mutant of the model plant *Arabidopsis*, whose chloroplasts don't move. They homed in on the defective gene and figured out that it codes for a protein that sits in the chloroplast membrane and has the ability to latch on to actin protein fibers. Actin is often involved in the movement of organelles. Using genetically modified *Arabidopsis* plants that produced actin-binding proteins linked to green fluorescent protein, Wada and his colleagues made actin filaments visible and traced their whereabouts.

Before the researchers turned on their strong light beam, the chloroplast was surrounded by actin filaments. But in the light, the filaments disappeared—likely depolymerizing—within 30 seconds. A minute later, they began to reappear but only on what became the leading edge of the moving chloroplast, Wada reported at the meeting and in the 4 August issue of the *Proceedings of the National Academy of Sciences*. "I think actin might pull the cell along," says Wada.

Next, Wada wants to pin down the signal that travels from the photoreceptor and causes the actin filaments to dissolve and reform. "The speed of signal transduction is very slow, so it must not simply be a diffusible, small molecule," he says. **–E.P.**

## Steak With a Side of Beta-Glucans

The quest for healthier food and better biofuels has taken one researcher deep into the plant cell wall. Plant cells are surrounded by a wall made up of molecules that are basically chains of sugars, so-called beta-glucans. Some, like cellulose, provide the scaffolding; others are gel-like, giving the cell wall some flexibility.

Grasses, including commercially important crops such as wheat, barley, sorghum, and rice, have a special beta-glucan not found in other plants, with an unusual arrangement of its atoms. Over the past 3 years, Geoff Fincher, a biochemist at the Australian Centre for Plant Functional Genomics at the University of Adelaide in Australia, and his colleagues have tracked down the genes involved in making this beta-glucan, and at the meeting he described progress in using those genes to increase the beta-glucan content of grains and other plant tissues. Those increases could translate into healthier foods by boosting fiber content. Moreover, "our ability to … manipulate beta-glucan content in plant cell walls can have a vast impact [on our ability] to fully utilize plant residue for many purposes" such as biofuels, says J. Perry Gustafson of the University of Missouri, Columbia.

The optimal amount of beta-glucan varies, says Fincher. In some instances, less is preferred. In brewing, barley grain's naturally induced enzymes are often unable to break down all the beta-glucans in malt, and the excess clogs up filtration steps. Low levels are also better for animal feed because the beta-glucans found in grasses can slow the gut's absorption of starch.

But for human health, more beta-glucan is better. Evidence suggests that this molecule, a

CREDIT: SAM-GEUN KONG

# A Question of Balance

What's a genome to do when a molecular hiccup causes it to swell to twice its normal size? Somehow it has to get back to a reasonably sized, smoothly functioning genome, often by shedding genes. Once thought to be quite rare except in plants, whole-genome duplications—in which every chromosome winds up with an extra copy—are showing up in many animal lineages as well. These DNA windfalls pave the way for new proteins, traits, and species, depending on the patterns of gene loss and change that follow.

James Birchler of the University of Missouri, Columbia, has proposed that genes that code for proteins that are part of complexes are most likely to survive purging. At the meeting, he discussed his latest experiments testing this idea, the so-called gene balance hypothesis. Increasing evidence from this and other meetings suggests that Birchler and colleagues may be right, says Yves Van de Peer, an evolutionary biologist at Ghent University in Gent, Belgium, who recently organized a conference on genome duplications. "So many people gave talks where they found support for the hypothesis," he says. "It's definitely catching on."

According to the gene-balance hypothesis, proteins destined to be part of a macromolecular complex must be produced in the proper proportion relative to their partners in the complex. Those proportions are maintained in whole-genome duplications, but if the genes for some of those proteins were subsequently lost, the balance would be disrupted, perhaps leading to lower fitness. Thus those genes tend to stay put, while one of the duplicate genes for a protein that works alone can disappear without consequence.

Following that same logic, similar disruptions might arise when a piece of chromosome with a gene whose protein is part of a complex gets duplicated. The hypothesis predicts that those extra genes would be purged from the genome to restore the balance. Because transcription factors tend to be part of complexes, they would likely be retained in whole-genome duplications and purged in smaller duplications.

In a series of experiments in maize, Birchler tracked the effect on protein production of adding extra chromosome arms. He started with maize that has one set of chromosomes instead of the usual two. He modified some of these haploid plants by adding a piece of a chromosome back to the genome. He also added an extra piece of chromosome to a normal diploid plant, making it trisomic, and took away a piece of chromosome from a diploid plant. He monitored the plants' growth and reproduction and took tissue samples to determine the amounts of individual proteins in the plant cells. He repeated the experiments, manipulating four different chromosome arms.

He found that the extra arm in the haploid plants caused most of the proteins to decrease, some by as much as 50%; trisomics had reductions down to two-thirds the protein quantities of diploids. "By looking at these different ploidy levels and gene expression, we can document [that] the level of imbalance has a respective global impact on gene expression," says Birchler. That imbalance translated into real effects: The greater the imbalance, the shorter the plants. He suspects that genes for regulatory protein subunits in the extra chromosome arms disrupt the balance of the complexes they belong to, negatively affecting gene expression.

**Out of whack.** An extra chromosome arm in maize plants (second and fourth from left) disrupts gene balance and leads to shorter plants.

Other researchers have looked at the distribution of genes in organisms with whole-genome duplications. From the three whole-genome duplications in *Arabidopsis*, 59% of the duplicates have stuck around, and they include 99% of all transcription factors and signal transducers and 92% of the developmental genes, Patrick Edger and J. Chris Pires of the University of Missouri, Columbia, wrote in the July issue of *Chromosome Research*. Researchers have observed similar trends in *Paramecium*. "That evolutionary data fits in with what we find experimentally," says Birchler. **–ELIZABETH PENNISI**

CREDIT: MAYA BENAVIDES AND FANGPU HAN

component of dietary fiber, helps prevent colorectal cancer, high cholesterol, heart disease, obesity, and diabetes. It passes intact through the small intestine and is fermented into short-chain fatty acids in the colon. Those fatty acids seem to improve the ability of the cells called colonocytes lining the gut to repair damaged DNA.

To increase the beta-glucan content in grains, Fincher and his colleagues put into barley a piece of oat regulatory DNA, a standard genetic engineering tool, that turns on a gene for making the beta-glucan only in the developing grain. "It worked much better than we expected," says Fincher. Beta-glucan levels in the grain increased 80%, and total dietary fiber climbed by more than 50%, Fincher reported. Fincher's ultimate goal is to enhance the beta-glucan content of wheat, which is low compared with barley.

Increasing beta-glucan content could also enhance the value of the currently unusable parts of corn and wheat for biofuels. When Fincher and his colleagues added a different stretch of regulatory DNA, one that turned on genes in vegetative tissues, it caused a sevenfold increase in beta-glucan in young barley leaves. "I was blown away that he could manipulate a gene and get seven and eight times [the amount]," says Gustafson. Wheat plants, for example, don't look promising for biofuels, but the equation could change if beta-glucan content could be increased enough, he adds. That's because this beta-glucan is more easily fermented by the industrial enzymes used than are other cell-wall components.

The process needs some refining, however: The beta-glucans gummed up the leaf vasculature, stopping nutrient flow and causing the leaf to die in some cases. So Fincher and his colleagues are evaluating other regulatory DNA. **–E.P.**

# LETTERS

*edited by Jennifer Sills*

## Getting His Goat

IN HIS BOOK REVIEW "TWO DOORS and a goat" (9 October, p. 231), the answer D. O. Granberg offers to the Monty Hall problem is incorrect. He assumes that the contestant should try to win the car. In reality, a car pollutes the environment and adds nothing to the car the contestant already owns. In contrast, a goat replaces noisy lawnmowers and provides milk, cheese, and (if absolutely necessary) a tasty curry.

**SIMON LEVAY**

West Hollywood, CA 90069, USA. E-mail: slevay@aol.com

## Cell Therapy Ahead for Parkinson's Disease

THE NEWS FOCUS STORY "FETAL CELLS AGAIN?" (C. Holden, 16 October, p. 358) indicates that fetal cell transplants for Parkinson's disease patients fell out of favor after control studies suggested that placebo effects may have accounted for positive results. However, there were no proven placebo effects in previous clinical trials. The reason that new trials are funded in Europe is that previous trials used outdated methods for cell therapy.

These outdated methods, combined with patient differences, obscured any difference in average improvement. However, some patients do show spectacular recovery in response to neuronal cell therapy. In the future, with the use of rapidly improving genetic tools and diagnostics, we may be able to identify in advance the patients who will be most responsive to cell therapy. According to available data, with improved cell therapy (very likely stem cell–derived), such patients could have a chance of significant motor and behavioral benefits for 10 to 15 years in the absence of drugs. It is true that Parkinson's disease is more complex than just a lack of dopamine, but those that use this argument to discourage physiological cell therapy miss the point: Many patients may respond better and have fewer long-term side effects in response to therapeutic dopamine neurons than they would with the available systemic drug therapy, which relies almost exclusively on dopamine pharmaceutical drugs. For these reasons, it is scientifically and medically shortsighted not to test major refinements of cell therapies for Parkinson's disease.

**OLE ISACSON**

Department of Neurology and Neuroscience, HNDC, Harvard Medical School, Boston, MA 02115, USA, and Neuroregeneration Laboratories, McLean Hospital, MRC, Belmont, MA 02478, USA. E-mail: isacson@hms.harvard.edu

## Environmental Markets: Concentrate on Criteria

IN THEIR PERSPECTIVE ("RESTORATION OF ecosystem services for environmental markets," 31 July, p. 575), M. A. Palmer and S. Filoso rightly promote rigorous science to link ecosystem functioning with the provision of ecosystem services, but they exaggerate the potential downside of market valuation in restoration outcomes. Well-defined markets delineate which services are relevant and, consequently, the biophysical processes that underlie them, not the other way around. In effect, environmental markets are indispensable compasses for restoration initiatives.

The focus should be on developing and improving valuation criteria, not on adding costly mechanisms that might discourage development. There is currently a large and growing research paradigm, informed by both economists and ecologists, that addresses how economic valuation can better approximate the complexity and nuance of ecosystems (*1*).

Ecological restoration in modern landscapes must be scientifically driven but socially based (*2*). As a matter of pragmatism, it is often better to have imperfectly functioning environmental markets, in which nature has some economic value, than to have no environmental markets, where nature possesses zero value. This fits into the broader notion of ecosystems as assets from which society derives vital services (*3*). Ecological restoration, then, is not merely a rehabilitation of biophysical processes, but an investment in natural capital.

**TONG WU[1]* AND YEON-SU KIM[2]**

[1]Ecological Restoration Institute, Northern Arizona University, Flagstaff, AZ 86011, USA. [2]School of Forestry, Northern Arizona University, Flagstaff, AZ 86011, USA.

*To whom correspondence should be addressed. E-mail: Tong.Wu@nau.edu

**References**

1. P. Dasgupta, K.-G. Mäler, Eds., *The Economics of Non-Convex Ecosystems* (Springer, New York, 2004).
2. R. J. Hobbs *et al.*, *Front. Ecol. Env.* **2**, 43 (2004).
3. G. C. Daily *et al.*, *Science* **289**, 395 (2000).

### Letters to the Editor

Letters (~300 words) discuss material published in *Science* in the previous 3 months or issues of general interest. They can be submitted through the Web (www.submit2science.org) or by regular mail (1200 New York Ave., NW, Washington, DC 20005, USA). Letters are not acknowledged upon receipt, nor are authors generally consulted before publication. Whether published in full or in part, letters are subject to editing for clarity and space.

Amazing maize
1071

Who killed the megafauna?
1072

## Environmental Markets: The Power of Regulation

IN THEIR PERSPECTIVE ("RESTORATION OF ecosystem services for environmental markets," 31 July, p. 575), M. A. Palmer and S. Filoso call for direct measurement of ecosystem processes and third-party verification. This step is a critical one for the burgeoning compensatory mitigation industry to preserve, or recover, its credibility. However, Palmer and Filoso did not mention those who actually control ecosystem markets and did not consider how more rigorous restoration quality checks could provide an economic incentive to reduce ecosystem impacts in the first place.

Ecosystem service markets are odd in that they are created and controlled by regulation. For aquatic ecosystems, for example, the Clean Water Act (CWA) and the first President Bush's administration created a cap-and-trade program for wetlands and later for streams. This produced a demand for restored ecosystems through fiat, not through an inherent consumer need for ecosystem service commodities. The U.S. Environmental Protection Agency (EPA) and the U.S. Army Corps of Engineers (USACE) determine the presence of wetlands and streams on the landscape, their condition, and any requirements for compensation when these ecosystems are affected by development. Thus, by regulating the presence of existing wetlands and streams that might be affected, these two federal agencies are responsible for creating demand for these ecosystem services. In turn, these two agencies bear responsibility for the presence of the supply of restored ecosystem services through approval and certification of specific restoration projects. If the quality and integrity of restoration are lacking in existing aquatic ecosystem service markets, the blame rests largely on the shoulders of EPA and USACE, and these are the agencies through which aquatic ecosystem restoration policy changes must occur.

We agree with Palmer and Filoso that more stringent criteria must be established for restoration as part of ecosystem markets, and we suggest that EPA and USACE quickly institute more stringent standards. But we also emphasize the economic and ecological implications of such changes. Making the success criteria of restoration more rigorous will undoubtedly increase the cost of restoration: Project engineering will initially prove more difficult and therefore more costly; financial risks will increase with greater uncertainty, causing investors to increase required rates of return; and verification of project success, whether direct or through third parties, will represent an additional expense.

The net result is an increase in mitigation costs, which will need to be recouped by charging more for mitigation credits. This will, in turn, drive up the costs of affecting aquatic ecosystems, serving as a deterrent to damaging them. That is, increased restoration quality requirements could reduce the demand for compensatory mitigation by providing incentives for avoidance. This is likely the most substantial benefit of more expensive restoration.

**ADAM RIGGSBEE[1]* AND MARTIN W. DOYLE[2]**

[1]RiverBank Ecosystems, Austin, TX 78755, USA. [2]Department of Geography, University of North Carolina, Chapel Hill, NC 27599–3220, USA.

*To whom correspondence should be addressed. E-mail: adam@riverbankecosystems.com

### Response

WE AGREE WITH WU AND KIM THAT WELL-defined markets can delineate relevant ecosystem services. However, contrary to Wu and Kim's assertion, the science underpinning aquatic ecosystem restoration is far too underdeveloped for a mere delineation of ecosystem service in a market context to serve as an adequate "compass for restoration initiatives." An ever-increasing number of peer-reviewed studies show that the effectiveness of aquatic restoration projects is falling short of expectations (*1*–*3*). This is particularly true for projects that attempt to create ecosystems or restore damaged ecosystems at sites that are inappropriate (e.g., lack needed hydrological linkages) or at sites vulnerable to impacts (e.g., downstream of a polluted tributary) (*4*, *5*).

To ensure sound investments in natural capital—which we whole-heartedly support—markets should provide incentives for conservation of natural resources. If the only alternative is restoration, then two steps are required. First, we must invest in science and engineering research aimed at improving methods to restore well-functioning aquatic ecosystems. Second, we should extend this research to include the development of cost-effective assessment metrics that dependably represent the ecosystem functions that support a service or suite of services (*6*–*9*).

Wu and Kim asserted that we exaggerated the potential downside of environmental markets. The focus of our Perspective was on the incomplete nature of ecological science needed to inform markets. We did not delve into the economic complexities associated with ecosystem service markets. However, even to us as ecologists it is obvious that the environmental markets are quite different from routine commodity markets that should be self-governing. Typically, the product bought or traded is a permit or an allowance to affect the environment—not an ecosystem service. The permit to affect the environment is the buyer's motivation for entering the market. Profit is the seller's motivation, and it is to his or her advantage to produce a (restoration) product at the lowest possible cost. If the product quality (restoration project outcome) is not easily assessed or if it is not properly evaluated by a regulatory entity, it may not matter to the buyer (*10*). Quality uncertainty is well known to influence markets.

Riggsbee and Doyle astutely point out that it is the regulator and those establishing the rules of the market that are in the position to evaluate quality. If the regulator does not ensure that the ecosystem services being sold or traded are actually delivered, then the market system will result in further environmental degradation. Furthermore, the potential for political influence on regulatory decisions is great. Regulators are under enormous pressures from multiple sources. Thus, the need for an independent entity that does not answer to elected officials and does not stand to benefit financially is required to complete evaluations and monitor trades.

**MARGARET A. PALMER* AND SOLANGE FILOSO**

Chesapeake Biological Laboratory, Center for Environmental Science, University of Maryland, Solomons, MD 20688, USA.

*To whom correspondence should be addressed. E-mail: mpalmer@umd.edu

#### References

1. J. M. R. Benayas, A. C. Newton, A. Diaz, J. M. Bullock, *Science* **235**, 1121 (2009).
2. M. A. Palmer, H. L. Menninger, E. S. Bernhardt, *Freshwat. Biol.* **55**, 1 (2010).
3. K. C. Reiss, E. Hernandez, M. T. Brown. *Wetlands* **29**, 907 (2009).
4. J. B. Zedler, *Trends Ecol. Evol.* **15**, 402 (2000).
5. M. A. Palmer, *Est. Coasts* **32**, 1 (2009).
6. G. C. Daily *et al.*, *Front. Ecol. Environ.* **7**, 21 (2009).
7. S. M. Hoeltje, C. A. Cole, *Env. Manage.* **43**, 597 (2009).
8. L. A. Wainger, J. W. Boyd, in *Ecosystem-Based*

*Management for the Oceans*, K. McLeod, H. Leslie, Eds. (Island Press, Washington, DC, 2009), chap. 6.
9. S. R. Carpenter *et al.*, *Proc. Natl. Acad. Sci. U.S.A.* **106**, 1305 (2009).
10. D. King, *Env. Law Rep.* **32**, 11317 (2002).

## Training Scientists to Manage

THE NEWS FOCUS STORY "RESHUFFLING GRADuate training" (J. Mervis, 31 July, p. 528) details Roald Hoffmann's proposal to improve the U.S. science system by making students more independent and empowered through an increase in government fellowships granted directly to students. Responses to this story included suggestions to increase funding for fellowships ("Increase grants, too," M. J. Castellano and K. E. Mueller, Letters, 18 September, p. 1498) and to provide more stable funding for students ("Stable funding is key," R. J. Butera, Letters, 18 September, p. 1499).

These suggestions are all related to the theme of financially supporting and maintaining the most important resource to modern scientific research: graduate students. However, although academic culture recognizes the importance of graduate students, it currently does almost nothing to train current and future principal investigators (PIs) to effectively manage this resource. Few Ph.D.s have substantial hands-on experience managing others before they land a faculty position, and even fewer have any formal training in management. Faculty are left to learn this skill on the job at the expense of productivity and the well-being of the people they are managing. Furthermore, there is an emphasis on student independence in this discussion, which is natural; independence is an essential quality in a career researcher. The unfortunate implication is that ideal students are independent from the start. In fact, independence is a skill that can be taught and nurtured, just like the other skills that are explicitly taught in graduate school.

To improve the efficiency of the science industry, I suggest improving the management of its most important resource. Unproductive students are a consequence of student inexperience and poor advising. Better management of students can be achieved through a range of mechanisms that involve both faculty and students (such as regular mutual evaluations and human resources training for current and future PIs). Such efforts may cost time initially, but will certainly pay off in the long run.

**MICHAEL TOWN**

Laboratoire de Glaciologie et Géophysique de l'Environnement/CNRS, St. Martin d'Hères, 38402, France. E-mail: town@lgge.obs.ujf-grenoble.fr

### CORRECTIONS AND CLARIFICATIONS

**News Focus:** "Looking for a target on every tumor" by J. Kaiser (9 October, p. 218). Lung cancer kills 160,000 Americans a year, not 16,000.

**Reports:** "Grueneberg ganglion cells mediate alarm pheromone detection in mice" by J. Brechbühl *et al.* (22 August 2008, p. 1092). The next-to-last sentence of the text read "The presence of a GG has been identified in all mammalian species looked at so far, including humans (*15*, *30*)." Instead, it should read "The presence of a GG has been identified in all mammalian orders looked at so far, including human embryos (*15*, *30*)."

BEHAVIOR

# Selfless Memes

**Johan J. Bolhuis**

**The Age of Empathy**
Nature's Lessons for a Kinder Society
***by Frans de Waal***
Harmony, New York, 2009. 304 pp. $25.99, £19.99. ISBN 9780307407764.

This year we celebrate the bicentennial of Charles Darwin's birth and the sesquicentennial of the publication of his magnum opus, *On the Origin of Species*. It was in a later work, *The Descent of Man* (*1*), that Darwin explicitly addressed the evolution of the human mind. He essentially argued for continuity of mind between humans and other animals. At the same time, he suggested that there is a kind of evolutionary hierarchy in which there is a greater cognitive gap between fishes and apes than between apes and man. It is only fitting that Frans de Waal, a professor of primatology at Emory University, publishes his latest book in the Darwin year, as he clearly has taken the master's lessons to heart.

As he has done in earlier books, de Waal gives a lively and colorful account of the behavior of our closest living relatives, the great apes. He also reports the exploits of other species, including his pet cat and, indeed, himself. *The Age of Empathy* is not a dry scholarly monograph but an appealing mixture of scientific findings, anecdotes, and his personal views of human behavior. Where his previous books focused on the behavioral similarities between apes and humans, here de Waal wants to apply the lessons learned from his scientific work (and that of others) to the way modern society should be structured. This is an admirable effort, and that's why it is such a shame that, ultimately, his arguments are flawed.

De Waal is quite right that the social Darwinists were badly mistaken when they sought to derive the essence of human nature from the theory of evolution. His critique, however, flogs a horse that has ceased to be for quite a while. I suspect most sensible people would agree that the supposed selfishness of our genes cannot be translated to human behavior. But, curiously, de Waal falls into the same trap when he attempts to derive some kind of moral code from the ways other animals behave. De Waal has recently revealed himself to be a fan of the great Scottish philosopher David Hume (*2*). Nonetheless, he seems to ignore Hume's famous contention that moral principles cannot be derived from nature—a type of reasoning known as the naturalistic fallacy. This is puzzling, because in his chapter "The Other Darwinism" de Waal acknowledges the naturalistic fallacy and concludes "[a]ll that nature can offer is information and inspiration, not prescription." Nevertheless, in the book he argues that lessons can be learned from nature as to how humans should conduct themselves. De Waal falls foul of another fallacy when he assumes that evolution can explain human behavior, when in fact it can't (*3*). To make matters worse, he espouses a particular, rather limited view of evolution, where common descent is all-important. Consequently, he focuses on apes (and the occasional monkey) in his quest for cognitive similarities with our own species.

**Trusting one another.** A monkey at a zoo cleaning a hippopotamus's mouth.

CREDIT: FRANS DE WAAL/FROM THE AGE OF EMPATHY

Frequently endowing animals with human feelings and thoughts, de Waal seems to enjoy anthropomorphizing. Although this may seem unscientific, throughout the book the author likes to highlight unconventional ways of studying animals. At one stage he states that pioneering Russian primatologist Nadia Kohts, who had studied one young, captive chimpanzee intensively, "looked into the ape's heart and was impressed by what she saw." Just as Konrad Lorenz used to do half a century ago, de Waal likes to dismiss his critics as "behaviorists," even when they clearly aren't. This is odd, as anthropomorphism has been criticized not only by American behaviorists but just as much by European ethologists, not in the least by de Waal's compatriot Niko Tinbergen, with Lorenz one of the founding fathers of ethology.

To be fair, de Waal does not base his arguments solely on anecdotes. He also discusses experimental studies of animal cognition, including his own. It is unfortunate, however, that the reader usually gets to hear only one side of the arguments. For instance, when the author writes about alleged "consolation" in chimpanzees or "inequity aversion" in capuchin monkeys, he does not discuss evidence from other sources (*4*, *5*) that shows the story is not quite as straightforward as he presents it.

*The Age of Empathy* is essentially a moral pamphlet—and a very eloquent and entertaining one at that. Few would disagree with de Waal's basic message that we should strive to create a more empathic society. But it is a mistake to suggest that we can derive any kind of moral values from nature. Comparing humans with other animals can be amusing, and the author is a master at recounting anecdotes. But no matter how desirable his goal of a kinder society is, anthropomorphic anecdotes have no place in science. Evolution is about history, not about how the human mind works—let alone about how humans ought to behave. In this year of celebration of Darwin's genius, we should finally lay such mistaken views to rest.

**References**
1. C. Darwin, *The Descent of Man, and Selection in Relation to Sex* (John Murray, London, 1871).
2. F. B. M. de Waal, *Nature* **460**, 175 (2009).
3. J. J. Bolhuis, C. D. L. Wynne, *Nature* **458**, 832 (2009).
4. S. E. Koski, E. H. M. Sterck, *Anim. Behav.* **73**, 133 (2007).
5. C. D. L. Wynne, *Nature* **428**, 140 (2004).

10.1126/science.1181554

The reviewer is in the Behavioral Biology Group, Utrecht University, Post Office Box 80086, 3508 TB Utrecht, Netherlands. E-mail: j.j.bolhuis@uu.nl

WOMEN IN SCIENCE

# Preferences and Penalties Differ

**Raegen T. Miller**

Two groups of people should care about the underrepresentation of women in math-intensive fields: academics and everyone else. In *The Mathematics of Sex: How Biology and Society Conspire to Limit Talented Women and Girls*, Stephen J. Ceci and Wendy M. Williams provide a valuable resource for both audiences. For academics, their book may help diffuse political tension inimical to the goals of the academy.

The reviewer is at the Center for American Progress, 1333 H Street NW, Washington, DC 20005, USA. E-mail: rmiller@americanprogress.org

**The Mathematics of Sex**
How Biology and Society Conspire to Limit Talented Women and Girls

***by Stephen J. Ceci and Wendy M. Williams***

Oxford University Press, New York, 2009. 286 pp. $34.95, £22.50. ISBN 9780195389395.

Currently, the issue of underrepresentation is a political lightning rod, and scholars are virtually guaranteed to attract abundant criticism for posing and testing any hypothesis explaining gender disparities among scientists in different fields. Such criticism is not always confined to the scientific merits of its recipient's work, and junior scholars, in particular, may jeopardize their careers by pursuing research agendas speaking to the relative scarcity of women in mathematically oriented fields. An intellectual climate more conducive to self-censorship than the pursuit of knowledge seems unlikely to help explain the issue of underrepresentation, much less address it. In other words, the academy has painted itself into a corner, and it needs help getting out. In this sense, *The Mathematics of Sex* is a lifeline.

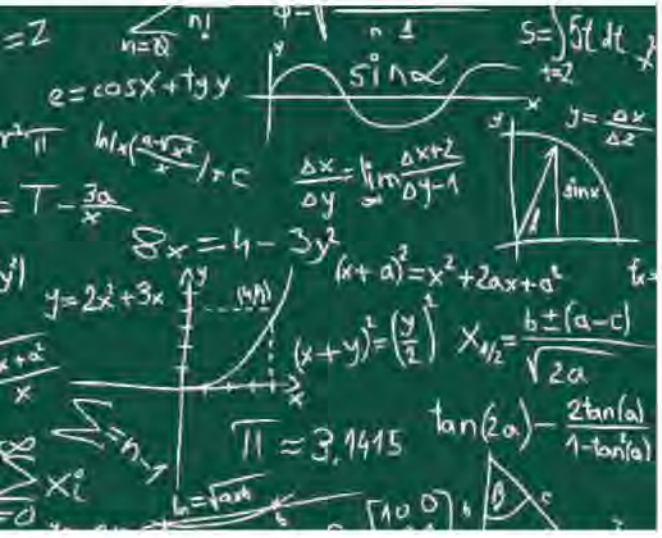


But why should everyone else care about the underrepresentation of women in fields such as mathematics, physics, chemistry, computer science, and engineering? One reason is that this gender imbalance does not exist in a vacuum. Recall, for example, that women are overrepresented in elementary-school teaching and nursing while men tend not to share equally with women the burdens of child and elder care. Especially when women are the primary breadwinners for 40% of households (*1*), failing to wonder whether cultural expectations, the education system, and workforce policies safeguard inequity, limit opportunity, and perpetuate poverty represents something like civic negligence. And it seems fair to expect that the best available explanation for women's underrepresentation in math-intensive fields, which tend to be highly remunerative, should inform urgent public policy questions (e.g., health care reform). In this sense, Ceci and Williams's account raises timely questions.

Another reason to care about the paucity of women in mathematically oriented disciplines is that many of the challenges facing us all in the 21st century are arguably math-intensive. Thus, to the extent that women do not take up careers in these fields for reasons other than their ability to grapple with science, technology, engineering, and mathematics (STEM) subjects, society may be shooting itself in the foot.

*The Mathematics of Sex* affords all concerned a chance to step back and weigh comprehensively the extant evidence pertaining to the underrepresentation of women in math-intensive fields. Ceci and Williams (developmental psychologists at Cornell University) draw on their detailed critique [previously published with colleague Susan M. Barnett (*2*)] of over 400 publications spanning at least seven fields. They explain that the research bases supporting the two dominant schools of thought—nature and nurture—are decidedly problematic.

Readers looking for support of the view that women are innately less capable than men of wrestling with STEM topics will be disappointed. Similarly, those looking to blame the underrepresentation of women in STEM careers squarely on cultural expectations enforced by parents, schools, and other institutions will be challenged to consider a more complex view. The evidence for the biological and socialization explanations is fraught with inconsistency and contradictions, and much of it does not jibe with the major inroads that women have made in math-intensive fields in recent decades. Readers will be left fairly convinced that, although more research is needed, gender per se and differences in how boys and girls are socialized should be relegated to the status of secondary factors.

Aware that few readers are comfortable with the jargon of psychology, sociology, economics, education, endocrinology, cognitive neuroscience, and genetics, the authors have taken pains to make their discussion of relevant evidence accessible to nonspecialists. Furthermore, they employ two strategies to humanize the material. First, they lace the text with dry, occasionally sardonic wit. Consider this summary of a finding that undermines the socialization position: "An observer from another planet, scanning the evidence, might think that boys must surmount negative stereotypes about their poor math ability that accrue from years of witnessing girls outperform them in math classes."

The authors' second strategy is to contextualize select scientific points with anecdotes from their experiences as parents and professors. This practice, which is anathema to research literatures, may infuriate professional scientists, but it does not affect the authors' treatment of evidence speaking to the biological or socialization arguments. The authors' reported experiences do, however, resonate with their preferred explanation of the underrepresentation of women in math-intensive professions. Namely, many mathematically capable women choose to work in non-STEM areas, and those who do enter STEM areas choose to leave them at twice the rate of men. The authors comment that because women are "far more likely to be equally talented in *both* math and verbal domains," they have more options for entering nonmath fields than do men. In addition, Ceci and Williams note that women pay a greater professional penalty for having children than do men, which makes them more susceptible to work-family conflicts.

This "choice" hypothesis is appealing. It does not lend itself to the victim narrative and paternalistic responses that poison debate, and it suggests that the remedy to women's underrepresentation in mathematically oriented fields may be largely a matter of getting the incentives right. From a public policy perspective, that is good because the focus of investigation shifts to money. This shift raises completely new questions. For instance, is there a relationship between the scarcity of women in particular STEM areas and the fact that an enormous proportion of resources, especially taxpayer dollars, in those fields is bound up in the research, development, and construction of weapon systems? We don't know, but the answer to this question may matter a great deal. In any event, *The Mathematics of Sex* provides reasons enough to turn away from the many minor distinctions that have to this point dominated inquiry into the underrepresentation of women in math-intensive careers.

**References**

1. H. Boushey, A. O'Leary, Eds., "The Shriver report: A woman's nation changes everything" (Center for American Progress, Washington, DC, 2009). www.americanprogress.org/issues/2009/10/womans_nation.html.
2. S. J. Ceci, W. M. Williams, S. M. Barnett, *Psychol. Bull.* **135**, 218 (2009).

10.1126/science.1182498

SCIENCE AND REGULATION

# New Science for Chemicals Policy

U.S. regulation of chemicals is in need of an overhaul, informed by European legislation and guided by new thinking about risk.

**Megan R. Schwarzman* and Michael P. Wilson**

Over the last century, industrial chemicals have become ubiquitous in materials, products, and manufacturing processes used throughout society. In 2006, more than 34 million metric tons of chemical substances were produced in, or imported into, the United States every day (*1*). Over the next quarter-century, global chemical production is projected to double, rapidly outpacing the rate of population growth (*2*). These substances ultimately enter Earth's environment; hundreds of chemicals are routinely detected in people and ecosystems worldwide (*3*, *4*). Long-standing public policies governing chemical design, production, and use need deep restructuring in light of new science on the health and environmental effects of anthropogenic chemicals. Such reforms are essential to safeguard ecosystem integrity, human health, and economic sustainability.

### Gaps in U.S. Chemicals Policy

The U.S. Toxic Substances Control Act (TSCA) is the primary mechanism by which the Environmental Protection Agency (EPA) is expected to oversee more than 80,000 chemicals. Just over 1000 of these substances are regulated by other major U.S. environmental statutes (e.g., the Clean Water Act) (*5*). But most health and ecological risks associated with industrial chemicals are still poorly understood because TSCA, like policies of many other nations, does not require producers to generate basic information on chemical uses, health effects, or exposures (*6*). The default assumption is that chemicals remain on the market unless or until government generates sufficient evidence to prove harm. Even then, chemicals policies worldwide have failed to grant governments sufficient means to control most chemicals, including those whose risks are well-established. It is a testament to the limitations of TSCA that, since 1976, the EPA has been able to apply the statute in regulating just five substances (*6*). Such failings have been documented for decades (*7*), yet the absence of federal action to date means that chemicals policy reform remains an urgent societal need (*8*). In response, some U.S. states are developing their own approaches to chemical regulation (*9*).

The lack of transparency and accountability in the chemicals market has hidden many human and environmental costs of chemical exposures. As a result, the market essentially "undervalues" the safety of chemicals relative to their function, price, and performance. Producers have thus had little incentive to develop safer substances according to the principles of green chemistry.

### Ecosystems and Endocrine Disruption

The lack of well-functioning chemicals policies worldwide has contributed to extensive ecosystem contamination by anthropogenic chemicals. These include hundreds of endocrine-disrupting chemicals (EDCs) whose distinct hazard traits are transforming our understanding of chemical risk. Many EDCs, such as polychlorinated biphenyls, phthalates, and bisphenol A, interfere with biological signaling mechanisms that govern development, reproduction, or immune function in humans and wildlife (*10*, *11*). EDCs have also been linked with population declines due to invertebrate imposex (masculinization or feminization); egg-shell thinning in birds and reptiles; and reduced reproductive capacity and immune function in fish, mammals, and amphibians (*12*). Many EDCs persist in the environment and biomagnify in higher trophic levels.

Improved understanding of the unique characteristics and impacts of EDCs upends many tenets of risk assessment on which chemicals policies are currently based. When exposures occur during critical periods of development, EDCs can produce lifelong, sometimes multigenerational, changes, which suggests that risk assessment should account for timing of exposure in addition to dose (*13*). Some EDCs are most potent at concentrations several orders of magnitude lower than those tested by toxicological methods commonly used for regulatory purposes. EDCs in combination can produce additive or synergistic effects (*14*) that cannot be predicted by assessing individual chemicals in isolation. Some hormone alterations caused by EDCs might appear slight in an individual but can have potentially large population-level effects (*15*) by reducing intelligence, reproductive capacity, or disease resistance.

EDCs demonstrate the contribution of chemical pollution to a set of interrelated factors, including biodiversity loss and climate change, that affect ecosystem resilience and threaten societal sustainability (*16*). Translating the emerging science of endocrine disruption into chemicals policy will require new toxicological tools and cumulative risk assessment methods (*17*). It will also demand a fundamentally new way of thinking about the risks associated with chemical exposures, one in which precaution informs the application of scientific evidence to public policy. This approach would acknowledge scientific uncertainty and the potential to deliver as-yet-unrecognized hazards to future generations (*18*). In practical terms, this will require that producers demonstrate the safety of a chemical as a condition of its use, and that governments have the means of acting on early indications of harm.

### A More Precautionary Policy: EU's REACH

The U.S. approach to chemicals policy has fallen behind global changes, led by the European Union (EU). Most important among the EU's new legislation is the 2006 regulation on the Registration, Evaluation, Authorization, and Restriction of Chemicals (REACH) (*19*). A core structural difference between REACH and TSCA is the European law's requirement that chemical manufacturers and importers, not the government, provide basic information on the identity and physical properties of ~30,000 chemicals sold in volumes of more than one metric ton per year, per producer. More comprehensive hazard data are required for a subset of ~12,000 substances whose sales exceed 10 metric tons per year.

REACH further designates some chemicals as Substances of Very High Concern (SVHCs) on the basis of properties such as environmental persistence and bioaccumulation, or because they are classified under EU law as carcinogens, mutagens, or reproductive toxicants. Authorization for continued use of these highest-risk chemicals will hinge on producers' demonstrating the safety of each intended use, or that, in the absence of suitable alternatives, the socioeconomic benefits outweigh the health and environmental risks. How these risks and benefits are calculated will determine the degree of health protection afforded by the authorization provision

Center for Occupational and Environmental Health, School of Public Health, University of California at Berkeley, Berkeley, CA 94720, USA.
*Author for correspondence. E-mail: mschwarzman@berkeley.edu

**CORE DISTINCTIONS BETWEEN CHEMICALS POLICIES OF THE UNITED STATES (TSCA) AND THE EUROPEAN UNION (REACH)**

| | TSCA | REACH |
|---|---|---|
| **Burden of proof** | Producers are not required to generate and disclose hazard data; government bears the burden of proof of harm.* | Producers must (i) supply hazard data for eligible chemicals on the basis of volume in commerce and (ii) demonstrate safety or adequate control of certain chemicals of concern. |
| **New chemicals** | Producers must submit premanufacture notification, but there is no minimum required set of hazard data. | Chemicals introduced since 1981 are subject to volume-based data requirements. |
| **Existing chemicals** | Chemicals in use before 1976 were assumed to be safe and were not subjected to the regulation. | Chemicals in use before 1981 are subject to the same volume-based data requirements as new chemicals. |
| **Prioritizing chemicals for regulatory action** | The lack of data requirements precludes effective prioritization. | Chemicals are prioritized by hazard and exposure potential; chemicals of concern are subject to use-by-use authorization. |
| **Supply chain transparency** | No requirements. | Two-way flow of hazard and exposure information is required between chemical producers and commercial users. |
| **Public access to information** | Extensive trade secret claims are allowed, including chemical names and uses. | A database of registered chemicals with clear criteria for trade secret claims will allow public access to a yet-to-be-determined body of information. |

*TSCA does give EPA authority to require a producer to test a chemical for health and environmental effects. But EPA must first establish that the substance poses "an unreasonable risk" to human health or the environment, or that there is either significant environmental release or human exposure potential. These restrictions in the statute place EPA in a logical paralysis: to require information for assessing a chemical's risk, EPA needs risk information that producers are under no obligation to provide.

of REACH. The regulation also provides a means of controlling substances not otherwise classified as hazards, such as EDCs, by creating a category of SVHCs called "substances of equivalent concern." Finally, REACH gives government the ability to regulate a substance irrespective of its toxicity, based instead on its designation as "very persistent, very bioaccumulative." REACH is thus the first comprehensive chemicals policy to codify a precautionary approach to some chemicals whose risks are not yet fully understood.

In addition to the anticipated (but not-yet-quantified) ecological benefits of reduced environmental contamination, REACH is expected to garner significant public health gains. Savings of $60 billion are predicted over 30 years due to prevention of occupational diseases alone (*20*). By improving overall transparency and accountability in the chemicals market, REACH is also expected to advance green chemistry innovation.

### International Impact

By placing conditions on access to European markets, REACH has set what may become a de facto global standard. The influx of chemical information expected under REACH, as well as the potential for countries outside Europe to become markets for toxic substances prohibited in the EU, presents other regions with an opportunity, and imperative, to retool their chemicals policies.

In the fall of 2009, the Obama Administration unveiled principles for U.S. chemicals policy reform, proposing that chemical producers be required to submit sufficient hazard, exposure, and use data for EPA to determine that chemicals meet a health-based safety standard (*21*). The principles further acknowledge the EPA's need for authority to act on priority chemicals, reducing risks they pose to sensitive subpopulations. These principles could influence development of TSCA reform. If implemented, they could improve EPA's ability to protect public health and the environment, while also providing the necessary incentive to move the chemicals market toward green chemistry, with the ultimate goal of placing the U.S. chemical industry on a more sustainable footing.

### Toward an Integrated Chemicals Policy

New chemicals policies must confront multiple challenges: a backlog of unexamined chemicals; ineffective means of phasing out chemicals of concern; and the need for methods to apply emerging science on chemical hazards, such as EDCs, to inform precautionary decision-making. New approaches should enable action in the face of scientific uncertainty and should account for interrelated factors affecting human health and ecosystems. Well-intentioned environmental regulation has been plagued by the substitution of one hazard for another, such as the shifting of chemical risks from air to water, from the general population to workers, or from energy solutions to chemical hazards. No one policy can single-handedly prevent these missteps, but the next generation of environmental decision-making can better reflect interconnectedness in nature and society.

### References and Notes


1. EPA, *2006 Inventory Update Reporting: Data Summary* (Publication 740S08001, EPA, Washington, DC, 2006); www.epa.gov/oppt/iur/pubs/2006_data_summary.pdf.
2. M. P. Wilson, M. R. Schwarzman, *Environ. Health Perspect.* **117**, 1202 (2009).
3. A. E. Nilsson, H. P. Huntington, *Arctic Pollution 2009* (Arctic Monitoring and Assessment Program, Oslo, Norway, 2009).
4. U.S. Centers for Disease Control and Prevention, *Third National Report on Human Exposure to Environmental Chemicals* (Publication 05-0570, CDC, Atlanta, GA, 2005); www.cdc.gov/exposurereport/pdf/thirdreport.pdf.
5. J. Dernbach, *Harv. Law Rev.* **21**, 1 (1997).
6. U.S. Government Accountability Office, *Chemical Regulation: Options Exist to Improve EPA's Ability to Assess Health Risks and Manage Its Chemicals Review Program* (Publication 05-458, GAO, Washington, DC, 2005), p. 18; www.gao.gov/new.items/d05458.pdf.
7. National Research Council (NRC), *Toxicology Testing: Strategies to Determine Needs and Priorities* (National Academies Press, Washington, DC, 1984).
8. GAO, *High-Risk Series: An Update* (GAO-09-271, GAO, Washington, DC, 2009); www.gao.gov/products/GAO-09-271.
9. University of Massachusetts at Lowell, *State Leadership in Formulating and Reforming Chemicals Policy: Actions Taken and Lessons Learned* (Univ. of Mass. at Lowell, Lowell, MA, 2009); www.chemicalspolicy.org/downloads/StateLeadership.pdf.
10. A. K. Hotchkiss *et al.*, *Toxicol. Sci.* **105**, 235 (2008).
11. World Health Organization, *Global Assessment of the State-of-the-Science of Endocrine Disruptors* (WHO, Geneva, 2002); www.who.int/ipcs/publications/new_issues/endocrine_disruptors/en/print.html.
12. J. G. Vos, E. Dybing, *Crit. Rev. Toxicol.* **30**, 71 (2000).
13. P. Grandjean *et al.*, *Basic Clin. Pharmacol. Toxicol.* **102**, 73 (2007).
14. D. O. Carpenter, K. Arcaro, D. C. Spink, *Environ. Health Perspect.* **110**, 25 (2002).
15. T. J. Woodruff *et al.*, *Environ. Health Perspect.* **116**, 1568 (2008).
16. J. Rockstrom *et al.*, *Nature* **461**, 472 (2009).
17. NRC, *Science and Decisions: Advancing Risk Assessment* (National Academies Press, Washington, DC, 2008).
18. D. Gee, *Environ. Health Perspect.* **114**, 152 (2006).
19. EU, Official Journal of the EU, Regulation (EC) No. 1907/2006 of the European Parliament and of the Council of 18 December 2006, concerning the Registration, Evaluation, Authorization, and Restriction of Chemicals (REACH) (EU, Brussels, 2006).
20. European Commission, Environment Directorate General, *Assessment of the Impact of the New Chemicals Policy on Occupational Health—Final Report* (Risk and Policy Analysts, Ltd., Norfolk, UK, 2003); http://ec.europa.eu/environment/chemicals/reach/background/docs/finrep_occ_health.pdf.
21. EPA, *Essential Principles for Reform of Chemicals Management Legislation* (EPA, Washington, DC, 2009); www.epa.gov/oppt/existingchemicals/pubs/principles.pdf.

22. Supported by the Berkeley Center for Environmental Public Health Tracking, CDC grant 5U19EH000097-04; the Stiefel Family Foundation; and the EU Center of Excellence, University of California at Berkeley.

10.1126/science.1177537

ENVIRONMENT

# Monitoring Earth's Critical Zone

Earth's rapidly changing near-surface environment needs systematic observation to better manage future crop production, climates, and water quality.

**Daniel deB. Richter Jr. and Megan L. Mobley**

Geologists tell us that we live in the Anthropocene, the period marked by humanity's global transformation of the environment (*1*). More than half of Earth's terrestrial surface is now plowed, pastured, fertilized, irrigated, drained, fumigated, bulldozed, compacted, eroded, reconstructed, manured, mined, logged, or converted to new uses. These activities have long-lasting effects on life-sustaining processes of the near-surface environment, recently termed Earth's "critical zone" (*2*). The full range of Anthropocene changes in Earth's critical zone is not well quantified, especially belowground (see the figure) (*3*–*6*), where observed changes justify a major expansion in monitoring to better ensure the sustainability of crop and soil productivity, and the functioning of the global atmosphere and hydrosphere (*3*).

Most existing environmental monitoring focuses on Earth's aboveground critical zone, especially the highly dynamic systems of the weather, atmospheric chemistry, wildlife populations, water quality, and river flow and flooding. Such monitoring has greatly improved environmental management (*3*), but as human demands on the environment continue to accelerate, changes in the soil, root zones, and hydro- and bio-active mantles challenge and even threaten the sustainability of land management and the wider environment (*3*, *6*–*12*). Critical zone monitoring uses a field-based approach, developed largely in the ecological and geological sciences, to study the dynamics and controls of the near-surface environment. Field plots, whole watersheds, and even river basins are the objects of studies aimed to enhance crop management, manage rising greenhouse gas emissions, and improve water quality.

To meet humanity's growing needs for food, fiber, and bioenergy, plant and soil productivity will be vastly expanded in the next few decades, with substantial effects on the belowground critical zone. Monitoring of critical zones is ongoing worldwide, but with uneven organization and scientific quality (*3*, *4*, *6*, *7*). Outstanding exceptions are found in developing nations of southern and southeast Asia (*8*), where dozens of long-term rice and wheat experiments test the sustainability of the intensively managed critical zones on which food supplies for several billion people depend. The results demonstrate sustainability in many experiments but also raise serious concerns: A number of sites have experienced serious rice-yield declines, attributed to degraded soil physical properties, soil toxicities, diminished availabilities of nutrients, and climate change (specifically, higher nighttime temperatures) (*8*). Due to their regional distribution, networking, and long-term continuity, the Asian rice experiments are an excellent model for the monitoring that needs to accompany expansions in food, fiber, and bioenergy in the coming decades.

Critical zone processes also control greenhouse-gas concentrations in the atmosphere, currently greatly exacerbated by land-use change and management. A notable example of how monitoring can quantify land-management's control over emissions of the greenhouse gases $CO_2$, methane, and nitrous oxide is found at the Kellogg Biological Station's Long-Term Ecological Research (LTER) in Michigan. Decades of data from Kellogg's permanent field plots indicate that substantial fractions of greenhouse emissions from agriculture and forestry can be mitigated by land-management strategies (*9*, *10*). This landmark study, along with monitoring networks such as U.S. Department of Agriculture's GRACEnet (*11*), will likely be instrumental in controlling agricultural greenhouse-gas emissions.

Finally, improved water quality also depends on increased understanding of the physics, chemistry, and biology of the critical zone. Especially promising is the National Science Foundation's new Critical Zone Observatory (CZO) program, which studies natural and human-affected processes that control water chemistry, from upper soil layers of first-order catchments to lower-lying aquifers and river basins. Much remains to be learned, however, as illustrated by the recent discovery that highly insoluble chemical compounds and colloids may be surprisingly mobile in belowground critical zones (*12*, *13*), specifically through preferential flow paths and macropores, the major conduits for drainage in many soils. Such pollutant transport provides strong support for expanded monitoring to quantify thresholds, lags, and resiliency of critical-zone controls over water quality (*6*).

The future of critical zone monitoring appears bright, given recent reports from the National Academies (*14*, *15*) and expansion of monitoring programs in NSF, U.S. Geological Survey, U.S. Department of Agricul-


**Critical depth.** The root systems of corn (*17*) (**left**), pine (**right**), and many other plants can often extend to more than 2 m belowground, yet most soil-monitoring studies are limited to the top 30 or at most 60 cm (*18*).

Nicholas School of the Environment, Duke University, Durham, NC 27708 drichter@duke.edu

ture, and internationally with monitoring networks such as SoilCrET (a newly organizing European network of nine CZOs) (*16*), and nearly 300 long-term soil-ecosystem experiments (*5*). Pushing these programs to their full potential requires expanded international collaboration, cooperation with educators, and financial and intellectual commitments over several human generations.

### References and Notes


1. J. Zalasiewicz *et al.*, *Geol. Soc. Am. Today* **18**, 4 (2008).
2. National Research Council, *Basic Research Opportunities in Earth Science* (National Academies Press, Washington, DC, 2001).
3. D. deB. Richter *et al.*, *Soil Sci. Soc. Am. J.* **71**, 266 (2007).
4. D. deB. Richter, D. Markewitz, *Understanding Soil Change* (Cambridge Univ. Press, Cambridge, UK, 2001).
5. http://ltse.env.duke.edu
6. H. H. Janzen, *Glob. Change Biol.* **15**, 2770 (2009).
7. G. P. Robertson, *Bioscience* **58**, 640 (2008).
8. J. K. Ladha *et al.*, Eds., *Integrated Crop and Resource Management in the Rice-Wheat System of South Asia* (International Rice Research Institute, Manila, Philippines, 2009).
9. G. P. Robertson *et al.*, *Science* **289**, 1922 (2000).
10. Kellogg Biological Station LTER, Hickory Corners, MI, 2009; http://lter.kbs.msu.edu/vignettes/global_warming.php.
11. A. J. Franzluebbers, R. F. Follett, *J. Soil Tillage Res.* **83**, 1 (2005).
12. X. Zhao *et al.*, *Geoderma* **142**, 237 (2007).
13. J. W. Fuchs *et al.*, *J. Environ. Qual.* **38**, 473 (2009).
14. National Research Council, *Observing the Weather and Climate from the Ground Up* (National Academies Press, Washington, DC, 2009).
15. National Research Council, *Restructuring Federal Climate Research to Meet the Challenges of Climate Change* (National Academies Press, Washington, DC, 2009).
16. http://eusoils.jrc.ec.europa.eu/events/Conferences/2009/Dessau.pdf
17. J. E. Weaver, F. C. Jean, J. W. Crist, Development and Activities of Roots of Crop Plants (Carnegie Institute, Washington, DC, 1922).
18. J. M. Baker *et al.*, *Agric. Ecosyst. Environ.* **118**, 1 (2007).


10.1126/science.1179117

MATERIALS SCIENCE

# The Hotter the Engine, the Better

Alloys based on molybdenum or niobium may allow the high-temperature components of jet engines to run hotter and more efficiently.

**John H. Perepezko**

Jet turbine engines have benefited from decades of development of nickel-based superalloys, which have allowed a steady increase in engine operating temperatures and led to improved performance and efficiency. However, operating temperatures are now reaching limits posed by the melting temperatures ($T_m$) of these materials. New materials, including alloys based on metals with higher melting points, such as molybdenum (Mo) and niobium (Nb) alloyed with silicon (Si), are now being seriously examined as alternatives by academic and industrial groups.

To be used in future jet engines, Nb and Mo alloys will have to match or surpass nickel (Ni) alloys in performance as well as high $T_m$. The nickel superalloys have many favorable properties beyond being able to operate at high temperatures—they have high tensile strength, they have sufficient ductility to be shaped mechanically, and they resist oxidation and fatigue. Nickel superalloy components in jet engines can reach temperatures approaching 1150°C, which is about 200°C below their $T_m$. Gas temperatures within the turbines, which define the engine operating temperature, are much higher. The parts do not melt because cooling air is forced through the single-crystal turbine blades, or airfoils (which are hollow), and they are also protected by ceramic thermal barrier coatings (*1*).

The development trend for these materials in gas-turbine engines (*2*) can best be summed up via the power produced as a function of the turbine rotor inlet temperature, the hottest part of the engine where combustion occurs (see the first figure). The ideal performance (given by the green curve) exceeds that of actual engines (blue bullets) and reflects inefficiencies.

These performance data reveal a troubling trend, but also an opportunity. Rotor inlet temperatures increased with each engine advance, but so did inefficiency, principally because extra work is needed to provide the flow of cooling air. The opportunity is that an almost 50% increase in output power could result for operation without auxiliary cooling at about 1300°C. This benefit is leveraged further by simplified manufacturing as well as the cascading effect of eliminating weight and complexity of auxiliary cooling requirements.

The choices of alternative materials are limited by numerous performance criteria. One empirical guideline, the Johnson relation, would require that $T_m$ be above 2500°C if the blades are not cooled or otherwise unprotected (*3*). Another issue is creep, the slow deformation of the blade as it is subjected to stress from centrifugal force. Lower creep rates translate into higher maximum operating temperatures, and creep rates tend to be lower for materials with higher $T_m$. There are only a limited number of ceramics, intermetallic compounds, and refractory metals (i.e., metals that keep their strength at high temperatures) that satisfy this initial $T_m$ criterion. As single components, the ceramic and intermetallic phases, which have good oxidation resistance and low density, suffer from severe embrittlement problems and flaw sensitivity at low temperatures that make them unacceptably prone to failure. Composite design strategies have addressed some of the limitations, and silicon carbide matrix composites are being considered for nonrotating engine components for temperatures up to 1200°C (*4*).

Of the refractory metals, Mo and Nb form alloys that satisfy many of the requirements for engine applications, but they suffer from a severe drawback that has only been addressed recently. As pure elements, both metals have poor oxidation resistance. The oxide layer that forms on Nb, $Nb_2O_5$, does not protect the metal from further oxidation, and Mo forms an oxide, $MoO_3$, that is volatile above about 700°C (*5*). However, silicon-

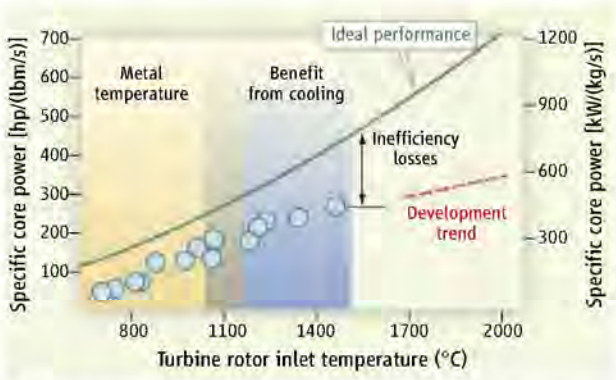


**Efficiency opportunities.** Jet turbine engines should run more efficiently at higher combustion gas temperatures. Here, the core power output is shown versus turbine inlet temperature for selected gas turbine engines. The data points for specific engines can be compared to the ideal or theoretical limit. Early efforts (the orange shaded region) reflect advantages gained from efficient design and the use of advanced materials in the turbine. Later efforts (blue shading) reflect more incremental gains from advanced cooling schemes Higher-temperature materials are needed to shift performance back toward the ideal limits.

Department of Materials Science and Engineering, University of Wisconsin-Madison, 1509 University Avenue, Madison, WI 53706, USA. E-mail: perepezk@engr.wisc.edu

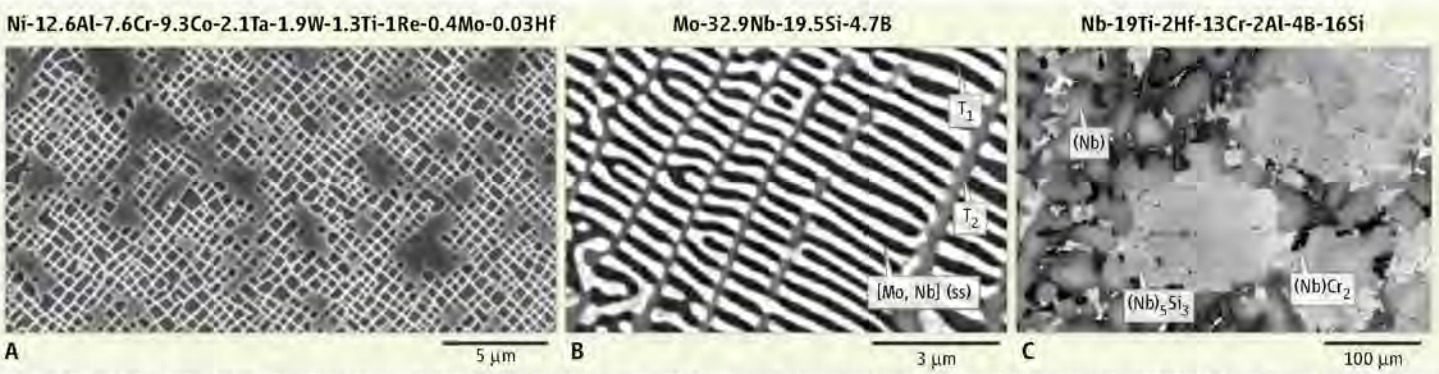


**Lessons from microstructure**. Candidate materials based on molybdenum (Mo) and niobium (Nb), alloyed with silicon (Si) and other elements, can withstand oxidation and could operate in the temperature range where nickel superalloys require thermal protection. They can also develop multiphase microstructures analogous to those of nickel superalloys, which are shown in backscattered electron micrographs. In (**A**), a nickel superalloy CMSX-4 has a continuous γ phase in white; the γ′ phase appears as dark blocks. (**B**) As-cast Mo-based alloy forms a (Mo, Nb) solid-solution matrix that contains inclusions of a $T_1$ phase, $(Mo, Nb)_5Si_3$, and a $T_2$ phase, $(Mo, Nb)_5SiB_2$. (**C**) A directionally solidified Nb alloy has inclusions of $(Nb)_5Si_3$ and $(NbCr_2$.

containing alloys (silicides) of these metals have been explored during the last decade that show promising oxidation resistance.

The route forward for Mo and Nb alloys borrows from lessons learned in the development of nickel superalloys along with some assistance from computational studies (*6–8*). One key aspect is that the many design requirements can be satisfied with a multiphase microstructure. For nickel superalloys, the γ phase, a face-centered-cubic Ni solid solution, acts as a matrix that holds together the other phases dispersed within it. About 60% of the volume within this matrix is a precipitate of nickel, aluminum, and titanium called the γ′ phase that strengthens the superalloy; small amounts of other intermetallic phases are also present (*9*).

The γ and γ′ phases have similar crystal structures and form a stable interface (see the second figure, panel A). Both phases have extensive solubility for additional transition metal alloying elements that can help increase $T_m$, add strength at high temperatures, and help adjust for any crystal-packing misfits. The oxidation resistance is derived mainly from aluminum (Al) and chromium (Cr) that form protective $Al_2O_3$ and $Cr_2O_3$ surface layers. The highest-performance superalloy parts are single crystals in which the crystal lattice is aligned to maximize creep strength.

A key difference between Nb/Mo and the nickel superalloys is that oxidation resistance cannot rely on alumina ($Al_2O_3$); at 1300°C and above, silica ($SiO_2$), which grows more slowly, does this job. Both the Nb and Mo base systems have a body-centered-cubic solid-solution phase that functions like the γ phase in nickel superalloys. In the Mo base alloys, whose typical composition includes boron (Mo containing 9 atomic % Si and 7 atomic % B, or Mo-9Si-7B), silicide ($Mo_3Si$ or $Mo_5Si_3$, called $T_1$) and borosilicide ($Mo_5SiB_2$ called $T_2$) phases are also present and act like the γ′ phase in superalloys, but do not exhibit the low interface energy of γ/γ′ (*7, 8, 10–12*). The modified form of the three-phase microstructure (see the second figure, panel B) developed through alloy design exhibits an organized interwoven morphology with exceptional high-temperature strength (*13*). During oxidation, after a transient period when the volatilization of $MoO_3$ enriches the surface in B and Si, a borosilicate surface layer develops that is protective to above 1300°C (*14, 15*).

For the Nb base alloys, the chemistry is more complex and includes other transition metals, such as Cr, titanium (Ti) and hafnium (Hf) (*16, 17*). The oxidation behavior is also more complex, but acceptable oxidation loss has been attained at 1200°C (*16*). An example of the microstructure in this system is shown in panel C of the second figure.

For both refractory metal systems, the microstructural stability exhibited under extreme conditions of high temperature and stress creates challenges for conventional processing, such as forging, which will modify this microstructure. The challenge is to design processing methods that yield the desired final microstructure during initial alloy synthesis. Some progress has been made in directional solidification, but reactivity with mold materials is an issue (*17*). Innovative powder metallurgy processing may be an effective approach to achieve large-scale synthesis of uniform multiphase microstructures (*18, 19*). These approaches include in situ reaction synthesis of the alloy and superplastic forming, in which deformation rates are enhanced by accelerated diffusion in grain boundaries between crystallites.

At present, it appears that the Nb base systems can serve in uncooled applications up to about 1200°C, and the Mo base systems can offer capability to above 1300°C. In the United States, there is industrial development of the Nb base system by General Electric (*16, 17*) and the Mo base system by Pratt & Whitney (*10, 11*), and a multi-institution development effort is ongoing in Europe (*18*). The refractory metal systems are in the early stages of evolution, but may well enter the forefront of meeting the demands for greater gas turbine efficiency that are driving the need for new high-temperature materials. They may also provide new materials for land-based power generation turbines and for hypersonic flight for access to space.



**References and Notes**

1. N. P. Padture, M. Gell, E. H. Jordan, *Science* **296**, 280 (2002).
2. D. M. Dimiduk, J. H. Perepezko, *MRS Bull.* **28**, 639 (2003).
3. R. L. Fleischer, *J. Met.* **37**, 16 (1985).
4. R. Naslain, *Compos. Sci. Technol.* **64**, 155 (2004).
5. R. W. Buckman, in *Alloying*, J. L. Walter, M. R. Jackson, C. T. Sims, Eds. (ASM, Metals Park, OH, 1988), pp. 419–445
6. C. L. Fu, X. Wang, *Philos. Mag. Lett.* **80**, 683 (2000).
7. N. I. Medvedeva, Y. N. Gornostyrev, A. J. Freeman, *Phys. Rev. Lett.* **94**, 136402 (2005).
8. R. Sakidja *et al.*, *Acta Mater.* **56**, 5223 (2008).
9. W. Ross, C. T. Sims, in *Superalloys II*, C. T. Sims, N. S. Stoloff, W. C. Hagel, Eds. (Wiley, New York, 1987), pp. 97–133.
10. D. M. Berczik, U.S. Patent 5,595,616 (1997).
11. D. M. Berczik, U.S. Patent 5,693,156 (1997).
12. J. H. Schneibel, R. O. Ritchie, J. J. Kruzic, P. F. Tortorelli, *Metall. Mater. Trans. A* **36**, 525 (2005).
13. J. H. Perepezko *et al.*, in *Advanced Structural Materials: Properties, Design, Optimization, and Applications*, W. Soboyejo, Ed. (CRC Press, Boca Raton, FL, 2007), p. 437.
14. R. Sakidja *et al.*, *Scr. Mater.* **53**, 723 (2005).
15. M. Akinc *et al.*, *Mater. Sci. Eng.* **261**, 16 (1999).
16. B. W. Bewlay *et al.*, *MRS Bull.* **28**, 622 (2003).
17. B. P. Bewlay, M. R. Jackson, J.-C. Zhao, P. R. Subramanian, *Metall. Mater. Trans. A* **34**, 2043 (2003).
18. P. Jehanno *et al.*, *Metall. Mater. Trans. A* **36**, 515 (2005).
19. J. M. R. Middlemas, J. K. Cochran, *J. Met.* **60**, 19 (2008).
20. Support was provided by the Office of Naval Research (grant N00014-07-1-1083) and Air Force Office of Scientific Research (grant FA9550-06-1-0233). B. Bewlay provided useful input on Nb-based alloys and D. Furrer advised on CMSX-4.

10.1126/science.1179327

CHEMISTRY

# Hydrate Molecular Ballet

An exceptionally long computer simulation offers a glimpse of molecular events leading to methane hydrate formation.

**Pablo G. Debenedetti and Sapna Sarupria**

Hydrates are crystalline solids in which guest molecules are trapped within polyhedral water cages (*1*). They are important in hydrocarbon processing (*2*) and could play a major role in sustainable energy production (*3*, *4*). Methane hydrate occurs naturally and in vast quantities on ocean floors and in permafrost, with implications for climate change and energy recovery (*2*). However, the molecular mechanisms leading to hydrate formation are poorly understood; this knowledge gap affects not just the science and technology of these materials, but our comprehension of hydrophobicity (*5*) and of disorder-order phase transitions. On page 1095 of this issue, Walsh *et al.* report a computational tour de force that offers a fascinating glimpse of the molecular events leading to methane hydrate formation (*6*).

When methane dissolves in water, a hydrate phase becomes thermodynamically stable at sufficiently low temperatures and high pressures (e.g., for pressures above 80 bar when the temperature is 10°C). The water-methane liquid mixture is then said to be metastable with respect to the hydrate. The basic mechanism by which a stable phase is formed within a metastable phase is called nucleation (*7*). Under the action of thermal motion, molecular fluctuations give rise to small nuclei of the new phase. The lower free energy of the new phase stabilizes nuclei, but an energetic penalty must be paid to form an interface with the liquid. Below a critical nucleus size, surface effects are dominant and nuclei redissolve spontaneously. Above the critical size, on the other hand, the lower free energy of the bulk stable phase overpowers the interfacial penalty, and nuclei grow, leading to the appearance of a new phase. Beyond these generalities, though, it is not known what a critical hydrate nucleus looks like or how large it is, nor is it understood how a bulk hydrate phase grows from a critical nucleus. Because the rate of nucleation depends exponentially on the energetic cost of forming a critical nucleus, the lack of detailed knowledge of hydrate nucleation prevents the accurate prediction of hydrate formation kinetics.

The inability to detect events over nanoscopic time and length scales has hindered the experimental study of hydrate nucleation mechanisms. Molecular dynamics, a computer simulation technique where the motions of atoms and molecules can be followed over nanosecond times and nanometer lengths, is ideally suited to investigating hydrate formation. However, the formation of a nucleus is a rare event, and for the typical volume sampled in a molecular dynamics simulation (~100 $nm^3$) the waiting time can be much longer than the nanosecond range normally sampled with such a technique. Accordingly, Walsh *et al.* perform exceptionally long simulations, extending to microseconds. They are thus able to observe the spontaneous formation of a water cage consisting of 12 pentagonal faces ($5^{12}$) containing a single methane molecule (see the figure). A surprisingly ordered shell of adsorbed methane molecules facilitates the formation of further $5^{12}$ cages. This type of cage cannot fill space, so a few of them rearrange to form an uncommon structure containing 12 pentagonal and three hexagonal faces ($5^{12}6^3$). This expansion enables the surrounding small cages to better fill space, and hydrate formation ensues.

The elaborate molecular ballet reported by Walsh *et al.* reveals the high degree of cooperativity and synchronized motion required for a liquid mixture to evolve into an ordered hydrate phase. The highly structured first-shell layer of adsorbed methane molecules needed for the hydrate to form points to the importance of including order metrics in the description of what constitutes a critical hydrate nucleus.

A unit cell of the thermodynamically stable form of methane hydrate, the so-called structure I (sI), contains two small $5^{12}$ cages and six large $5^{12}6^2$ cages, adding up to 46 water molecules (*1*, *2*). Another common hydrate crystal is the so-called structure II (sII), whose unit cell contains 16 small $5^{12}$ cages and eight large $5^{12}6^4$ cages, adding up to 136 water molecules (*1*, *2*). Small guest molecules such as Ar or Kr form sII hydrate, filling both small and large cages. Methane and $CO_2$ form sI hydrate, partially filling the small $5^{12}$ cages, whereas larger guest molecules such as isobutane or propane form sII hydrates with empty small cages. An intriguing observation of Walsh *et al.* is that their final hydrate phase is a combination of sI and sII. The uncommon $5^{12}6^3$ cage plays a crucial role by allowing the coexistence of sI and sII without the need to form an energetically unfavorable interface.

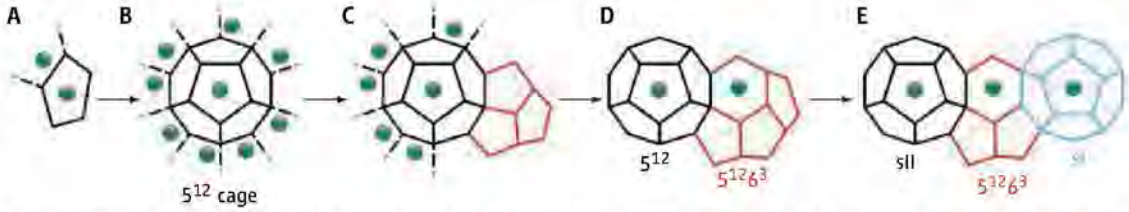


**Fluctuating on the road to hydrate formation.** The molecular mechanism of methane hydrate formation found by Walsh *et al.* (**A**) Water pentagons are stabilized by the adsorption of methane molecules. (**B**) Water pentagons form $5^{12}$ cages (12 pentagonal faces), which are stabilized by ordered adsorbed methane molecules. (**C** and **D**) The faces of $5^{12}$ cages undergo rearrangement and form $5^{12}6^3$ cavities (shown in red). (**E**) These unusual $5^{12}6^3$ cavities allow sI and sII structures to coexist.

Under naturally occurring conditions, sI is the thermodynamically stable form of methane hydrate. However, the coexistence of sI and sII methane hydrates has been observed under moderate conditions (*8*). The calculations of Walsh *et al.* provide a plausible mechanism underlying the subtle interplay of kinetics and thermodynamics implicit in the appearance of a metastable form of hydrate (sII). It will be interesting to explore the temperature range over which the sI and sII appear simultaneously, as well as to test the extent to which this phenomenon occurs when different water models are used in the simulations. The nucleation rates inferred from these calculations are very large, on the order of $10^{25}$ nuclei $cm^{-3}$ $s^{-1}$. It is important to validate these numbers in simulations using different force fields, in particular by using atomically detailed representations of methane.

Department of Chemical Engineering, Princeton University, Princeton, NJ 08544, USA. E-mail: pdebene@princeton.edu

The rare and random events reported by Walsh *et al.* are helpful to develop a physical intuition about plausible mechanisms of hydrate formation. It is reassuring that the two independent trajectories reported in the body of the paper and in the supporting online material lead to similar results. Still, going from these useful but anecdotal snapshots of hydrate birth to the prediction of nucleation rates is a major challenge. It requires the use of path-sampling techniques (*9*, *10*) to generate a statistically significant set of trajectories linking the starting liquid mixture to the final hydrate solid. Only after bringing the powerful theoretical superstructure of statistical mechanics to bear on this problem will quantitative and predictive knowledge of hydrate nucleation kinetics emerge. In the meantime, the computer experiment of Walsh *et al.* has allowed a tantalizing glimpse into the type of concerted molecular motions required to form a methane hydrate.


**References**

1. E. D. Sloan, C. A. Koh, *Clathrate Hydrates of Natural Gases* (CRC Press, Boca Raton, FL, ed. 3, 2008).
2. E. D. Sloan, *Nature* **426**, 353 (2003).
3. L. J. Florusse *et al.*, *Science* **306**, 469 (2004).
4. C. A. Rochelle *et al.*, *Geol. Soc. London Spec. Pub.* **319**, 171 (2009).
5. D. Chandler, *Nature* **437**, 640 (2005).
6. M. R. Walsh, C. A. Koh, E. D. Sloan, A. K. Sum, D. T. Wu, *Science* **326**, 1095 (2009); published online 8 October 2009 (10.1126/science.1174010).
7. P. G. Debenedetti, *Metastable Liquids: Concepts and Principles* (Princeton Univ. Press, Princeton, NJ, 1996).
8. J. M. Schicks, J. A. Ripmeester, *Angew. Chem. Int. Ed.* **43**, 3310 (2004).
9. R. J. Allen, D. Frenkel, P. R. ten Wolde, *J. Chem. Phys.* **124**, 024102 (2006).
10. P. G. Bolhuis, D. Chandler, C. Dellago, P. L. Geissler, *Annu. Rev. Phys. Chem.* **53**, 291 (2002).


10.1126/science.1183027

PLANT SCIENCE

# Solving the Maze

The maize genome sequence will allow further analyses of genetic diversity and the genetic basis for traits critical to plant breeding.

**Catherine Feuillet[1] and Kellye Eversole[2]**

Almost 400 years after Native Americans introduced maize to the pilgrims and joined in celebrating what would become an annual day of giving thanks for the bounty of the harvest, insights from the maize genome sequence, reported on page 1112 (*1*) of this issue by Schnable *et al.*, will pave the way for sequencing other economically important crops. Vielle-Calzada *et al.* on page 1078 (*2*), Swanson-Wagner *et al.* on page 1118 (*3*), and Gore *et al.* on page 1115 (*4*) describe the immediate exploitation of the maize genome sequence. These and companion studies (*5*) represent a milestone in genetics and plant biology, as well as the crowning achievement of a group of corn growers and scientists who envisioned changing the world of agriculture.

For more than 100 years, maize has been a major food, feed, and industrial feedstock for biofuels and bioproducts. The maize genome sequence is now poised to launch the next revolution in genetics and breeding for cereals to meet the challenges of ensuring an abundant supply of food, feed, and fuel in an environmentally sustainable manner. Maize is important not only for its socioeconomic benefits, however. It is also a model system for addressing fundamental questions in genetics such as the impact of domestication on genome structure, the molecular basis of heterosis (the superior performance of hybrid progeny relative to their parents), and the role of transposons—mobile segments of DNA—in genome evolution (*6*). Over the past two decades, the maize genome project has been the main driver for acquiring knowledge and developing methods to sequence plant genomes (*7*–*9*).

Beginning in 1994, the U.S. National Corn Growers Association's vision of a world with a publicly available corn genome sequence was based on the conviction that "the future of corn is written in its genetic code" and "the most important thing we could do is to map the corn genome" (*10*). Fifteen years later, this major goal has been achieved with the first improved draft genome sequence of a reference inbred line of maize (B73). With a physical map-based sequencing strategy focused on a high-quality annotation of the gene space, Schnable *et al.* located over 32,000 genes, characterized the content and distribution of transposable elements, observed their impact on the genome structure (particularly at the centromeres), and gained insight into the mechanisms (gene loss) that returned the ancient allotetraploid maize genome (four sets of chromosomes) to a genetically diploid state. The B73 sequence will serve as the foundation for studies that include linking the sequence to traits, characterizing the structure and evolution of microRNAs, identifying structural variations between the B73 and other inbred lines, and characterizing the distribution and regulation of transposable elements. Some of these analyses have begun already (*5*).

Having a reference maize sequence enables intra- and interspecific comparative analyses such as the one performed by Vielle-Calzada *et al.*, in which highly conserved regions between the genome sequence of a Mexican landrace popcorn (*Palomero Toluqueño*) and that of B73 were identified. The conservation of these regions in other landraces but not in teosinte indicated their potential role in domestication. Some contain genes related to abiotic stress or metal responses, leading the authors to propose that environmental factors, possibly relating to volcanic activity 8500 to 10,500 years ago, played a key role in driving maize domestication.

One of the most extraordinary characteristics of maize is the high level of heterosis observed in hybrids, a feature that has been exploited widely and enabled the maize breeding success story without, however, any explanation for the underlying factors. Swanson-Wagner *et al.* combined a genome-wide comparative transcript analysis between reciprocal hybrids generated from B73 and another reference inbred line (Mo17) with an elaborately designed analysis of expression quantitative trait loci (eQTL) to show that differential gene expression in maize hybrids is driven primarily by the paternally inherited allele of trans-eQTL (DNA elements located on chromosomes that control the differential expression of genes located on other chromosomes). Furthermore, Schnable *et al.* suggest a role for the presence-absence variant regions that contain hundreds of expressed genes

**The corn of plenty.** An improved draft of the maize genome sequence is poised to revolutionize crop improvement.

CREDIT: ISTOCKPHOTOS

[1]UMR INRA-UBP, Génétique, Diversité et Ecophysiologie des Céréales, 63100 Clermont-Ferrand, France. [2]Eversole Associates, Bethesda, MD 20814, USA. E-mail: catherine.feuillet@clermont.inra.fr

in heterosis (*5*). These breakthroughs in understanding a fundamental phenomenon of plant biology are leading the way to identifying the underlying genes or small RNAs with the prospect of improving heterosis in maize and other crops.

The full potential of a genome sequence for elucidating complex agronomically important traits (such as yield, quality, and stress tolerance) can be achieved only if there is sufficient resolution in genetic mapping and phenotyping of the target traits. In maize, this has been accomplished with the recent development of a nested association mapping (NAM) population (*11*) that is based on B73 (5000 recombinant inbred lines generated by crossing B73 with 25 diverse maize lines) and captures ~136,000 chromosomal crossover events. This powerful resource has revealed already the genetic basis of flowering time in maize, which is driven by numerous (50 to 100) small-effect QTL (*12*). Using knowledge from the B73 genome sequence features, Gore *et al.* (*4*) targeted the gene fraction of the maize genome for resequencing in the founder inbred lines of the NAM population. Two data sets comprising 3.3 million single-nucleotide polymorphisms (DNA sequence variations) were used to produce a first haplotype map ("HapMap") and analyze the recombination and diversity distribution along the maize chromosomes. The relative distance along a chromosome arm and the repeat density were identified as the two major drivers of recombination distribution, while 21% of the genic fraction was found in low-recombination pericentromeric regions. Moreover, Gore *et al.* established the relation between low recombination and the residual heterozygosity found in the pericentromeric regions that likely underpins heterosis. This maize HapMap and comparative genome hybridization experiments (*5*) permitted the identification of more than 100 low-diversity regions that are possibly associated with domestication and geographic differentiation of maize. These analyses set up the next goals for maize, including overcoming recombinational constraints that limit the full exploitation of the genetic diversity present in the maize gene pool.

The results reported around the maize genome sequence will have a broad impact on plant breeding and provide far-reaching benefits for humans and animals. Years of hard work by the maize community to accumulate resources, populations, phenotypic data, and agronomic knowledge can now be integrated with sequence information to accelerate crop improvement. Moreover, this will open the floodgates for genome sequencing and genome-enabled breeding of other economically important crops such as wheat, barley, or pine whose larger and more complex genomes have long been viewed as making these plants "unapproachable."


**References**

1. P. S. Schnable *et al.*, *Science* **326**, 1112 (2009).
2. J.-P. Vielle-Calzada *et al.*, *Science* **326**, 1078 (2009).
3. R. A. Swanson-Wagner *et al.*, *Science* **326**, 1118 (2009).
4. M. A. Gore *et al.*, *Science* **326**, 1115 (2009).
5. 2009 Maize Genome Collection, *PLoS Genet.* http://collections.plos.org/plosgenetics/maize.php.
6. *Handbook of Maize, Genetics and Genomics*, J. Bennetzen, S. Hake, Eds. (Springer, New York 2009), vol. 2.
7. P. SanMiguel *et al.*, *Science* **274**, 765 (1996).
8. C. A. Whitelaw *et al.*, *Science* **302**, 2118 (2003).
9. P. D. Rabinowicz, J. L. Bennetzen, *Curr. Opin. Plant Biol.* **9**, 149 (2006).
10. E. H. Coe, *Proc. Natl. Acad. Sci. U.S.A.* **95**, 2029 (1998).
11. M. D. McMullen *et al.*, *Science* **325**, 737 (2009).
12. E. S. Buckler *et al.*, *Science* **325**, 714 (2009).


10.1126/science.1183463

PALEONTOLOGY

# Megafaunal Decline and Fall

Declines in North American megafauna populations began before the Clovis period and were the cause, not the result, of vegetation changes and increased fires.

**Christopher Johnson**

One of the most dramatic environmental changes in recent Earth history has been the disappearance of very big animals—mammoths, mastodons, ground sloths, giant kangaroos, moa and hundreds of others—from most of the land area of the globe. What caused these extinctions? And how did they affect the world's ecosystems? The first question has generated such intense debate that few scientists have got past it to confront the second. On page 1100 of this issue, Gill *et al.* (*1*) give answers to both questions.

Twenty thousand years ago, North America had a more impressive array of big mammals than Africa does today; by 10,000 years ago, 34 genera of these mammals were gone, including the 10 species that weighed more than a ton. Many other drastic changes occurred in this interval, all of which have been advocated as possible causes of megafaunal extinction. The climate flipped from cold to warm, then back to cold in a 1000-year chill (the Younger Dryas), before rapidly rewarming. There were more, larger fires (*2*), and the structure and species composition of vegetation changed drastically. People arrived, and the Clovis culture—with a characteristic style of beautifully crafted stone spear points—flourished for less than 1000 years (*3*). Some scientists have argued that an extraterrestrial object struck Earth ~13,000 years ago, triggering the Younger Dryas, starting fires, killing the megafauna, and putting an end to the Clovis culture (*4*).

The power of the new study (*1*) comes from the use of a tiny organism to reconstruct the decline of the very biggest animals. *Sporormiella* is a fungus that produces spores in the dung of large herbivorous vertebrates. Lots of dung means lots of spores, so *Sporormiella* gives an index of the biomass of large herbivores. The spores accumulate in sediments along with pollen and charcoal, allowing changes in biomass of large herbivores to be matched exactly to sediment records of vegetation and fire, which can in turn be dated and aligned with other archaeological and environmental records.

Gill *et al.* analyzed sediments from a lake in Indiana in this way, and found that megafaunal decline began ~14,800 years ago and took more than a thousand years (see the figure). Large vegetation changes and an increase in fire followed this decline. All this happened long before the proposed extraterrestrial impact. This rules out vegetation change, fire, and cosmic disaster as primary causes of megafaunal extinction. Climate change as a cause also looks implausible: Climate would most likely have affected megafauna by changing vegetation, but vegetation changes followed megafaunal decline.

What about people? It has long been argued that Clovis artifacts signal the first arrival of people in North America south of the boreal ice sheets and that the Clovis people were specialized big-mammal hunters

School of Marine and Tropical Biology, James Cook University, Townsville, Queensland 4811, Australia. E-mail: christopher.johnson@jcu.edu.au

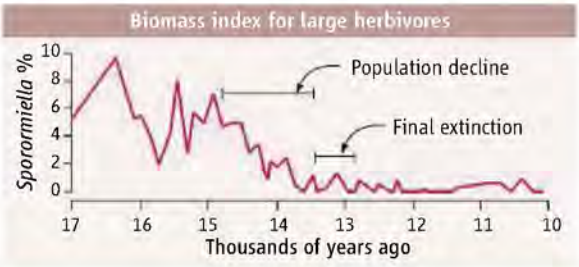


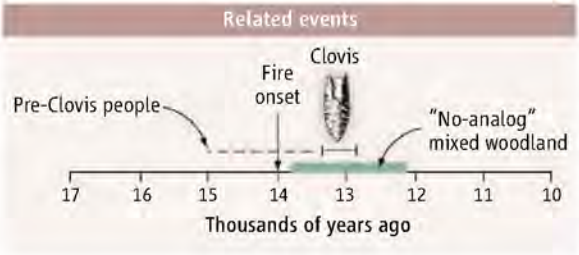


**Pushed to the brink.** Megafauna such as mastodons (**top**) lived in North America until about 13,300 to 12,900 years ago and maintained open savanna-like vegetation. Gill *et al.* have now used the abundance of the dung fungus *Sporormiella* as an indicator of megafaunal populations to study the pattern of megafaunal decline around Appleman Lake in Indiana. They show that this decline began about 14,800 years ago (**middle**). The decline of the megafauna was followed by an increase of fire and development of novel plant communities; although the megafaunal extinction coincides with the presence of the Clovis people, earlier human communities may have been responsible for the initial decline (**bottom**).

who caused a crash of megafaunal populations from prehuman abundance to extinction within a few hundred years. This "blitzkrieg" scenario is supported by the fact that terminal dates on megafaunal fossils range from 13,300 to 12,900 years ago (*5*), which coincides almost exactly with the Clovis period (*3*). But the new data show that the megafaunal decline had begun more than a thousand years earlier. If people were responsible for that decline, they must have been pre-Clovis settlers. The existence of such people has been controversial, but archaeological evidence is slowly coming to light (*6*) and is consistent with their arrival around the beginning of the megafaunal decline (*1*). It is beginning to look as if the greater part of that decline was driven by hunters who were neither numerous nor highly specialized for big-game hunting. Clovis technology may have been a feature of the endgame, possibly reflecting an intensified hunting strategy that developed once megafauna had become rare, possibly wary, and harder to hunt.

The results of Gill *et al.* thus help to elucidate the cause of megafaunal extinction in North America and raise new questions on how people and megafauna interacted. But they also show that this extinction caused a major ecological transformation. Before 14,800 years ago, the environment around the site studied by Gill *et al.* was an open savanna or parkland, probably with scattered spruce and rare broad-leaved trees growing over a short grass-dominated pasture, and almost no fire. As the megafauna declined, woody biomass increased, mainly by growth of broad-leaved trees that had presumably been suppressed by the large herbivores. The result was a transitory spruce/broadleaf woodland, the like of which does not exist today. Big fires broke out ~14,000 years ago, and for the next few thousand years, major fires returned every few centuries. These changes were widespread (*7*): Fire increased throughout North America ~14,000 years ago (*2*), and the transitory "no-analog" woodland extended over a vast area (*8*).

None of this should surprise us. The interactions of mega-herbivores with vegetation and fire can still be seen at work in Africa (*9*). Megafaunal extinctions elsewhere should have had similarly dramatic consequences (*10*). The world's ecosystems must have been profoundly restructured as megafaunal extinctions stepped around the globe. Describing these ecological transformations, and understanding the development of today's ecosystems in light of them, is the next big challenge for ecologists.


**References**

1. J. L. Gill, J. W. Williams, S. T. Jackson, K. B. Linninger, G. S. Robinson, *Science* **326**, 1100 (2009).
2. J. R. Marlon *et al.*, *Proc. Natl. Acad. Sci. U.S.A.* **106**, 2519 (2009).
3. M. R. Waters, T. W. Stafford Jr., *Science* **315**, 1122 (2007).
4. R. B. Firestone *et al.*, *Proc. Natl. Acad. Sci. U.S.A.* **104**, 16016 (2007).
5. S. Fiedel, in *American Megafaunal Extinctions at the End of the Pleistocene*, G. Haynes, Ed. (Springer, Dordrecht, 2009), pp. 21–37.
6. M. T. P. Gilbert *et al.*, *Science* **320**, 786 (2008).
7. G. S. Robinson, L. P. Burney, D. A. Burney, *Ecol. Monogr.* **75**, 295 (2005).
8. J. W. Williams *et al.*, *Ecology* **82**, 3346 (2001).
9. M. Waldram, W. Bond, W. Stock, *Ecosystems* **11**, 101 (2008).
10. C. N. Johnson, *Proc. R. Soc. Lond. B. Biol. Sci.* **276**, 2509 (2009).


10.1126/science.1182770

# Controlling the Velocity of Light Pulses

Robert W. Boyd[1]* and Daniel J. Gauthier[2]

It is now possible to exercise a high degree of control over the velocity at which light pulses pass through material media. This velocity, known as the group velocity, can be made to be very different from the speed of light in a vacuum $c$. Specifically, the group velocity of light can be made much smaller than $c$, greater than $c$, or even negative. We present a survey of methods for establishing extreme values of the group velocity, concentrating especially on methods that work in room-temperature solids. We also describe some applications of slow light.

For the past decade or more, the optical physics community has been fascinated by the related phenomena known figuratively as slow and fast light (*1*–*3*). These names refer to situations in which the group velocity of light $v_g$ is very different from the speed of light in a vacuum $c$. The group velocity gives approximately the velocity at which light pulses propagate through a dispersive material. One refers to light as being "slow" for $v_g << c$ (*4*, *5*) or "fast" for $v_g > c$ or $v_g < 0$ (*6*–*12*). For $v_g < 0$, the pulse envelope appears to travel backward in the material (*12*), and hence it is sometimes referred to as "backward light."

Interest in slow and fast light dates back to the early days of the 20th century. Sommerfeld and Brillouin (*13*) were intrigued by the fact that theory predicts that $v_g$ can exceed $c$, which leads to apparent inconsistencies with Einstein's special theory of relativity. Experimental investigations of extreme propagation velocities were performed soon after the invention of the laser (*6*, *7*).

A great impetus for much of the recent interest in slow and fast light is the experiment of Hau *et al.* (*4*), which showed that light could be slowed down to the "human" scale of 17 m/s. The result was obtained in ultracold atom clouds with the use of electromagnetically induced transparency (EIT), which induces transparency in a material while allowing it to retain strong linear and nonlinear optical properties (*14*). Slow light can also be obtained through the use of the optical response of hot atomic vapors (*5*). To date, the largest slow-light optical delay measured in pulse widths is 80 pulse widths (*15*) for 740-ps-long pulses propagating between two absorbing resonances in a cesium vapor.

More recently, extreme values of $v_g$ were realized in room-temperature, solid-state materials, which are more suited for many practical applications. Here we review some of the physical mechanisms that can be used to induce slow- and fast-light effects in room-temperature solids (*16*–*18*), and we describe some of the exotic propagation effects that can thereby be observed. We also survey some applications of slow and fast light within the fields of quantum electronics and photonics.

## Slow- and Fast-Light Fundamentals

The concept of velocity is well defined for a point particle but becomes murky for wave phenomena. For example, a light pulse tends to spread and distort as it propagates through a material system such a glass. For this reason, it is not possible to use a single definition of velocity to describe the speed at which a pulse of light propagates through a material (*2*). Nonetheless, under conditions described below, $v_g$ gives a reasonable measure of the speed at which a pulse travels.

To understand the consequences of dispersion of the refractive index, we first consider the propagation of a monochromatic beam of light through a material. The phase velocity ($v_p$) describes the speed at which the wavefronts move through the material and is given by

$$v_p = c/n \tag{1}$$

Here, $n$ is the refractive index of the material, which describes effects such as refraction at an interface between two dissimilar materials.

A pulse of light is a wavepacket that is composed of an infinite number of monochromatic component waves, where constructive and destructive interference among the waves defines the shape and location of the pulse envelope in space and time. When the pulse propagates through a material system, each monochromatic component wave travels at a different speed because of the frequency dependence of $n$, resulting in a shift (relative to vacuum propagation) of the regions of constructive and destructive interference. Pulse distortion can also occur. For sufficiently short propagation distances, pulse distortion is not too severe, and the motion of the pulse can be described by $v_g$ (*2*) given by $v_g = c/n_g$, where

$$n_g = n + \omega \frac{dn}{d\omega} \tag{2}$$

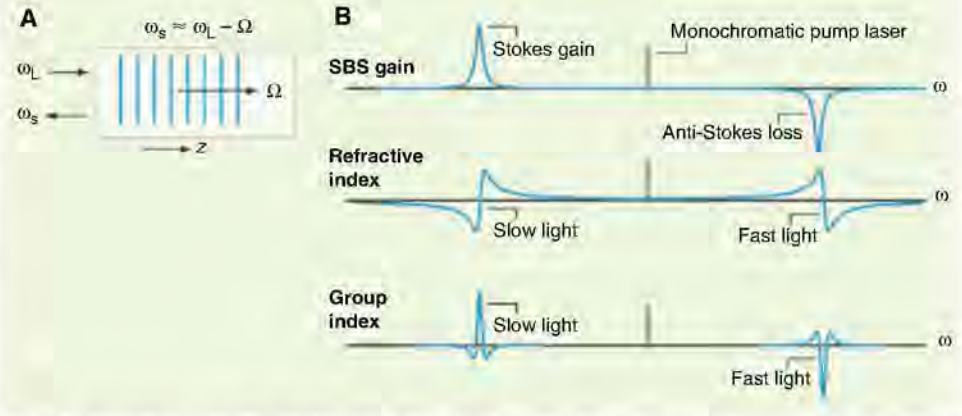


**Fig. 1.** Slow light via SBS. (**A**) Schematic of the SBS process. A laser beam (frequency $\omega_L$) and a signal beam (frequency $\omega_S$) interact to produce an ultra–high-frequency acoustic wave (frequency $\Omega$, typically ~10 GHz for standard optical fibers) through the process of electrostriction. The acoustic wave produces an optical wavelength–scale variation in the refractive index of the material, which acts as a moving diffraction grating. For the case of $\omega_S \approx \omega_L - \Omega$, the grating travels in the same direction as the pump laser beam and scatters light coherently from the pump beam into the signal beam. This process thus gives rise to a narrow isolated amplifying resonance, known as the Stokes resonance, as shown in (**B**). For the opposite case in which $\omega_S \approx \omega_L + \Omega$, the diffraction grating moves in the opposite direction, and light from the signal beam is scattered into the pump laser beam, resulting in an anti-Stokes absorbing resonance. General considerations (the Kramers-Kronig relations) require that a peak in the gain or loss be accompanied by a rapid variation in the refractive index $n$. According to Eq. 2, this rapid variation gives rise to a large contribution to $n_g$. Thus, a large slow-light effect occurs near the center of the Stokes gain, or a fast-light effect occurs near the center of the anti-Stokes absorption resonance. The SBS process is noteworthy in that the resonances can be created at any frequency by adjusting the pump laser frequency, and the time delay can be adjusted continuously by adjusting the laser intensity.

[1]The Institute of Optics and Department of Physics and Astronomy, University of Rochester, Rochester, NY 14627, USA. [2]Department of Physics, Duke University, Box 90305, Durham, NC 27708, USA.

*To whom correspondence should be addressed. E-mail: boyd@optics.rochester.edu

is known as the group index, where $\omega$ is the light's frequency. A fascinating result of recent investigations is the extreme range of values of $n_g$ that can be observed in the laboratory. For example, one can readily observe extremely slow light with $n_g \sim 10^8$ or can observe backward light with $n_g < 0$. These values should be put in the context of the refractive index, which lies in the range of ~1.4 to ~3 for typical materials in the visible part of the electromagnetic spectrum. As can be seen from Eq. 2, $n_g$ can be adjusted either by modifying $n$ or by modifying $dn/d\omega$ (the dispersive contribution to $n_g$). Most demonstrations of extreme values of $n_g$ rely on the dominance of the dispersive contribution to $n_g$. However, recent developments in the field of metamaterials have led to the demonstration of negative values of $n$ (*19*).

## Slow Light in Room-Temperature Solids

Many applications of slow light require the use of room-temperature solids, rather than crystals at cryogenic temperatures (*8*), hot atomic vapors (*5*, *15*), or ultracold atomic ensembles (*4*, *20*). In our view, three methods involving room-temperature solids have emerged as being particularly well suited for use in applications of low light. These methods are reviewed below.

*Slow light via stimulated Brillouin scattering.* Stimulated Brillouin scattering (SBS) is a nonlinear optical process that occurs readily in any transparent material. It results from the mutual interaction of applied pump and signal laser beams with an acoustic wave that is itself created by the laser beams through the process of electrostriction (*21*). For the case in which the signal beam has a slightly lower frequency than the pump beam, the mutual interaction gives rise to a narrow gain resonance (Fig. 1). There will be a large slow-light effect near the center of this gain line. For the case in which the signal beam has a slightly higher frequency than the pump, the opposite happens, giving rise to an absorption resonance and a fast-light effect. The induced time delay for the slow-light situation is proportional to the intensity of the pump beam, allowing $v_g$ to be readily controlled. Slow light based on this process was first observed in standard telecommunication optical fibers at a wavelength of 1550 nm (*17*, *18*).

A limitation to the usefulness of the SBS process, however, is that the Brillouin linewidth for typical optical fibers is only 30 to 50 MHz. This linewidth sets the characteristic frequency bandwidth over which slow-light effects can be observed. Data transmission rates are hence limited to this value, which is much too small for many applications in optical telecommunication. Several procedures have been introduced to broaden this linewidth, such as broadening the linewidth of the laser that pumps the SBS process. This method was used to achieve a 12-GHz bandwidth (*22*) and to delay 100-ps-long pulses by up to three pulse widths (*23*). More details on recent advances in SBS slow light can be found in a recent review (*24*).

*Slow light via coherent population oscillations.* Another method for producing slow light is based on the process of coherent population oscillation (CPO). The CPO process has been studied since the 1960s and has successfully been exploited for slow- and fast-light research (*12*, *16*, *25*–*27*). The idea behind CPO (see Fig. 2) is that, when pump and probe beams of slightly different frequencies interact inside a saturable absorbing material, the atomic population is driven coherently between the ground and excited states at the beat frequency of the light beams. These population oscillations lead to a dip in the absorption spectrum that is experienced by the probe beam, which then leads to a greatly reduced $v_g$ over a spectral region surrounding the dip.

In the first reported experimental study of slow light based on CPO (*25*), saturation of the strong green absorption band of ruby was used to produce the slow-light effect. Group velocities as low as 60 m/s, corresponding to an $n_g$ of $5 \times 10^6$, were observed for waveforms with time scales on the order of 16 ms.

A follow-up experiment made use of the nonlinear optical properties of the crystal alexandrite (*16*). Alexandrite is a saturable absorber at some frequencies but an inverse saturable absorber at others. At frequencies at which alexandrite is an inverse saturable absorber, it displays fast and backward light as a result of the CPO effect. In one situation, a velocity of −800 m/s was measured. The implications of a negative $v_g$ are described in the following section. CPO typically produces a maximum delay or advance of about 0.25 pulse widths. However, by careful choice of material parameters and by cascading more than one CPO delay element, greater delays can be obtained. In one study, a delay of approximately 1.3 pulse widths was achieved (*28*).

*Tunable time delays based on $v_g$ dispersion.* The simplest method for controlling the velocity of light is to make use of a medium with a large dispersion in $v_g$ (*29*). By varying the frequency of the carrier wave of the signal, the time delay can be controlled directly. In practice, this method is often implemented by starting with a signal at a prescribed carrier frequency, shifting the carrier frequency with a nonlinear optical conversion method, passing this frequency-shifted signal through a highly dispersive medium, and finally converting the carrier frequency back to the original frequency. This method is often called the conversion/dispersion (C/D) method for this reason.

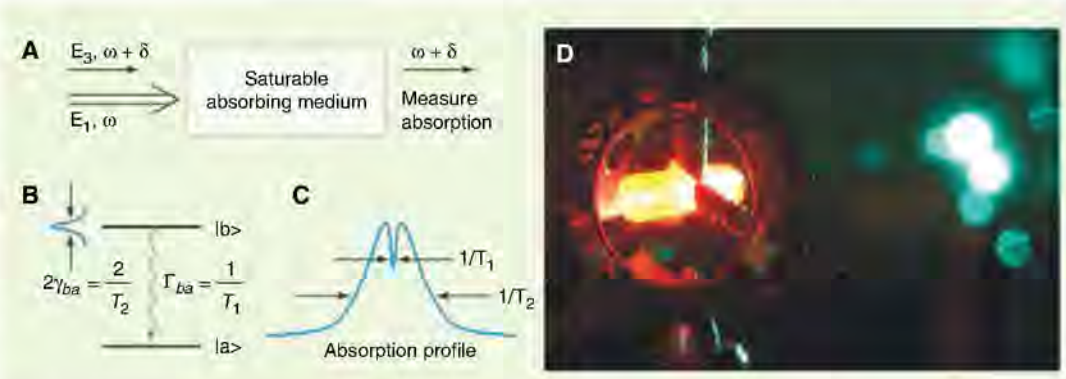


**Fig. 2.** Origin of slow light due to CPO. **(A)** A strong pump laser beam ($E_1$, frequency $\omega$) copropagates with a weak probe beam ($E_3$, frequency $\omega + \delta$) through a saturable absorber. **(B)** Energy-level diagram of a typical saturable absorbing medium. The width of the resonance is governed by the inverse of the dipole dephasing time $T_2$. Here $2\gamma_{ba}$ is the resonance linewidth and $\Gamma_{ba}$ is the spontaneous emission rate of |b⟩. **(C)** Absorption profile in the presence of CPO. The pronounced dip is created by the following process: A beat note is induced at the frequency difference of the two input beams. When the beat-note period is so long that the atomic population can follow the beat frequency (the time scale for atomic population to respond is the $T_1$ relaxation time), the resonance is more easily saturated, resulting in smaller signal-beam absorption. When the beat-note period is much shorter than the $T_1$ lifetime, the material senses only the average of the field (that is, the beat notes are washed out), resulting in lower saturation of the resonance and larger signal-beam absorption. If $T_1$ is much greater than $T_2$, a well-defined hole is thus induced in the absorption profile of the saturable absorber, even if the absorption profile is homogeneously broadened in the conventional sense. This spectral hole then leads, through the usual Kramers-Kronig relations, to a rapid spectral variation of the refractive index and thus to a strong slow-light effect. Detailed calculation (*25*) shows that the resulting $n_g$ scales linearly with the intensity of the pump laser, as long as the pump intensity is not too large. Thus, the slow-light delay via CPO can be tuned continuously by adjusting the pump beam intensity. **(D)** Part of the experimental setup.

## Fast Light and Its Interpretation

As mentioned above, $v_g$ can become greater than $c$ or can even become negative (Fig. 3). Fast light

is sometimes taken to constitute a highly exotic phenomenon, perhaps because of some fear that superluminal propagation constitutes a violation of relativity theory. However, slow light occurs when $dn/d\omega$ is positive, and fast light occurs when $dn/d\omega$ is negative. Thus, there is nothing fundamentally different between slow light and fast light. Here we show that fast light is entirely consistent with accepted physical laws.

Experimental studies of fast-light propagation include those of (*7*–*10*). More-recent work was motivated by a suggestion (*30*) to make use of a Raman gain doublet to induce a spectral region within which $v_g$ exceeds $c$ and pulse distortion effects are minimized. This idea was successfully implemented (*10*) by using a gain doublet produced in a laser-pumped cesium vapor. Soon thereafter, an experiment directly measured the speed at which information propagates through a fast-light material (*11*). Figure 3A shows an example for the case of a smooth Gaussian-shaped pulse propagating through the fast-light medium in comparison to the same pulse propagating through vacuum.

*Causality implications.* It is well established that the superluminal transfer of information is inconsistent with the concept of Einstein causality. In particular, if information could be transmitted from one observer to another in a superluminal fashion, then there is always some other inertial reference frame in which the information reaches the receiver before it leaves the sender. Because causality is believed to be a universal property of nature, it is commonly thought that the superluminal transfer of information is therefore impossible.

So why do laboratory results of fast light not necessitate the superluminal transfer of information? It is believed that the explanation lies in the distinction between $v_g$ and the information velocity. The group velocity can take on any value. However, the information velocity can never exceed $c$ and, according to many models, is always equal to $c$ (*2*, *13*, *31*). To understand why this is so, we note that the encoding of information onto an optical waveform necessarily entails impressing points of discontinuity onto the waveform. New information is encoded at each discontinuity. In concept, no information is carried by the smooth portions of the waveform, because, in principle, the future behavior can be predicted in terms of the past behavior for any analytic function. Points of discontinuity propagate at the speed of light in a vacuum $c$ because no physical material can respond instantaneously to a change in the waveform (*13*).

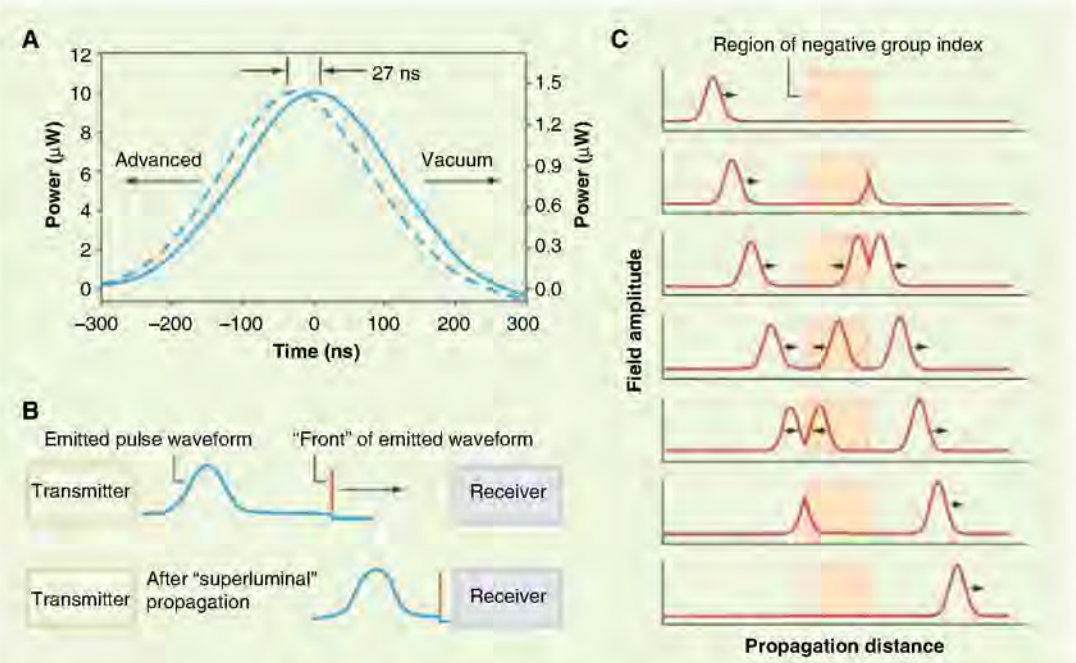


**Fig. 3.** Some exotic propagation effects can occur when light pulses pass through a dispersive material. One of these is superluminal pulse propagation. In (**A**), a 260-ns-long (full width at half maximum) pulse propagates through a laser-pumped potassium vapor with $n_g$ of approximately −20 (dashed line). The peak of the pulse is seen to be advanced by 27 ns with respect to vacuum propagation (solid line) (*11*). Such superluminal propagation effects may appear to violate principles of causality, but in fact they do not for reasons illustrated in (**B**). Any real pulse has a "front": the first moment in time at which the intensity becomes nonzero, as indicated by the vertical line. In superluminal propagation experiments, the peak of the pulse moves at a superluminal velocity, but the front of the pulse moves at velocity $c$. Because the information content of the pulse is contained in the front, no information is transmitted at a velocity exceeding $c$. For propagation distances longer than those shown here, for which the pulse peak begins to overtake the pulse front, severe pulse distortion always occurs and no pulse energy ever precedes the pulse front. (**C**) Another exotic propagation effect is backward pulse propagation. This effect occurs for a sufficiently long material with a negative $n_g$ and leads to the result that the peak of the transmitted pulse appears to emerge from the material medium before the peak of the incident pulse enters the medium. Backward propagation has been observed in the laboratory (*12*). The plots are based on a simple model that assumes that all spectral components of the pulse propagate without loss at the same $v_g$.

*Backward light.* Under certain extreme conditions, $v_g$ can actually become negative. Numerical simulations of the sort shown in Fig. 3C (*32*, *33*) demonstrate that the peak of the pulse leaving a slab of material appears to exit before the peak of the input pulse enters the slab. Moreover, the pulse envelope appears to propagate backward inside the material (although the flow of power is still from the entrance to the exit of the slab), justifying the name backward light. These predictions were verified experimentally (*12*) using the highly dispersive response of an erbium-doped fiber amplifier. When driven into saturation, an amplifier shows fast light by means of the CPO effect (*12*) for the same reason that an absorber shows slow light (Fig. 2C). The peak of the pulse did propagate in the backward direction within the fiber, in agreement with the standard meaning of $v_g$.

## Applications of Slow and Fast Light

*Telecommunication.* Slow-light methods have direct applicability to the field of optical telecommunication for applications such as buffering and regeneration. Figure 4A shows how a slow-light delay line acting as a buffer might be used to increase the throughput of an optical telecommunication system.

To implement this idea, the delay line needs to be able to store as many bits of information (data pulses) as are contained in a data packet. This number is determined by the system architecture. In most implementations, a typical packet has at least 1024 bits of data (or 1024 pulses in the return-to-zero data format). In fundamental terms, the number of stored pulses is known as the delay-bandwidth product of the delay line. There have been a number of analyses of the theoretical limit to how large the delay-bandwidth product of a slow-light delay line can be (*34*, *35*). The general conclusion of these analyses seems to be that there is no fundamental limit to the size of the delay-bandwidth product, although there can be serious practical problems involved in obtaining large values of this quantity. One important implementation of slow-light methods in optical telecommunication is the demonstration of optical data packet synchronization and multiplexing based on the C/D method (*36*).

By careful selection of the slow-light mechanism and operating conditions, delays of many pulse lengths have been obtained in laboratory

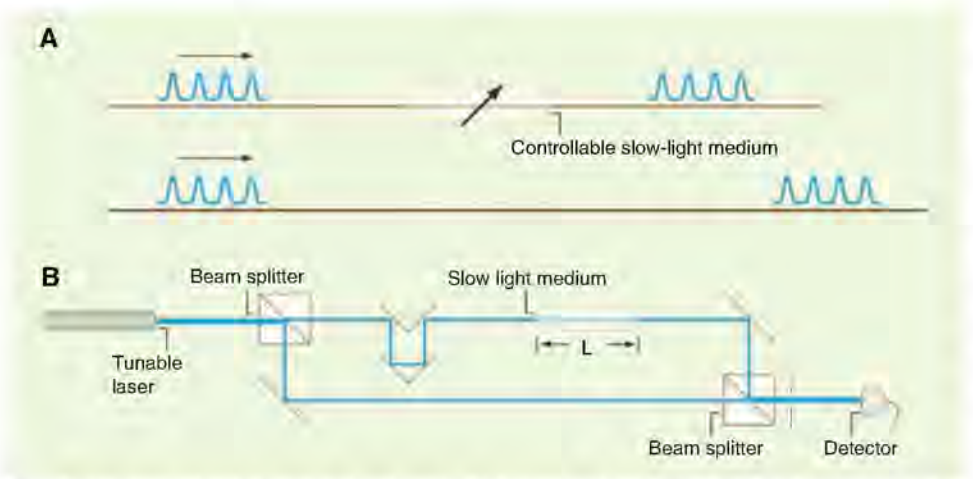


**Fig. 4.** Two applications of slow and fast light. **(A)** A slow-light buffer for use in a telecommunication system. If two optical data packets arrive simultaneously at an optical switch, a problem occurs because the switch cannot handle the two data packets simultaneously. In the worst case, one of the data packets is simply dropped and must be retransmitted at a later time. This procedure, of course, simply makes the problem of system overload worse, because the data packet has to be transmitted more than once. This problem can be avoided by constructing a controllable delay line that can act as a buffer for a complete data packet, as shown. In this scenario, one data packet is directed into the buffer and is released only after the other data packet has cleared the switch. **(B)** Slow-light–enhanced optical interferometer. By placing a slow-light medium of length $L$ in one arm of the interferometer, the spectral resolution can be increased by a factor as large as the $n_g$ of the slow-light material. This procedure holds great promise for the development of spectrometers with extremely high spectral resolution or for miniaturizing the size of spectrometers of more modest resolution.

measurements. By combining slow-light methods with self-phase modulation, a total advancement/delay bandwidth product of ~10 for 370-fs-long optical pulses has been obtained using a semiconductor optical amplifier (*37*). Recently, using the C/D method, delays of 20,000 pulse widths have been obtained at a data rate of 40 Gb/s (*38*). These delays are large enough to prove useful in actual communication systems.

*Microwave photonics.* Microwave photonics is an emerging field in which high-frequency electrical signals in the radio-frequency or microwave-frequency bands are impressed onto a light beam using amplitude or phase modulators and are subsequently processed using all-optical methods. These all-optical methods tend to have very high bandwidth, fast reconfiguration speeds, and low loss. Already, microwave photonic devices are being integrated into broadband wireless access networks, phased-array antennas, and high-speed signal processing engines.

At the heart of many of these devices is a unit that gives a true time delay (as opposed to mechanisms that would delay some spectral components but not others) of an optical waveform (*39*). For device reconfigurability, it is important that the time delay be continuously tunable. Thus, slow- and fast-light methods are well suited to the development of microwave photonic devices. In fact, only modest delays are needed (a delay-bandwidth product of unity is often sufficient) in comparison to what is needed for data buffering in telecommunication systems described above. One example of a microwave component based on slow light is a phase shifter with a continuously tunable phase shift of ~240° at a microwave frequency of approximately 19 GHz (*40*).

*Interferometry.* The performance of many types of interferometers can be dramatically improved by placing a highly dispersive material within the interferometer. One example is the slow-light Mach-Zehnder interferometer shown in Fig. 4B. One finds by direct calculation (*41*) that the spectral sensitivity of the interferometer, defined as the change in phase difference between the two arms per change in input frequency, is proportional to the product of the length $L$ and $n_g$ of the slow-light material. Thus, dramatic increases in the spectral sensitivity of the interferometer are enabled by using large values of $n_g$. A slow-light spectrometer of this sort was constructed (*41*) and was found to achieve an increase in spectral sensitivity by a factor of approximately 2; more recent work has demonstrated a 100-fold enhancement of the sensitivity.

## Summary and Outlook

Slow- and fast-light methods have advanced dramatically in recent years. Many of the fundamental aspects of slow and fast light are currently well understood. Thus, research has turned to the equally exciting task of developing applications of this new technology.

### References and Notes

1. R. W. Boyd, D. J. Gauthier, *Progress in Optics* (Elsevier, Amsterdam, 2002), p. 497.
2. P. W. Milonni, *Fast Light, Slow Light, and Left-Handed Light* (Institute of Physics Publishing, Bristol, UK, 2005).
3. J. B. Khurgin, R. S. Tucker, Eds., *Slow Light: Science and Applications* (CRC Press, Boca Raton, FL, 2008).
4. L. V. Hau, S. E. Harris, Z. Dutton, C. Behroozi, *Nature* **397**, 594 (1999).
5. M. M. Kash *et al.*, *Phys. Rev. Lett.* **82**, 5229 (1999).
6. N. G. Basov, R. V. Ambartsumyan, V. S. Zuev, P. G. Kryukov, V. S. Letokhov, *Sov. Phys. JETP* **23**, 16 (1966).
7. F. R. Faxvog, C. N. Y. Chow, T. Bieber, J. A. Carruthers, *Appl. Phys. Lett.* **17**, 192 (1970).
8. S. Chu, S. Wong, *Phys. Rev. Lett.* **48**, 738 (1982).
9. B. Segard, B. Macke, *Phys. Lett.* **109**, 213 (1985).
10. L. J. Wang, A. Kuzmich, A. Dogariu, *Nature* **406**, 277 (2000).
11. M. D. Stenner, D. J. Gauthier, M. A. Neifeld, *Nature* **425**, 695 (2003).
12. G. M. Gehring, A. Schweinsberg, C. Barsi, N. Kostinski, R. W. Boyd, *Science* **312**, 895 (2006).
13. The work of A. Sommerfeld and L. Brillouin from 1914 is translated into English and collected in a book (*42*).
14. S. E. Harris, J. E. Field, A. Imamoğlu, *Phys. Rev. Lett.* **64**, 1107 (1990).
15. R. M. Camacho, M. V. Pack, J. C. Howell, A. Schweinsberg, R. W. Boyd, *Phys. Rev. Lett.* **98**, 153601 (2007).
16. M. S. Bigelow, N. N. Lepeshkin, R. W. Boyd, *Science* **301**, 200 (2003).
17. K. Y. Song, M. G. Herráez, L. Thévenaz, *Opt. Express* **13**, 9758 (2005).
18. Y. Okawachi *et al.*, *Phys. Rev. Lett.* **94**, 153902 (2005).
19. D. R. Smith, J. B. Pendry, M. C. K. Wiltshire, *Science* **305**, 788 (2004).
20. S. Inouye *et al.*, *Phys. Rev. Lett.* **85**, 4225 (2000).
21. R. W. Boyd, *Nonlinear Optics* (Academic Press, Amsterdam, 2008), chap. 9.
22. Z. Zhu, A. M. C. Dawes, D. J. Gauthier, L. Zhang, A. E. Willner, *J. Lightwave Technol.* **25**, 201 (2007).
23. E. Cabrera-Granado, O. G. Calderón, S. Melle, D. J. Gauthier, *Opt. Express* **16**, 16032 (2008).
24. L. Thévenaz, *Nat. Photon.* **2**, 474 (2008).
25. M. S. Bigelow, N. N. Lepeshkin, R. W. Boyd, *Phys. Rev. Lett.* **90**, 113903 (2003).
26. P.-C. Ku *et al.*, *Opt. Lett.* **29**, 2291 (2004).
27. H. Su, S. L. Chuang, *Appl. Phys. Lett.* **88**, 061102 (2006).
28. W. Xue, S. Sales, J. Company, J. Mørk, *Opt. Lett.* **34**, 929 (2009).
29. J. Sharping *et al.*, *Opt. Express* **13**, 7872 (2005).
30. A. M. Steinberg, R. Y. Chiao, *Phys. Rev. A* **49**, 2071 (1994).
31. R. Y. Chiao, A. M. Steinberg, in *Progress in Optics*, E. Wolf, Ed. (Elsevier, Amsterdam, 1997), pp. 347–406.
32. C. G. B. Garrett, D. E. McCumber, *Phys. Rev. A* **1**, 305 (1970).
33. A. Dogariu, A. Kuzmich, H. Cao, L. Wang, *Opt. Express* **8**, 344 (2001).
34. D. A. B. Miller, *Phys. Rev. Lett.* **99**, 203903 (2007).
35. B. Macke, B. Ségard, *Phys. Rev. A* **78**, 013817 (2008).
36. I. Fazal *et al.*, *Opt. Express* **15**, 10492 (2007).
37. B. Pesala, F. G. Sedgwick, A. V. Uskov, C. Chang-Hasnain, *Opt. Express* **17**, 2188 (2009).
38. T. Kurosu, S. Namiki, *Opt. Lett.* **34**, 1441 (2009).
39. F. Öhman, K. Yvind, J. Mørk, *IEEE Photon. Technol. Lett.* **19**, 1145 (2007).
40. W. Xue, S. Sales, J. Capmany, J. Mørk, *Opt. Lett.* **34**, 929 (2009).
41. Z. Shi, R. W. Boyd, D. J. Gauthier, C. C. Dudley, *Opt. Lett.* **32**, 915 (2007).
42. L. Brillouin, *Wave Propagation and Group Velocity* (Academic Press, New York, 1960).
43. We acknowledge valuable discussions with A. M. C. Dawes, A. L. Gaeta, G. M. Gehring, S. E. Harris, J. C. Howell, A. Liapis, J. R. Lowell, M. A. Neifeld, M. Scully, Z. Shi, M. D. Stenner, J. E. Vornehm Jr., A. E. Willner, and Z. Zhu and financial support through the Defense Advanced Research Projects Agency Defense Sciences Office slow-light program and through NSF.

10.1126/science.1170885

# The Palomero Genome Suggests Metal Effects on Domestication

Jean-Philippe Vielle-Calzada,* Octavio Martínez de la Vega,* Gustavo Hernández-Guzmán, Enrique Ibarra-Laclette, Cesar Alvarez-Mejía, Julio C. Vega-Arreguín,† Beatriz Jiménez-Moraila, Araceli Fernández-Cortés, Guillermo Corona-Armenta, Luis Herrera-Estrella,‡ Alfredo Herrera-Estrella

Maize was domesticated from Balsas teosinte (*Zea mays* ssp *parviglumis*) ~9000 years ago (*1*), resulting in a wide variety of landraces.

To gain insight into maize genomic diversity, we sequenced the *EDMX-2233* genotype of the *Palomero Toluqueño* (*Palomero*) landrace, a highland popcorn from San Lorenzo Teotuitlán, Mexico (*2*) (Fig. 1A), and compared its features with those of the inbred B73 genome (*3*). The *Palomero* genome is ~22% smaller and contained ~20% less repetitive DNA (*3*) (fig. S1). A total of 653 *Palomero* regions (0.5 kb to 2.5 kb) had 100% identity to the *B73* genome across all chromosomes (*2*) (table S4). These identical sequence regions (IDSRs) represent 544.6 kb and include 458 nonprotein-coding and 188 protein-coding regions (82% with evidence of expression) (*4*). One IDSR mapped 62.2 kb upstream of the domestication gene *teosinte branched1* (*tb1*), confirming a selective sweep 5′ to the *tb1* transcribed sequence (*5*). Two IDSRs mapped to 156 kb and 166 kb upstream and downstream, respectively, of the domestication gene *teosinte glume architecture1* (*6*) (fig. S3). Additional regions dense in IDSRs include a 1.7-Mb genomic segment near position 95 Mb of chromosome 4 (ctg171; six IDSRs) and a 1.5-Mb segment between positions 89.5 Mb and 91 Mb of chromosome 10 [ctg411; five IDSRs (*2*)], of which a 1.3-kb region (SMS43) is significant for domestication under a coalescent model ($P < 0.001$; table S8), confirming that some IDSRs may contain regions selected by humans.

Because null nucleotide variability between *Palomero* and B73 could represent mutational cold spots specific to *Zea* or regions under weak negative selection, we selected 30 random IDSRs across the genome and sequenced them in 16 Mexican landraces and 11 Balsas teosinte accessions (*2*) (table S6). In the landraces, 27 of the 30 IDSRs had reduced numbers of segregating sites ($S$) and haplotypes ($h$) compared with the corresponding values for previously reported neutral genes [$S \leq 9$ and $h \leq 8$ versus $S \geq 17$ and $h \geq 8$ (*2*)], suggesting that the majority of IDSRs could be considered artificially selected loci. The nucleotide diversity index, $\pi$, was also significantly smaller in landraces compared with in teosintes (*2*) (Mann-Whitney U test, $P < 0.001$; table S7). Neutral loci retained about 70% of the genetic diversity of teosinte ($\pi_M/\pi_T \sim 0.7$), which was reduced in 11 of the 30 sequenced IDSRs ($\pi_M/\pi_T < 0.15$), suggesting maize-specific selection (*3*). Six of these segments showed a complete absence of nucleotide variability in maize but not among teosintes.

Coalescent simulation (CS) tests were used to identify putative domestication loci (*7*, *8*). Assuming that the ancestral population follows a neutral equilibrium model, CS on the 12 genomic regions showing the lowest $\pi_M/\pi_T$ ratio (*2*) identified eight putative domestication loci that contain several genes encoding proteins involved in the epigenetic control of plant development (*2*) or heavy-metal detoxification (table S8 for details). Among the latter, one contains a member of the E1-E2 superfamily predicted to transport cadmium (SMS1), whereas another encodes a multicopper oxidase protein (MCO) predicted to be involved in metal transport (SMS33). A third gene encoding a P-type copper translocator that also detoxifies heavy metals has a $\pi_M/\pi_T$ ratio suggestive of selection (SMS18), although CS cannot discard the possibility that this is due to demographic bottlenecks. An additional gene encodes a phosphatidylinositol transporter protein involved in responses to abiotic stress (SMS15). These genes are all transcriptionally active (*4*). Moreover, SMS1 and SMS33 map to the short arm of chromosome 5, colocalizing with a domestication quantitative trait locus (QTL) (Fig. 1B) (*9*). Regions disqualified as domestication loci by CS exhibited a loss of genetic diversity in both landraces and teosintes (*2*). At least 11 other genomic IDSRs contain genes involved in abiotic stress or metal responses (table S9), suggesting that environmental factors related to the metal contents of local soils may have been important in maize domestication. Thus, the *Palomero* landrace genome offers information for exploring allelic variants selected during early maize cultivation.

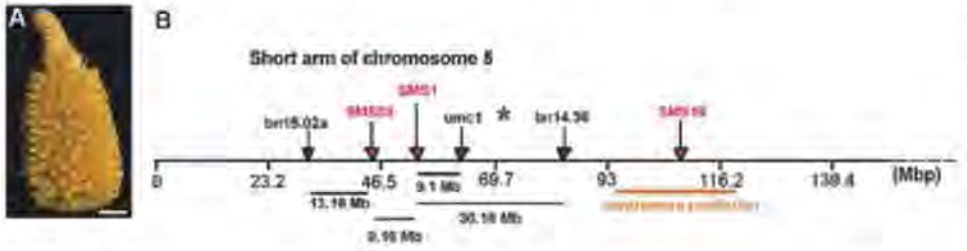


**Fig. 1.** (**A**) Cob of *Palomero Toluqueño EMX-2233*; scale bar indicates 1 cm. (**B**) Colocalization of SMS1 and SMS33 (each containing a heavy-metal–detoxification gene) with the predicted location of a major QTL for domestication (blue asterisk) in the short arm of chromosome 5 (*2*). SMS18 (also containing a heavy-metal–detoxification gene) maps within the range of the centromere.


## References and Notes

1. Y. Matsuoka *et al.*, *Proc. Natl. Acad. Sci. U.S.A.* **99**, 6080 (2002).
2. Materials and methods are available as supporting material on *Science* Online.
3. P. S. Schnable *et al.*, *Science* **326**, 1112 (2009).
4. J. C. Vega-Arreguín *et al.*, *BMC Genomics* **10**, 299 (2009).
5. R. M. Clark, E. Linton, J. Messing, J. F. Doebley, *Proc. Natl. Acad. Sci. U.S.A.* **101**, 700 (2004).
6. J. Dorweiler, A. Stec, J. Kermicle, J. Doebley, *Science* **262**, 233 (1993).
7. M. I. Tenaillon *et al.*, *Proc. Natl. Acad. Sci. U.S.A.* **98**, 9161 (2001).
8. A. Eyre-Walker, R. L. Gaut, H. Hilton, D. L. Feldman, B. S. Gaut, *Proc. Natl. Acad. Sci. U.S.A.* **95**, 4441 (1998).
9. W. H. Briggs, M. D. McMullen, B. S. Gaut, J. Doebley, *Genetics* **177**, 1915 (2007).

10. We thank D. Torrent (Barcelona Supercomputing Center, Spain) for facilities and technical support; J. Sánchez, J. M. Hernández Casillas, and Centro Internacional de Mejoramiento de Maíz y Trigo (CIMMYT) for access to their seed collections; G. Palomino and G. Acosta for help with flow cytometry; J. Bennetzen, S. Wessler, and N. Jiang for help with repetitive DNA analysis; J. Sánchez and A. Avendaño (Centro Universitario de Ciencias Biológicas y Agropecuarias) for providing plant material; J. Doebley, J. Yan, and C. Bedolla for backup DNA samples; and two anonymous reviewers for helpful suggestions. Funded by Consejo Nacional de Ciencia y Tecnología and the ZEA-2006 grant from la Secretaría de Agricultura, Ganadería, Desarrollo Rural, Pesca y Alimentación. Genbank assession numbers are GU112491 to GU112502.

## Supporting Online Material

www.sciencemag.org/cgi/content/full/326/5956/1078/DC1
Materials and Methods
Figs. S1 to S4
Tables S1 to S11
References

30 June 2009; accepted 16 October 2009
10.1126/science.1178437

Laboratorio Nacional de Genómica para la Biodiversidad, CINVESTAV Irapuato, Km 9.6 Libramiento Norte Carretera Irapuato-León, 36500 Irapuato, Mexico.

*These authors contributed equally to this work.
†Present address: Boyce Thompson Institute for Plant Research, Ithaca, NY 14853, USA.
‡To whom correspondence should be addressed. E-mail: lherrera@ira.cinvestav.mx

# Strengthening Individual Memories by Reactivating Them During Sleep

John D. Rudoy,[1] Joel L. Voss,[1,2] Carmen E. Westerberg,[1] Ken A. Paller[1]*

Initially fragile memories can gain stability via consolidation, but the extent to which sleep contributes to this process is unresolved (*1*, *2*). Sleep between encoding and retrieval, relative to wakefulness, promotes memory storage in some circumstances, perhaps from internally generated memory reactivation (*3*, *4*). Moreover, reinstating a learning context (an odor) during slow-wave sleep enhances retrieval of spatial information learned in that context (*5*). It remains unclear whether exposure during sleep to cues associated with newly learned information can selectively enhance the storage of individual memories.

We taught people to associate each of 50 unique object images with a location on a computer screen before a nap (Fig. 1A). Each object was paired with a characteristic sound delivered over a speaker (e.g., cat with meow and kettle with whistle). For the entirety of the nap, white noise was presented at an unobtrusive intensity (about 62 dB sound-pressure level). During non–rapid eye movement (non-REM) sleep, the sounds for 25 of the objects were presented, with white-noise intensity lowered such that overall sound levels were approximately constant (Fig. 1B).

After waking, individuals viewed all 50 objects and attempted to position each one in its original location. Absolute distance measures showed that object placements were more accurate for objects that were cued by their sounds during sleep than for those not cued [1.07 ± 0.08 cm (SE) versus 1.23 ± 0.10 cm (SE), respectively; $t_{11}$ = 2.6; $P < 0.05$]. Forgetting occurred between the final stage of learning and the postnap test, with a smaller decline for cued compared with uncued objects (Fig. 1C). An advantage for cued-object locations computed in this manner was evident in 10 of the 12 participants.

Electroencephalographic (EEG) recordings provided information for determining sleep stages (*6*). Additionally, EEG responses to sound cues were sorted into two conditions via a median split on the difference between pre- and postnap accuracy: (i) less-forgetting accuracy was superior postnap compared with prenap [placements 0.51 ± 0.1 cm (SE) closer to correct]; (ii) more-forgetting accuracy was superior prenap compared with postnap [placements 0.60 ± 0.1 cm (SE) closer to correct]. Average EEG amplitudes measured over the interval from 600 to 1000 ms after sound onset were 15.3 μV greater when there was less forgetting ($t_{11}$ = 3.2, $P < 0.01$). Thus, the degree of recall improvement or decline appeared to have been influenced by sound-induced memory processing during sleep, as indexed by brain potentials.

Participants professed no knowledge that sounds were presented during sleep. Moreover, they performed at chance when forced to guess which sounds were presented during sleep (*6*).

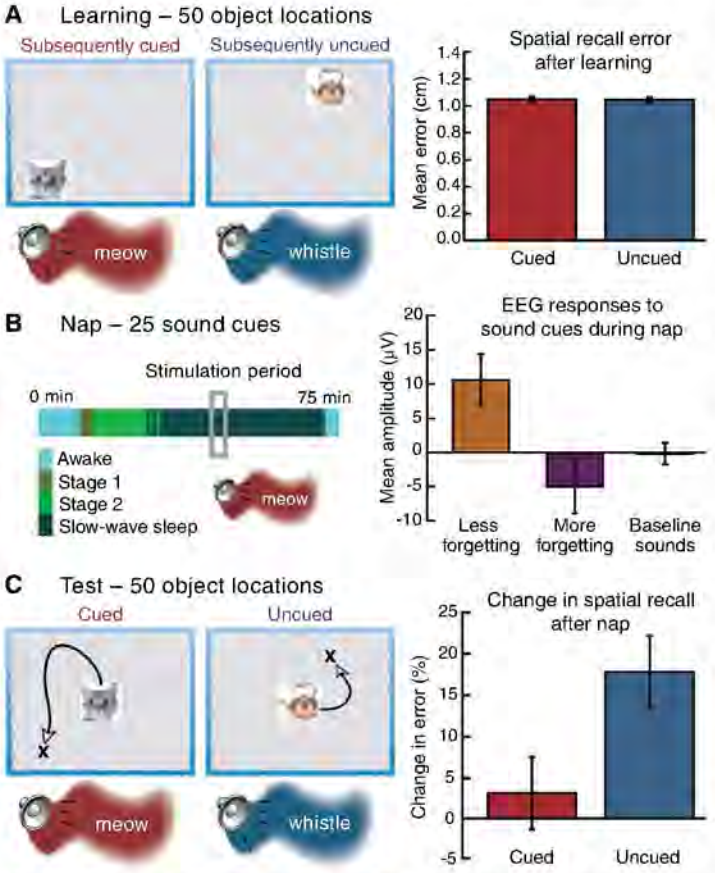


**Fig. 1.** **(A)** Individuals learned object-location associations while hearing object sounds. Accuracy at the final stage of learning was matched for objects subsequently cued or not cued by the sounds (mean ± SE). **(B)** Sleep-staging data are shown for a representative participant, including the 3.5-min sequence of 25 sound cues. Vertex brain potentials differed according to level of forgetting for corresponding object locations. **(C)** After the nap, individuals attempted to place each object in its correct location (arrows simulate motion of objects as individuals complete the task). Better spatial-location retention for cued compared with uncued objects was reflected by a smaller change in error ($t_{11}$ = 3.2, $P < 0.01$).

These results show that information presented during sleep can influence subsequent retrieval during waking. In an additional control experiment with 12 other participants who remained awake, sounds presented after learning did not reliably influence recall accuracy [1.15 cm from target ± 0.07 (SE) versus 1.32 cm ± 0.14 (SE) for cued versus uncued items, respectively; $t_{11}$ = 1.4; $P$ = 0.18].

The extent to which cues affect consolidation in waking subjects may depend on how strongly individuals attend to the cues (*6*). Regardless, we propose that sound cues presented during sleep prompted preferential processing of corresponding object-location associations. The hippocampus has previously been implicated in sleep-mediated consolidation (*3*, *5*). Memory storage in our study likely depends on representations of objects, sounds, and locations in multiple cortical regions, along with hippocampal networks capable of linking these representations together (*2*). Although some sleep theories emphasize general plasticity mechanisms that could benefit all information learned before sleep (*7*), our results show that memory processing during sleep can be highly specific. Certain associations may be preferentially reactivated during sleep as a normal part of memory stabilization and consolidation.

Whereas opportunities for enhancement of memory storage may be available every time we sleep, reminders during sleep can be used to target the reactivation and strengthening of individual memories.

## References and Notes

1. J. L. McGaugh, *Science* **287**, 248 (2000).
2. K. A. Paller, in *Encyclopedia of Neuroscience*, L. R. Squire, Ed. (Academic Press, Oxford, 2009), pp. 741–749.
3. J. Born, B. Rasch, S. Gais, *Neuroscientist* **12**, 410 (2006).
4. R. Stickgold, J. A. Hobson, R. Fosse, M. Fosse, *Science* **294**, 1052 (2001).
5. B. Rasch, C. Büchel, S. Gais, J. Born, *Science* **315**, 1426 (2007).
6. Materials and methods are available as supporting material on *Science* Online.
7. G. Tononi, C. Cirelli, *Brain Res. Bull.* **62**, 143 (2003).
8. Supported by NSF under grant BCS-0818912, by the National Institute of Neurological Disorders and Stroke, and by the Alzheimer's Association.

## Supporting Online Material

www.sciencemag.org/cgi/content/full/326/5956/1079/DC1
Materials and Methods
Tables S1 to S3

13 July 2009; accepted 23 September 2009
10.1126/science.1179013

[1]Northwestern University, Evanston, IL 60208, USA. [2]Beckman Institute for Advanced Science and Technology, Urbana, IL 61801, USA.

*To whom correspondence should be addressed. E-mail: kap@northwestern.edu

# Detection of Gamma Rays from a Starburst Galaxy

F. Acero,[1] F. Aharonian,[2,14] A. G. Akhperjanian,[3] G. Anton,[16] U. Barres de Almeida,[9] A. R. Bazer-Bachi,[4] Y. Becherini,[13] B. Behera,[15] K. Bernlöhr,[2,6] A. Bochow,[2] C. Boisson,[7] J. Bolmont,[19] V. Borrel,[4] J. Brucker,[16] F. Brun,[19] P. Brun,[8] R. Bühler,[2] T. Bulik,[29] I. Büsching,[10] T. Boutelier,[17] P. M. Chadwick,[9] A. Charbonnier,[19] R. C. G. Chaves,[2] A. Cheesebrough,[9] L.-M. Chounet,[11] A. C. Clapson,[2] G. Coignet,[12] M. Dalton,[6] M. K. Daniel,[9] I. D. Davids,[22,10] B. Degrange,[11] C. Deil,[2] H. J. Dickinson,[9] A. Djannati-Ataï,[13] W. Domainko,[2] L. O'C. Drury,[14] F. Dubois,[12] G. Dubus,[17] J. Dyks,[24] M. Dyrda,[28] K. Egberts,[2] D. Emmanoulopoulos,[15] P. Espigat,[13] C. Farnier,[1] S. Fegan,[11] F. Feinstein,[1] A. Fiasson,[12] A. Förster,[2] G. Fontaine,[11] M. Füßling,[6] S. Gabici,[14] Y. A. Gallant,[1] L. Gérard,[13] D. Gerbig,[21] B. Giebels,[11] J. F. Glicenstein,[8] B. Glück,[16] P. Goret,[8] D. Göring,[16] D. Hauser,[15] M. Hauser,[15] S. Heinz,[16] G. Heinzelmann,[5] G. Henri,[17] G. Hermann,[2] J. A. Hinton,[25] A. Hoffmann,[18] W. Hofmann,[2] P. Hofverberg,[2] S. Hoppe,[2] D. Horns,[5] A. Jacholkowska,[19] O. C. de Jager,[10] C. Jahn,[16] I. Jung,[16] K. Katarzyński,[27] U. Katz,[16] S. Kaufmann,[15] M. Kerschhaggl,[6] D. Khangulyan,[2] B. Khélifi,[11] D. Keogh,[9] D. Klochkov,[18] W. Kluźniak,[24] T. Kneiske,[5] Nu. Komin,[8] K. Kosack,[2] R. Kossakowski,[12] G. Lamanna,[12] J.-P. Lenain,[7] T. Lohse,[6] V. Marandon,[13] O. Martineau-Huynh,[19] A. Marcowith,[1] J. Masbou,[12] D. Maurin,[19] T. J. L. McComb,[9] M. C. Medina,[7] J. Méhault,[1] R. Moderski,[24] E. Moulin,[7] M. Naumann-Godo,[11] M. de Naurois,[19] D. Nedbal,[20]* D. Nekrassov,[2] B. Nicholas,[26] J. Niemiec,[28] S. J. Nolan,[9] S. Ohm,[2] J-F. Olive,[4] E. de Oña Wilhelmi,[2] K. J. Orford,[9] M. Ostrowski,[23] M. Panter,[2] M. Paz Arribas,[6] G. Pedaletti,[15] G. Pelletier,[17] P.-O. Petrucci,[17] S. Pita,[13] G. Pühlhofer,[18,15] M. Punch,[13] A. Quirrenbach,[15] B. C. Raubenheimer,[10] M. Raue,[2,30] S. M. Rayner,[9] O. Reimer,[31,32] M. Renaud,[13,2] F. Rieger,[2,30] J. Ripken,[5] L. Rob,[20] S. Rosier-Lees,[12] G. Rowell,[26] B. Rudak,[24] C. B. Rulten,[9] J. Ruppel,[21] V. Sahakian,[3] A. Santangelo,[18] R. Schlickeiser,[21] F. M. Schöck,[16] U. Schwanke,[6] S. Schwarzburg,[18] S. Schwemmer,[15] A. Shalchi,[21] M. Sikora,[24] J. L. Skilton,[25] H. Sol,[7] Ł. Stawarz,[23] R. Steenkamp,[22] C. Stegmann,[16] F. Stinzing,[16] G. Superina,[11] A. Szostek,[23,17] P. H. Tam,[15] J.-P. Tavernet,[19] R. Terrier,[13] O. Tibolla,[2] M. Tluczykont,[5] C. van Eldik,[2] G. Vasileiadis,[1] C. Venter,[10] L. Venter,[7] J. P. Vialle,[12] P. Vincent,[19] M. Vivier,[8] H. J. Völk,[2] F. Volpe,[2] S. J. Wagner,[15] M. Ward,[9] A. A. Zdziarski,[24] A. Zech[7]

Starburst galaxies exhibit in their central regions a highly increased rate of supernovae, the remnants of which are thought to accelerate energetic cosmic rays up to energies of ~$10^{15}$ electron volts. We report the detection of gamma rays—tracers of such cosmic rays—from the starburst galaxy NGC 253 using the High Energy Stereoscopic System (H.E.S.S.) array of imaging atmospheric Cherenkov telescopes. The gamma-ray flux above 220 billion electron volts is $F = (5.5 \pm 1.0_{stat} \pm 2.8_{sys}) \times 10^{-13}$ cm$^{-2}$ s$^{-1}$, implying a cosmic-ray density about three orders of magnitude larger than that in the center of the Milky Way. The fraction of cosmic-ray energy channeled into gamma rays in this starburst environment is five times as large as that in our Galaxy.

Starburst galaxies are characterized by a boosted formation rate of massive stars and an increased rate of supernovae in localized regions, which also exhibit very high densities of gas and of radiation fields. Their optical and infrared (IR) luminosity is dominated by radiation from numerous young massive stars, most of which later explode as supernovae. Given that most cosmic rays in normal galaxies are expected to be accelerated in supernova remnants (*1*), starburst regions represent a favorable environment for the acceleration of cosmic rays, resulting in cosmic-ray energy densities orders of magnitude higher compared with the local value in our Galaxy [e.g., (*2*)]. Cosmic-ray protons can produce gamma radiation by inelastic collisions with ambient gas particles and subsequent $\pi^0$-decay. Primary and secondary cosmic-ray electrons can also produce gamma radiation by Bremsstrahlung and up-scattering of low-energy photons from massive stars or from ambient radiation fields. Starburst galaxies are therefore considered promising sources of gamma-ray emission (*3*, *4*). Here, we report the detection of very high energy (VHE) (>100 GeV) gamma rays from the starburst galaxy NGC 253.

NGC 253, at a distance of 2.6 to 3.9 Mpc (*5*–*7*), is one of the closest spiral galaxies outside the Local Group. It is similar to our Milky Way in its overall star formation rate. Its nucleus, however, is a starburst region (*8*) of very small spatial extent (a few 100 pc), characterized by a very high star formation rate per volume and thus also by a very large mechanical energy production in the form of supernova explosions. Star formation activity is estimated to have been going on for 20 to 30 million years (*8*) and can therefore be considered to be in a steady state for the time scales governing cosmic-ray transport. A supernova rate of ~0.1 year$^{-1}$ has been inferred for the entire galaxy from radio (*9*) and infrared (*10*) observations. The rate is most pronounced in the central starburst region, where a conservative estimate yields a rate of super-

[1]Laboratoire de Physique Théorique et Astroparticules, Université Montpellier 2, CNRS/IN2P3, CC 70, Place Eugène Bataillon, F-34095 Montpellier Cedex 5, France. [2]Max-Planck-Institut für Kernphysik, P.O. Box 103980, D 69029 Heidelberg, Germany. [3]Yerevan Physics Institute, 2 Alikhanian Brothers Street, 375036 Yerevan, Armenia. [4]Centre d'Etude Spatiale des Rayonnements, CNRS/UPS, 9 avenue du Colonel Roche, BP 4346, F-31029 Toulouse Cedex 4, France. [5]Universität Hamburg, Institut für Experimentalphysik, Luruper Chaussee 149, D 22761 Hamburg, Germany. [6]Institut für Physik, Humboldt-Universität zu Berlin, Newtonstrasse 15, D 12489 Berlin, Germany. [7]Laboratoire Univers et Théories, Observatoire de Paris, CNRS, Université Paris Diderot, 5 Place Jules Janssen, 92190 Meudon, France. [8]Institut de Recherche sur les Lois Fondamentales de l'Univers/La Direction des Sciences de la Matière/Commissariat à l'Energie Atomique, CE Saclay, F-91191 Gif-sur-Yvette, Cedex, France. [9]University of Durham, Department of Physics, South Road, Durham DH1 3LE, UK. [10]Unit for Space Physics, North-West University, Potchefstroom 2520, South Africa. [11]Laboratoire Leprince-Ringuet, Ecole Polytechnique, CNRS/IN2P3, F-91128 Palaiseau, France. [12]Laboratoire d'Annecy-le-Vieux de Physique des Particules, Université de Savoie, CNRS/IN2P3, F-74941 Annecy-le-Vieux, France. [13]Astroparticule et Cosmologie (APC), CNRS, Université Paris 7 Denis Diderot, 10, rue Alice Domon et Leonie Duquet, F-75205 Paris Cedex 13, France. UMR 7164 (CNRS, Université Paris VII, CEA, Observatoire de Paris). [14]Dublin Institute for Advanced Studies, 5 Merrion Square, Dublin 2, Ireland. [15]Landessternwarte, Universität Heidelberg, Königstuhl, D 69117 Heidelberg, Germany. [16]Universität Erlangen-Nürnberg, Physikalisches Institut, Erwin-Rommel-Strasse 1, D 91058 Erlangen, Germany. [17]Laboratoire d'Astrophysique de Grenoble, Institut National des Sciences de l'Univers CNRS, Université Joseph Fourier, BP 53, F-38041 Grenoble Cedex 9, France. [18]Institut für Astronomie und Astrophysik, Universität Tübingen, Sand 1, D 72076 Tübingen, Germany. [19]Laboratoire de Physique Nucléaire et des Hautes Energies, Université Pierre et Marie Curie Paris 6, Université Denis Diderot Paris 7, CNRS/IN2P3, 4 Place Jussieu, F-75252, Paris Cedex 5, France. [20]Charles University, Faculty of Mathematics and Physics, Institute of Particle and Nuclear Physics, V Holesovickách 2, 180 00, Prague, Czech Republic. [21]Institut für Theoretische Physik, Lehrstuhl IV: Weltraum und Astrophysik, Ruhr-Universität Bochum, D 44780 Bochum, Germany. [22]University of Namibia, Private Bag 13301, Windhoek, Namibia. [23]Obserwatorium Astronomiczne, Uniwersytet Jagielloński, ul. Orla 171, 30-244 Kraków, Poland. [24]Nicolaus Copernicus Astronomical Center, ul. Bartycka 18, 00-716 Warsaw, Poland. [25]School of Physics and Astronomy, University of Leeds, Leeds LS2 9JT, UK. [26]School of Chemistry and Physics, University of Adelaide, Adelaide 5005, Australia. [27]Toruń Centre for Astronomy, Nicolaus Copernicus University, ul. Gagarina 11, 87-100 Toruń, Poland. [28]Instytut Fizyki Jadrowej PAN, ul. Radzikowskiego 152, 31-342 Kraków, Poland. [29]Astronomical Observatory, The University of Warsaw, Al. Ujazdowskie 4, 00-478 Warsaw, Poland. [30]European Associated Laboratory for Gamma-Ray Astronomy, 4 Place Jussieu, F-75252, Paris Cedex 5, France. [31]Institut für Astro und Teilchenphysik, Leopold-Franzens-Universität Innsbruck, A6020 Innsbruck, Austria. [32]KIPAC Kavli Institute for Particle Physics and Cosmology, Stanford University, Stanford, CA 94305, USA.

*To whom correspondence should be addressed. E-mail: nedbal@ipnp.troja.mff.cuni.cz

novae ~0.03 year$^{-1}$, which is comparable to that in our Galaxy (*8*). This suggests a very high local cosmic-ray energy density. The mean density of the interstellar gas in the central starburst region is $n \cong 600$ protons cm$^{-3}$ (*11*), which is almost three orders of magnitude higher than the average density of the gas in the Milky Way. The thermal continuum emission of NGC 253 peaks in the far infrared (FIR) energy band at ~100 μm, with a luminosity that is ~5 times the total radiation from our own Galaxy (*12*). This FIR emission originates from interstellar dust, which reprocesses starlight from the numerous young massive stars. The emission is highly concentrated toward the small central starburst nucleus. Therefore, the density of the radiation field in the starburst region is about a factor $10^5$ larger than the average value in the inner 100 pc around the Galactic Center. The activity of NGC 253 has been shown to be of a pure starburst nature and not due to an active supermassive black hole (*13*, *14*). Observations of radio (*15*, *16*) and thermal x-ray emission (*17*, *18*) show a hot diffuse halo, consistent with the existence of a galactic wind extending out to ~9 kpc from the galactic plane that transports matter and cosmic rays from the nucleus to intergalactic space and reaches asymptotically a bulk speed of ~900 km/s (*19*).

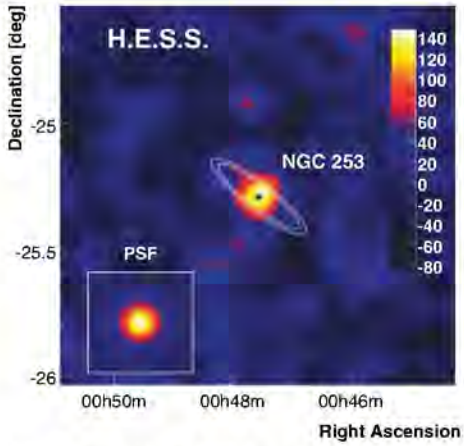


**Fig. 1.** A smoothed map of VHE gamma-ray excess of the 1.5° by 1.5° region around NGC 253. A Gaussian with root mean square of 4.2′ was used to smooth the map in order to reduce the effect of fluctuations. The star shows the optical center of NGC 253. The inlay represents an image of a Monte Carlo simulated point source (i.e., the point-spread function of the instrument). The white contours represent the optical emission of the whole NGC 253, demonstrating that the VHE emission originates in the nucleus and not in the disk. The contours correspond to constant surface brightness of 25 magnitudes arc sec$^{-2}$—traditionally used to illustrate the extent of the optical galaxy—and 23.94 magnitudes arc sec$^{-2}$ according to (*34*).

Given its proximity and its extraordinary properties, NGC 253 was predicted to emit gamma rays at a detectable level (*4*). Recent calculations give similar results (*20*, *21*). Previously, only upper limits have been reported in the gamma-ray range, in the MeV-GeV range by the Energetic Gamma-Ray Experiment Telescope (EGRET) (*22*), and in the TeV range by the High Energy Stereoscopic System (H.E.S.S.) [based on 28 hours of observation (*23*)] and by the Collaboration of Australia and Nippon (Japan) for a Gamma-Ray Observatory in the Outback (CANGAROO) III (*24*). We report the result of continued observations of NGC 253 with the H.E.S.S. telescope system with a much larger data sample. [See the Supporting Online Material (SOM) for a description of the experiment and the detection technique.]

We obtained observations in 2005, 2007, and 2008. After rejecting those data that did not have the required quality, we analyzed 119 hours of live-time data. Even with this extremely long exposure, the measured VHE gamma-ray flux of NGC 253 is at the limit of the H.E.S.S. sensitivity. Thus, advanced image analysis techniques were required to extract a significant signal on top of the uniform background of local cosmic rays impinging on Earth's atmosphere—only one out of $10^5$ recorded air showers represents a gamma ray from NGC 253. We used the Model Analysis technique (*25*) (SOM), based on which we detected an excess of 247 events from the direction of NGC 253 above 220 GeV, corresponding to a statistical significance of 5.2 standard deviations (Fig. 1). The signal is steady and stable (a fit over the period of 3 years to a constant has a chance probability of 47%). The source position is $\alpha_{J2000} = 0^h47^m33^s.6 \pm 30^s$, $\delta_{J2000} = -25°18'8'' \pm 27''$ consistent with the position of the optical center of NGC 253 ($\alpha_{J2000} = 0^h47^m33^s.1$, $\delta_{J2000} = -25°17'18''$). The distribution of excess events is consistent with the point spread function of the H.E.S.S. instrument, implying a source size of less than 4.2′ (at a 1σ confidence level) (see Fig. 2 for a comparison of the angular distribution of the gamma events with a point-like simulated signal). The integral flux of the source above the threshold of 220 GeV is $F(>220\ \text{GeV}) = (5.5 \pm 1.0_{stat} \pm 2.8_{sys}) \times 10^{-13}$ cm$^{-2}$ s$^{-1}$. This corresponds to 0.3% of the VHE gamma-ray flux from the Crab Nebula (*26*); given the well-known uncertainties in the diffusion part of the particle transport properties, as well as the only approximate knowledge of the starburst parameters, it is consistent with the original prediction (*4*) (Fig. 3).

As an external galaxy detected in gamma rays that, as a key property, does not contain a massive black hole of sizeable associated luminosity,

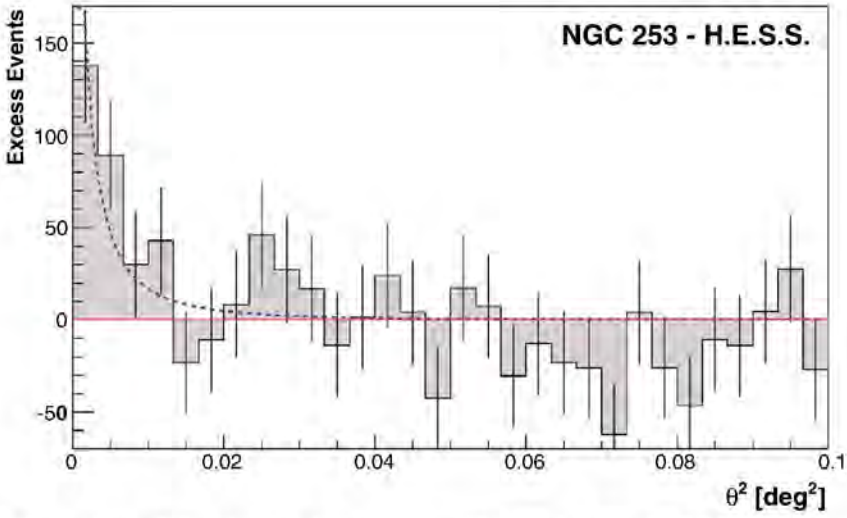


**Fig. 2.** Reconstructed directions of the gamma-ray–like events around NGC 253. θ denotes the angular distance between the arrival direction and the position of the object. The background estimated from off-source regions is uniform in the $\theta^2$ representation and has been subtracted here. The signal is consistent with a H.E.S.S. point source (blue dashed line), corresponding to $\theta <$ 4.2′ or < 3.2 kpc at a distance of 2.6 Mpc.

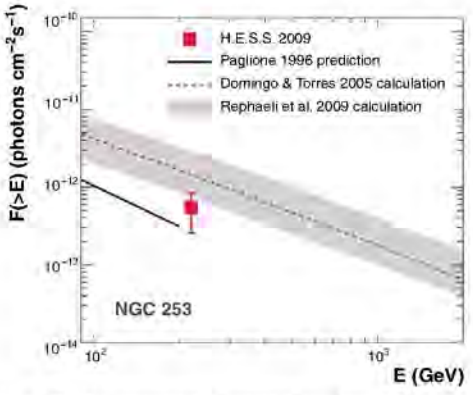


**Fig. 3.** The observed integral flux of gamma rays from NGC 253 (red point) is compared to theoretical estimates (*4*, *20*, *23*). The solid line corresponds to the prediction by (*4*). The dashed line corresponds to the model (*20*). The gray-shaded band denotes the estimate (*21*). The error of the H.E.S.S. measurement includes systematic errors.

NGC 253 is a member of a class of gamma-ray emitters external to the Milky Way and the associated Large Magellanic Cloud (LMC). These gamma-ray emitters apparently produce their own cosmic-ray population. Except for the starburst, NGC 253 is a normal galaxy. So far, only the LMC, a small and close satellite of the Milky Way, was detected in gamma rays with the EGRET instrument (*27*). In contrast, there exists a class of external galaxies detected in gamma rays whose emission is—according to present knowledge—exclusively due to an active galactic nucleus (AGN), driven by a supermassive black hole in their center. Their physical characteristics are quite distinct from normal galaxies and not the subject of the discussion here.

The detection of NGC 253 in VHE gamma rays implies a high energy density of cosmic rays in this system. One can calculate a corresponding cosmic-ray density directly from the H.E.S.S. observations. Assuming a dominant hadronic origin of the gamma-ray emission, the spatial density $N_p(>E_p)$ of the gamma-ray generating protons in the starburst region with an energy exceeding $E_p \approx 220/0.17$ GeV $\approx 1300$ GeV is about $4.9 \times 10^{-12}$ cm$^{-3}$ for the measured gamma-ray flux above 220 GeV, independent of the distance to NGC 253. This is about 2000 times as large as the corresponding Galactic cosmic-ray number density at the solar system and about 1400 times as high as the density at the center of our Galaxy (*28*). Taking $E_p N_p(>E_p)$ as a rough measure of the energy density of cosmic rays above energy $E_p$ in NGC 253, $E_p N_p(>E_p) \approx 6.4$ eV cm$^{-3}$ for $E_p > 1300$ GeV. This is larger than the entire cosmic-ray energy density in the Galaxy near the solar system, which is dominated by GeV-particles.

Gamma-ray production represents one channel for conversion and loss of cosmic rays at TeV energies. The time between inelastic collisions of hadronic cosmic rays and target protons and nuclei at $E_p \approx 1300$ GeV is of the order of $10^5$ years for a mean gas density of about 600 protons cm$^{-3}$. These collisional losses compete with two other processes in starbursts: spatial losses of particles convected out of the considered region by the wind, and diffusive losses (see the SOM for a summary of the cosmic-ray transport characteristics in NGC 253). Because of the very high gas density in the nucleus of NGC 253, the ratio of hadronic gamma-ray production to energy loss by transport is considerably higher than for a galaxy like ours. In the Milky Way, the ~1300-GeV gamma-ray–generating charged particles encounter about 0.6 g cm$^{-2}$ of matter before they escape, extrapolating results from (*29*). Their mean free path for inelastic nuclear collisions is equivalent to about 56 g cm$^{-2}$. Therefore, the Galactic ratio of gamma-ray production probability to the escape probability of 1300 GeV particles is about $10^{-2}$. If the cosmic-ray energy production in the starburst region of NGC 253 is in equilibrium with losses caused by nuclear collisions, then, for the measured gas density and supernova rate—together with an assumed cosmic-ray production efficiency of $10^{50}$ erg per event and a production spectrum $\propto E^{-2.1}$ (*3*, *23*)—the expected integral gamma-ray flux above 220 GeV would be $\approx 10^{-11}$ cm$^{-2}$ s$^{-1}$. The observed flux is smaller than this calorimetric flux by a factor of $\approx 5 \times 10^{-2}$—again independent of the distance. Therefore, the starburst region is only mildly calorimetric. For a comparison, see (*23*, *30*). Nevertheless, the numbers imply that the conversion efficiency of protons into gamma rays in the starburst region of NGC 253 exceeds that in our Galaxy by almost an order of magnitude. This comparatively high efficiency has another consequence: Assuming that the remaining structure of NGC 253 is about the same as in our Galaxy, then the starburst nucleus is about 5 times as bright in VHE gamma rays as in the associated galaxy, and the starburst nucleus should outshine the rest of NGC 253. This is consistent with the detection of a H.E.S.S. point source (Fig. 1).

Given these results, one may ask whether they have a wider importance regarding the nonthermal particle population in the universe. A starburst galaxy such as NGC 253 is a potential model for a phase of galaxy formation as well as for two-body galaxy-galaxy interactions, especially in the dense environment of large galaxy clusters. High-energy gamma-ray emission as a result of these processes should accompany the thermal IR emission of such luminous infrared galaxies. The galactic winds present in these systems are expected to massively populate intergalactic space with nucleosynthesis products and cosmic rays.

## References and Notes


1. F. A. Aharonian *et al.*, *Nature* **432**, 75 (2004).
2. H. J. Völk, U. Klein, R. Wielebinski, *Astron. Astrophys.* **213**, L12 (1989).
3. H. J. Völk, F. A. Aharonian, D. Breitschwerdt, *Space Sci. Rev.* **75**, 279 (1996).
4. T. A. D. Paglione, A. P. Marscher, J. M. Jackson, D. L. Bertsch, *Astrophys. J.* **460**, 295 (1996).
5. D. Puche, C. Carignan, *Astron. J.* **95**, 1025 (1988).
6. R. Rekola *et al.*, *Mon. Not. R. Astron. Soc.* **361**, 330 (2005).
7. The following description is based on a distance of 2.6 Mpc; the final conclusions are, however, independent of distance.
8. C. W. Engelbracht, M. J. Rieke, G. H. Rieke, D. M. Kelly, J. M. Achtermann, *Astrophys. J.* **505**, 639 (1998).
9. R. R. J. Antonucci, J. S. Ulvestad, *Astrophys. J.* **330**, L97 (1988).
10. D. van Buren, M. A. Greenhouse, *Astrophys. J.* **431**, 640 (1994).
11. K. Sorai, N. Nakai, N. Kuno, K. Nishiyama, T. Hasegawa, *Publ. Astron. Soc. Jpn.* **52**, 785 (2000).
12. W. Rice *et al.*, *Astrophys. J. Suppl. Ser.* **68**, 91 (1988).
13. A. Brunthaler *et al.*, *Astron. Astrophys.* **497**, 103 (2009).
14. M. Bauer *et al.*, *Astron. Astrophys.* **467**, 979 (2007).
15. C. L. Carilli, M. A. Holdaway, P. T. P. Ho, C. G. de Pree, *Astrophys. J.* **399**, L59 (1992).
16. V. Heesen, R. Beck, M. Krause, R.-J. Dettmar, *Astron. Astrophys.* **494**, 563 (2009).
17. M. Dahlem, K. A. Weaver, T. M. Heckman, *Astrophys. J. Suppl. Ser.* **118**, 401 (1998).
18. M. Bauer *et al.*, *Astron. Astrophys.* **489**, 1029 (2008).
19. V. N. Zirakashvili, H. J. Völk, *Astrophys. J.* **636**, 140 (2006).
20. E. Domingo-Santamaría, D. F. Torres, *Astron. Astrophys.* **444**, 403 (2005).
21. Y. Rephaeli, Y. Arieli, M. Persic, *Mon. Not. R. Astron. Soc.*, in press; available at http://arXiv.org/abs/0906.1921.
22. J. J. Blom, T. A. D. Paglione, A. Carramiñana, *Astrophys. J.* **516**, 744 (1999).
23. F. Aharonian *et al.*, H.E.S.S. Collaboration. *Astron. Astrophys.* **442**, 177 (2005).
24. C. Itoh *et al.*, CANGAROO Collaboration. *Astron. Astrophys.* **462**, 67 (2007).
25. The Model Analysis is based on a comparison and fit of observed air shower images with a precomputed library of images (*31*); another analysis technique, based on a machine learning algorithm called boosted decision trees (BDT) (*32*), was used to verify the results. It was trained with simulated gamma rays and with real cosmic-ray data from background fields (*33*). Both algorithms yield an improvement by a factor 1.5 to 1.7 in the statistical significance of faint sources compared with the standard image analysis (*26*), as verified with a number of other gamma-ray sources. The Model Analysis result is found to be consistent with the one obtained with the BDT analysis. Details are given in the SOM.
26. F. Aharonian *et al.*, H.E.S.S. Collaboration. *Astron. Astrophys.* **457**, 899 (2006).
27. P. Sreekumar *et al.*, *Astrophys. J.* **400**, L67 (1992).
28. F. Aharonian *et al.*, H.E.S.S. Collaboration. *Nature* **439**, 695 (2006).
29. S. P. Swordy, D. Müller, P. Meyer, J. L'Heureux, J. M. Grunsfeld, *Astrophys. J.* **349**, 625 (1990).
30. T. A. Thompson, E. Quataert, E. Waxman, *Astrophys. J.* **654**, 219 (2007).
31. M. de Naurois, L. Rolland, *Astroparticle Phys.*, in press; available at http://arXiv.org/abs/0907.2610.
32. L. Breiman, J. Friedman, C. J. Stone, R. A. Olshen, *Classification and Regression Trees* (Wadsworth, Stamford, CT, 1984)
33. S. Ohm, C. van Eldik, K. Egberts, *Astroparticle Phys.* **31**, 383 (2009).
34. W. D. Pence, *Astrophys. J.* **239**, 54 (1980).


35. The support of the Namibian authorities and of the University of Namibia in facilitating the construction and operation of H.E.S.S. is gratefully acknowledged, as is the support by the German Ministry for Education and Research (BMBF), the Max Planck Society, the French Ministry for Research, the CNRS-IN2P3 and the Astroparticle Interdisciplinary Programme of the CNRS, the UK Science and Technology Facilities Council (STFC), the IPNP of Charles University, the Polish Ministry of Science and Higher Education, the South African Department of Science and Technology and National Research Foundation, and the University of Namibia. U. Barres de Almeida is supported by the CAPES Coordenação de Aperfeiçoamento de Pessoal de Nível Superior Foundation, Ministry of Education of Brazil. The European Associated Laboratory for Gamma-Ray Astronomy is jointly supported by CNRS and Max-Planck-Gesellschaft. We appreciate the excellent work of the technical support staff in Berlin, Durham, Hamburg, Heidelberg, Palaiseau, Paris, Saclay, and Namibia in the construction and operation of the equipment.


## Supporting Online Material

www.sciencemag.org/cgi/content/full/1178826/DC1
Materials and Methods
SOM Text
Figs. S1 to S5
References


8 July 2009; accepted 15 September 2009
Published online 24 September 2009;
10.1126/science.1178826
Include this information when citing this paper.

# Shape-Controlled Colloidal Interactions in Nematic Liquid Crystals

Clayton P. Lapointe,[1,2] Thomas G. Mason,[2] Ivan I. Smalyukh[1]*

Robust control over the positions, orientations, and assembly of nonspherical colloids may aid in the creation of new types of structured composite materials that are important from both technological and fundamental standpoints. With the use of lithographically fabricated equilateral polygonal platelets, we demonstrate that colloidal interactions and self-assembly in anisotropic nematic fluids can be effectively tailored via control over the particles' shapes. The particles disturb the uniform alignment of the surrounding nematic host, resulting in both a distinct equilibrium alignment and highly directional pair interactions. Interparticle forces between polygonal platelets exhibit either dipolar or quadrupolar symmetries, depending on whether their number of sides is odd or even, and drive the assembly of a number of ensuing self-assembled colloidal structures.

Self-assembly of micrometer- and nanometer-scale colloidal particles into ordered structures is of wide-ranging interest for both fundamental science and technological applications (*1*). In isotropic liquids such as water, the electrostatic and entropic forces that drive the assembly of spherical colloids are typically isotropic, limiting the overall landscape of possible structures. Concentrated suspensions of monodisperse spherical particles are an important example; these can form three-dimensional (3D) colloidal crystals that are markedly similar to their atomic counterparts. However, colloidal crystals formed in this fashion are restricted to lattices with high packing fractions, such as hexagonal close-packed or face-centered cubic (*2*). The generation of anisotropic interactions is necessary to increase the complexity and diversity of colloidal architectures formed by such interactions (*3*–*6*). Oriented assemblies of particles can be produced by means such as nonuniform patterning of their surfaces (*3*), anisotropic deposition of colloids onto solid substrates (*4*), or application of external fields (*5*). Alternatively, introducing anisotropy directly into a solvent by using a nematic liquid crystal (NLC), one can engender anisotropic interaction forces between colloids that are not present in ordinary fluids (*7*). NLCs are composed of rod-shaped molecules with long molecular axes aligned along a common direction (*8*). The local average molecular orientation is often represented by a unit vector $\mathbf{n}$ with inversion symmetry $\mathbf{n} \equiv -\mathbf{n}$, referred to as the director. The dependence of $\mathbf{n}$ as a function of spatial position $\mathbf{r}$ is described with a director field $\mathbf{n}(\mathbf{r})$. Anisotropic molecular interactions at NLC surfaces, known as surface anchoring, result in a preferential alignment and boundary conditions for $\mathbf{n}(\mathbf{r})$. Colloids immersed in NLCs deform the surrounding director field because of this surface anchoring and induce point or line defects [regions where $\mathbf{n}(\mathbf{r})$ is discontinuous] in the nematic bulk (Fig. 1, A and B) or at the nematic-particle interface (Fig. 1C), unless the surface anchoring is weak or the particles are small (supporting online material fig. S1) (*9*). The particles and accompanying defects introduce long-range gradients in $\mathbf{n}(\mathbf{r})$ that depend on particle size (*9*), type and strength of surface anchoring (*10*), confinement (*11*, *12*), and external fields (*13*). The elastic energy due to these gradients depends on the particles' relative positions and gives rise to interactions mediated by elasticity. Even for spherical particles in NLCs (Fig. 1, A to C), elastic interactions are highly anisotropic and can lead to a host of self-assembled structures ranging from linear and branched chains to 2D crystals (*7*, *9*–*16*). Reminiscent of electrostatic interactions exhibited by charge distributions, elastic colloidal interactions bear qualitatively different symmetries that mimic the dipolar (Fig. 1A) or quadrupolar (Fig. 1, B and C) symmetries of $\mathbf{n}(\mathbf{r})$ around isolated particles.

We demonstrate that altering the shapes of particles can lead to marked changes in the symmetry of their elastic interactions and the resulting colloidal assemblies in NLCs. Optical polarizing microscopy (PM) and fluorescence confocal polarizing microscopy (FCPM) show

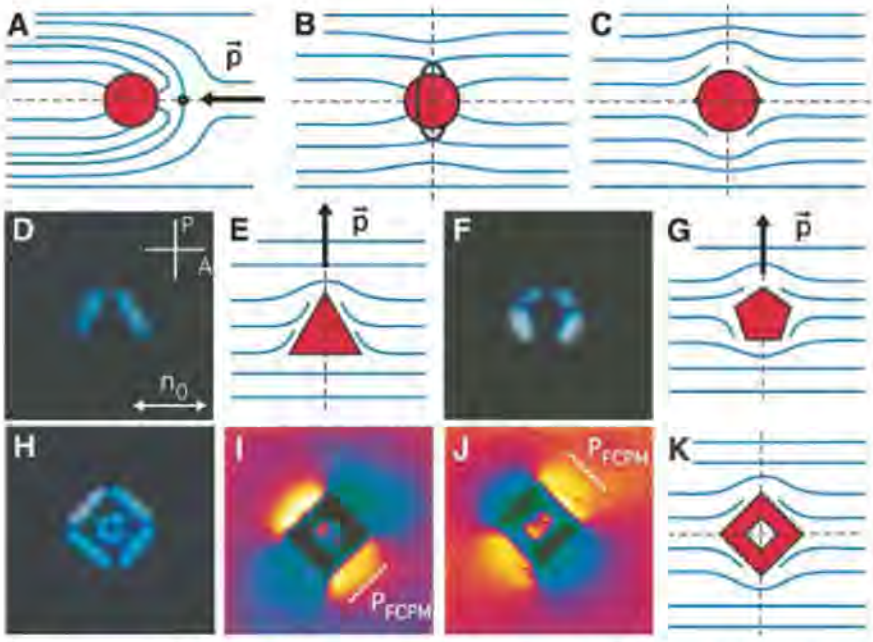


**Fig. 1.** Shape-controlled director field configurations around colloidal particles immersed in a uniformly aligned NLC. (**A**) A spherical colloid with strong vertical anchoring induces a hyperbolic point defect (black dot) in the bulk of the NLC forming a dipolar $\mathbf{n}(\mathbf{r})$ structure (blue lines) with the elastic dipole moment $\mathbf{p}$ parallel to $\mathbf{n}_0$. (**B**) A spherical particle with vertical anchoring and encircled by a line defect in the equatorial plane (black line) gives a quadrupolar director structure. (**C**) A colloidal sphere with planar degenerate anchoring induces two surface point defects (black dots) at the poles along $\mathbf{n}_0$ and forms a quadrupolar configuration of $\mathbf{n}(\mathbf{r})$. Optical PM micrographs show that polygons with an odd number of sides, such as triangles (**D** and **E**) and pentagons (**F** and **G**), in 5CB orient with one side parallel to $\mathbf{n}_0$ and, as shown in (E and G), induce dipolar $\mathbf{n}(\mathbf{r})$ with elastic dipole moments $\mathbf{p}$ perpendicular to $\mathbf{n}_0$. (**H**) PM image showing a square platelet oriented with its diagonal axis parallel to $\mathbf{n}_0$ producing quadrupolar distortions. (**I** and **J**) FCPM images of $\mathbf{n}(\mathbf{r})$ obtained for linear polarizations ($P_{FCPM}$) at ±45° to $\mathbf{n}_0$, and color-coded fluorescence intensity varying from minimum (black) to increasingly higher intermediate (green, blue, red) and maximum (yellow) values. (**K**) Reconstructed quadrupolar director field for a square platelet in 5CB. Dashed lines denote mirror symmetry planes of the $\mathbf{n}(\mathbf{r})$ configurations. The lateral edge lengths of triangles, squares, and pentagons are 3.0 μm, 4.5 μm, and 1.5 μm, respectively. All platelets have a thickness of 1 μm. The square-shaped particles contain a square hole with 2-μm sides.

[1]Department of Physics, Renewable and Sustainable Energy Institute, and Liquid Crystals Materials Research Center, University of Colorado at Boulder, Boulder, CO 80309, USA. [2]Department of Chemistry and Biochemistry, Department of Physics and Astronomy, and California NanoSystems Institute, University of California at Los Angeles, Los Angeles, CA 90095, USA.

*To whom correspondence should be addressed. E-mail: ivan.smalyukh@colorado.edu

that platelet colloids with equilateral polygonal shapes exhibit well-defined alignment and elastic deformations of $\mathbf{n}(\mathbf{r})$ that have either dipolar or quadrupolar symmetry. Colloidal polygons with an odd number of sides form elastic dipoles, whereas even-sided particles form elastic quadrupoles. Using model polygonal platelets shaped as triangles, squares, and pentagons, we demonstrate that their shape dictates the resulting $\mathbf{n}(\mathbf{r})$ symmetry as well as the symmetry of the ensuing elastic interactions. Particle tracking video microscopy (*17*), combined with optical tweezing of particle pairs, provides direct measurements of anisotropic interaction forces.

Monodisperse platelet colloids of uniform thickness and predesigned shapes are fabricated with the use of photolithography (*18*). Micron-sized polygonal colloids of triangular, square, and pentagonal shapes are produced using an ultraviolet-sensitive photoresist (SU-8) on Si wafers (*19*). After exposure and development, the particles are released from the wafers into an organic solvent and transferred into pentylcyanobiphenyl (5CB), a room temperature NLC. Sample cells consisting of parallel glass plates separated by 10- to 60-μm spacers are filled with colloidal dispersions in 5CB by capillary action and sealed with epoxy. The far-field alignment direction $\mathbf{n}_0$ is set by unidirectional rubbing of the polyimide coated inner surfaces of the cell. The samples are studied with an inverted optical microscope equipped with a confocal laser scanning unit and a holographic optical tweezers system (*20*) operating at $\lambda = 1064$ nm. The 3D structure of $\mathbf{n}(\mathbf{r})$ around the colloids is determined with lateral and vertical resolution of ~0.5 μm with the use of FCPM (*21*). For FCPM observations, 0.01 weight percent of anisotropic fluorescent dye was dissolved homogeneously in 5CB (*19*); at this concentration, the rodlike dye molecules do not alter the NLC properties and orient parallel to 5CB molecules so that the contrast in the fluorescence image arises from spatial changes in $\mathbf{n}(\mathbf{r})$ (*21*). Imaging and optical tweezing are performed simultaneously with a 100× oil-immersion objective.

PM images reveal the $\mathbf{n}(\mathbf{r})$ deformations surrounding isolated particles of each type suspended in aligned 5CB (Fig. 1). When $\mathbf{n}_0$ is oriented along the linear polarization of incident light, distorted regions where $\mathbf{n}(\mathbf{r})$ departs from $\mathbf{n}_0$ alter the polarization state of transmitted light and appear bright when viewed through the analyzer. Polygonal platelets always orient with their larger-area top and bottom surfaces parallel to $\mathbf{n}_0$, suggesting planar degenerate anchoring at the interface of SU-8 and 5CB. Polygons that have an odd number of sides ($N$), such as triangles and pentagons, orient with one of their sides along $\mathbf{n}_0$, and bright lobes are visible near their other sides (Fig. 1, D and F). However, colloids with even $N$, such as squares, align with one diagonal axis along $\mathbf{n}_0$, and bright regions appear symmetrically along all outer and inner edges (Fig. 1H). PM and FCPM textures indicate the presence of three mirror symmetry planes of the $\mathbf{n}(\mathbf{r})$ deformations, which intersect the particle's center of mass: one coplanar with both $\mathbf{n}_0$ and the unit vector $\mathbf{v}$ normal to the platelet's larger-area faces, a second parallel to the faces, and a third plane orthogonal to $\mathbf{n}_0$. Thus, the $\mathbf{n}(\mathbf{r})$ structure is quadrupolar, as schematically shown in Fig. 1K, resembling the symmetry of elastic quadrupoles formed by spherical particles (Fig. 1, B and C). Further, because the strongest FCPM signal corresponds to regions where $\mathbf{n}(\mathbf{r})$ is parallel to the linear FCPM polarization, the fluorescence images in Fig. 1, I and J, demonstrate that $\mathbf{n}(\mathbf{r})$ is indeed quadrupolar and consistent with surface anchoring of 5CB on SU-8 photoresist being degenerate planar (*22*).

In the case of triangles and pentagons with odd $N$, however, the mirror symmetry plane that is coplanar with both $\mathbf{n}_0$ and $\mathbf{v}$ is broken so that the $\mathbf{n}(\mathbf{r})$ structure is dipolar (Fig. 1, E and G), unlike that of other previously studied colloids promoting planar surface anchoring (*15*, *23*). Moreover, the elastic dipole moment $\mathbf{p}$ is orthogonal to $\mathbf{n}_0$ (Fig. 1E), in contrast to what is seen for colloids with vertical surface anchoring and $\mathbf{p}$ parallel to $\mathbf{n}_0$ (*7*, *11*, *14*, *24*), as shown in Fig. 1A. Examples of dipoles that align orthogonally to field lines are rare but can be formed by dipolar pairs of line defects in NLCs (*19*) and vortex spin configurations in ferromagnets (*8*). Similar to a sphere with planar anchoring shown in Fig. 1C, the shape-dictated dipolar structures of odd-$N$ platelets do not give rise to point or line defects in the NLC bulk. The dipolar $\mathbf{n}(\mathbf{r})$ symmetry of odd-$N$ platelets should be stable with respect to varying particle size and the strength of surface anchoring at their interfaces (fig. S1) (*19*). This is different from the case of dipoles formed by spherical colloids accompanied by bulk point defects (Fig. 1A) observed only for strong anchoring and for particle sizes larger than ~1 μm, but not for smaller colloids for which a quadrupolar $\mathbf{n}(\mathbf{r})$ (Fig. 1B) is of lower energy (*9*). For odd-$N$ polygonal platelets, although the magnitude of $\mathbf{p}$ decreases with decreasing particle size or weakening anchoring strength (fig. S1), the alignment and dipolar symmetry should retain down to particle sizes of ~50 to 100 nm, at which the planar boundary conditions at the platelet surfaces are expected to partially relax (*19*). For $N = 5$, the magnitude of $\mathbf{p}$ is smaller than that for $N = 3$ (Fig. 1), and we expect that it decreases further as $N$ increases and ultimately vanishes in the limit $N \rightarrow \infty$, corresponding to a circular disc with quadrupolar $\mathbf{n}(\mathbf{r})$ (*9*).

The director field configurations surrounding regular polygons (Fig. 1) can be understood within an elegant theoretical framework that is built on an analogy with electrostatics (*25*–*27*). Within the one-elastic constant approximation (*19*), minimization of the NLC elastic energy $U_{el} = (K/2)\int d^3\mathbf{r}(\nabla\mathbf{n})^2$ [where $K$ is an average Frank elastic constant, and $(\nabla\mathbf{n})^2 = (\nabla \cdot \mathbf{n})^2 + (\nabla \times \mathbf{n})^2$] leads to Laplace's equation for $\mathbf{n}(\mathbf{r})$. Far from the particle, deviations from $\mathbf{n}_0$ are small, and $\mathbf{n}(\mathbf{r})$ can be expanded in a multipole series containing elastic monopole, dipole, and quadrupole terms that decay with distance $r$ as $1/r$, $1/r^3$, and $1/r^5$, respectively. The predicted absence of an elastic monopole, when no external torque is present (*25*), is consistent with the observed dipolar symmetry of $\mathbf{n}(\mathbf{r})$, as well as the equilibrium orientation of polygons with odd $N$. For example, $\mathbf{n}(\mathbf{r})$ would have no planes of mirror symmetry for a triangle or pentagon oriented so that all edges are neither parallel nor perpendicular to $\mathbf{n}_0$. Consequently, an elastic torque would be present, and the system would not be in mechanical equilibrium. There are two possible ori-

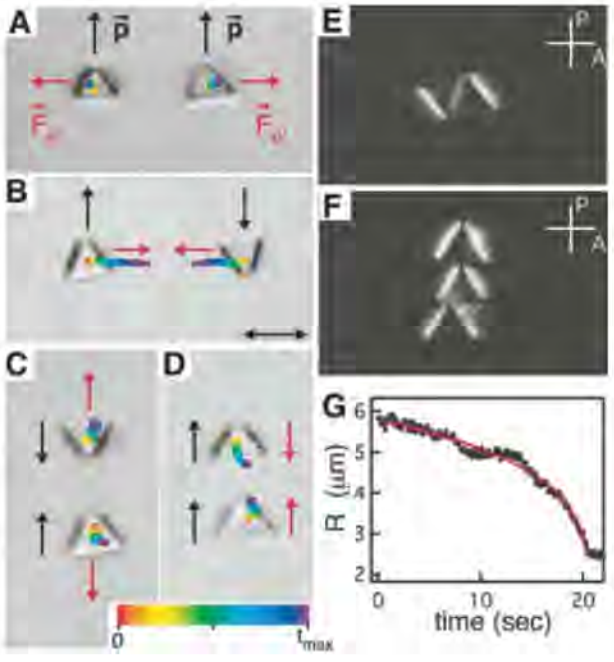


**Fig. 2.** Elastic dipole-dipole pair interactions of triangular colloids in 5CB and their assembly into chains. (**A** to **D**) Color-coded trajectories of triangles with parallel [(A) and (D)] and antiparallel [(B) and (C)] dipole moments; the trajectories are overlaid on top of the first video frame, with colors representing time according to the scale in the inset. Maximum elapsed times $t_{max}$: (A) 20.5 s, (B) 29.6 s, (C) 53.3 s, and (D) 24.8 s. Red arrows show the direction of the elastic force $\mathbf{F}_{el}$. PM images of two types of aggregates: (**E**) antiparallel dipole chain along $\mathbf{n}_0$ and (**F**) parallel dipole chain oriented perpendicular to $\mathbf{n}_0$. (**G**) Time dependence of the pair separation for the trajectories shown in (D). The red curve shows a fit with the expected $R(t)$ for a dipole-dipole attraction balanced by a viscous drag. The direction of the far-field director $\mathbf{n}_0$ is shown by the double-headed arrow in (B).

entations for a triangle or a pentagon with ensuing $\mathbf{n}(\mathbf{r})$ having at least two planes of mirror symmetry: (i) one with a side along $\mathbf{n}_0$ giving an elastic dipole with $\mathbf{p}$ perpendicular to $\mathbf{n}_0$ and (ii) another with a side oriented perpendicular to $\mathbf{n}_0$ (in this case, $\mathbf{p}$ would be parallel to $\mathbf{n}_0$). Evidently, the former has lower elastic energy because this is the equilibrium orientation observed in the experiments. The alignment of colloidal polygons with even $N$, such as square-shaped particles, can be understood in a similar fashion. Orientations for which neither of the diagonals are parallel to $\mathbf{n}_0$ would give rise to an elastic torque and are unstable. When the sample is heated into the isotropic phase, no preferred orientation is observed (fig. S2), confirming the elastic nature of the alignment of polygons in the nematic phase. Furthermore, observations during multiple heating and cooling cycles show that different sides (odd $N$) and diagonals (even $N$) can align along $\mathbf{n}_0$ each time the sample is quenched into the nematic phase, demonstrating that there is no preference in the selection of these sides or diagonals.

Although the orientations of the polygonal edges are constrained relative to $\mathbf{n}_0$, a platelet's surface normal $\mathbf{v}$ is free to rotate about $\mathbf{n}_0$ in the bulk of a ≈60-μm-thick NLC cell, indicating that the elastic energy is independent of such rotations (*28*). Confinement to cells of thickness comparable to the lateral size of platelets (≈10 μm) inhibits rotations about $\mathbf{n}_0$, and the platelike colloids orient parallel to the cell substrates to minimize the elastic energy due to the planar anchoring at the top and bottom surfaces of the colloids. To explore the directionality and strength of anisotropic elastic-pair interactions, we control the initial positions and orientations of particles with the use of optical tweezers (*11*, *12*, *15*) and then track their motion using video microscopy after release from the laser traps. When the center-to-center separation vector $\mathbf{R}$ for two triangles is along $\mathbf{n}_0$, elastic repulsion occurs for parallel dipoles (Fig. 2A), whereas attraction takes place for antiparallel dipoles (Fig. 2B). The opposite is true for situations when $\mathbf{R}$ is perpendicular to $\mathbf{n}_0$; antiparallel dipoles repel (Fig. 2C) and parallel dipoles attract (Fig. 2D). Two types of self-assembled chainlike aggregates are observed: (i) antiparallel dipole chains in which the triangles aggregate along $\mathbf{n}_0$ (Fig. 2E) and (ii) chains perpendicular to $\mathbf{n}_0$ consisting of parallel dipoles (Fig. 2F). Chaining of triangular colloids perpendicular to $\mathbf{n}_0$ is a consequence of the dipoles' alignment orthogonal to $\mathbf{n}_0$. The dipolar nature of the elastic interaction is further evidenced by the time dependence of particle separation $R(t)$ for a pair of triangles aggregating along $\mathbf{n}_0$ (Fig. 2G). Because the system is highly overdamped (Reynolds number << 1), inertial forces are negligible and the elastic force $F_{el}$ is balanced by a viscous Stokes drag $F_{drag} = -\zeta dR/dt$, where $\zeta$ is a drag coefficient, and $dR/dt$ is the time-derivative of the particle separation $R(t)$. For an elastic dipolar force $F_{el} = -\kappa_d/R^4$ (where $\kappa_d$ is a constant that depends on $K$ and the geometry and size of the particle), integration of the equation of motion $F_{el} + F_{drag} \approx 0$ yields $R(t) = (R_0^5 - 5\alpha_d t)^{1/5}$, where $\alpha_d = \kappa_d/\zeta$, and $R_0$ is the initial separation at time $t = 0$ when particles are released from the traps. $R(t)$ fits the data well with one adjustable parameter $\alpha_d = 63.1 \pm 0.5\ \mu m^5/s$ (red curve in Fig. 2G). Using an estimate of the drag coefficient $\zeta \sim (2 \text{ to } 4) \times 10^{-6}$ kg/s (*29*) and the maximum relative velocity $dR/dt \approx 1$ μm/s determined from the data in Fig. 2G, one obtains a maximum attractive elastic force of 2 to 4 pN near contact at $R \approx 2.6$ μm. This force and the corresponding binding energy $\approx 5 \times 10^{-18}$ J ($\approx 1200 k_B T$, where $k_B$ is Boltzmann's constant) for a pair of triangles are comparable to those measured for spherical colloids of similar size (*11*, *12*, *15*).

Square-shaped platelets aggregate at angles intermediate between 0 and 90° relative to $\mathbf{n}_0$, suggesting a nondipolar symmetry of elastic interactions. A time series of video frames in Fig. 3A shows two interacting squares after release from the optical traps used to position them initially with $\mathbf{R}$ parallel to $\mathbf{n}_0$. The squares repel while gradually moving sideways (frames 1 and 2), then attract along ≈45° to $\mathbf{n}_0$ (frames 3 and 4), and ultimately aggregate with adjacent sides touching to form a chain that equilibrates at ≈40° to $\mathbf{n}_0$. This equilibration angle decreases with the addition of more particles into the linear chain, consistent with the planar anchoring at the NLC-colloid surfaces. Kinked chains as well as more symmetric structures are also possible. For example, a square and a two-particle chain can attract (Fig. 3, C and D) and form a structure in which the individual square orientations match those of isolated ones.

To elucidate the angular dependence of elastic interactions between square particles, two are positioned at a fixed center-to-center separation of $R = 12.3$ μm and various angles between $\mathbf{R}$ and $\mathbf{n}_0$: $\theta = 0, \pm\pi/8, \pm\pi/4$, and $3\pi/8$, as shown in the inset of Fig. 3E. For each $\theta$, the particles are released from the optical traps, tracked with video microscopy for 13 s while the traps are off, and then moved back to the same initial locations. Because the elastic forces at $R = 12.3$ μm are weak ($\sim 10^{-2}$ pN), we time-average an ensemble of 10 particle trajectories for each $\theta$ to mitigate the effects of Brownian motion. The average relative trajectories at various $\theta$ are shown in Fig. 3E. Elastic repulsion occurs for pair orientations parallel ($\theta = 0$) and perpendicular ($\theta = \pi/2$) to $\mathbf{n}_0$, whereas strong attraction along $\mathbf{R}$ takes place at $\theta = \pm\pi/4$. At $\theta = \pm\pi/8$, the elastic force drives the particles sideways toward $\theta = \pm\pi/4$ while gradually becoming attractive. The angular dependence of the expected force between quadrupoles at a large fixed separation

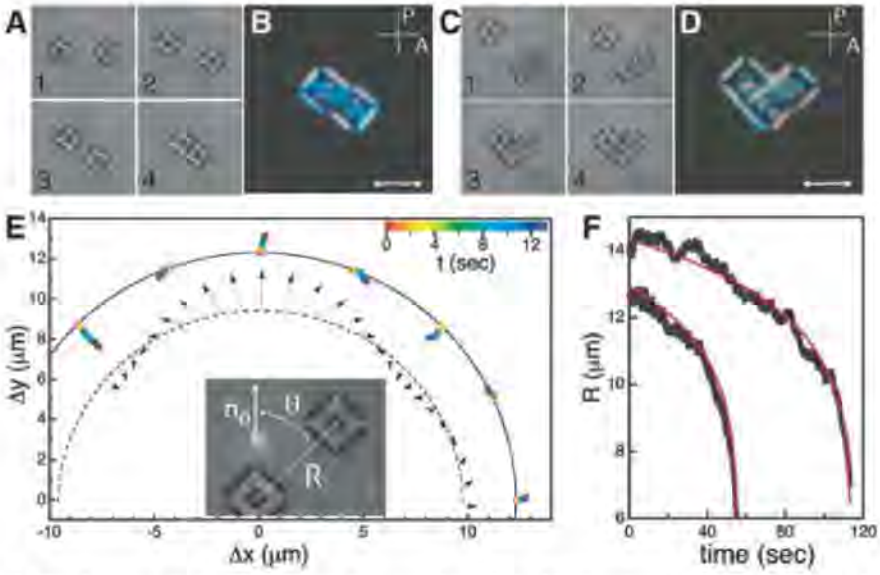


**Fig. 3.** Quadrupolar elastic interactions of square platelets and their assembly in 5CB. (**A**) Video frames (1 to 4) showing squares released from optical traps with their initial center-to-center separation $\mathbf{R}$ parallel to $\mathbf{n}_0$ (horizontal). Elastic interactions drive the particles to form a chain at ≈40° to $\mathbf{n}_0$. The elapsed times for each frame are: (1) 0 s, (2) 60.2 s, (3) 77.7 s, and (4) 81.3 s. (**B**) PM image of the two-square chain formed in (A). (**C**) Video frames (1 to 4) showing the aggregation of a square with a two-square chain resulting in a structure symmetric about the plane orthogonal to $\mathbf{n}_0$. The elapsed times in each frame are: (1) 0 s, (2) 40.5 s, (3) 53.3 s, and (4) 56.2 s. (**D**) PM micrograph of the aggregate formed in (C). (**E**) Relative displacements $\Delta x$, $\Delta y$ of square platelets that are color-coded as a function of elapsed time (inset) after being released with the initial separation $R = 12.3$ μm. The data sets are obtained by particle tracking and provided for the initial pair-separation vector $\mathbf{R}$ at angles $\theta = 0, \pm\pi/8, \pm\pi/4$, and $3\pi/8$ relative to $\mathbf{n}_0$. Black arrows indicate the quadrupolar pair interaction force at large fixed separation $R$ and various $\theta$. (**F**) $R(t)$ dependences for a pair of squares with initial separations $R_0 = 14.3$ μm and 12.9 μm. Red lines show least-squares fits with the $R(t)$ expected for a quadrupolar interaction balanced by a viscous drag. The orientation of the far-field director $\mathbf{n}_0$ is shown by the white double-headed arrows in (B) and (D).

(shown by black arrows in Fig. 3E) (*9*, *15*) exhibits marked correlation with the measured displacements, confirming the quadrupolar nature of elastic forces between colloidal squares. These results imply that the presence of the hole in a colloidal square and, more generally, other modifications to the platelet's topology are inconsequential to the anisotropy of interactions, as long as the quadrupolar $\mathbf{n}(\mathbf{r})$ symmetry is preserved.

Quadrupolar forces are expected to decay with distance as $\sim R^{-6}$ (*9*, *15*). To test if square platelets interact in this manner, we have measured the relative positions of two colloidal squares along $\theta = \pi/4$ from initial separations $R_0 = 14.3$ and 12.9 μm (Fig. 3F). From a balance of a quadrupolar elastic force $F_{elq} = -\kappa_q/R^6$ with a viscous drag, one obtains the time-dependent particle separation $R(t) = (R_0^7 - 7\alpha_q t)^{1/7}$, where $\alpha_q = \kappa_q/\zeta$. The two sets of data in Fig. 3F can be fit with $R(t)$ using only one adjustable parameter $\alpha_q = (1.6 \pm 0.1) \times 10^5$ μm$^7$/s. Taking the average elastic constant $K \approx 7$ pN (*30*), an effective viscosity $\eta \approx 0.075$ Pa·s for 5CB, as well as the side length $L = 4.5$ μm of the platelet, dimensional analysis gives an estimate of $\alpha_q \sim KL^5/\eta = 1.7 \times 10^5$ μm$^7$/s, in reasonable agreement with these experiments. Using a drag coefficient $\zeta \approx 1.9 \times 10^{-6}$ kg/s of a square platelet in 5CB [determined by probing its diffusive motion with video microscopy (fig. S3)] and $\alpha_q = 1.6 \times 10^5$ μm$^7$/s, we calculate a maximum attractive elastic force of ≈20 pN near contact at $R = 4.5$ μm and corresponding binding energy $\approx 3 \times 10^{-17}$ J ($\approx 7000 k_B T$).

In conclusion, elastic colloidal interactions in NLCs are sensitive to the colloids' shapes. Equilibrium director field configurations around equilateral polygonal colloids exhibit dipolar symmetry if they have odd $N$ (i.e., triangles or pentagons) and quadrupolar symmetry if $N$ is even, giving rise to dipolar and quadrupolar elastic colloidal interactions, respectively. Elastic dipole moments of polygonal platelets orient perpendicular to the far-field director $\mathbf{n_0}$. Dipole-dipole forces drive their assembly into chains perpendicular to $\mathbf{n_0}$ if their dipoles are parallel and chains along $\mathbf{n_0}$ if their dipoles are antiparallel. Although the symmetry of these highly directional elastic forces should not change over a broad range of particle sizes (~50 nm to tens of microns), the strength can vary substantially. One can envision the design of such interactions for the assembly of colloidal architectures ranging from anisotropic aggregates to new types of colloidal crystals and optical metamaterials with well-defined alignment relative to the far-field director.

### References and Notes


1. G. M. Whitesides, B. Grzybowski, *Science* **295**, 2418 (2002).
2. V. J. Anderson, H. N. Lekkerkerker, *Nature* **416**, 811 (2002).
3. K. Zhao, T. G. Mason, *Phys. Rev. Lett.* **99**, 268301 (2007).
4. K. J. Stebe, E. Lewandowski, M. Ghosh, *Science* **325**, 159 (2009).
5. T. C. Halsey, *Science* **258**, 761 (1992).
6. S. C. Glotzer, *Science* **306**, 419 (2004).
7. P. Poulin, H. Stark, T. C. Lubensky, D. A. Weitz, *Science* **275**, 1770 (1997).
8. P. M. Chaikin, T. C. Lubensky, *Principles of Condensed Matter Physics* (Cambridge Univ. Press, Cambridge, 2000).
9. H. Stark, *Phys. Rep.* **351**, 387 (2001).
10. I. I. Smalyukh, A. V. Kachynski, A. N. Kuzmin, P. N. Prasad, *Proc. Natl. Acad. Sci. U.S.A.* **103**, 18048 (2006).
11. I. Musevic, M. Skarabot, U. Tkalec, M. Ravnik, S. Zumer, *Science* **313**, 954 (2006).
12. M. Vilfan *et al.*, *Phys. Rev. Lett.* **101**, 237801 (2008).
13. I. Dierking, G. Biddulph, K. Matthews, *Phys. Rev. E* **73**, 011702 (2006).
14. J.-C. Loudet, P. Barois, P. Poulin, *Nature* **407**, 611 (2000).
15. I. I. Smalyukh, O. D. Lavrentovich, A. N. Kuzmin, A. V. Kachynski, P. N. Prasad, *Phys. Rev. Lett.* **95**, 157801 (2005).
16. A. B. Nych *et al.*, *Phys. Rev. Lett.* **98**, 057801 (2007).
17. J. C. Crocker, D. G. Grier, *J. Colloid Interface Sci.* **179**, 298 (1996).
18. C. J. Hernandez, T. G. Mason, *J. Phys. Chem. C* **111**, 4474 (2007).
19. Materials and methods are available as supporting material on *Science* Online.
20. D. G. Grier, *Nature* **424**, 810 (2003).
21. I. I. Smalyukh, S. V. Shiyanovskii, O. D. Lavrentovich, *Chem. Phys. Lett.* **336**, 88 (2001).
22. C. Tsakonas, A. J. Davidson, C. V. Brown, N. J. Mottram, *Appl. Phys. Lett.* **90**, 111913 (2007).
23. C. Lapointe *et al.*, *Science* **303**, 652 (2004).
24. U. Tkalec, M. Skarabot, I. Musevic, *Soft Matter* **4**, 2402 (2008).
25. F. Brochard, P. G. de Gennes, *J. Phys. (Paris)* **31**, 691 (1970).
26. T. C. Lubensky, D. Pettey, N. Currier, H. Stark, *Phys. Rev. E* **57**, 610 (1998).
27. B. I. Lev, S. B. Chernyshuk, P. M. Tomchuk, H. Yokoyama, *Phys. Rev. E* **65**, 021709 (2002).
28. Because of a density mismatch of ~0.2 g/cm$^3$ between SU-8 and 5CB, particles tend to sediment toward the lower half of the cell and come to rest at a height ≈5 μm at which the repulsive particle-substrate interaction due to the $\mathbf{n}(\mathbf{r})$ deformations balances gravity (*23*).
29. The drag coefficient of a triangular platelet can be estimated as that of a thin disk with the radius $a$ circumscribing the edges of the triangle: $\zeta \approx 32\eta a/3$. Using a representative value of shear viscosity $\eta \approx 0.075$ Pa·s for 5CB (*9*), one finds $\zeta \approx 2 \times 10^{-6}$ kg/s. Although this analysis is only approximate, it gives reasonable estimates for platelet colloids, as verified experimentally (*19*).
30. L. M. Blinov, V. G. Chigrinov, *Electrooptic Effects in Liquid Crystal Materials* (Springer, New York, 1996).


31. We thank K. Zhao for assistance with the fabrication of colloids, and we acknowledge support from the Institute for Complex and Adaptive Matter and from NSF grants DMR 0645461, DMR 0847782, CHE 0450022, and DMR 0820579.


### Supporting Online Material

www.sciencemag.org/cgi/content/full/326/5956/1083/DC1
Materials and Methods
Figs. S1 to S3
References

20 May 2009; accepted 15 September 2009
10.1126/science.1176587

# Atmospheric Sulfur in Archean Komatiite-Hosted Nickel Deposits

**Andrey Bekker,[1, 2]*† Mark E. Barley,[3]* Marco L. Fiorentini,[3] Olivier J. Rouxel,[4] Douglas Rumble,[1] Stephen W. Beresford[3]**

Some of Earth's largest iron-nickel (Fe-Ni) sulfide ore deposits formed during the Archean and early Proterozoic. Establishing the origin of the metals and sulfur in these deposits is critical for understanding their genesis. Here, we present multiple sulfur isotope data implying that the sulfur in Archean komatiite-hosted Fe-Ni sulfide deposits was previously processed through the atmosphere and then accumulated on the ocean floor. High-temperature, mantle-derived komatiite magmas were then able to incorporate the sulfur from seafloor hydrothermal sulfide accumulations and sulfidic shales to form Neoarchean komatiite-hosted Fe-Ni sulfide deposits at a time when the oceans were sulfur-poor.

Submarine Fe-Ni sulfide deposits hosted in komatiites (mantle-derived ultramafic rocks with high magnesium content) produce ~10% of the world's annual Ni, making them an important type of ore-bearing deposits (*1*). Mineralization of komatiite-hosted Fe-Ni sulfides can form either massive ores at the base of, or disseminated/blebby ores within, komatiite lava flows and sills (fig. S1). Komatiite-hosted massive Fe-Ni sulfide deposits are most abundant during periods of elevated mantle plume magmatism and continental crustal growth. In the Neoarchean and Paleoproterozoic, such events occurred around 2.95, 2.7, and 1.9 billion years ago (Ga), which correspond to global peaks in the abundance of banded iron formations, sulfidic black shales, and volcanogenic massive Fe-Cu-Zn sulfide deposits (*2*, *3*).

Initial efforts to determine the source of sulfur in these deposits suggested that sulfides were transported directly from the mantle (*4*, *5*). It was later proposed based on a wide range of volcanological, stratigraphic, geochemical, sulfur isotopic, thermodynamic, and fluid dynamic constraints that the magmas assimilated sulfur either during ascent or emplacement on the sea floor [see (*1*) for case studies] because the sulfur content of the mantle is too low (*6*), komatiites result from high degrees of melting in the mantle, and a negative pressure feedback on sulfur content limits sulfide saturation in mafic magmas (*7*). Analysis of multiple sulfur isotopes makes it

possible to further test sulfur assimilation models. Most Archean sedimentary sulfides show $\delta^{34}S$ values (*8*) near that of the mantle (*9*–*12*), whereas hydrothermal alteration and metamorphism tend to homogenize variability in primary $\delta^{34}S$ values (*13*). Therefore, $\delta^{34}S$ data alone do not unambiguously constrain the sulfur source for Archean komatiite-hosted Fe-Ni sulfides. However, the products of non–mass-dependent fractionation of sulfur isotopes (*14*, *15*) by photochemical reactions in the Archean oxygen-free atmosphere—oxidized water-soluble sulfur species with negative $\Delta^{33}S$ values (*8*) and reduced sulfur species with positive $\Delta^{33}S$ values—can be readily distinguished from mantle-derived magmatic sulfides (*13*, *16*). For example, it was shown that sulfur from sulfate aerosols was preferentially incorporated into hydrothermally influenced deposits such as banded iron formations, barites, volcanogenic massive sulfides (VMS), and sedimentary exhalative deposits, as well as early diagenetic pyrite nodules in black shales resulting in negative $\Delta^{33}S$ values (*15*–*21*). Sulfur from elemental sulfur aerosols preferentially contributed to disseminated sulfides in sedimentary rocks, including black shales, yielding positive $\Delta^{33}S$ values (*14*, *19*).

Archean sedimentary rocks are also characterized by highly variable iron isotope signatures that can be reflective of their origin. A range of $\delta^{56}Fe$ values for banded iron formations, VMS deposits, and black shales has been linked to abiogenic and/or biogenic redox-controlled processes in the Archean oceans. In contrast, magmatic minerals and mantle-derived mafic rocks experience little iron isotope fractionation (*22*, *23*).

Here, we combine $\Delta^{33}S$ and $\delta^{56}Fe$ analyses to determine the source(s) of sulfur in Archean komatiite-hosted Fe-Ni sulfide deposits. Samples were collected from the ~2.71-Ga Agnew-Wiluna and Norseman-Wiluna greenstone belts of Western Australia and the time-equivalent Abitibi greenstone belt, Canada (*24*). The samples represent massive, blebby, and disseminated komatiite-hosted Fe-Ni sulfides, sulfidic black shales, and massive sulfide lenses in felsic metavolcanic and volcaniclastic sedimentary rocks underlying the komatiite sequences. The isotope signatures of Fe-Ni sulfide deposits were then compared with those of possible sulfur sources in host rocks such as sulfidic organic matter–rich shales and massive sulfide lenses (*24*) to determine their origin.

The magmatic komatiite-hosted Fe-Ni sulfides show significant ranges in sulfur isotope values, which can be directly compared with those of sulfur-rich crustal lithologies (Fig. 1). The magmatic Fe-Ni sulfides have a 10.6 per mil (‰) range in $\delta^{34}S$ values that overlaps with the $\delta^{34}S$ range of sulfidic black shales and VMS deposits. The volcanogenic massive sulfides have consistently negative $\Delta^{33}S$ values as low as −0.7‰, within the range of values obtained for Archean hydrothermal barites and sulfides (*14*–*18*, *20*, *21*). In contrast, sulfidic black shales underlying komatiite-hosted Fe-Ni sulfide deposits have near 0‰ or positive $\Delta^{33}S$ values, as high as +2.3‰, within the range of values for disseminated pyrites in fine-grained siliciclastic sediments of this age (*14*, *15*, *19*). Basal komatiite-hosted massive Fe-Ni sulfides from the Agnew-Wiluna greenstone belt and the Alexo deposit of the Abitibi greenstone belt display negative $\Delta^{33}S$ values ranging from −1.0 to −0.4‰, suggesting that almost all sulfur in these deposits came from the assimilated hydrothermal massive sulfides. Magmatic matrix, disseminated, and blebby komatiite-hosted Fe-Ni sulfides from the Agnew-Wiluna greenstone belt display more variable $\Delta^{33}S$ values, ranging from +0.3 to −0.6‰, which is consistent with mixing between multiple crustal and mantle sulfur sources. In contrast, subeconomic blebby Fe-Ni sulfides from a komatiitic sill at Dundonald, Abitibi greenstone belt, which intruded into a sulfidic black shale, have essentially the same positive $\Delta^{33}S$ values as the pyrite in the enclosing shale. The massive sulfide lenses have negative $\Delta^{33}S$ values, suggesting that some fraction of sulfur was derived from thermochemical seawater sulfate reduction.

The negative $\delta^{56}Fe$ values of the VMS and shale-hosted sulfides (Fig. 2) are within the range of sulfides in Archean fine-grained sediments and modern seafloor hydrothermal deposits (*22*, *25*). The highly negative $\delta^{56}Fe$ values of massive sulfide lenses are consistent with direct pyrite precipitation at the sea floor from iron-rich

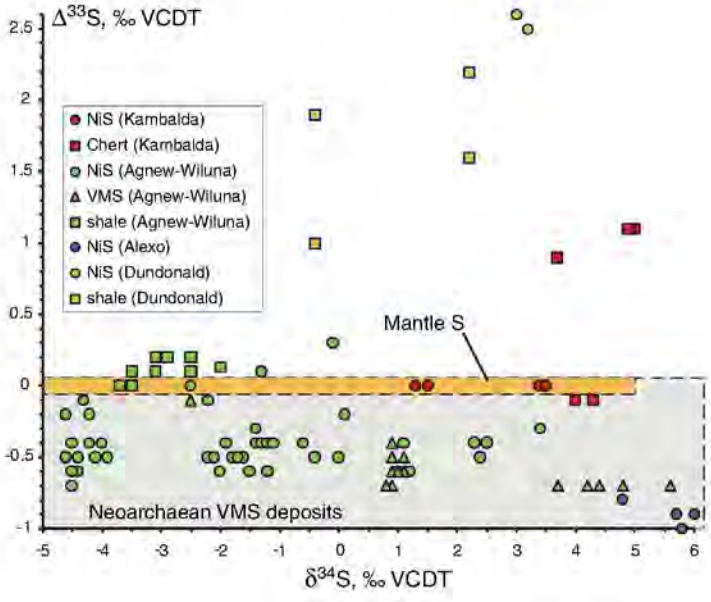


**Fig. 1.** $\Delta^{33}S$ versus $\delta^{34}S$ data for the studied samples and fields for mantle sulfur and Neoarchean VMS deposits. $\delta^{34}S$ values for mantle sulfur are from (*12*) and those for Neoarchean VMS deposits are from (*33*). $\Delta^{33}S$ values for the Archean mantle are inferred from (*13*, *16*) and those for the Neoarchean VMS deposits are from the current study and (*15*, *16*, *18*, *21*).

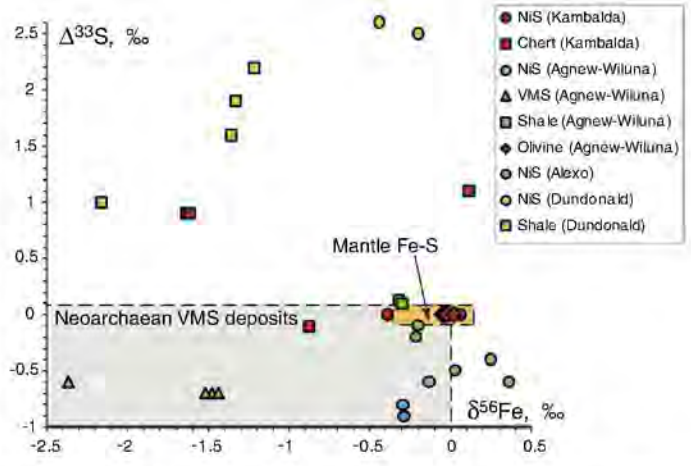


**Fig. 2.** $\Delta^{33}S$ and $\delta^{56}Fe$ data. The range of $\Delta^{33}S$ values for magmatic mantle-derived Fe-S and Neoarchean VMS deposits is from Fig. 1. $\delta^{56}Fe$ values (0.09 ± 0.05‰) for the bulk silicate Earth (*23*) were expanded down to −0.35‰ based on a fractionation factor between pyrrhotite and peralkaline rhyolitic melt (*26*) to infer the iron isotope composition of magmatic mantle-derived Fe-S. We assume that the fractionation factor for pentlandite is similar or very close to the one for pyrrhotite. The origin of Fe-Ni sulfides with positive $\delta^{56}Fe$ values (up to 0.4‰) and negative $\Delta^{33}S$ values (down to −0.6‰) is enigmatic; however, assimilation of in situ sulfidized iron oxides may explain their iron and sulfur isotope systematics. The range of iron isotope composition of Neoarchean VMS deposits (−2.4 to 0.0‰) is very close to that of modern submarine VMS deposits (−2.1 to −0.1‰) (*25*).

[1]Geophysical Laboratory, Carnegie Institution of Washington, 5251 Broad Branch Road, NW, Washington, DC 20015, USA. [2]Department of Geological Sciences, University of Manitoba, Winnipeg, MB, R3T 2N2, Canada. [3]Centre for Exploration Targeting, School of Earth and Environment, University of Western Australia, 35 Stirling Highway, Crawley WA 6009, Australia. [4]Marine Chemistry and Geochemistry Department, Woods Hole Oceanographic Institution, Woods Hole, MA 02543, USA.

*These authors contributed equally to this work.
†To whom correspondence should be addressed. E-mail: bekker@cc.umanitoba.ca

Archean seawater or high-temperature hydrothermal fluids. In contrast, the $\delta^{56}$Fe values for Fe-Ni sulfide samples display a limited range from +0.4 to −0.4‰. This range is much smaller than that in both the VMS and shale-hosted sulfides and might reflect either minor crustal iron contribution to iron-rich komatiite magmas or high-temperature iron isotope fractionations. Indeed, recent experimental studies (*26*) have demonstrated a significant iron isotope fractionation between pyrrhotite and peralkaline rhyolitic melts ($\Delta^{56}Fe_{FeS\text{-}melt}$ = −0.35 ± 0.04‰), but smaller fractionation factors are expected at a lower oxidation state in komatiite melts. Olivine $\delta^{56}$Fe values tightly clustered at 0 ± 0.1‰ (Fig. 2) likely reflect magma composition, minor iron isotope fractionation during olivine crystallization (*23*, *27*), and postdepositional alteration (*24*). Because iron isotope values of Fe-Ni sulfides are fractionated toward both positive and negative values, it seems unlikely that magmatic processes alone are responsible for this range. Iron oxide minerals in banded iron formations typically have strongly positive to slightly negative iron isotope values, whereas iron sulfides in Archean black shales and VMS deposits of various ages systematically show negative iron isotope values (*25*, *28*). We therefore infer that the iron isotope composition of komatiite-hosted Fe-Ni sulfides reflects a mixture of locally assimilated crustal materials with heterogeneous iron isotope compositions and mantle-derived melts with iron isotope values close to 0‰.

Multiple sulfur and iron isotope signatures of Fe-Ni sulfides indicate assimilation of sulfur-rich crustal lithologies with a large range of $\Delta^{33}$S and $\delta^{56}$Fe values into sulfur-poor komatiitic magma with $\Delta^{33}$S and $\delta^{56}$Fe values close to 0‰. Consequently, whereas the sulfur isotope composition of Fe-Ni sulfides was dominated by crustal sources, their iron isotope composition was buffered by komatiite melt. The only notable exception in our data set to an unambiguous crustal sulfur source for Fe-Ni sulfide deposits is the basal komatiite-hosted massive Fe-Ni sulfide ore of the Kambalda deposit, which does not show non–mass-dependent fractionation of sulfur isotopes and has unfractionated to moderately negative iron isotope values. These data can be explained by either a magmatic sulfur source (*29*) or assimilation of multiple crustal sulfur sources and mixing with mantle-derived sulfur in a dynamic lava channel during transport (*30*), leading to dilution of weak non–mass-dependent sulfur isotope signal and equilibrium iron isotope fractionation between pyrrhotite and silicate magma (*26*). In this case, when non–mass-dependent fractionation in magmatic sulfides is lacking or small, sulfur isotopes neither prove nor disprove assimilation of Archean wall-rock sulfides.

Our data suggest that most Neoarchean komatiites achieved sulfide saturation by assimilating wall-rock crustal sulfur. Most Archean deeper-water sediments were sulfur-poor due to low sulfate contents in the Archean anoxic oceans (*11*) except for those deposited during the short-lived mantle plume breakout events when extensive subaerial and submarine volcanism delivered larger amounts of sulfur compounds to the atmosphere and oceans (*2*, *3*, *31*). Even these sulfidic black shales were largely restricted to shallow margins in basins far from komatiite plumbing systems (Fig. 3). The ~2.7-Ga mineralized komatiites correspond to a peak in the global abundance of VMS deposits (*2*). The sulfur in the latter deposits is a mixture of mantle-derived sulfur with $\delta^{34}S \approx \Delta^{33}S = 0$‰ leached at depth from the underlying volcanic rocks with a minor, but significant, component derived by thermochemical reduction of seawater sulfate with negative $\Delta^{33}$S values that was produced by atmospheric photochemical reactions (*15*, *18*). Consequently, VMS deposits within or near active volcanic plumbing systems would have been an abundant and easily accessible sulfur source in ~2.7-Ga submarine environments (Fig. 3).

Recent studies of mineralized komatiites at Mount Keith, Western Australia, indicate magma emplacement in a proximal felsic volcanic environment, with both felsic and komatiitic magmas most likely using the same plumbing system (*32*). Formation of basal massive Fe-Ni sulfide deposits in komatiites such as Mount Keith therefore likely involved cannibalization of VMS deposits during magma emplacement along preexisting plumbing systems in submarine felsic volcanic successions or in lava channels (Fig. 3). However, our results also indicate that there is no single unique process to achieve sulfide saturation in komatiite magmas. Whereas Agnew-Wiluna and, possibly, Alexo deposits used sulfur from volcanogenic massive sulfide deposits, Dundonald and Kambalda deposits likely derived sulfur from wall-rock sediments. The style and size of Fe-Ni sulfide deposits are therefore largely determined by the sulfur source in country rock. Consequently, emplacement of hot komatiite magmas during a peak in magmatic activity in submarine volcanic arc environments and in mantle plume breakouts appears to be the key to formation of komatiite-hosted Fe-Ni sulfide deposits in Archean greenstone belts at a time when the oceans and sediments were sulfur-poor.

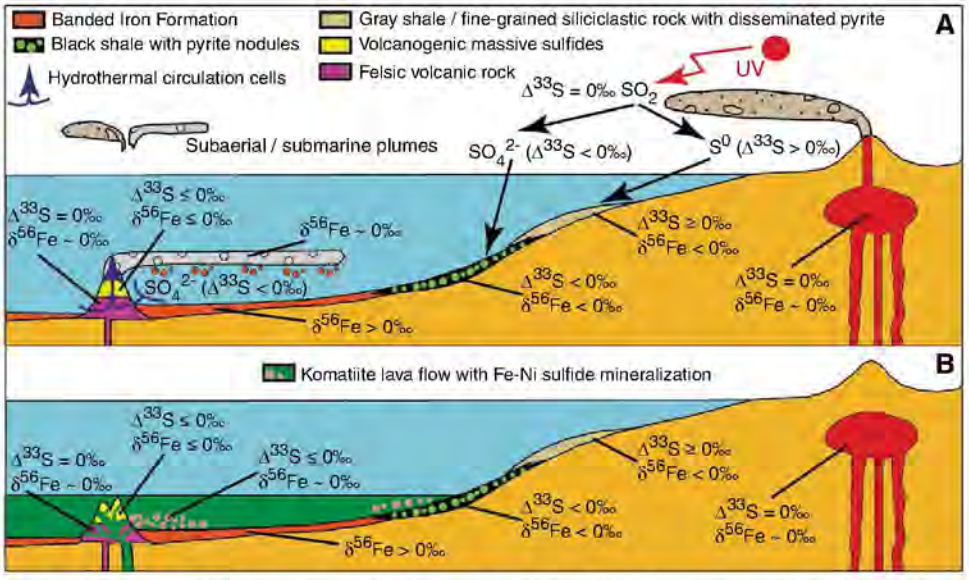


**Fig. 3.** **(A)** Schematic diagram illustrating iron and multiple sulfur isotope composition of depositional environments in the footwall of Fe-Ni sulfide–bearing komatiites associated with the ~2.7-Ga mantle plume breakout event that were influenced by non–mass-dependent sulfur isotope fractionation in the Archean anoxic atmosphere. UV: ultraviolet. **(B)** Volcanogenic massive sulfide deposits associated with felsic volcanic rocks in the footwall were cannibalized when komatiite magma was emplaced along the preexisting plumbing systems (e.g., Mount Keith deposit of the Agnew-Wiluna greenstone belt), thus providing sulfur for large, economic Fe-Ni sulfide deposits. Some Fe-Ni sulfide deposits derived sulfur from sulfidic black shales. The schematically shown Mount Keith komatiite flow is up to 500 m thick and several kilometers in width and length.

## References and Notes


1. N. T. Arndt, *Komatiite* (Cambridge Univ. Press, Cambridge, 2008).
2. M. E. Barley, B. Krapez, D. I. Groves, R. Kerrich, *Precambrian Res.* **91**, 65 (1998).
3. K. C. Condie, *Earth Planet. Sci. Lett.* **163**, 97 (1998).
4. A. J. Naldrett, *Can. Inst. Min. Metal. Bull.* **66**, 45 (1973).
5. A. J. Naldrett, A. R. Turner, *Precambrian Res.* **5**, 43 (1977).
6. W. F. McDonough, S.-S. Sun, *Chem. Geol.* **120**, 223 (1995).
7. R. F. Wendlandt, *Am. Mineral.* **67**, 877 (1982).
8. $\delta^{33}$S and $\delta^{34}$S values are conventional δ notations with respect to VCDT (Vienna–Canyon Diablo Troilite) defined as $\delta'S = 1000[(^{x}S/^{32}S)_{sample}/(^{x}S/^{32}S)_{VCDT} - 1]$, where $x$ is 33 and 34, respectively. $\Delta^{33}$S value ($\Delta^{33}S = \delta^{33}S^{*} - 0.515\delta^{34}S^{*}$), a measure of non–mass-dependent fractionation of S isotopes, is based on $\delta^{33}S^{*}$ and $\delta^{34}S^{*}$ values defined as $\delta'S^{*} = 1000\ln[(\delta'S/1{,}000) + 1]$, where $x$ is 33 and 34, respectively.
9. C. M. Lesher, *Rev. Econ. Geol.* **4**, 45 (1989).
10. A. J. Naldrett, *Econ. Geol.* **75**, 628 (1981).
11. D. E. Canfield, *Annu. Rev. Earth Planet. Sci.* **33**, 1 (2005).
12. R. R. Seal, *Rev. Mineral. Geochem.* **61**, 633 (2006).
13. S. C. Penniston-Dorland *et al.*, *Geology* **36**, 979 (2008).
14. J. Farquhar, H. Bao, M. Thiemens, *Science* **289**, 756 (2000).

15. J. Farquhar, B. A. Wing, in *Mineral Deposits and Earth Evolution*, I. McDonald, A. J. Boyce, I. B. Butler, R. J. Herrington, D. A. Polya, Eds. (Geological Society of London Special Publication, London, 2005), vol. 248, pp. 167–177.
16. Y. Ueno, S. Ono, D. Rumble, S. Maruyama, *Geochim. Cosmochim. Acta* **72**, 5675 (2008).
17. H. Bao, D. Rumble III, D. R. Lowe, *Geochim. Cosmochim. Acta* **71**, 4868 (2007).
18. J. W. Jamieson, B. A. Wing, M. D. Hannington, J. Farquhar, *Econ. Geol.* **101**, 1055 (2006).
19. S. Ono, N. J. Beukes, D. Rumble III, *Precambrian Res.* **169**, 48 (2009).
20. Y. Shen, J. Farquhar, A. Masterson, A. J. Kaufman, R. Buick, *Earth Planet. Sci. Lett.* **279**, 383 (2009).
21. P. Philippot *et al.*, *Science* **317**, 1534 (2007).
22. O. Rouxel, A. Bekker, K. Edwards, *Science* **307**, 1088 (2005).
23. B. L. Beard *et al.*, *Chem. Geol.* **195**, 87 (2003).
24. Supporting material is available on *Science* Online.
25. O. Rouxel, W. C. Shank III, W. Bach, K. J. Edwards, *Chem. Geol.* **252**, 214 (2008).
26. J. A. Schuessler, R. Schoenberg, H. Behrens, F. Von Blanckenburg, *Geochim. Cosmochim. Acta* **71**, 417 (2007).
27. F.-Z. Teng, N. Dauphas, R. T. Helz, *Nature* **320**, 1620 (2008).
28. C. M. Johnson, B. L. Beard, N. J. Beukes, C. Klein, J. M. O'Leary, *Contrib. Mineral. Petrol.* **144**, 523 (2003).
29. J. G. Foster, D. D. Lambert, L. R. Frick, R. Mass, *Nature* **382**, 703 (1996).
30. C. M. Lesher, M. O. Burnham, *Can. Mineral.* **39**, 421 (2001).
31. M. E. Barley, A. Bekker, B. Krapez, *Earth Planet. Sci. Lett.* **238**, 156 (2005).
32. N. M. Rosengren, S. W. Beresford, B. A. Grguric, R. A. F. Cas, *Econ. Geol.* **100**, 149 (2005).
33. M. D. Hannington, W. Bleeker, I. Kjarsgaard, in *The Giant Kidd Creek Volcanogenic Massive Sulfide Deposit, Western Abitibi Subprovince, Canada*, M. D. Hannington, C. Tucker Barrie, Eds. (Economic Geology, Monograph 10, 1999), pp. 163–224.
34. Supported by a NAI International Collaboration grant (M.L.F.); AMIRA and the Australian Research Council DP 0988326 grants (M.E.B., M.L.F., and S.W.B.); NSF grant EAR-937 05-45484 (A.B.); NAI award NNA04CC09A (A.B.); Natural Sciences and Engineering Research Council of Canada 938 Discovery grant (A.B.); NAI, Carnegie Institution of Washington Node, and NASA Cosmochemistry program (D.R.); and NSF OCE-0622982 and EAR-0820661 grants (O.J.R.). We acknowledge R. Cas, M. Houlé, M. Lesher, J. Farquhar, A. L. Masterson, and M. Auro for helpful discussions and experimental assistance and two anonymous reviewers for constructive comments.

**Supporting Online Material**

www.sciencemag.org/cgi/content/full/326/5956/1086/DC1
Materials and methods
SOM Text
Figs. S1 to S4
Table 1
References

15 June 2009; accepted 14 September 2009
10.1126/science.1177742

# Geophysical Detection of Relict Metasomatism from an Archean (~3.5 Ga) Subduction Zone

**Chin-Wu Chen,[1]* Stéphane Rondenay,[1] Rob. L. Evans,[2] David B. Snyder[3]**

When plate tectonics started on Earth has been uncertain, and its role in the assembly of early continents is not well understood. By synthesizing coincident seismic and electrical profiles, we show that subduction processes formed the Archean Slave craton in Canada. The spatial overlap between a seismic discontinuity and a conductive anomaly at ~100 kilometers depth, in conjunction with the occurrence of mantle xenoliths rich in secondary minerals representative of a metasomatic front, supports cratonic assembly by subduction and accretion of lithospheric fragments. Although evidence of cratonic assembly is rarely preserved, these results suggest that plate tectonics was operating as early as Paleoarchean times, ~3.5 billion years ago (Ga).

Archean cratons form the core of many of Earth's continents. By virtue of their longevity, they offer important clues about plate tectonic processes during early geological times. A question of particular interest is whether subduction is the main mechanism of cratonic assembly and, if so, when this process began to operate. Answers to these questions may be found in the lithosphere of the Archean Slave craton, which is located in the northwestern Canadian Shield (Fig. 1) and represents the oldest known fragment of the North American continent (*1*). The Slave craton has been studied extensively to reveal processes of cratonic assembly as it is well exposed and has been insulated from plate margin processes for more than 2 billion years. In the center of the Slave craton, inclusions of rock fragments from the mantle indicate that the lithospheric mantle is separated into two distinct layers at 140- to 150-km depth, with a harzburgitic upper layer exhibiting a very high degree of iron depletion (*2*, *3*) and a lherzolitic lower layer that is less depleted in iron (*2*). Previous seismic studies identified remnants of subducted oceanic lithosphere (*4*–*6*), believed to be linked to the final stages of assembly of the Slave craton during the late Archean (~2.6 Ga) and to its stabilization during the Proterozoic (~1.84 Ga). Despite these results, there remains much uncertainty over the timing and mechanisms of the formation of the Slave craton. For example, it is unknown when its >200-km-thick lithospheric root was in place, and if it was constructed solely by subduction accretion (*7*) or by successive accretion-collision episodes (*8*).

Here, we investigate coincident seismic receiver-function (*9*) and electrical profiles across the Slave craton to further understand the mechanisms of cratonic assembly. Two main features in the seismic profile reveal the structure of the underlying lithosphere (Fig. 2). First, the crust-mantle boundary, or Moho, appears as a positive (downward slow-to-fast) velocity gradient across the entire profile at depths ranging from 34 to 41 km, marking a southward thickening of the crust. Second, a pronounced negative (downward fast-to-slow) velocity gradient dips southward from 96- to 124-km depth beneath the center of the craton. Portions of this seismic discontinuity have been identified previously (*5*, *6*), but here it is seen as a continuous profile. The lack of *SH*-response by the seismic discontinuity (*9*) suggests that it is not caused by anisotropic parameters (*4*). Thus, the amplitude of the discontinuity suggests a 9 to 21% isotropic velocity contrast (*9*).

The electrical image was constructed by means of the magnetotelluric (MT) technique, which measures time variations of the magnetic and electric fields at Earth's surface to infer electrical resistivity structure in the subsurface, and reveals a conductive anomaly in the central Slave mantle (*10*) (Fig. 2B). The anomaly has a conductivity of 0.01 to 0.03 S/m, which is two orders of magnitude higher than that of the surrounding mantle and therefore prevents penetration of the signal (and imaging) at greater depths. It has a depth ranging from ~80 to 120 km with a southward dip, and may be caused by interconnected graphite films deposited along grain boundaries (*10*).

When displayed simultaneously in vertical cross section (Fig. 2, A and B), the seismic discontinuity and the conductive anomaly exhibit a pronounced spatial coincidence. Although the conductive anomaly appears slightly shallower (by ~4 to 9 km) than the seismic discontinuity, this difference is within reasonable error of the depth estimates associated with each technique—namely, 10 km for the seismic profile and 15 km for the MT image (*9*, *10*). In map projection, the regions over which these structures are observed overlap with the lateral extent of the upper-mantle harzburgitic layer (*2*) (Fig. 1).

The coexistence of the seismic and electrical discontinuities suggests that they have a common origin. A review of the possible causes for these anomalies, with support from petrological analy-

[1]Department of Earth, Atmospheric, and Planetary Sciences, Massachusetts Institute of Technology (MIT), 77 Massachusetts Avenue, Cambridge, MA 02139, USA. [2]Department of Geology and Geophysics, Woods Hole Oceanographic Institution, MS 22, Woods Hole, MA 02543, USA. [3]Geological Survey of Canada, 615 Booth Street, Ottawa, Ontario K1A 0E9, Canada.

*To whom correspondence should be addressed. E-mail: cwchen@mit.edu

ses of xenoliths, favors a mineralogical explanation (*9*). A positive thermal anomaly, a layer of partial melt, or the presence of water could all lower seismic velocities (*9*), but they cannot be sustained over long time scales (millions of years) in the cold, stable lithosphere of the Slave craton. Similarly, compositional variations due to the juxtaposition of different mantle domains or to variable degrees of melt depletion cannot account for more than 1.5% of seismic velocity variation (*11*) or one-third of an order of magnitude reduction in electrical resistivity (*12*). Although no single mineral can produce both anomalies, secondary minerals that formed from metasomatic alteration may be responsible. For the seismic anomaly, phlogopite is the most likely candidate, as it is stable at pressure and temperature conditions corresponding to the location of the anomaly (*13*) and represents up to ~50% of the bulk composition of the eclogitic mantle xenoliths that originated ~100 km below the central Slave craton (*14*). This quantity of phlogopite could reduce *S*-wave velocities by ~17% relative to the host eclogite and surrounding mantle peridotite (*15*), which is in agreement with the observed seismic discontinuity. Phlogopite also increases electrical conductivity (*13*), but experimental data show that it can contribute at most 1% of the observed conductive anomaly (*16*). We attribute the additional conductivity increase to thin, interconnected films of graphite deposited along grain boundaries, the presence of which has been invoked to explain this and other conductivity anomalies in cratonic lithosphere (*10*, *17*).

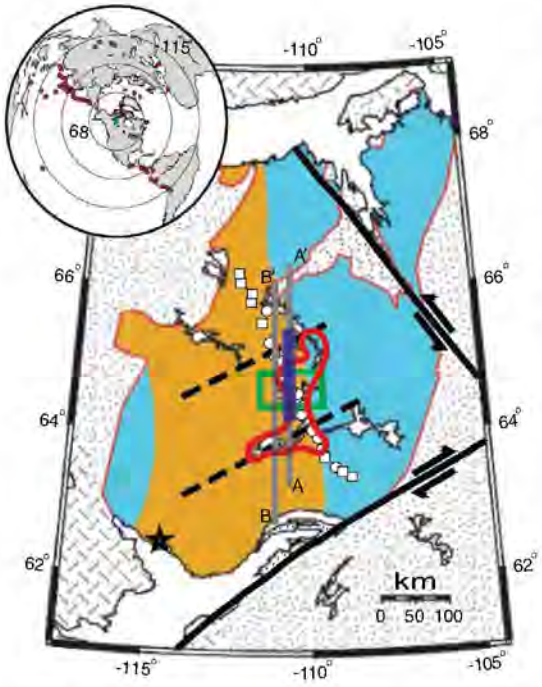


**Fig. 1.** Map of the Slave craton. The boundaries of the exposed craton are outlined in red. Inset shows a polar projection of the world centered on the craton (green square), with the 62 earthquakes (red circles) used for the analysis. Crustal topology and geochemical signatures broadly subdivide the Slave craton into two distinct regions (*27*): the older (4.03 to 2.83 Ga) Central Slave Basement Complex to the west, filled in brown, and isotopically juvenile rocks (2.67 to 2.6 Ga) to the east, filled in blue. The lateral extent of an ultradepleted harzburgitic layer of the mantle lithosphere has been inferred from petrological analysis of mantle xenoliths (*2*) (outlined in green) and geochemical analyses of garnet xenocrysts (*3*) (region between the two black dashed lines). The seismic stations used in this study are denoted by white circles and squares for POLARIS and MIT stations, respectively, which form a ~400-km-long linear array with ~20-km average station spacing. The line A-A′ marks the location of the seismic profile shown in Fig. 2A. The lateral extent of the central Slave seismic discontinuity (Fig. 2, A and C) is indicated by blue shading, and that of the conductive anomaly (Fig. 2B) is outlined in red. The line B-B′ is the nominal projected location of the MT array (*10*).

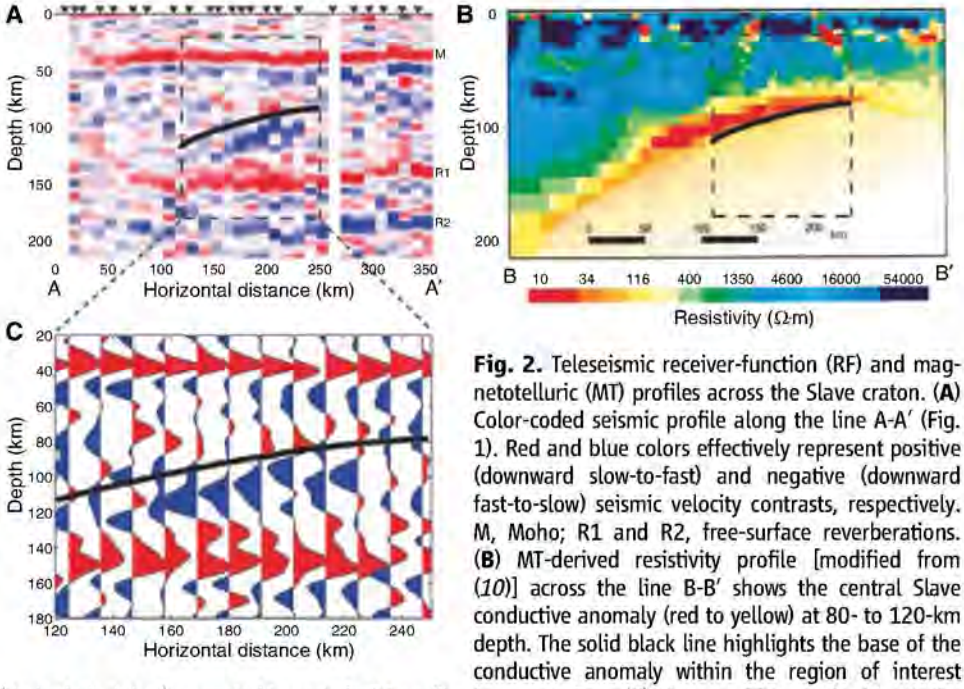


**Fig. 2.** Teleseismic receiver-function (RF) and magnetotelluric (MT) profiles across the Slave craton. **(A)** Color-coded seismic profile along the line A-A′ (Fig. 1). Red and blue colors effectively represent positive (downward slow-to-fast) and negative (downward fast-to-slow) seismic velocity contrasts, respectively. M, Moho; R1 and R2, free-surface reverberations. **(B)** MT-derived resistivity profile [modified from (*10*)] across the line B-B′ shows the central Slave conductive anomaly (red to yellow) at 80- to 120-km depth. The solid black line highlights the base of the conductive anomaly within the region of interest (dashed black box), repeated to scale in RF profiles for comparison. **(C)** Close-up RF traces for bins in the region of interest (*9*).

We propose that the two minerals, phlogopite and graphite, are related to metasomatic alteration, consistent with dehydration within a subduction zone complex where large quantities of sediments (source of carbon) were subducted (*18*). The existence of a metasomatized layer at 100-km depth beneath the central Slave fits well within the context of subduction related to the assembly of Archean cratons (*5*, *7*, *19*). Two possible subduction models can cause the observed metasomatic front and underlying harzburgitic layer. In one model, the discontinuity is due to the underplating of a subducted oceanic slab (fig. S4A) and marks the interface between the overriding plate and a layer of eclogitized and metasomatized oceanic crust. An alternative scenario of assembly involves an episode of shallow subduction (fig. S4B), in which the mantle wedge becomes stagnant and freezes due to low subduction angle—a process that has been documented in Phanerozoic times, for example, in parts of the Andes (*20*). Regardless of the exact subduction model, the discontinuity appears to represent the base of an ancient lithosphere that preceded cratonization.

The subduction event may be constrained by the age of minerals found in local xenoliths and by the lateral extent of the observed discontinuity. Lu-Hf dating of clinopyroxenes in the phlogopite-bearing eclogites indicates a minimum age of ~2.7 Ga (*14*), which approaches closely the timing of collision between the younger eastern Slave terranes and the older Central Slave Basement Complex (Fig. 1) (*21*). However, this event caused a north-south suture that runs nearly parallel to the seismic line (*21*), and a related subduction should therefore be observed over the entire length of the profile, which is not

the case. Moreover, robust Re-Os age constraints on peridotitic diamonds from the harzburgitic layer suggest that the central Slave's lithospheric mantle down to 150 km was formed and stabilized by 3.5 Ga (*22*). Therefore, the central Slave seismic discontinuity is likely caused by metasomatized mantle from a Paleoarchean subduction zone.

The presence of a Paleoarchean cratonic lithosphere in the Slave does not conflict with the occurrence of craton-wide arc volcanism and plutonism during later Neoarchean time (*21*); rather, it suggests that the blocks that aggregated in the final stage of cratonic assembly may themselves have been fragments of older, thick proto-cratonic entities. This is consistent with the limited lateral extent of the discontinuity, which may mark the outline of a broken block (fig. S4), and is supported by the unique geochemical signature and high concentration of diamondiferous kimberlites found in the same region (*2*).

If subduction has been active since the Paleoarchean, similar or related structures with limited lateral extent should be expected in other parts of the craton and in other cratons worldwide. Indeed, anisotropic seismic discontinuities have been detected below the southwest edge of the Slave craton (*4*) and the adjacent Wopmay orogen (*23*). These have been inferred to mark Proterozoic collision-subduction events associated with the final assembly and stabilization of a large part of the Laurentian continent (*24*). Away from cratonic edges, similar seismic discontinuities have been detected in the Kaapvaal craton of South Africa (*25*). Moreover, a global compilation of long-aperture seismic refraction data indicates the existence of a widespread (albeit not ubiquitous) negative discontinuity in the 90- to 120-km depth range beneath several Archean cratons (*26*). The character of the discontinuities (i.e., their spatial extent, depth, dip, and physical properties) depends on the details of each subduction event, including the amount of metasomatism, the subduction geometry, and history of much younger events of accretion and magmatism. Given the limited detailed geophysical sampling of cratons and the nonuniform nature of these subduction-related discontinuities, it is thus not surprising that not many of them have been observed to date.

### References and Notes


1. S. A. Bowring, I. S. Williams, W. Compston, *Geology* **17**, 971 (1989).
2. W. L. Griffin *et al.*, *J. Petrol.* **40**, 705 (1999).
3. H. S. Grütter, D. B. Apter, J. Kong, in *Proceedings of the 7th International Kimberlite Conference*, J. J. Gurney *et al.*, Eds. (Red Roof Design, Cape Town, 1999), vol. 1, pp. 307–313.
4. M. G. Bostock, *J. Geophys. Res.* **103**, 21183 (1998).
5. D. B. Snyder, *Tectonics* **27**, TC4006 (2008).
6. M. Moorkamp, A. G. Jones, D. W. Eaton, *Geophys. Res. Lett.* **34**, L16311 (2007).
7. H. H. Helmstaedt, J. D. Schulze, in *Kimberlites and Related Rocks, Their Composition, Occurrence, Origin, and Emplacement*, J. Ross, Ed. (Geological Society of Australia, Canberra, 1989), vol. 1, pp. 358–368.
8. T. H. Jordan, *Nature* **274**, 544 (1978).
9. Supporting material is available on *Science* Online.
10. A. G. Jones *et al.*, *Geology* **29**, 423 (2001).
11. C.-T. A. Lee, *J. Geophys. Res.* **108**, 2441 (2003).
12. A. G. Jones, R. L. Evans, D. W. Eaton, *Lithos* **109**, 131 (2009).
13. D. E. Boerner *et al.*, *Science* **283**, 668 (1999).
14. S. Aulbach, N. J. Pearson, S. Y. O'Reilly, B. J. Doyle, *J. Petrol.* **48**, 1843 (2007).
15. B. R. Hacker *et al.*, *J. Petrol.* **46**, 1661 (2005).
16. A. A. Guseinov, I. O. Gargatsev, R. U. Gabitova, *Izv. Phys. Solid Earth* **41**, 670 (2005).
17. M. Mareschal, W. S. Fyfe, J. Percival, T. Chan, *Nature* **357**, 674 (1992).
18. D. M. Kerrick, J. A. D. Connolly, *Nature* **411**, 293 (2001).
19. C.-T. A. Lee, in *Archean Geodynamics and Environments*, K. Benn, J.-C. Mareschal, K. C. Condie, Eds. (American Geophysical Union, Washington, DC, 2006), vol. 164, pp. 89–114.
20. L. S. Wagner, S. Beck, G. Zandt, M. N. Ducea, *Earth Planet. Sci. Lett.* **245**, 289 (2006).
21. W. J. Davis, A. G. Jones, W. Bleeker, H. Grütter, *Lithos* **71**, 575 (2003).
22. K. J. Westerlund *et al.*, *Contrib. Mineral. Petrol.* **152**, 275 (2006).
23. J.-P. Mercier *et al.*, *J. Geophys. Res.* **113**, B04308 (2008).
24. P. F. Hoffman, *Annu. Rev. Earth Planet. Sci.* **16**, 543 (1988).
25. D. B. Snyder, S. Rondenay, M. G. Bostock, G. D. Lockhart, *Lithos* **77**, 859 (2004).
26. H. Thybo, E. Perchuć, *Science* **275**, 1626 (1997).
27. W. Bleeker, L. Ketchum, V. Jackson, M. Villeneuve, *Can. J. Earth Sci.* **36**, 1083 (1999).


28. We thank S. Bowring for thoughtful and insightful comments on earlier drafts of this paper. We thank A. Jones for permission to use his figure in Fig. 2B. We thank S. Shirey, S. Aulbach, C. Till, L. Elkins-Tanton, and M. Moorkamp for helpful discussions, the POLARIS consortium for making data available, and members in the Northwest Territories Geoscience Office, BHP-Billiton Diamonds Inc., De Beers Canada Inc., and Tahera Diamond Corp. for logistical support of our field work in the Slave province. This work is funded by NSF grant EAR-0409509 (S.R.). C.-W.C. is partially supported by an MIT Praecis Presidential Fellowship. This is Natural Resources Canada Earth Sciences Sector (ESS) contribution 20090244.


### Supporting Online Material

www.sciencemag.org/cgi/content/full/326/5956/1089/DC1
SOM Text
Figs. S1 to S4
Table S1
References

30 June 2009; accepted 17 September 2009
10.1126/science.1178477

# Nanoplasmonic Probes of Catalytic Reactions

**Elin M. Larsson,* Christoph Langhammer, Igor Zorić, Bengt Kasemo**

**Optical probes of heterogeneous catalytic reactions can be valuable tools for optimization and process control because they can operate under realistic conditions, but often probes lack sensitivity. We have developed a plasmonic sensing method for such reactions based on arrays of nanofabricated gold disks, covered by a thin (~10 nanometer) coating (catalyst support) on which the catalyst nanoparticles are deposited. The sensing particles monitor changes in surface coverage of reactants during catalytic reaction through peak shifts in the optical extinction spectrum. Sensitivities to below $10^{-3}$ monolayers are estimated. The capacity of the method is demonstrated for three catalytic reactions, CO and $H_2$ oxidation on Pt, and $NO_x$ conversion to $N_2$ on Pt/BaO.**

In heterogeneous catalysis, reactants in gas or liquid phase are converted to desired product molecules on the surface of a solid catalyst, which is usually composed of catalytically active nanoparticles (1 to 10 nm) dispersed on a porous, high-surface-area support material. In order to understand and improve these systems, it is important to be able to monitor the catalyst's state and to follow the reaction in real time. An important quantity is the surface coverage of reactants. However, experimental difficulties arise from the complexity of the catalyst and the atmospheric or higher pressures in which the reactions occur. Model systems (commonly single-crystal surfaces) and model reactions are frequently investigated at idealized ultrahigh vacuum (UHV) conditions, allowing use of powerful experimental probes (such as electrons, photons, or ions). A major challenge is to correlate results obtained by using the idealized and thoroughly scrutinized model catalysts in UHV with those of the less characterized real nanostructured catalysts at real reaction conditions (*1*–*3*).

We describe a method that, with a simple optical transmission (or reflection) measurement (Fig. 1A), can follow catalytic reactions in real time for both model and real supported catalysts. The principle is "nanoplasmonic" [localized surface plasmon resonance (LSPR)] sensing, currently intensely explored for biosensing, down toward single-molecule sensitivity (*4*). We show that LSPR can monitor changes in adsorbate coverages on "realistic" supported catalysts (Fig. 2) with a sensitivity corresponding to much less than 0.1 monolayer (ML).

For demonstrators, we used two types of Pt catalysts (Fig. 1, B to G) and three well-known catalytic reactions: oxidation of hydrogen ($H_2 + 1/2O_2 \rightarrow H_2O$), oxidation of carbon monoxide ($CO + 1/2O_2 \rightarrow CO_2$), and $NO_x$ storage and

Chemical Physics Group, Department of Applied Physics, Chalmers University of Technology, SE-41296 Gothenburg, Sweden.

*To whom correspondence should be addressed. E-mail: elarsson@chalmers.se

reduction over Pt/BaO catalysts. The first reaction is a common model reaction (*5*) relevant for hydrogen fuel cells, whereas the latter two are of key importance in automotive emission cleaning (*1*, *6*).

An optical transmission measurement (Fig. 1A) is made through a quartz reactor in which a transparent sample is mounted (alternatively, measurements can be made in reflection). The sample consists of the LSPR sensing structure and the catalyst, deposited on a glass substrate by using nanofabrication techniques and evaporation (Fig. 1, B to G). The transmission of white light through the sample, via the reactor walls, was detected as a function of wavelength by use of an array spectrometer (*7*). In some cases, scanning the spectral region of interest with monochromatic light or measuring the extinction at a particular wavelength may be preferable. This technique is suitable for use in either harsh environments, a remote sensing setup, or both.

The LSPR sensing structures are, in the present work, nanoscale disks of gold or platinum. The light transmitted through the sample has an intensity minimum (maximum extinction) at the wavelength at which the LSPR excitation in the sensing particles is strongest (Fig. 1A, bottom). The excitation creates a strongly enhanced electromagnetic near field, which acts as a probe of the nanoparticle's surrounding (*8*). The wavelength of maximum extinction, $\lambda_{max}$, is very sensitive to changes of the dielectric properties near the sensing nanoparticles [within a few tens of nanometers; see discussion below and in (*7*)]. It is the shift of $\lambda_{max}$, measured with a resolution of 0.01 nm, that provides the sensing function (Fig. 1A, bottom) and allows sub-monolayer changes in surface coverage to be monitored.

For the Pt-catalyzed oxidation of hydrogen, we used a sample (Fig. 1, B to D) consisting of an array of nanofabricated (*9*) plasmonic gold disks ($\lambda_{max} \approx 570$ nm, 76 nm diameter, and 30 nm high) that were covered by a 10-nm-thick film of $SiO_2$, on which a nanogranular Pt catalyst was deposited by means of electron-beam evaporation. The amount of Pt is small enough so that individual Pt nanoparticles of sizes in the range of 5 to 20 nm are formed (see Fig. 1D) (*7*), which mimics the size range of real supported Pt catalysts. We call this sensing method "indirect sensing" (*10*) because in this case the LSPR sensing structure is not the catalyst, contrary to the case in a previous demonstration by Novo *et al.*, of using gold nanocrystals as both catalysts and LSPR sensor to follow a liquid-phase charge-transfer reaction (*11*).

The experiment was performed by slowly varying the relative $H_2$ concentration, $\alpha^{H2} = [H_2]/([H_2] + [O_2])$, from hydrogen-rich to oxygen-rich and back again while continuously recording $\Delta\lambda_{max}$ (Fig. 2A) (*7*). The $H_2$ scan rate was slow enough so that steady state was established at each concentration, except possibly for very slow structural or chemical changes of the catalyst. The sample temperature was measured with a thermocouple in contact with the sample surface. The reactant ($H_2 + O_2$) concentration was kept constant at 4% in Ar carrier gas at atmospheric pressure by means of a gas flow of 16.7 ml/s (3.4 cm/s plug flow velocity). The sample temperature ($T$), without reaction, was 509 K.

We observed discontinuous steps up and down in $\Delta\lambda_{max}$ at a critical reactant mixture of $\alpha^{H2}_{cr} = 0.5$ (Fig. 2A, blue curves), depending on whether the $H_2$ fraction was increasing or decreasing. This step is completely absent in control measurements on an identical structure without Pt particles. The step in $\Delta\lambda_{max}$ coincides with a peak ($\Delta T_{max} = 16$ K) in the simultaneously measured sample temperature (Fig. 2A, red and brown curves), which is caused by the exothermicity of the reaction. $\Delta\lambda_{max}$ varies only slowly above and below $\alpha^{H2}_{cr}$. All data measured with the sample structure in Fig. 1B were corrected for a small background signal, which was caused by the interaction of reactant gases with the $SiO_2$ surface (*7*, *12*). This correction slightly affects the slopes of $\Delta\lambda_{max}$ on both sides of $\alpha^{H2}_{cr}$ but does not affect the position or magnitude of the step in $\Delta\lambda_{max}$.

The $\Delta\lambda_{max}$ step is assigned to the well-known kinetic phase transition in the $H_2 + O_2$ reaction, occurring at a critical gas mixture, $\alpha^{H2}_{cr}$, at which a sudden transition occurs from an oxygen-covered surface at low $\alpha^{H2}$ to a partially hydrogen-covered surface at high $\alpha^{H2}$ (*13*). This transition occurs where the overall exothermic reaction has a rate maximum, which is the reason for the peak in temperature.

Because the kinetic phase transition at $\alpha^{H2} = \alpha^{H2}_{cr}$ involves a transition from an essentially oxygen-saturated to a partially hydrogen-covered surface, this example shows that LSPR can (i) detect surface coverage changes at the sub-monolayer level on small supported Pt nanoparticles and (ii) follow the kinetics of a catalytic reaction. The slopes of the LSPR peak position versus $\alpha^{H2}$, on both sides of the kinetic phase transition, are not primarily due to coverage changes but are the result of the reaction-induced temperature variation (*14*). This effect can, if needed, be subtracted by separate calibration measurements of $\Delta\lambda_{max}$ versus temperature with a non-reactive gas. The fact that the LSPR resonance position is also sensitive to temperature has, however, no influence on the measured $\Delta\lambda_{max}$ step at $\alpha^{H2}_{cr}$. The temperature variation over the region of the step is minor and estimated to be less than 1 K. Raw data of the LSPR resonance position versus time (as $\alpha$ was changed), and the accompanying temperature change, is shown in fig. S3. According to these data, the $\Delta\lambda_{max}$ step at the kinetic phase transition point is not compromised by temperature (see also the next example), which essentially is constant over that narrow $\alpha$ regime.

Further proof that the temperature sensitivity of $\Delta\lambda_{max}$ does not affect the step in $\Delta\lambda_{max}$ at the kinetic phase transition was obtained from measurements with diluted reactant concentrations of $H_2 + O_2$, from 6 to 1% (fig. S5). Such dilution did not change the magnitude of the $\Delta\lambda_{max}$ step at all (as expected, if it is due to a coverage change from or to a saturated oxygen adlayer) but changed the maximum temperature rise from 4 K to 24 K because of the increasing chemical power generation at higher concentrations. The temperature sensitivity of the LSPR, which at first sight might seem as a complication, can be used for an independent LSPR-based temperature measurement, as discussed in (*7*).

In the above measurements, there was potentially a difference in the temperature measured by the thermocouple and the actual catalyst particle temperature because of very local temperature gradients. However, this does not change the general analysis or conclusions above because such a gradient if at all present would not change the analysis at the kinetic phase transition (which is the most important part).

Qualitatively similar results with larger Pt particles were also obtained for "direct sensing," in which Pt disks were simultaneously acting as the catalyst and the LSPR-sensing particles (*7*). Pt nanoparticles have previously been found to exhibit optical excitations similar to those of Au nanoparticles (*15*). In some cases, this type of sensing—which is somewhat similar to the results by Novo *et al.* (*11*)—may be preferred because, for example, the Pt disks can be converted to well-defined single crystals (*16*) and thus can represent model catalysts. However, here our focus and emphasis is on the indirect sensing, in which the sensing particles are not the catalyst, because this is a much more versatile and entirely new approach.

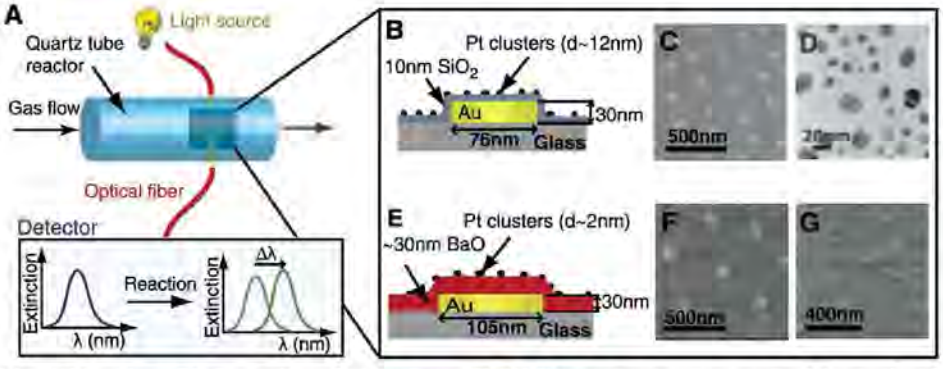


**Fig. 1.** Experimental setup and sensing structures (*7*). (**A**) Flow reactor arrangement and (bottom) optical readout. (**B**) Catalyst and sensing structure used to monitor changes in adsorbate coverage. (**C**) Scanning electron microscopy image of the sensing structure in (B). (**D**) TEM image of Pt catalyst clusters identical to those on the sensing structure in (B). (**E**) Sensing structure used to monitor the $NO_2$ storage/release from BaO. (**F** and **G**) Top-view (F) and 70° tilt (G) SEM images of the sensing structure in (E).

We next explored the practically important and most-studied catalytic model reaction CO + $O_2$ (*17*) in the same way as for $H_2$ + $O_2$, using the same Pt catalyst sample. A representative example is shown in Fig. 2B (8% reactants, 506 K, and 16.7 ml/min). As in the $H_2$ + $O_2$ reaction, an almost discontinuous step in $\Delta\lambda_{max}$ occurs of nearly the same amplitude but for a mixing ratio of $\alpha^{CO}$ = [CO]/([CO] + [$O_2$]) around 0.07. This is the kinetic phase transition in the CO + $O_2$ reaction from an oxygen- to a CO-covered surface, which is known to occur at very low relative CO concentration (*18*), much lower than for the $H_2$ + $O_2$ reaction, which explains the small $\alpha^{CO}_{cr}$ value. The kinetic phase transition and the associated coverage change can be sensitively detected with LSPR sensing.

A difference from the $H_2$ + $O_2$ reaction is that the temperature versus α profile is asymmetric around $\alpha^{CO}_{cr}$. This asymmetry arises from the strong blocking (poisoning) effect of CO for oxygen adsorption, preventing $O_2$ from dissociating and reacting when the surface is CO-saturated. Thus, the temperature profile is flat at $\alpha^{CO} > \alpha^{CO}_{cr}$, and there is no temperature-induced slope of the wing of $\Delta\lambda_{max}$, such as for $H_2$ + $O_2$ in Fig. 2A, because there is no reaction and no chemical energy dissipated, and the coverage is fixed at 1 ML CO. Similar behavior (an asymmetric *T* versus α peak) was seen also for the $H_2$ + $O_2$ reaction, but at lower temperatures [supporting online material (SOM) text]. The latter is caused by hydrogen poisoning (*13*) of the reaction at low temperature, similar to CO poisoning for the CO reaction. This occurs at lower temperature for the hydrogen reaction because the chemisorption energy is much smaller for hydrogen as compared with CO.

As seen in Fig. 2B, there is an irreversibility in closing the cycle going from oxygen-rich to CO-rich and back to oxygen-rich conditions. The origin of this is probably some irreversibility in the oxidation-reduction cycle. This minor effect does not change the main analysis of the $\Delta\lambda_{max}$ step at the kinetic phase transition point. Carbonyls or other similar poisoning effects were ruled out because they would have monotonically reduced the activity of the samples, which was not the case.

We now turn to a more complex but practically important reaction in automotive emission cleaning for diesel and so-called "lean burn" engines (engines operated at oxygen excess) in which the conventional three-way catalyst cannot reduce $NO_x$ efficiently. The latter has led to the development of so-called $NO_x$ storage/reduction catalysts, in which $NO_x$ is temporarily (~1 min) accumulated in the catalyst, whereas the engine operates at $O_2$ excess [typically 30 to 600 parts per million (ppm) levels of NO + $NO_2$], and then the stored $NO_x$ is reduced to $N_2$ by switching the air/fuel mixture to excess fuel, HC (or $H_2$), for a few seconds. A key to this solution is the $NO_x$ storage material, usually barium oxide (BaO), which upon $NO_x$ storage is converted to $Ba(NO_3)_2$ or related compounds (*6*). Pt (and in practice usually also Rh) is needed for the reduction step and also for oxidation of NO (when present) to $NO_2$ during the storage phase.

To test whether LSPR detection can monitor these reactions, we used a similar catalyst and sensing structure as above but with the passive $SiO_2$ layer replaced by an evaporated, ~30-nm-thick $NO_x$-active BaO layer (Fig. 1, E to G) deposited over the Au LSPR-sensing particles (140 nm diameter, 30 nm high, and $\lambda_{max} \approx 660$ nm). A similar nanogranular Pt film as above was then deposited on the BaO film (*7*). To mimic the $NO_x$ storage period, the sample was exposed for 30 min to a gas mixture of 30 to 1000 ppm $NO_2$ + 6% $O_2$. It was subsequently exposed to 2% $H_2$ to mimic the reduction period, in which the catalyst is restored to be able to store $NO_x$ again.

The results of both the storage period (*t* = 8 to 38 min in Fig. 3) and the reduction step are shown in Fig. 3A. For all curves, there is an initial rapid upward shift of $\Delta\lambda_{max}$ within 20 s after exposure to $NO_2$ and $O_2$ and then a slowly continuing increase, which is greater for higher $NO_2$ concentrations. We interpret this as LSPR detection of the BaO + $NO_2$ storage reaction, converting a thin surface layer of BaO to $Ba(NO_3)_2$, which changes the effective refractive index that is sensed by the LSPR sensor (see below). The larger signals for larger $NO_2$ concentrations (quantified in Fig. 3B) are caused by a combination of reversible and irreversible $NO_x$ storage, both increasing with increasing $NO_x$ concentration. Exposing the sample to $H_2$ (at 38 min in Fig. 3A) results as expected in a shift of $\Delta\lambda_{max}$ back to the original value before the $NO_2$ exposure because of the hydrogen reduction of stored $NO_x$ to $N_2$ and concerted $Ba(NO_3)_2 \rightarrow$ BaO conversion (creating partly reduced BaO). The immediate shift also at 0 ppm $NO_2$ is due to the oxidation of the partially reduced BaO in the presence of $O_2$ after the hydrogen treatment.

Regarding the sensing mechanisms, in the sensing of the kinetic phase transitions for the CO and $H_2$ reactions (Fig. 2) the major change is a conversion of the adsorbate layer on the Pt nanoparticles from (or to) an oxygen-saturated to (or from) a CO- or (partially) hydrogen-covered surface. Oxygen adsorption/removal on Pt involves charge rearrangement in the surface layer manifested, for example, in a change of work function (*19*, *20*). In the standard treatment of LSPR sensing (*4*), this charge rearrangement can be associated with a change in the dielectric properties of the surface layer. Based on the collected data for the indirect sensing examples, including calibration data (SOM text) (*7*), we conclude that the oxygen-coverage change is the main contributor to the measured shift in $\Delta\lambda_{max}$, whereas the CO and H coverages have less influence (although they create a measurable signal, at least for CO). From the observed $\Delta\lambda_{max}$ shifts of ~1 nm (Fig. 2) and the spectral resolution in the experimental setup, we estimate a lower sensitivity limit for the current measurements with the same type of sample to be 0.02 monolayer of oxygen. For a more detailed discussion on sensitivity and how it compares with other studies (*21*–*25*), see the SOM text. We estimate that this sensitivity can be improved down to around 0.001 monolayer by use of improved optical measurements (*26*) and even further by optimizing the sensing structure (SOM text). This estimate is for a Pt coverage of only ~20% on the sample surface. This sensitivity is high enough to detect similar coverage changes with a real supported catalyst, which in addition can be a three-dimensional (3D) porous structure with more catalytic material within the LSPR sensing range. The sensing volume is estimated to extend to at least 20 nm away from the Au sensing particles. With a nanoporous support with supported particles in the <5-to-10-nm range, several monolayers of nanoparticles would thus be sensed. Such a structure would also represent a very typical catalyst structure. Work is in progress to make measurements with such structures.

In the $NO_x$ sensing, the Pt/BaO/Au–LSPR structure senses changes in the dielectric constant near the Au particles, which is caused by incorporation of $NO_x$ in the BaO layer. The corresponding LSPR signal is approximately an order of magnitude greater than for the CO and $H_2$ reactions; this is a very sensitive (and fast) method for $NO_x$ sensing. We attribute the larger signal to a combination of three effects: (i) the involved surface area is greater, close to 80 to 90% as compared with 20%, because only a minor part of the BaO is covered by Pt; (ii) there is most likely a 3D rather than 2D $NO_x$ layer involved in the storage (*27*); and (iii) the volume

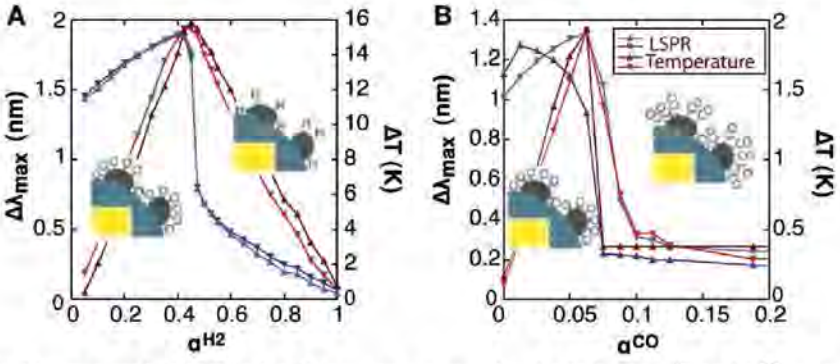


**Fig. 2.** Plasmon peak shift (blue) and temperature variation (red) during $\alpha^{H2}$ and $\alpha^{CO}$ sweeps. The indirect sensing structure in Fig. 1, B to D, was used. Triangles pointing up and down represent α sweeps up and down, respectively. (**A**) $\alpha^{H2}$ sweeps at 509 K, 4% $H_2$ + $O_2$ reactant, and 16.7 ml/s. The pictures to the left and right of the step in $\Delta\lambda_{max}$ illustrate the change in surface coverage upon passing the kinetic phase transition. (**B**) $\alpha^{CO}$ sweeps at 506 K, 8% CO + $O_2$ reactant, and 16.7 ml/s.

expansion upon $NO_x$ storage is very large, causing a large change in overall dielectric response.

Although demonstrated here for only two materials, one metal and one nonmetal (Pt and BaO), there is in principle no limitation with respect to the catalytic materials for which the indirect sensing can be applied because the basic principle is that a change in surface coverage—in the composition of the chemisorption or thin surface layer—causes a change in the polarizibility/dielectric properties of that layer, which is sensed by the LSPR. This statement is generic and applicable to all catalytic materials. What may vary is the absolute sensitivity to different combinations of materials and chemisorbed molecules, which in turn will influence the sensitivity and degree of applicability of the method. Also, the material in the separating layer imposes no restriction, except possibly from a technical point of view, because any dielectric of interest as a catalyst support such as alumina, titania, zirconia, iron oxides, or various carbides, will work similarly well as $SiO_2$. This lack of limitation regarding the support material derives from the ability of the LSPR-induced electromagnetic field to penetrate through the separating layer and sense changes in the coverage of the actual catalyst particles, which in turn induces a LSPR frequency shift that is measured. It is in practice therefore the ability to make thin separating layers of various materials, rather than their dielectric properties, that may impose some limitations.

We are not claiming that the method is applicable to every situation; few methods are. However, we claim to have demonstrated a method with high potential for many important situations in catalysis. Regarding limitations, they may occur for reactions with mixtures of several reactants that have substantial coverage simultaneously or very low total coverage. However, the opposite cases are abundant in catalysis. For example, many catalytic reactions are, even under practical conditions, dominated by the coverage of one species, and the coverage frequently changes from dominance of one species to dominance of a second species at the rate maximum. For more complex situations, multiplexing approaches (as discussed below and in the SOM text) may be used.

The very high sensitivity of the LSPR sensing as demonstrated here is mainly a virtue but potentially also a cause of interpretation problems in some cases. For example, catalyst restructuring and changes of the support may interfere with the detection of the actual coverage changes of interest (in other situations, it might be these side effects that are of interest to measure). However, there are several ways of dealing with these and similar effects, if at hand. (i) Irreversible restructuring can be detected by returning to an identical reaction situation (such as temperature or coverage) and noting the corresponding LSPR shifts. (ii) Such effects can, as was done in the present measurements, be eliminated by using the common "running in" approach in catalysis, in which the catalyst is cycled through the reaction conditions several times before the actual measurements are done in order to stabilize the catalyst structurally and chemically. (iii) Temperature effects can be calibrated away (see above). (iv) Support effects can be calibrated away (see above and SOM text). (v) However, for the future, a more elegant approach would be to build in such eliminations by means of multiplexing—by using different areas on a single sample, with each area optimized to detect one change or correction of interest. The parameters at hand for such multiplexing are, for example, the size and shape of the sensing Au (or other material) LSPR particles and the thickness of the separating layer while keeping the actual catalyst particles the same everywhere. LSPR is ideal for such an approach because very small areas are required for each measurement area (such as 10 by 10 μm) and because parallel detection is possible through spectroscopic imaging. For example, one area of the multiplexing structure could then be optimized for coverage monitoring, another for temperature measurement, and yet another to monitor support interactions. Some such functions may even be achieved by using elongated sensing particles and two light polarizations, as demonstrated in (*28*), because the short and long particle directions have different spectral sensing regions and probably also different relative sensitivity factors for, for example, adsorbates and temperature.

The sensing structures we used have not been optimized with respect to shape, size, and material of the LSPR-sensing particles or of the separating layer. For example, it is possible to improve the sensitivity by optimizing the thickness of the $SiO_2$ (or other oxide) layer (*29*) between the sensing particles and the actual catalyst. The same type of structures as described here can also be combined with simultaneous, LSPR-enhanced Fourier transform infrared (*30*) or Raman spectroscopy (*31*), which would provide simultaneous spectroscopic information about specific adsorbates or adsorbate-substrate bonds.

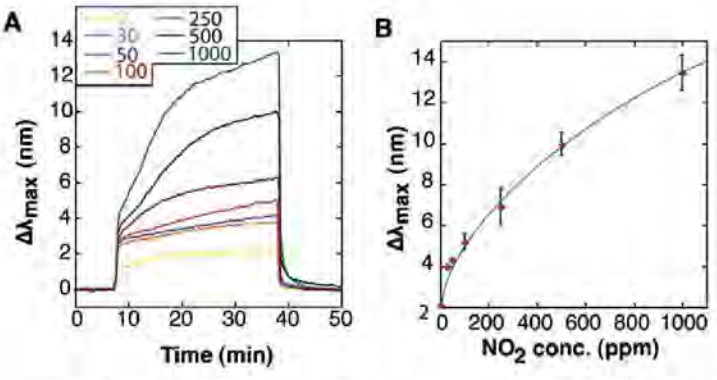


**Fig. 3.** $NO_x$ storage and release (as $N_2$) from BaO measured with the catalyst structure in Fig. 1, E to G. (**A**) Plasmon peak shift during 30 min $NO_2$ storage (at $t$ = 8 to 38 min), at seven different concentrations (0, 30, 50, 100, 250, 500, and 1000 ppm), and subsequent release by exposure to 2% $H_2$ (at $t$ = 38 min). (**B**) Total plasmon peak shift after 30 min of $NO_2$ exposure as a function of $NO_2$ concentration [same concentrations as in (A)].


**References and Notes**

1. G. Ertl, *Angew. Chem. Int. Ed.* **47**, 3524 (2008).
2. G. A. Somorjai, J. Y. Park, *Catal. Lett.* **115**, 87 (2007).
3. D. W. Goodman, *Chem. Rev.* **95**, 523 (1995).
4. J. N. Anker *et al.*, *Nat. Mater.* **7**, 442 (2008).
5. S. Völkening, K. Bedurftig, K. Jacobi, J. Wintterlin, G. Ertl, *Phys. Rev. Lett.* **83**, 2672 (1999).
6. N. Takahashi *et al.*, *Catal. Today* **27**, 63 (1996).
7. Materials and methods are available as supporting material on *Science* Online.
8. U. Kreibig, M. Vollmer, *Optical Properties of Metal Clusters: Springer Series in Materials Science* (Springer Verlag, Berlin, 1995), vol. 25.
9. H. Fredriksson *et al.*, *Adv. Mater.* **19**, 4297 (2007).
10. C. Langhammer, E. Larsson, I. Zoric, B. Kasemo, Swedish Patent application P180305E00 (2009).
11. C. Novo, A. M. Funston, P. Mulvaney, *Nat. Nanotechnol.* **3**, 598 (2008).
12. M. Wallin, H. Grönbeck, A. Lloyd Spetz, M. Eriksson, M. Skoglundh, *J. Phys. Chem. B* **109**, 9581 (2005).
13. V. P. Zhdanov, B. Kasemo, *Surf. Sci. Rep.* **20**, 111 (1994).
14. G. Weick, G.-L. Ingold, R. A. Jalabert, D. Weinmann, *Phys. Rev. B* **74**, 165421 (2006).
15. C. Langhammer, Z. Yuan, I. Zoric, B. Kasemo, *Nano Lett.* **6**, 833 (2006).
16. K. Wong, S. Johansson, B. Kasemo, *Faraday Discuss.* **105**, 237 (1996).
17. G. Ertl, *Surf. Sci.* **299–300**, 742 (1994).
18. M. Bär, C. Zulicke, M. Eiswirth, G. Ertl, *J. Chem. Phys.* **96**, 8595 (1992).
19. D. H. Parker, M. E. Bartram, B. E. Koel, *Surf. Sci.* **217**, 489 (1989).
20. G. A. Somorjai, M. A. Van Hove, *Prog. Surf. Sci.* **30**, 201 (1989).
21. G. H. Chan, J. Zhao, E. M. Hicks, G. C. Schatz, R. P. Van Duyne, *Nano Lett.* **7**, 1947 (2007).
22. C. Langhammer, M. Schwind, B. Kasemo, I. Zori, *Nano Lett.* **8**, 1461 (2008).
23. E. M. Larsson, J. Alegret, M. Käll, D. S. Sutherland, *Nano Lett.* **7**, 1256 (2007).
24. T. Rindzevicius *et al.*, *Nano Lett.* **5**, 2335 (2005).
25. L. J. Sherry, R. C. Jin, C. A. Mirkin, G. C. Schatz, R. P. Van Duyne, *Nano Lett.* **6**, 2060 (2006).
26. A. B. Dahlin, J. O. Tegenfeldt, F. Hook, *Anal. Chem.* **78**, 4416 (2006).
27. J. Szanyi, J. H. Kwak, D. H. Kim, S. D. Burton, C. H. F. Peden, *J. Phys. Chem. B* **109**, 27 (2005).
28. C. Hagglund, M. Zach, G. Petersson, B. Kasemo, *Appl. Phys. Lett.* **92**, 053110 (2008).
29. T. Rindzevicius, Y. Alaverdyan, M. Käll, W. A. Murray, W. L. Barnes, *J. Phys. Chem. C* **111**, 11806 (2007).
30. D. Enders, T. Nagao, T. Nakayama, M. Aono, *Langmuir* **23**, 6119 (2007).
31. S. Nie, S. R. Emory, *Science* **275**, 1102 (1997).



32. The Swedish foundation for strategic research (program PhotoNano), the Chalmers Foundation, and the Swedish energy agency (project N2E2) are acknowledged for their financial support. We are grateful to S. Gustafsson and E. Olsson at our department for the TEM picture in Fig. 1D.


**Supporting Online Material**

www.sciencemag.org/cgi/content/full/1176593/DC1
Materials and Methods
SOM Text
Figs. S1 to S6
References


20 May 2009; accepted 8 September 2009
Published online 22 October 2009;
10.1126/science.1176593
Include this information when citing this paper.

# Microsecond Simulations of Spontaneous Methane Hydrate Nucleation and Growth

Matthew R. Walsh,[1] Carolyn A. Koh,[1] E. Dendy Sloan,[1] Amadeu K. Sum,[1]* David T. Wu[1,2]*

Despite the industrial implications and worldwide abundance of gas hydrates, the formation mechanism of these compounds remains poorly understood. We report direct molecular dynamics simulations of the spontaneous nucleation and growth of methane hydrate. The multiple-microsecond trajectories offer detailed insight into the process of hydrate nucleation. Cooperative organization is observed to lead to methane adsorption onto planar faces of water and the fluctuating formation and dissociation of early hydrate cages. The early cages are mostly face-sharing partial small cages, favoring structure II; however, larger cages subsequently appear as a result of steric constraints and thermodynamic preference for the structure I phase. The resulting structure after nucleation and growth is a combination of the two dominant types of hydrate crystals (structure I and structure II), which are linked by uncommon $5^{12}6^3$ cages that facilitate structure coexistence without an energetically unfavorable interface.

A solution of methane and water crystallizes to a clathrate hydrate upon cooling and/or pressurization (*1*). Such hydrates, which are ice-like inclusion compounds with guest molecules trapped (enclathrated) inside hydrogen-bonded water cages, are relevant in a variety of scientific and industrial contexts, including climate change modeling (*2*), carbon dioxide sequestration (*3*), hydrocarbon extraction (*4*), hydrogen and natural gas storage (*4*–*6*), separation and refrigeration technologies (*7*, *8*), marine biology (*9*), and planetary surface chemistry (*10*). Of particular interest are the hydrocarbon hydrates that can form blockages in oil and natural gas pipelines; this phenomenon severely affects the safety of production and currently represents the most expensive hindrance to pipeline flow assurance (*1*, *4*). Hydrates also exist naturally in arctic regions and in marine sediments along continental margins, and have gained attention as a potential energy resource (*11*, *12*); even by the most conservative estimates, the energy dormant in natural gas hydrates worldwide is double that of all conventional fossil fuel deposits combined (*1*, *11*).

Curiously, gas hydrates seem to defy intuition about hydrophobic compounds, as the concentration of a nonpolar gas in the solid hydrate lattice is more than two orders of magnitude higher than the solubility of such a gas in liquid water. For example, the solubility of methane in water is about one molecule for every 4000 water molecules, whereas in sI hydrates, there are about six water molecules for every methane molecule. Depending on the guest molecules, hydrates can

[1]Center for Hydrate Research, Department of Chemical Engineering, Colorado School of Mines, Golden, CO 80401, USA. [2]Department of Chemistry, Colorado School of Mines, Golden, CO 80401, USA.

*To whom correspondence should be addressed. E-mail: asum@mines.edu (A.K.S.); dwu@mines.edu (D.T.W.)

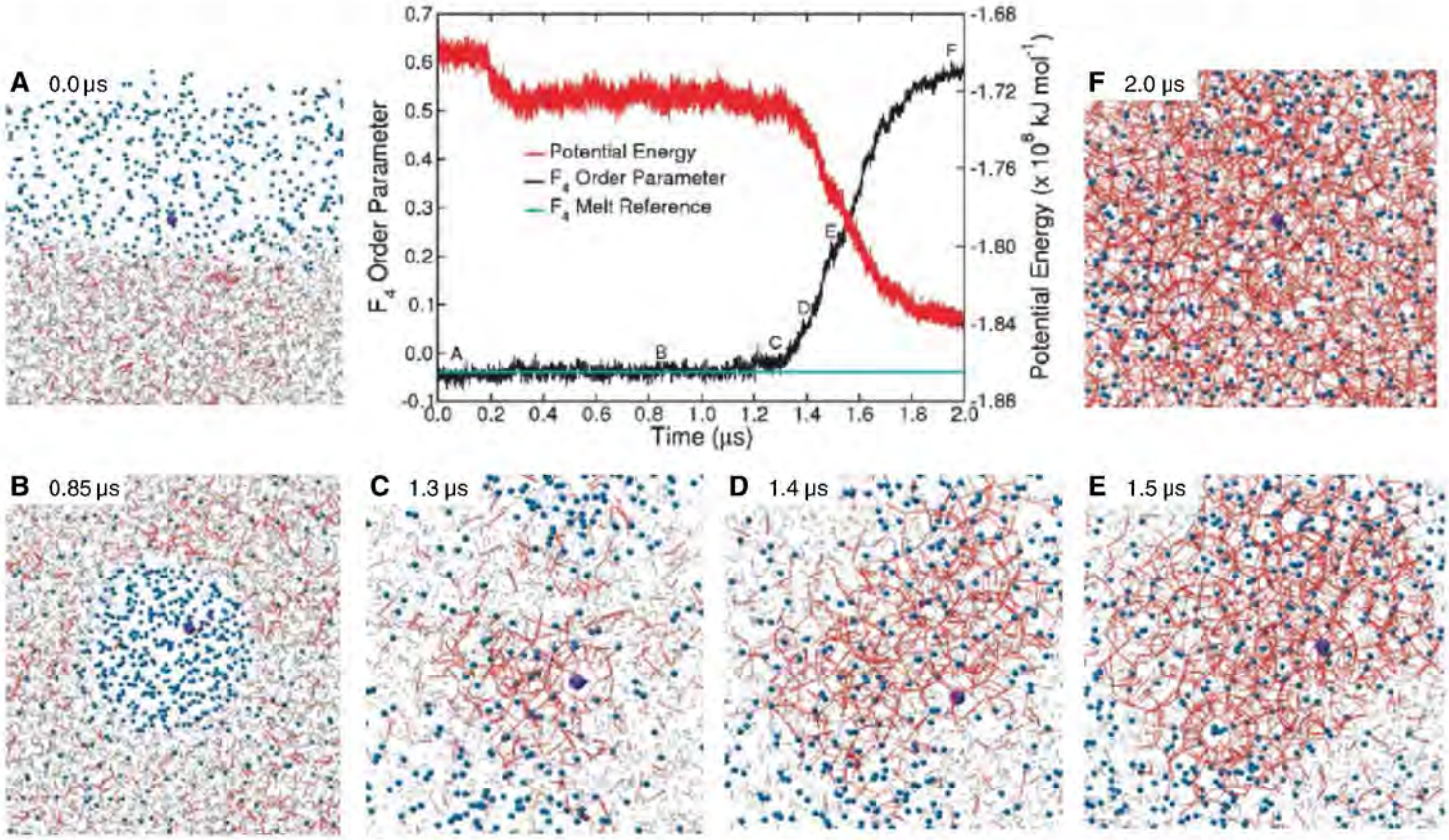


**Fig. 1.** Potential energy and $F_4$ order parameter for the methane-water system over the course of the simulation. A similar plot of the nucleation data and system snapshots for the 5-μs trajectory is shown in fig. S1. The reference $F_4$ value (–0.04) for a fully melted hydrate (horizontal blue line) helps to identify the beginning of nucleation at ~1.2 μs. Snapshots (**A**) through (**F**) show the system evolution during the simulation (images are only a portion of the periodic simulation box). Water is represented as gray lines, methane as blue spheres, and hydrogen bonds between water molecules as red lines. The larger violet sphere represents the first methane molecule to become permanently enclathrated. During the time preceding nucleation, this methane molecule migrates from the vapor to the liquid and back several times. The water molecules are time-averaged over 2 ns to aid in the visualization. Movie S1 shows the complete nucleation trajectory. The methane concentration in the water phase and the gas density during the simulation are given in table S1.

form a variety of crystal types, although there are two dominant structures of gas hydrates: structure I (sI) and structure II (sII). Both sI and sII crystals have cages made from 12 planar pentagonal faces (denoted $5^{12}$ or small cages); in addition, sI contains $5^{12}6^2$ (large sI) cages, and sII contains $5^{12}6^4$ (large sII) cages (*1*). In sI hydrate, the $5^{12}$ cages do not share faces because they are separated by the large sI cages, but in sII hydrate, face-sharing $5^{12}$ cages are present. A full description of the molecular mechanism of hydrate formation remains an elusive yet important objective, as it would address outstanding issues related to order-disorder transitions and hydrophobic-hydrophilic interactions.

Laboratory measurements have been unsuccessful in identifying the molecular mechanism of hydrate nucleation because of the inability to precisely target the time and spatial domain of a nucleation event, which may occur in nanoseconds and on the nanometer length scale (*13*, *14*). Because classical molecular dynamics (MD) simulations can follow the nanoscale trajectories of molecules, MD has been the preferred technique to investigate the formation of hydrates (*15*–*21*). However, because hydrate nucleation is a rare event, with induction times longer than typical MD trajectories in the nanosecond range, the molecular simulation of hydrate formation from a disordered and phase-separated state has been hindered. Here we present the results of two independent MD simulations of methane hydrate nucleation made possible by extending simulations into the microsecond domain (*22*). Because the two trajectories are qualitatively and quantitatively similar, we focus our analysis on a 2-μs simulation at 250 K and 50 MPa; analogous results for a 5-μs trajectory at 260 K and 45 MPa are given in (*23*).

The initial configuration was obtained by melting 64 unit cells of sI methane hydrate at 425 K for a period of 3.5 ns, resulting in a two-phase liquid-vapor system with a mole fraction of methane in water of 0.0015 (two orders of magnitude lower than actually found in hydrates). This system was then cooled and pressurized to hydrate-forming conditions (250 K and 50 MPa) and monitored for nucleation; this method is analogous to that used by Matsumoto *et al.* in the direct simulation of ice nucleation (*24*). A detailed description of the methods used is provided in (*23*). Figure 1 shows the evolution of the potential energy and a four-body structural order parameter ($F_4$) of the methane-water system, along with snapshots taken from various stages of the simulation. The $F_4$ order parameter is a function of the torsion angle between oxygen atoms within 0.3 nm and the outermost hydrogen atoms in the water-water pair (*15*, *16*). The average values of $F_4$ for hydrate, liquid water, and ice are 0.7 (for both sI and sII hydrate), −0.04, and −0.4, respectively, and thus $F_4$ is an effective quantitative indication of the phase (*20*).

The first several hundred nanoseconds of the simulation involve the dissolution of methane into water induced by the high-pressure and low-temperature conditions. At ~0.18 μs, a methane bubble forms, causing the initial decrease in the potential energy. The density of methane gas increases by ~5% upon bubble formation (table S1), possibly resulting from an increase in the effective vapor pressure due to the surface tension of the methane-water interface (*25*). Moreover, the concomitant increase in the methane mole fraction in the bulk water to 0.039 (26% of that found in hydrate) may also be a consequence of an increase in the vapor-phase pressure due to interfacial effects. On at least three occasions during the first 1.2 μs, with the first occurring at ~0.3 μs, small networks of water cages form around dissolved methane molecules, only to dissociate several nanoseconds later, illustrating the stochastic nature of nucleation. At ~1.2 μs, a clear departure in $F_4$ from the melt reference line is observed, indicating spontaneous hydrate nucleation. After ~1.3 μs, rapid hydrate growth is indicated by the precipitous rise of $F_4$ and fall of the potential energy.

Figure 2 shows snapshots detailing successive events during nucleation occurring at ~1.2 μs. At 1.139 μs, the two orange methane molecules and five water molecules cooperatively organize into a stable structure, with the methane molecules adsorbed on opposite sides of a single planar pentagonal ring of water molecules. These methane molecules retain their positions relative to each other throughout the fluctuating partial formation and dissociation of hydrogen-bonded cavities surrounding them. This initial structure in turn allows

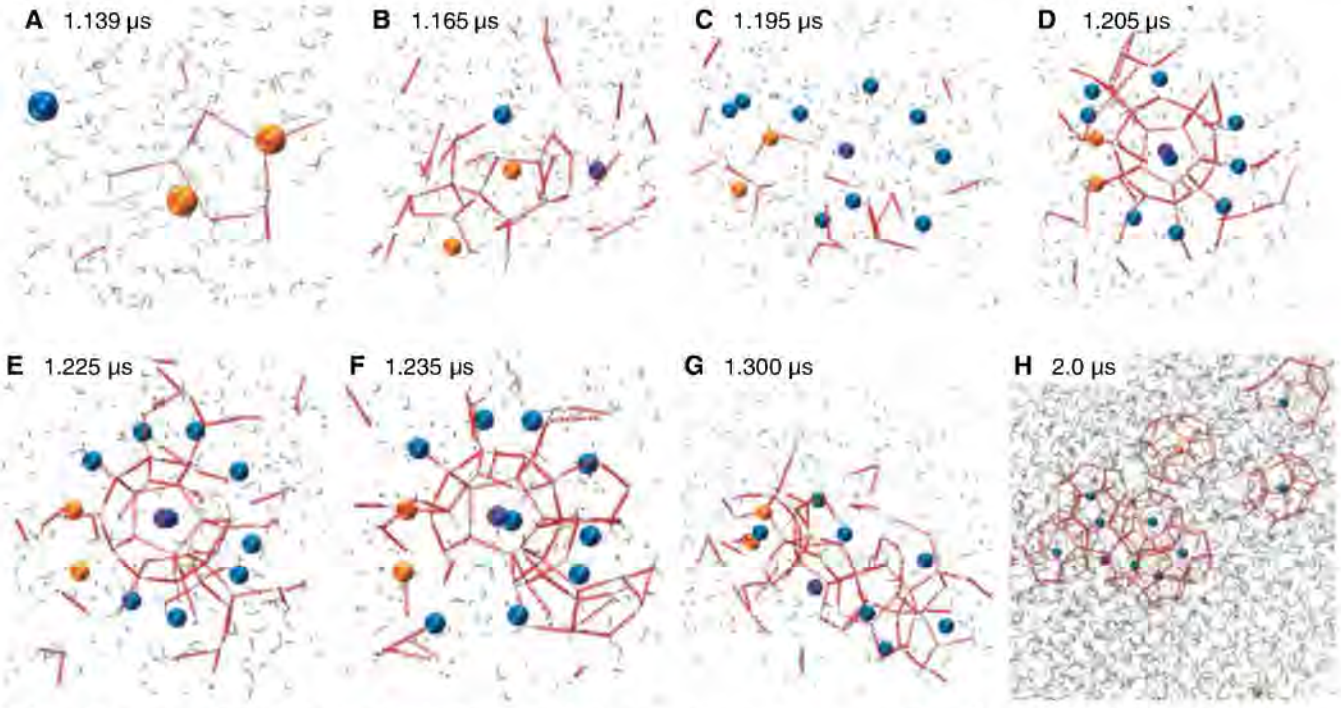


**Fig. 2.** Fluctuating nature of the first cages involved in the hydrate nucleation. A similar sequence is shown for the 5-μs trajectory in fig. S2. (**A** to **C**) A pair of methane molecules is adsorbed on either side of a single pentagonal face of water molecules. Partial cages form around this pair, near the eventual central violet methane molecule, only to dissociate over several nanoseconds. (**D** and **E**) A small cage forms around the violet methane and other methane molecules adsorb to 11 of the 12 pentagonal faces of the cage, creating the bowl-like pattern shown. (**F** and **G**) The initial central cage opens on the end opposite to the formation of a network of face-sharing cages, and rapid hydrate growth follows. (**H**) A snapshot of the system after hydrate growth, showing the fates of those methane molecules that make up the initial bowl-like structure (other cages not shown). Movie S2 shows the formation of the initial small cage, the bowl-like pattern, and subsequent breakup and rearrangement; movie S3 highlights the process leading to the breakup of the central cage. These nucleation events occur in the liquid phase.

the growth of more water faces and adsorbed methane. These observations of methane-water cooperativity toward ordering are consistent with prior studies showing that the faces of rigid or constrained cages can adsorb methane molecules, and that the adsorbed methane molecules prolong the lifetime of the faces of unconstrained hydrate cages (*26*, *27*). This process leads to the gradual formation of a small ($5^{12}$) cage (containing the violet methane) at 1.225 μs surrounded by a bowl-like pattern in the first shell of adsorbed methane molecules (viewed from the top in Fig. 2). In this early stage with an absence of other constraints, the small $5^{12}$ cage is locally preferred.

The faces and edges of the hydrogen bond network fluctuate as a result of fleeting (~1 ns) exchange or insertion of water molecules from the surrounding liquid, while a flickering halo (*20*) of partial cages forms around the adsorbed methane molecules in the bowl-like structure. At this stage, extended growth of the halo into face-sharing $5^{12}$ cages around a central $5^{12}$ cage is hindered by steric constraints (as $5^{12}$ cages alone cannot fill space). After persisting for ~30 ns, the central $5^{12}$ cage opens when two new water molecules are inserted into the only face not adsorbing a methane molecule, on the side opposite to that where several new full cages are completed (movies S2 and S3). This breakup facilitates the ability of the surrounding small cages to fill space, and rapid hydrate growth ensues. Over the course of 240 ns, the original small cage rearranges around the violet methane molecule to become an uncommon $5^{12}6^3$ cage (12 pentagonal and three hexagonal faces). $5^{12}6^3$ cages are present in neither sI nor sII hydrate, but they have been suggested to allow the coexistence of sI and sII hydrates without an energetically unfavorable interface (*28*, *29*). Although the cage that becomes a $5^{12}6^3$ cage was observed in this trajectory to be the $5^{12}$ cage central to the initial bowl-like structure, the fluctuating nature of the network suggests that other cages in the initially formed network of small cages could also be the first to rearrange to a $5^{12}6^3$ cage. This is in fact observed in the 5-μs trajectory reported in (*23*). The cage central to the bowl-like pattern of adsorbed methane molecules (shown in fig. S2) partially dissociates, but over the course of several hundred nanoseconds it rearranges to another $5^{12}$ cage, while an adjacent cage rearranges to a $5^{12}6^3$ cage.

A few connected $5^{12}$ cages form first before yielding to larger cages, as a result of steric constraints and the thermodynamic preference for sI hydrate. Figure 3 shows the evolution of the number of the various types of hydrate cages present during nucleation and growth. The $5^{12}$ cages clearly dominate the system in the early stages of nucleation. The large $5^{12}6^2$ sI cages, which together with the $5^{12}$ cages make up sI hydrate, are next in abundance, appear ~100 ns afterward, and reflect the thermodynamic preference of the system. The large $5^{12}6^4$ sII cages, which are known to be too large to be stabilized effectively by methane (*1*), represent the smallest fraction of cages, and they likely exist because of the large number of face-sharing small cages, which provide a pattern for sII cage formation. The rate of formation of $5^{12}6^3$ linking cages initially matches that of large sI cages but then comparatively slows, consistent with a role for the $5^{12}6^3$ cages early in the formation process as a template for sI cage growth from an otherwise sII-like structure, as discussed below.

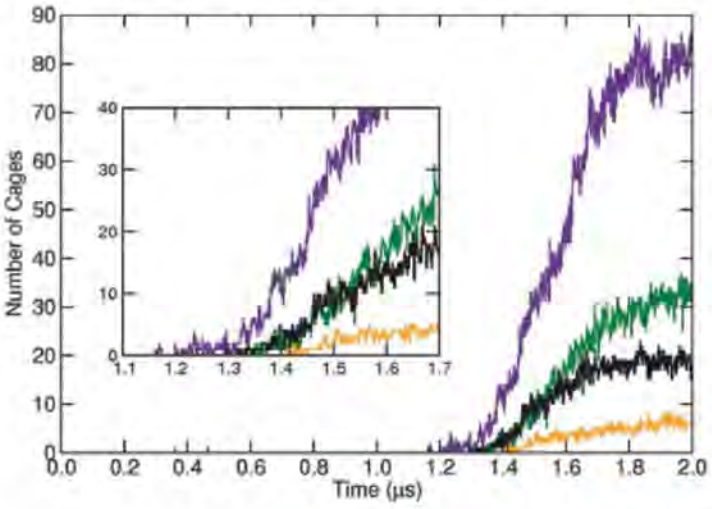


**Fig. 3.** Evolution of cage types during nucleation and growth over the course of the simulation, including the complete induction time, nucleation, and growth. The inset focuses on the period of nucleation and initial growth. An analogous plot for the 5-μs trajectory is shown in fig. S3. The lines shown in the graph are color-coded as follows: violet, small $5^{12}$ cages; green, large $5^{12}6^2$ sI cages; black, $5^{12}6^3$ cages; orange, large $5^{12}6^4$ sII cages.

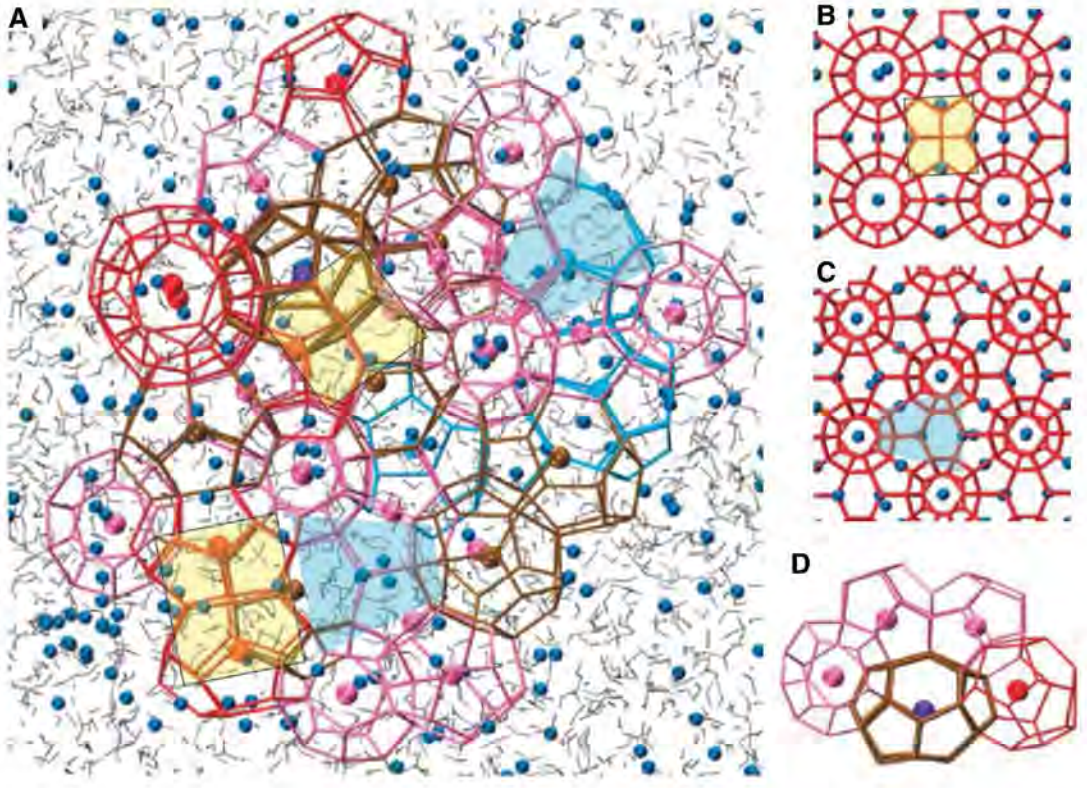


**Fig. 4.** (**A**) Simulation snapshot at 2 μs, after most of the system has transformed into hydrate. (**B** and **C**) sI (yellow squares) and sII motifs (blue trapezoids) are highlighted for comparison with perfect sI (B) and sII (C) hydrate crystals. Cages that make up sI and sII motifs are color-coded to further highlight sI/sII coexistence: red for large $5^{12}6^2$ sI cages; light blue for large $5^{12}6^4$ sII cages; brown for $5^{12}6^3$ linking cages; pink for small $5^{12}$ cages. (**D**) Snapshot taken after hydrate growth with a $5^{12}6^3$ linking cage (solid brown hydrogen bonds) around the violet methane originally at the center of the bowl of adsorbed methane molecules. Two of the three hexagonal faces can be seen at the top of the cage opposite each other; the other hexagonal face is on the bottom of the cage. The pink face-sharing small cages are characteristic of sII hydrate; the red cage is a large sI cage ($5^{12}6^2$). Excluding the violet methane in its $5^{12}6^3$ cage, the methane molecules shown follow the same color scheme as their respective cages. Movie S4 shows the color-coded hydrate nucleation trajectory using this same color scheme.

The hydrate structure at the end of the simulation is a mixture of sI and sII motifs (Fig. 4 and fig. S4). Despite the thermodynamic preference for sI, the coexistence of the two major types of structures for typical sI hydrate guests is well documented experimentally (*30*–*32*). Furthermore, configurations containing face-sharing $5^{12}$ cages have been observed in previous attempts to simulate methane hydrate nucleation and growth (*17*, *20*) and are observed in our simulations. Because $5^{12}$ cages present the smallest deviation from tetrahedrality of all hydrate cavities (*1*), it is reasonable that these cages would predominate in the initial structure and that they would share their pentagonal faces. Additionally, sII hydrate contains more $5^{12}$ cages per unit cell than sI by a factor of 8. For the aforementioned reasons, it is understandable that traces of sII would form in the initial stages of sI methane hydrate nucleation. Remarkable, though, is the cooperation between the sI and sII motifs via $5^{12}6^3$ cages; these uncommon cages appear to form as a link to facilitate growth of the thermodynamically preferred sI phase from the kinetically preferred sII phase formed initially (*28*).

One of the most intriguing results observed from the simulations is the unforeseen molecular order of the adsorbed methane molecules in the bowl-like arrangement immediately before hydrate formation and the minuscule nucleus size needed to initiate hydrate growth; clearly the relative positions of the guest molecules, and not only the nucleus size, have bearing on the control of hydrate nucleation. The mechanism described may reflect the high methane concentration in the water phase that developed spontaneously upon quenching. Nonetheless, because the system naturally evolved from equilibrated liquid and vapor to the experimentally observed coexistence of sI and sII cages, a molecular description of these simulation trajectories aids the understanding of the hydrate nucleation process. The immediate implications from these results are that the nucleation of hydrates is more complex than previously thought, involving cooperativity between methane and water, and that hydrate nucleation must be investigated over time scales considerably longer than those of most conventional simulation studies.

### References and Notes


1. E. D. Sloan, C. A. Koh, *Clathrate Hydrates of Natural Gases* (CRC Press, Boca Raton, FL, 2008).
2. K. Kaiho *et al.*, *Paleoceanography* **11**, 447 (1996).
3. Y. Park *et al.*, *Proc. Natl. Acad. Sci. U.S.A.* **103**, 12690 (2006).
4. E. D. Sloan, *Nature* **426**, 353 (2003).
5. L. J. Florusse *et al.*, *Science* **306**, 469 (2004).
6. W. L. Mao *et al.*, *Science* **297**, 2247 (2002).
7. T. Ogawa *et al.*, *Appl. Therm. Eng.* **26**, 2157 (2006).
8. V. M. Vorotyntsev, V. M. Malyshev, P. G. Taraburov, G. M. Mochalov, *Theor. Found. Chem. Eng.* **35**, 513 (2001).
9. C. R. Fisher *et al.*, *Naturwissenschaften* **87**, 184 (2000).
10. D. J. Milton, *Science* **183**, 654 (1974).
11. M. R. Walsh *et al.*, *J. Energy Econ.* **31**, 815 (2009).
12. R. Boswell, *Science* **325**, 957 (2009).
13. C. A. Koh, J. L. Savidge, C. C. Tang, *J. Phys. Chem.* **100**, 6412 (1996).
14. C. A. Koh, R. P. Wisbey, X. Wu, R. E. Westacott, A. K. Soper, *J. Chem. Phys.* **113**, 6390 (2000).
15. P. M. Rodger, T. R. Forester, W. Smith, *Fluid Phase Equilib.* **116**, 326 (1996).
16. L. A. Baez, P. Clancy, *Ann. N.Y. Acad. Sci.* **715**, 177 (1994).
17. C. Moon, P. C. Taylor, P. M. Rodger, *J. Am. Chem. Soc.* **125**, 4706 (2003).
18. H. Nada, *J. Phys. Chem.* **110**, 16526 (2006).
19. J. Vatamanu, P. G. Kusalik, *J. Phys. Chem.* **110**, 15896 (2006).
20. C. Moon, P. C. Taylor, P. M. Rodger, *Faraday Discuss.* **136**, 367 (2007).
21. J. Zhang *et al.*, *J. Phys. Chem. B* **112**, 10608 (2008).
22. Note that the time required for nucleation is volume-dependent, and induction times in simulations have no meaning unless a volume is specified. The system size reported here is comparable to previous similar studies in the literature, and thus it was necessary to extend the simulations several orders of magnitude in time to achieve nucleation.
23. See supporting material on *Science* Online.
24. M. Matsumoto, S. Salto, I. Ohmine, *Nature* **416**, 409 (2002).
25. P. Attard, M. P. Moody, J. W. G. Tyrell, *Physica A* **314**, 696 (2002).
26. E. A. Mastny, C. A. Miller, J. J. D. Pablo, *J. Chem. Phys.* **129**, 034701 (2008).
27. G. J. Guo, Y.-G. Zhang, H. Liu, *J. Phys. Chem. C* **111**, 2595 (2007).
28. J. Vatamanu, P. G. Kusalik, *J. Am. Chem. Soc.* **128**, 15588 (2006).
29. L. C. Jacobson, W. Hujo, V. Molinero, *J. Phys. Chem. B* **113**, 10298 (2009).
30. J. M. Schicks, J. A. Ripmeester, *Angew. Chem. Int. Ed.* **43**, 3310 (2004).
31. F. Fleyfel, J. P. Devlin, *J. Phys. Chem.* **95**, 3811 (1991).
32. D. K. Staykova, W. F. Kuhs, A. Salamatin, T. Hansen, *J. Phys. Chem.* **107**, 10299 (2003).


33. Supported by the NSF Materials Research Science and Engineering Center (NSF-MRSEC award DMR0820518), the U.S. Department of Energy–Basic Energy Sciences (DOE-BES award DE-FG02-05ER46242), and the CSM Hydrate Consortium (which is currently sponsored by BP, Champion Technologies, Chevron, ConocoPhillips, ExxonMobil, Halliburton, Multi-Chem Group, Nalco, Petrobras, Schlumberger, Shell, SPT Group, StatoilHydro, and Total). A.K.S. and D.T.W. were supported by NSF grant CBET-0933856. The simulations were carried out on facilities at the Golden Energy Computing Organization at the Colorado School of Mines, using resources acquired with financial assistance from NSF and the National Renewable Energy Laboratory. All graphics were prepared with VMD (S8). We thank T. Kaiser, M. Robbert, P. Rensing, T. Strobel, P. Prasad, Z. Aman, and L. Zerpa for support in computing efforts, and L. Jacobson, W. Hujo, and V. Molinero for generously sharing their cage recognition code.


### Supporting Online Material

www.sciencemag.org/cgi/content/full/1174010/DC1
SOM Text
Figs. S1 to S4
Table S1
Movies S1 to S4
References


24 March 2009; accepted 10 September 2009
Published online 8 October 2009;
10.1126/science.1174010
Include this information when citing this paper.


# Aragonite Undersaturation in the Arctic Ocean: Effects of Ocean Acidification and Sea Ice Melt


**Michiyo Yamamoto-Kawai,[1]* Fiona A. McLaughlin,[1] Eddy C. Carmack,[1] Shigeto Nishino,[2] Koji Shimada[2,3]**



The increase in anthropogenic carbon dioxide emissions and attendant increase in ocean acidification and sea ice melt act together to decrease the saturation state of calcium carbonate in the Canada Basin of the Arctic Ocean. In 2008, surface waters were undersaturated with respect to aragonite, a relatively soluble form of calcium carbonate found in plankton and invertebrates. Undersaturation was found to be a direct consequence of the recent extensive melting of sea ice in the Canada Basin. In addition, the retreat of the ice edge well past the shelf-break has produced conditions favorable to enhanced upwelling of subsurface, aragonite-undersaturated water onto the Arctic continental shelf. Undersaturation will affect both planktonic and benthic calcifying biota and therefore the composition of the Arctic ecosystem.


The increased rate of anthropogenic carbon dioxide ($CO_2$) released to the atmosphere in the 20th century has contributed to global warming and climate change because of the greenhouse effect (*1*). Because approximately one third of the $CO_2$ released has been absorbed by oceans, they are becoming more acidic (*2*, *3*). The uptake of $CO_2$ by seawater increases the concentration of hydrogen ions, which lowers pH and, in changing the chemical equilibrium of the inorganic carbon system, reduces the concentration of carbonate ions ($CO_3^{2-}$). Carbonate ions are required by marine calcifying organisms such as plankton, shellfish, and fish to produce calcium carbonate ($CaCO_3$) shells and skeletons. Therefore, the effects of decreased $CO_3^{2-}$ concentrations on marine organisms may place some species at risk (*3*, *4*). For either aragonite or calcite, the two types of $CaCO_3$ produced by marine organisms, the saturation state of $CaCO_3$


[1]Department of Fisheries and Oceans, Institute of Ocean Sciences, 9860 West Saanich Road, Sidney, British Columbia V8L 4B2, Canada. [2]Research Institute for Global Change, Japan Agency for Marine-Earth Science and Technology, 2-15 Natsushima, Yokosuka, Kanagawa 237-0061, Japan. [3]Tokyo University of Marine Science and Technology, 4-5-7, Konan, Minato-ku, Tokyo 108-8477, Japan.

*To whom correspondence should be addressed. E-mail: michiyo.kawai@dfo-mpo.gc.ca

($\Omega$) is expressed by the product of the concentrations of $CO_3^{2-}$ and $Ca^{2+}$ in seawater relative to the stoichiometric solubility product at a given temperature, salinity, and pressure. Waters with $\Omega > 1$ are favorable to forming $CaCO_3$ shells and skeletons, but waters with $\Omega < 1$ are corrosive, and in the absence of protective mechanisms, dissolution of $CaCO_3$ will commence. In surface waters, $\Omega$ is lower in high-latitude oceans than tropical or temperate oceans (*4*, *5*) because colder water absorbs more $CO_2$ and this reduces $CO_3^{2-}$. Therefore, apart from intermittent upwelling of undersaturated subsurface water as observed along the North American coast (*6*), surface waters are expected to become undersaturated ($\Omega < 1$) first in high-latitude oceans as atmospheric $CO_2$ concentrations increase. The Southern Ocean is predicted to become undersaturated with respect to aragonite-type $CaCO_3$ (aragonite is more soluble than calcite) by 2030 (*7*) and the North Pacific by 2100 (*8*). Model simulations of the Arctic Ocean predict $\Omega$ will decrease because of freshening and increased carbon uptake as a result of sea ice retreat and that Arctic surface waters will become undersaturated with aragonite within a decade (*9*).

In the Arctic Ocean, the decrease in the summer extent of Arctic sea ice has accelerated during the 2000s (*10*, *11*). Our data show that surface waters in the Canada Basin have freshened from 1997 to 2008 (fig. S1), and oxygen isotope tracer methods have shown that the major source of this additional freshwater is sea ice meltwater (Fig. 1A) (*12*, *13*). In 2008, total alkalinity (TA) and dissolved inorganic carbon (DIC) were analyzed in surface waters to calculate $\Omega$ aragonite (*13*). Compared with observations in 1997 (*14*), $\Omega$ aragonite was significantly lower in 2008, and undersaturated waters were found in the same region marked by low-salinity (S) and high–sea ice meltwater (Fig. 1A). Because meltwater has much lower concentrations of TA and DIC (~300 $\mu$mol kg$^{-1}$) than that of seawater (~2300 $\mu$mol kg$^{-1}$) (fig. S2) (*15*, *16*), mixing with sea ice meltwater decreases not only S but also TA and DIC. Altogether, decreases in S, TA, and DIC diminish concentrations of $CO_3^{2-}$ and, therefore, $\Omega$ (fig. S2). Although mixing with river water also dilutes seawater, river water has higher TA and DIC (~1000 $\mu$mol kg$^{-1}$) than that of meltwater (*15*). Therefore, the decrease in TA, DIC, and $\Omega$ is greater when the freshwater source is sea ice meltwater rather than river water (fig. S2). The $\Omega$ aragonite values are well correlated with both the fraction of sea ice meltwater [correlation factor ($r$) = –0.87] (Fig. 1B) and TA ($r$ = 0.84) and less well correlated with S ($r$ = 0.61). This indicates that the undersaturation of surface waters is a direct consequence of the recent and substantial increase in admixture of meltwater into the surface layer.

Furthermore, because sea ice limits air-sea gas exchange, the disappearance of sea ice in summer enhances $CO_2$ exchange between the ocean and atmosphere. Surface partial pressure of $CO_2$ ($Pco_2$) is lower in the Arctic Ocean than in the atmosphere (*17*, *18*) because of intense cooling, mixing with freshwater, and photosynthesis in summer, and, therefore, ice-free conditions increase $CO_2$ uptake and decrease $\Omega$. A comparison between the 1997 (*14*) and 2008 mean profiles of $\Omega$ aragonite in the Canada Basin shows that $\Omega$ aragonite has decreased in the top 50 m (Fig. 1C), the depth of the winter mixed layer. This is the layer in which rapid uptake of $CO_2$ occurs and increased freshwater inputs are found.

Models indicate sea ice will continue to decrease and predict that the Arctic Ocean may be ice-free in summer by the year 2030 (*19*). Thus, the amount of sea ice meltwater will probably continue to increase in the Canada Basin. An earlier onset of seasonal sea ice melt, together with global warming, will cause an increase in surface water temperature that will in turn act to increase $\Omega$ but to a small extent (fig. S2). Responses of phytoplankton to such changes are difficult to predict. Increased light availability and temperature may enhance photosynthesis during summer (which increases $\Omega$ by reducing seawater $CO_2$), but increased stratification of the seasonal layer by freshening and warming may decrease photosynthesis by blocking the resupply of nutrients from below. Nevertheless, it is clear that the melting of sea ice in the Arctic Ocean has indeed lowered $\Omega$ aragonite in the surface water to <1, and the Canada Basin is the first deep ocean where such surface undersaturation has been observed. We expect $\Omega$ will continue to decrease until the multiyear ice melts completely. Surface waters in the Canada Basin will exit the Arctic Ocean within ~10 years (*20*) and thus may contribute to a decrease in $\Omega$ in northern North Atlantic waters.

Moreover, as shown in Fig. 1C, waters with $\Omega$ aragonite of <1 are found at 100 to 200 m in the Canada Basin (*14*). The origin of this layer is Pacific water (fig. S3) that has been modified in winter on the highly productive Bering and Chukchi shelves (*21*). The characteristics of this so-called Pacific winter water (PWW) are cold temperatures (<–1°C), high nutrient concentrations, high content of $CO_2$ from the remineralization of organic matter, and therefore low $\Omega$ (*14*). Uptake of anthropogenic $CO_2$ has also influenced PWW properties. Calculations (*13*) indicate that $\Omega$ aragonite was ~1.2 during the preindustrial period when atmospheric $Pco_2$ was 280 parts per

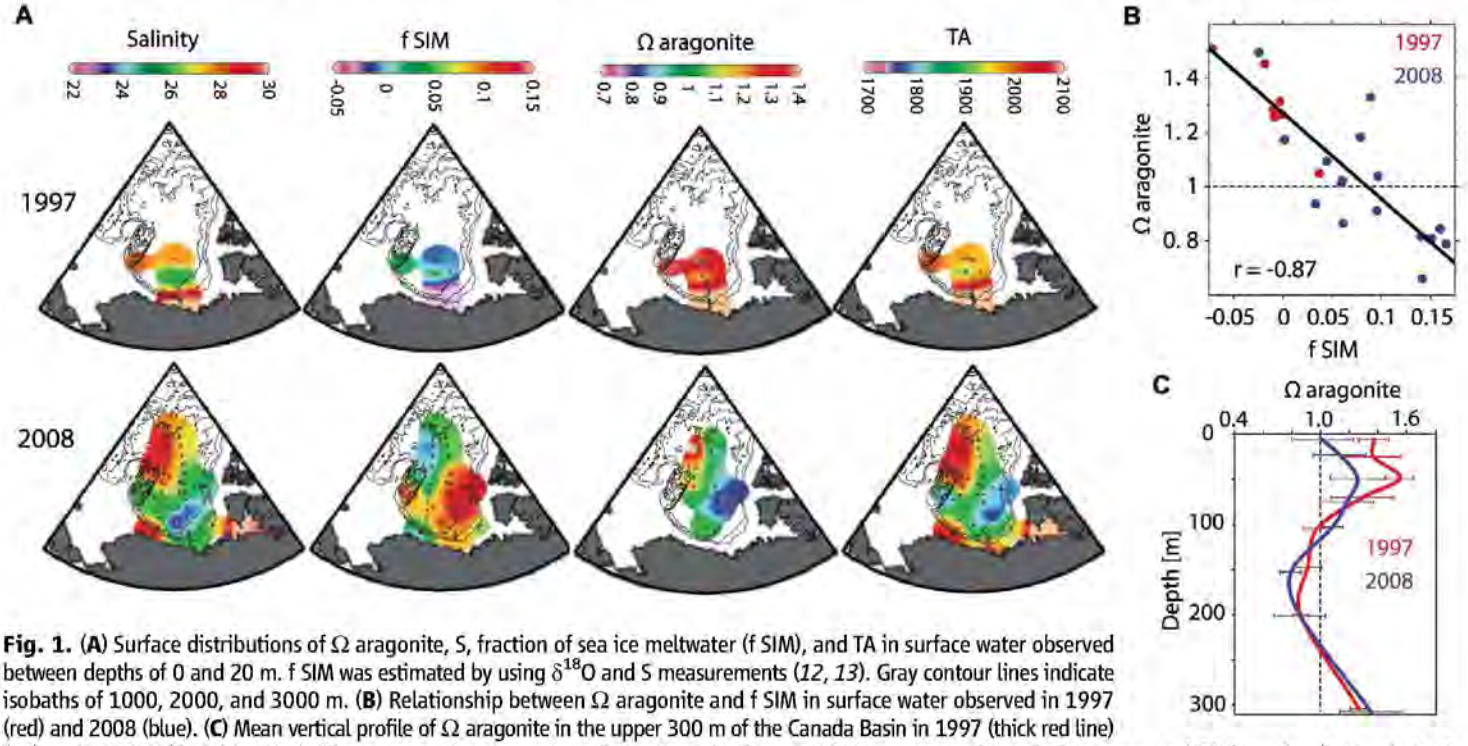


**Fig. 1.** (**A**) Surface distributions of $\Omega$ aragonite, S, fraction of sea ice meltwater (f SIM), and TA in surface water observed between depths of 0 and 20 m. f SIM was estimated by using $\delta^{18}O$ and S measurements (*12*, *13*). Gray contour lines indicate isobaths of 1000, 2000, and 3000 m. (**B**) Relationship between $\Omega$ aragonite and f SIM in surface water observed in 1997 (red) and 2008 (blue). (**C**) Mean vertical profile of $\Omega$ aragonite in the upper 300 m of the Canada Basin in 1997 (thick red line) (*14*) and in 2008 (thick blue line). Observations at stations where the bottom depth was >2000 m were used to calculate mean and SD (error bars) at each depth.

million (ppm) and then decreased to ~1.0 in the 1970s when atmospheric $P_{CO_2}$ was 330 ppm. Models indicate that retreat of the ice edge past the continental shelf break will greatly enhance upwelling (*22*). In the Canada Basin, the summer ice edge has been located northward of the shelf break almost yearly since 1997 (fig. S4), and thus upwelling will bring water with Ω aragonite of <1 onto the continental shelves.

Although the possible impact of decreased Ω and undersaturation with respect to aragonite on the ecosystem is not fully understood, laboratory experiments on marine biota in an elevated $CO_2$ environment show that changes in Ω cause substantial changes in overall calcification rates for many species of marine organisms, including coccolithophore, foraminifera, pteropods, mussels, and clams (*4*). In the Arctic Ocean, the larvae of aragonite shell–forming pteropods *Limacina helicina* are concentrated in the top 50 m (*23*), and this is where the decrease in Ω and increase in sea ice meltwater is the most profound. Upwelling of low Ω subsurface water onto the continental shelves will also affect benthic communities, such as bivalve molluscs (*4*). Therefore, we expect that populations of both planktonic and benthic calcifying organisms in the Canada Basin are now being affected because of the rapid decrease in Ω, which is due to the melting of sea ice and upwelling. Because they are important elements of the food web, the Arctic ecosystem may be at risk and requires observation in order to predict future possible impacts on marine organisms, fisheries, and biogeochemical cycles on both regional and global scales.

### References and Notes


1. Intergovernmental Panel on Climate Change, *Climate Change 2007: The Physical Science Basis; Contribution of Working Group I to the Fourth Assessment Report of the Intergovernmental Panel of Climate Change*, S. D. Solomon *et al.*, Eds. (Cambridge Univ. Press, Cambridge, 2007).
2. C. L. Sabine *et al.*, *Science* **305**, 367 (2004).
3. The Royal Society, "Ocean Acidification Due to Increasing Atmospheric Carbon Dioxide" (Policy Document 12/05, The Royal Society, London, 2005).
4. V. J. Fabry, B. A. Seibel, R. A. Feely, J. C. Orr, *ICES J. Mar. Sci.* **65**, 414 (2008).
5. R. M. Key *et al.*, *Global Biogeochem. Cycles* **18**, 10.1029/2004GB002247 (2004).
6. R. A. Feely *et al.*, *Science* **320**, 1490 (2008).
7. B. I. McNeil, R. J. Matear, *Proc. Natl. Acad. Sci. U.S.A.* **105**, 18860 (2008).
8. J. C. Orr *et al.*, *Nature* **437**, 681 (2005).
9. M. Steinacher, F. Joos, T. L. Frölicher, G.-K. Plattner, S. C. Doney, *Biogeoscience* **6**, 515 (2009).
10. J. Stroeve, M. M. Holland, W. Meier, *Geophys. Res. Lett.* **34**, 10.1029/2007GL029703 (2007).
11. J. C. Comiso, C. L. Parkinson, R. Gersten, L. Stock, *Geophys. Res. Lett.* **35**, 10.1029/2007GL031972 (2008).
12. M. Yamamoto-Kawai *et al.*, *J. Geophys. Res.* **114**, 10.1029/2008JC005000 (2009).
13. Materials and methods are available as supporting material on *Science* Online.
14. S. Jutterström, L. G. Anderson, *Mar. Chem.* **94**, 101 (2005).
15. L. W. Cooper *et al.*, *Geophys. Res. Lett.* **35**, 10.1029/2008GL035007 (2008).
16. L. G. Anderson, K. Olsson, M. Chierici, *Global Biogeochem. Cycles* **12**, 455 (1998).
17. L. G. Anderson, S. Kaltin, *Polar Res.* **20**, 225 (2001).
18. N. R. Bates, S. B. Moran, D. A. Hansell, J. T. Mathis, *Geophys. Res. Lett.* **33**, 10.1029/2006GL027028 (2006).
19. J. Stroeve *et al.*, *Eos* **89**, 13 (2008).
20. M. Yamamoto-Kawai, F. A. McLaughlin, E. C. Carmack, S. Nishino, K. Shimada, *J. Geophys. Res.* **113**, 10.1029/2006JC003858 (2008).
21. F. A. McLaughlin *et al.*, *Deep-Sea Res.* **51**, 107 (2004).
22. E. C. Carmack, D. C. Chapman, *Geophys. Res. Lett.* **30**, 10.1029/2003GL017526 (2003).
23. H. A. Kobayashi, *Mar. Biol. (Berl.)* **26**, 295 (1974).


24. We thank A. Proshutinsky as coinvestigator of the Beaufort Gyre project and acknowledge support provided by Fisheries and Oceans Canada, the Canadian International Polar Year program, and NSF. We are grateful to S. Zimmerman and other members of the scientific teams as well as the officers and crews on the CCGS Louis S. St-Laurent. We thank M. Davelaar, A. Ross, J. McKay, and K. Tamura for their careful analyses of TA, DIC, and $\delta^{18}O$ and H. Yoshikawa, S. Noriki, N. Kurita, and T. Takamura for their help in $\delta^{18}O$ analysis.


### Supporting Online Material

www.sciencemag.org/cgi/content/full/326/5956/1098/DC1
Materials and Methods
Figs. S1 to S4
References

30 March 2009; accepted 16 September 2009
10.1126/science.1174190

# Pleistocene Megafaunal Collapse, Novel Plant Communities, and Enhanced Fire Regimes in North America

**Jacquelyn L. Gill,[1,2] John W. Williams,[1,2] Stephen T. Jackson,[3] Katherine B. Lininger,[1] Guy S. Robinson[4]**

**Although the North American megafaunal extinctions and the formation of novel plant communities are well-known features of the last deglaciation, the causal relationships between these phenomena are unclear. Using the dung fungus *Sporormiella* and other paleoecological proxies from Appleman Lake, Indiana, and several New York sites, we established that the megafaunal decline closely preceded enhanced fire regimes and the development of plant communities that have no modern analogs. The loss of keystone megaherbivores may thus have altered ecosystem structure and function by the release of palatable hardwoods from herbivory pressure and by fuel accumulation. Megafaunal populations collapsed from 14,800 to 13,700 years ago, well before the final extinctions and during the Bølling-Allerød warm period. Human impacts remain plausible, but the decline predates Younger Dryas cooling and the extraterrestrial impact event proposed to have occurred 12,900 years ago.**

In North America, Pleistocene-Holocene deglaciation [18 to 6 thousand years ago (ka); 1 ka = 1000 calendar years ago] was marked by massive biotic upheaval, including the extinction of 34 megafaunal genera (*1*), species migration and reorganization of terrestrial communities (*2*), the rise and decline of plant communities without modern analogs (*3*), and increased biomass burning (*4*). Individualistic plant species' responses to climate change transformed the composition and distribution of vegetation formations, with rates of change highest between 13 and 10 ka (all ages are reported as calendar years before the present) (*2*). Many North American fossil pollen assemblages between 17 and 9 ka lack modern analogs, suggesting parent vegetation formations that were compositionally unlike any today (*5*). In the upper Midwest of the United States, "no-analog" pollen assemblages contained high percentages of temperate broadleaved trees, particularly *Fraxinus* (ash), *Ostrya*/*Carpinus* (hophornbeam/ironwood), and *Ulmus* (elm), coexisting with boreal conifers such as *Picea* (spruce) and *Larix* (larch) (*2*, *3*). These no-analog communities apparently formed in response to higher-than-present insolation and temperature seasonality, but it has been suggested that they may have been linked to the Pleistocene megafauna (*3*).

Deglaciation and vegetation turnover coincided with the end-Pleistocene megafaunal extinctions in North America, which was part of a global time-transgressive extinction wave that was taxonomically selective and more severe for species of large body size (*6*, *7*). In North America, >50% of all mammal species >32 kg and all species >1000 kg were extirpated (*1*). Hypothesized extinction drivers include climate change, human hunting, or a combination of the two; the relative importance of these mechanisms is debated (*1*, *8*). An extraterrestrial impact at 12.9 ka has also been proposed (*9*) but is disputed (*4*, *10*).

The apparent coincidence between megafaunal extinction, peak rates of vegetation change, and the rise of the no-analog communities (*3*) in eastern North America suggests causal relationships, but the direction of causation remains unclear. Hypothesized extinction mechanisms linked to vegetation change include habitat loss and fragmentation, disruption of coevolved plant and animal communities, and loss of vegetation mosaics (*1*, *8*). Conversely, the removal of keystone megaherbivores might have triggered trophic

[1]Department of Geography, University of Wisconsin, Madison, WI 53706, USA. [2]Center for Climatic Research, University of Wisconsin, Madison, WI 53706, USA. [3]Department of Botany, University of Wyoming, Laramie, WY 82071, USA. [4]Department of Natural Science, Lincoln Center Campus, Fordham University, New York, NY 10023, USA.

effects (*11*). Contemporary exclusion experiments have highlighted megafaunal influences on plant community composition and structure though edaphic disturbance, selective herbivory, and seed dispersal and propagation (*12*). In African savannas, megaherbivores can suppress fire by reducing fuel loads and facilitating the growth of less-flammable species (*13*).

Testing causal hypotheses has been hampered by difficulties in establishing the precise temporal sequence of events, due to fossil scarcity and uncertainties in dating and cross-site correlations. Megafaunal remains are rare, particularly in the lakes and mires that archive late Quaternary pollen records, and changes in population densities cannot be inferred from most megafaunal fossil records. Many bone radiocarbon dates are erroneously young because of contamination by humic acids, although dating of purified bone collagen can remove this effect (*14*). The last-dated fossil for a species is unlikely to be from the last surviving individual.

We precisely established local lead-lag relationships among the no-analog plant communities, changes in fire regimes, and megafaunal population declines through a multiproxy sedimentary study of *Sporormiella* dung fungal spores, fossil pollen, and charcoal from a lake in mid-continental North America. *Sporormiella* is a genus of coprophilous fungi in the family Sporormiaceae that requires herbivore digestion to complete its life cycle, producing spores on the dung of mammals and some birds (*15*). *Sporormiella* spores have been found in mammoth (*Mammuthus* spp.) gut contents and coprolites (*16*, *17*). *Sporormiella* spores track the end-Pleistocene megafaunal population decline: They are abundant in late-glacial sediments, scarce through the Holocene, and return to high abundances after the historic introduction of domestic grazers (*16*, *18*). The spores are transported to lakes by slopewash, so *Sporormiella* abundances in lake sediments reflect both dung loadings in the watershed and distance to their source (*19*). Thus, *Sporormiella* abundances cannot be simply converted to dung volume and herbivore biomass, but *Sporormiella* abundances <2% of the arboreal pollen sum consistently indicate the extinction of megafauna at sites in Pleistocene North America (*16*) and in late Holocene Madagascar (*20*).

Appleman Lake (LaGrange County, Indiana; 41.6237°N, 85.2136°W), a 21-ha kettle pond situated on glacial till and outwash from the Lake Michigan Lobe, is centrally located within the no-analog vegetation formations (Fig. 1). An 11.5-m sediment core was extracted in 2005 (*21*). Thirteen wood, pollen, and charcoal samples were submitted for radiocarbon analysis (table S1), four anomalous dates were rejected, and a linear age model was constructed from the remaining dates (fig. S1). No-analog communities were identified by plotting the minimum squared chord dissimilarities (SCDs) between Appleman pollen assemblages and their closest matches from the North American Modern Pollen Database; fossil samples with minimum dissimilarities >0.3 were considered to have no modern analog.

At Appleman Lake, *Sporormiella* was initially abundant, began declining at ~14.8 ka, fell below 2% at 13.7 ka (Fig. 2G), and remained <2% thereafter. The youngest-dated bones of most North American megafauna cluster between 13 and 11.5 ka (*22*), so the *Sporormiella* decline apparently indicates local population collapse and func-

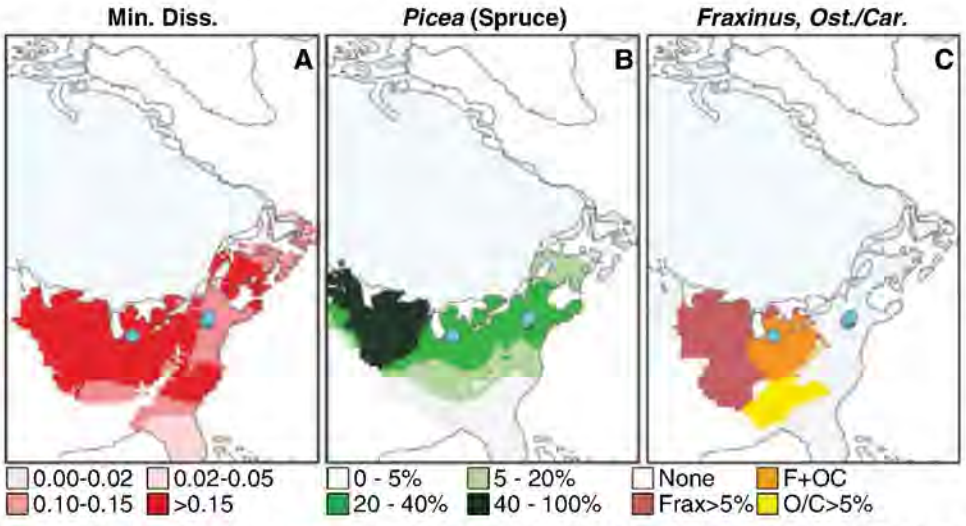


**Fig. 1.** Position of Appleman Lake, Indiana, and New York sites (blue circles) relative to (**A**) minimum squared chord dissimilarity for fossil pollen assemblages in eastern North America, (**B**) *Picea* pollen percentages, and (**C**) the distributions of *Fraxinus* and *Ostrya/Carpinus* pollen, all mapped for 14 ka. The mapped SCDs are based on a smaller list of taxa (25 pollen types) than used elsewhere in this paper; therefore, values >0.15 indicate fossil samples with no modern analog.

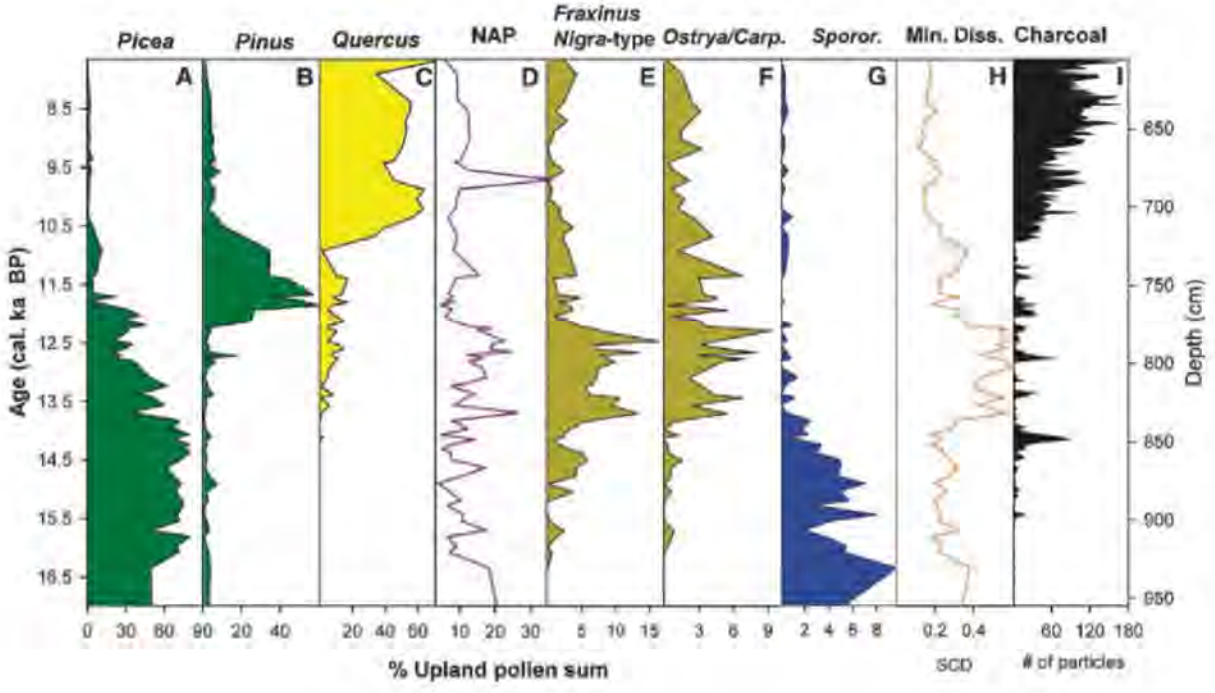


**Fig. 2.** Appleman Lake time series for (**A** to **F**) percent pollen abundances of selected taxa (NAP, nonarboreal pollen), (**G**) *Sporormiella*, (**H**) minimum squared chord dissimilarity, and (**I**) charcoal counts. Pollen abundances are expressed as a percentage of the upland pollen sum.

tional species extinction, not final extinction. The *Sporormiella* decline roughly coincided with the initiation of the Bølling-Allerød warm period, dated in Greenland at 14.69 ka (*23*). No-analog plant communities developed at 13.7 ka (Fig. 2H), after *Sporormiella* declined below 2%, and were marked by rises in *Fraxinus nigra*–type (black ash) and *Ostrya/Carpinus* (hophornbeam/ironwood) pollen abundances while *Picea* (spruce) abundances remained high (Fig. 2, A, E, and F). No-analog communities persisted until 11.9 ka (Fig. 2H) and were followed by a period of high *Pinus* (pine) abundances (Fig. 2B), then high abundances of *Quercus* (oak), marking the early Holocene establishment of deciduous forests in northern Indiana.

Fire regimes at Appleman had three stages. Before 14.3 ka, charcoal was uncommon, indicating few or no local fires (Fig. 2I) or insufficient biomass to produce abundant charcoal. After 14.3 ka, charcoal peaks were intermittent against low background rates of charcoal deposition. Charcoal first peaked at 14.1 ka, during the *Sporormiella* decline and before the increase in hardwood pollen abundances. This stage persisted until 10.7 ka, when rates of charcoal deposition and *Quercus* pollen abundances increased rapidly.

The close linkage between *Sporormiella* and changes in vegetation and fire at Appleman Lake is consistent with evidence from several New York sites (Fig. 3) (*18*). There, the onset of the *Sporormiella* decline ranged from <13 ka to >14 ka; dating is less certain than at Appleman due to hard-water contamination of bulk sediment radiocarbon dates (*24*). The New York sites are on the periphery of the late-glacial no-analog communities (Fig. 1) (*3*), and minimum SCDs are lower than at Appleman Lake (Fig. 3). Nevertheless, as at Appleman, hardwood abundances increased immediately after the *Sporormiella* decline, contributing to an increase in vegetation dissimilarity, and charcoal abundances peaked during or after the *Sporormiella* decline (Fig. 3).

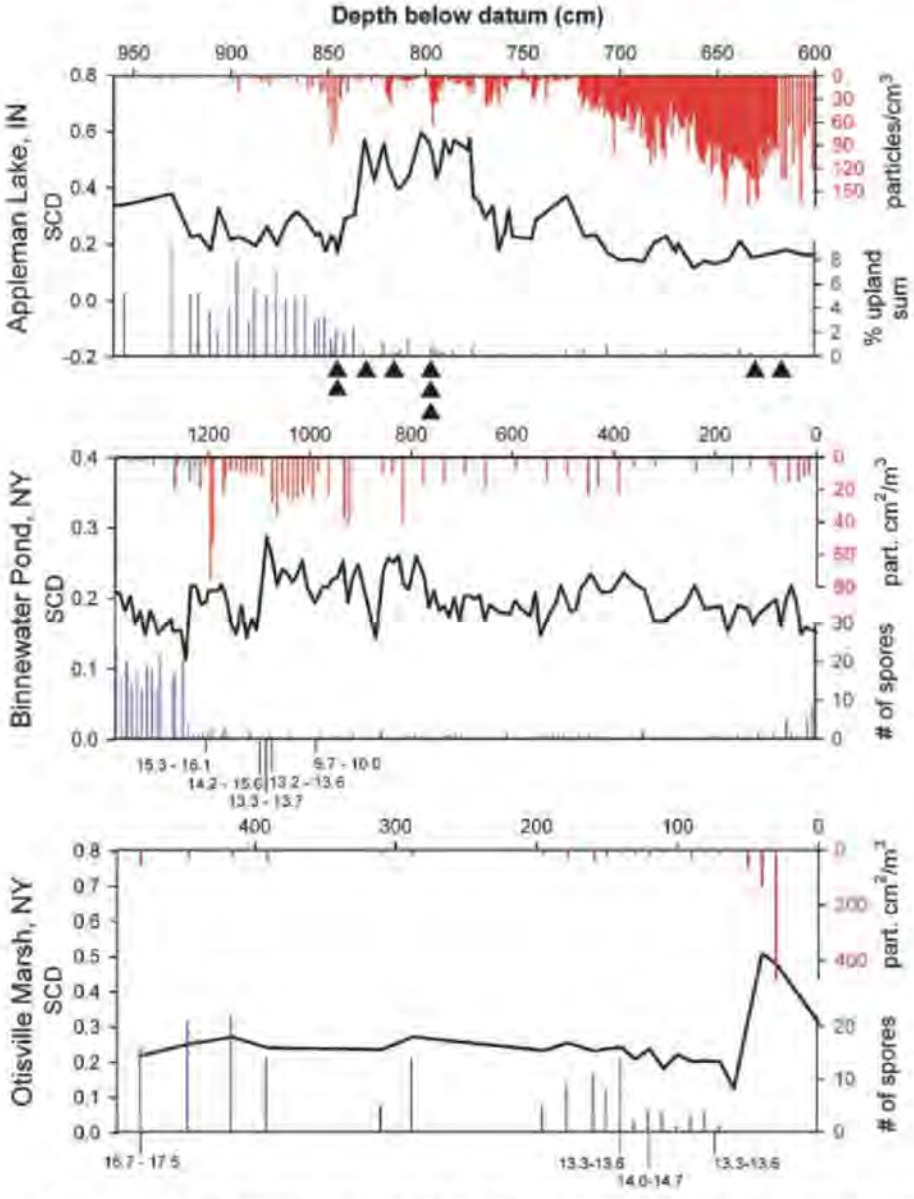


**Fig. 3.** Comparison of the Appleman record with two New York sites reinforces the close connection among the *Sporormiella* decline (blue histogram), the first large pulse of sedimentary charcoal (red histogram, inverted axis), and increased vegetation dissimilarity from that of the present (black line). Black triangles indicate locations of radiocarbon dates from Appleman.

Our data thus rule out hypotheses that (i) climate-forced changes in vegetation drove the megafaunal decline, and (ii) no-analog plant communities were created by megaherbivory. The first hypothesis is rejected because the *Sporormiella* decline preceded the major palynological events (particularly the shift from *Picea* to *Pinus* and increased abundances of hardwood taxa). However, climate change might have directly forced the megafaunal population declines, given the similar timing between the *Sporormiella* decline and the onset of Bølling-Allerød warming in Greenland (*23*). If so, climatic forcing apparently did not operate through habitat change, which is the mechanism underlying most climate-based extinction hypotheses (*1*).

The second hypothesis is excluded because the no-analog communities arose after *Sporormiella* declined. Thus, the increase in hardwood taxa (*Fraxinus*- and *Ostrya/Carpinus* at Appleman and *Ulmus*, *Acer*, and others in New York) may represent both a response to warming and a release from herbivory pressure. Many extant megaherbivores prefer broadleaf forage because of its higher nutrient and water content (*12*, *25*). For example, moose (*Alces alces*) dietary preferences have reduced tree density and promoted shrubs and needle-leaved trees (*26*). Tradeoffs between fire and megafaunal consumption of biomass are documented in modern African ecosystems (*13*). A switch from herbivory- to fire-dominated disturbance regimes may explain why the first post-*Sporormiella* charcoal peak was consistently the largest across sites (Fig. 3), if this first fire burned both live biomass and litter untouched by herbivores.

The possibility that late-glacial vegetation and fire regimes were influenced by herbivory does not rule out climatic drivers of late Quaternary landscape change, which are well established (*27*, *28*). Rather, we suggest a hierarchy of controls on deglacial vegetation history, with climate driving changes in plant and megafaunal ranges and abundances, which engendered further herbivory- and fire-regulated biotic interactions. The rise in *Fraxinus nigra*–type and *Ostrya/Carpinus* pollen ~15.0 ka (Fig. 2, E and F) may indicate the establishment of small tree populations under newly favorable climates, whereas secondary increases at 13.7 ka may indicate the expansion of populations under decreased herbivory pressure and a new fire regime. Thus, the formation of no-analog plant communities may have been jointly controlled by novel climates (highly seasonal insolation and temperatures) (*5*) and release from herbivory.

Humans may have affected late Quaternary vegetation history by intensifying fire regimes and contributing to the megafaunal extinctions. Increased sedimentary charcoal is associated with human arrival and megafaunal extinctions on islands (*20*), and

the globally time-transgressive wave of late Pleistocene extinctions closely tracks human colonization history. Butchered mammoth bones excavated in southeastern Wisconsin date regional human presence to between 14.8 and 14.1 ka (*29*), coeval with the *Sporormiella* decline at Appleman Lake.

At all sites, the *Sporormiella* decline substantially predated initiation of the Younger Dryas, ruling out abrupt climatic cooling and the hypothesized extraterrestrial impact at 12.9 ka as a cause (*9*). More generally, the megafaunal declines apparently progressed over several thousand years, given the 1000-year duration of the *Sporormiella* decline at Appleman and the difference in timing between the onset of the *Sporormiella* decline (14.8 ka) and the final extinctions (~11.5 ka) (*1*). This evidence excludes rapid-extinction hypotheses such as an extraterrestrial impact or a Paleo-Indian blitzkrieg (*30*).

Our work thus shows close connections among the late-glacial histories of fire, vegetation, and mammalian herbivores and suggests that the loss of a broad guild of consumers contributed to substantial restructuring of plant communities and an enhanced fire regime. The sequence of events at Appleman rules out several hypothesized causes and effects of the megafaunal extinction but does not conclusively resolve the debate over climatic versus human causation (or both) of the North American megafaunal extinctions. However, several promising avenues exist. One is to search for spatial and temporal patterns in the late Pleistocene *Sporormiella* decline (time-transgressive versus synchronous) and to further check its association with vegetation and fire history. Another is to analyze the *Sporormiella* record at sites spanning the penultimate deglaciation (when humans were absent from North America) and in sites near well-dated records of Paleo-Indian activity. Such analyses should be extended to other continents, to study the ecological effects of the end-Pleistocene extinctions under different contexts of human, climate, and vegetation history (*31*). By resolving the causes and consequences of the late Pleistocene megafaunal extinctions, such work would address concerns about trophic effects arising from the contemporary widespread declines, extinctions, and restorations of megaherbivores.

### References and Notes


1. P. L. Koch, A. D. Barnosky, *Annu. Rev. Ecol. Evol. Syst.* **37**, 215 (2006).
2. J. W. Williams, B. N. Shuman, T. Webb III, P. J. Bartlein, P. L. Leduc, *Ecol. Monogr.* **74**, 309 (2004).
3. J. W. Williams, B. N. Shuman, T. Webb III, *Ecology* **82**, 3346 (2001).
4. J. R. Marlon *et al.*, *Proc. Natl. Acad. Sci. U.S.A.* **106**, 2519 (2009).
5. J. W. Williams, S. T. Jackson, *Front. Ecol. Environ* **5**, 475 (2007).
6. S. K. Lyons, F. A. Smith, J. H. Brown, *Evol. Ecol. Res.* **6**, 339 (2004).
7. J. Alroy, in *Extinctions in Near Time: Causes, Contexts and Consequences*, R. D. E. MacPhee, Ed. (Kluwer Academic, New York, 1999), pp. 105–140.
8. D. A. Burney, T. F. Flannery, *Trends Ecol. Evol.* **20**, 395 (2005).
9. R. B. Firestone *et al.*, *Proc. Natl. Acad. Sci. U.S.A.* **104**, 16016 (2007).
10. N. Pinter, S. E. Ishman, *GSA Today* **18**, 37 (2008).
11. N. Owen-Smith, *Paleobiolgy* **13**, 351 (1987).
12. K. Danell, R. Bergstrom, P. Duncan, J. Pastor, *Large Herbivore Ecology, Ecosystem Dynamics, and Conservation* (Cambridge Univ. Press, Cambridge, 2006).
13. M. Sankaran *et al.*, *Nature* **438**, 846 (2005).
14. D. Overstreet, T. Stafford Jr., *Curr. Res. Pleistocene* **14**, 70 (1997).
15. S. E. Ahmed, R. F. Cain, *Can. J. Bot.* **50**, 419 (1972).
16. O. K. Davis, D. S. Shafer, *Palaeogeogr. Palaeoclimatol. Palaeoecol.* **237**, 40 (2006).
17. B. Van Geel *et al.*, *Quat. Res.* **69**, 361 (2008).
18. G. S. Robinson, L. P. Burney, D. A. Burney, *Ecol. Monogr.* **75**, 295 (2005).
19. D. Raper, M. B. Bush, *Quat. Res.* **71**, 490 (2009).
20. D. A. Burney, G. S. Robinson, L. P. Burney, *Proc. Natl. Acad. Sci. U.S.A.* **100**, 10800 (2003).
21. Materials and methods are available as supporting material on *Science* Online.
22. S. Fiedel, G. Haynes, *J. Archaeol. Sci.* **31**, 121 (2004).
23. S. O. Rasmussen *et al.*, *J. Geophys. Res.* **111**, D06102 (2006).
24. E. C. Grimm, L. J. Maher Jr., D. M. Nelson, *Quat. Res.* **72**, 301 (2009).
25. P. D. Coley, *New Phytol.* (suppl.) **106**, 251 (1987).
26. P. F. McInnes, R. J. Naiman, J. Pastor, Y. Cohen, *Ecology* **73**, 2059 (1992).
27. I. C. Prentice, P. J. Bartlein, T. Webb III, *Ecology* **72**, 2038 (1991).
28. P. J. Bartlein *et al.*, *Quat. Sci. Rev.* **17**, 549 (1998).
29. D. J. Joyce, *Quat. Int.* **142-143**, 44 (2006).
30. P. S. Martin, in *Quaternary Extinctions: A Prehistoric Revolution*, P. S. Martin, R. G. Klein, Eds. (Univ. of Arizona Press, Tucson, AZ, 1984).
31. C. N. Johnson, *Proc. R. Soc. London Ser. B* **276**, 2509 (2009).


32. We thank E. Grimm, J. Mason, and S. Hotchkiss for discussions and T. Minckley, S. Lucas, J. Marsicek, D. Alhambra, G. Schellinger, and S. Hernandez for field and laboratory assistance. Initial core analyses were performed at the National Lacustrine Core Facility at the University of Minnesota. This work was supported by NSF (grants DEB-0716471 and DEB-0716951) and the Graduate School and the Climate, People and Environment Program at the University of Wisconsin.


### Supporting Online Material

www.sciencemag.org/cgi/content/full/326/5956/1100/DC1
Materials and Methods
Figs. S1 to S4
Tables S1 and S2
References

10.1126/science.1179504

# High Symbiont Relatedness Stabilizes Mutualistic Cooperation in Fungus-Growing Termites

**Duur K. Aanen,[1]* Henrik H. de Fine Licht,[2] Alfons J. M. Debets,[1] Niels A. G. Kerstes,[1] Rolf F. Hoekstra,[1] Jacobus J. Boomsma[2]**

**It is unclear how mutualistic relationships can be stable when partners disperse freely and have the possibility of forming associations with many alternative genotypes. Theory predicts that high symbiont relatedness should resolve this problem, but the mechanisms to enforce this have rarely been studied. We show that African fungus-growing termites propagate single variants of their *Termitomyces* symbiont, despite initiating cultures from genetically variable spores from the habitat. High inoculation density in the substrate followed by fusion among clonally related mycelia enhances the efficiency of spore production in proportion to strain frequency. This positive reinforcement results in an exclusive lifetime association of each host colony with a single fungal symbiont and hinders the evolution of cheating. Our findings explain why vertical symbiont transmission in fungus-growing termites is rare and evolutionarily derived.**

Horizontal symbiont transmission is the rule in ancient and ecologically important mutualisms, such as those between plants and mycorrhizas or nitrogen-fixing bacteria. The stability of such interactions is puzzling, because multiple symbiont lineages compete for host resources, and hosts have frequent opportunities to exchange resident symbionts with new and potentially superior lineages (*1*–*3*). Here we address the evolutionary stability of an analogous animal-microbial mutualism in the fungus-growing termites (subfamily Macrotermitinae), which coevolved with a single genus of basidiomycete fungi, *Termitomyces*, while retaining horizontal symbiont transmission in most genera (*4*).

The termite-fungus mutualism is of major ecological importance in Old World tropical regions for decomposition and mineral cycling (*5*). The termites cultivate their fungal symbiont in well-protected gardens inside the nests on a substrate (comb) of predigested plant material (Fig. 1A). The mutualistic fungus provides most of the termite food, both directly, when termites eat nodules of fungal material containing asexual spores (Fig. 1B), and indirectly, when they ingest the partially degraded comb biomass later on (*6*, *7*). The symbiosis has a single African rain forest origin, more than 30 million years ago (*8*–*11*) and has radiated into 10 extant genera with about 330 described species (*12*).

No reversals to a solitary life-style are known (*4*). This is remarkable, as partners in most genera have retained independent reproduction by means

[1]Laboratory of Genetics, Wageningen University, 6700 AH Wageningen, Netherlands. [2]Centre for Social Evolution, Department of Biology, University of Copenhagen, 2100 Copenhagen, Denmark.

*To whom correspondence should be addressed. E-mail: duur.aanen@wur.nl

of termite swarming and growing mushrooms to disperse sexual spores. New colonies therefore need to acquire their garden symbionts de novo by collecting spores from the habitat (*13*). Similarly to most basidiomycetes, *Termitomyces* life cycles alternate between a homokaryotic and heterokaryotic stage, having one and two genetically different types of haploid nuclei, respectively (*14*), and fungus garden mycelium is heterokaryotic in all natural colonies studied so far. This implies that incipient termite colonies must be colonized by at least two compatible, and genetically different, sexual spores and that the homokaryotic stage is relatively short-lived [(*14*–*16*) and this study].

Following recently developed theory (*1*, *17*, *18*), we hypothesized that fungus-growing termites have evolved mechanisms to increase relatedness among symbionts to overcome the genetic heterogeneity of symbionts incurred at the start of a colony cycle. High symbiont relatedness reduces competition among strains and will therefore select for prudent horizontal transmission, causing minimal harm to the host (*1*). However, high symbiont relatedness needs to serve the short-term interests of both the fungi and the termites to remain stable over evolutionary time (*1*), and it has remained unclear how that might be achieved.

We used a highly variable intron of the single-copy gene *Elongation Factor 1 alpha* (*16*) to characterize symbiont diversity in multiple nests of *Macrotermes natalensis* (113 fungal samples collected from 49 different nests), *Odontotermes transvaalensis* (11 fungal samples from seven nests), and *Odontotermes badius* (13 samples from seven nests) (*19*). All but 2 of the 49 *Macrotermes natalensis* nests had a genetically unique strain of fungus (Fig. 1C), but we found no variation among multiple samples taken from the same nest. The difference between among- and within-colony diversity was highly significant ($P \ll 0.00001$) (*19*), and the detection power for genotypic diversity in a sample of this size was high (*19*). Similarly, we found genetic variation among symbionts from different nests in the two *Odontotermes* species, but never within nests. It therefore appears that *Termitomyces* is cultivated in single-strain monocultures (*4*, *20*).

We undertook a series of in vitro experiments on agar plates to simulate within-nest propagation of *Termitomyces*, using similarly high densities of asexual spores as in natural comb substrate (fig. S1). The propagation cycle starts with termites harvesting modified unripe mushrooms or nodules (Fig. 1B) containing asexual spores (conidia) (*21*, *22*). The spores are ingested, mixed with fragmented plant material, and homogeneously deposited as primary feces to build new layers of fungus comb. We harvested nodules from petri dish cultures and suspended the conidia in sterile water then used this suspension to inoculate fresh agar plates, emulating the termite fecal deposition behavior (fig. S1). The strains used were isolated from five colonies of *Macrotermes natalensis* (Fig. 1C), a species associated with a single species of *Termitomyces* (*14*–*16*). To investigate whether competing strains facilitate some form of positive reinforcement that would result in single-strain monocultures, we inoculated mixtures of five strains such that one strain provided 50% of the spores, while the remaining four strains made up 12.5% each. The results were consistent with positive frequency-dependent selection enhancing the representation of the majority inoculum strain among the asexual spores produced by the next cohort of nodules ($\chi^2 = 30.45$; df = 1; $P < 0.0001$; three of the five combinations, $P < 0.01$) (Fig. 1D).

We also compared the yield of asexual spores from monocultures of the five strains with that of mixed cultures with varying strain frequencies in high-density cultures and found that monoculture fungus farming gives a significantly higher yield than mixed cultures (Fig. 2, A and B). Next, we tested whether the scale of asexual spore production is dependent on the extent of successful fusion between clonally related mycelia, because it is well established that successful fusion between basidiomycete heterokaryons only happens when mycelia are clonally related, whereas fusion between genetically different clones is invariably followed by cell death at the interface of interacting mycelia (*23*). The frequency of successful fusion in a mixture of genetically different strains should therefore be lower than in a monoculture because clonal patches are smaller (fig. S4). However, this would not necessarily increase yield in monocultures, because fungal reproduction is often triggered by contact between genetically different mycelia [reviewed in (*24*)]. Our experimental results resolved this paradox by showing that average symbiont relatedness is indeed negatively correlated with the number of nodules produced (Fig. 2D), but positively correlated with average nodule size:

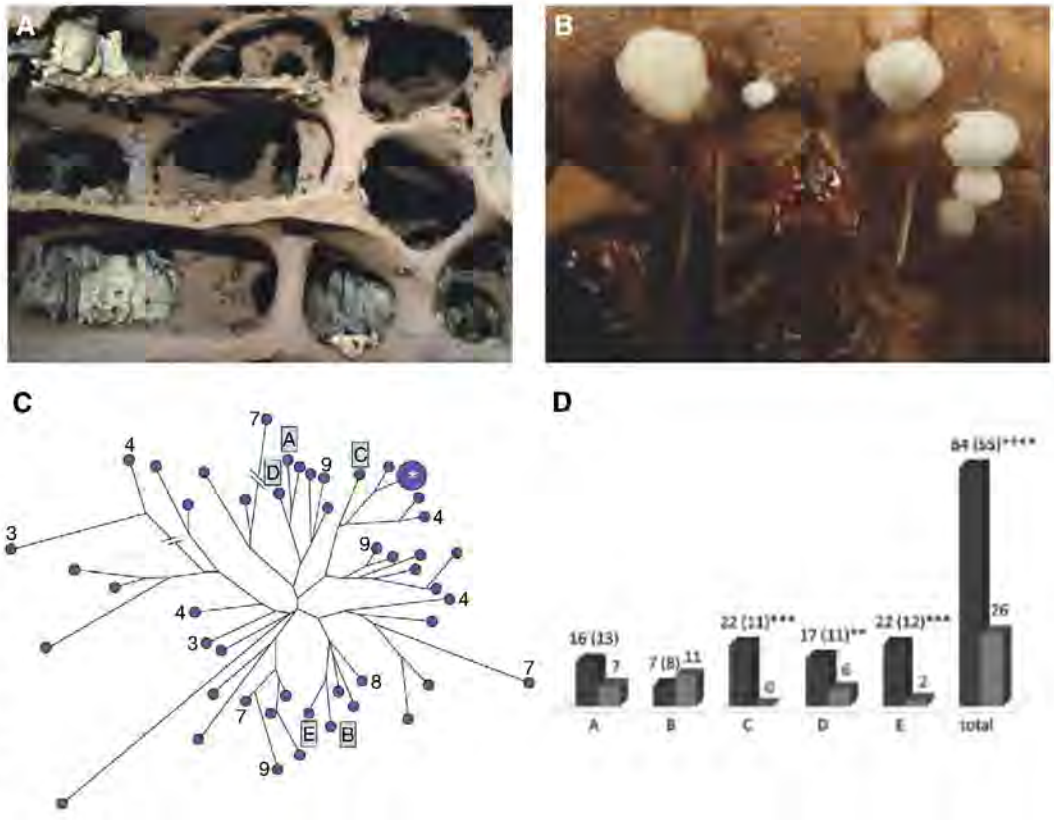


**Fig. 1.** Fungus cultivation by macrotermitine termites. (**A**) The inside of a colony of *Macrotermes natalensis* in South Africa. Fungus gardens are arranged in an interconnected network of chambers, each containing a mass of masticated plant substrate in which *Termitomyces* grows. (**B**) Close-up of a fungus garden of a *Macrotermes* sp. with multiple asexual fruiting bodies (nodules). The spores survive passage through the termite gut and are mixed with predigested plant material to be deposited as inoculated fresh garden substrate (*21*, *22*). (**C**) Genetic diversity of *Termitomyces* symbionts associated with *Macrotermes natalensis* in South Africa. Each circle represents a fungal genotype. Only two colonies shared the same fungal genotype [larger circle marked with an asterisk (*)]. No within-colony variation was found in 13 multiply sampled nests (number of samples per nest indicated; $n = 5.9$ samples on average). (**D**) Experimental demonstration of positive frequency-dependent selection on *Termitomyces* strains in mixtures of asexual spores indicated by letters in (C) with one of them being inoculated at 50% (the *x* axis label strain and the darker bars) and the others at 12.5% each (pooled in the lighter bars). The expected frequencies of the dominant strain without frequency-dependent selection are given in parentheses. $^{**}P < 0.01$; $^{***}P < 0.001$; $^{****}P < 0.0001$.

The mixed cultures have about three times as many nodules, but their total spore production is only ~15% of what monoculture nodules produce [(*19*) and supporting online text] (fig. S4). This shows that coordinated reproduction after successful fusion of neighboring mycelia belonging to the same clone is more efficient because mycelia mergers allow "division of labor" between mycelial growth and asexual reproduction.

The higher yield of *Termitomyces* monocultures relative to mixed cultures is caused by two effects: (i) synergism between successfully fusing mycelia and (ii) lack of supposedly costly cell death in monocultures. In some fungi (e.g., the *Leucoagaricus* associated with fungus-growing ants), cell death after unsuccessful fusion of mycelia is followed by further antagonistic destruction of mycelium on both sides (*25*), but this effect is not always found when genetically different mycelia of free-living fungi meet [compare (*23*) and (*26*)]. When we tested this, we found that there were no visible zones of mycelial antagonism in plated cultures of genetically different *Termitomyces* strains (Fig. 2C). Fungal propagation by termites thus provides a positive-feedback mechanism that leads to monocultures within colonies in spite of promiscuous acquisition of multiple symbionts during colony foundation. This process reinforces the occurrence of genetic bottlenecks, which also happens at each crop-rotation cycle within colonies (*21*), and stabilizes the mutualism, as it maximizes the short-term fitness interests of both termites and fungal crops.

Our results show that the comparative study of the convergently evolved fungus-farming systems of the attine ants (*27*–*29*) and the macrotermitine termites (*4*, *5*, *30*) provides insight into the general principles that govern the stability of obligate ectosymbiotic mutualisms. In both systems, the fungal symbionts are reared as single-strain monocultures, in spite of substantial genetic variation among fungal clones across colonies [(*14*-*16*) and this study], but this common characteristic is independent of the default symbiont transmission mode (vertical in the ants and horizontal in the termites) [(*24*) and this study]. Rather than transmission mode, it appears that the lifetime commitment between each farming society and a specific clonal crop is decisive for making both these fungus-farming mutualisms evolutionarily stable. Lifetime commitment is an extreme form of partner fidelity (*3*) and removes every incentive for cheating by reducing symbiont performance. However, this does not imply that host-symbiont conflict over transmission by independent reproduction cannot be further reduced, so that the occasional secondary evolution of vertical, uniparental symbiont inheritance in two genera of fungus-growing termites is not surprising (*13*, *19*).

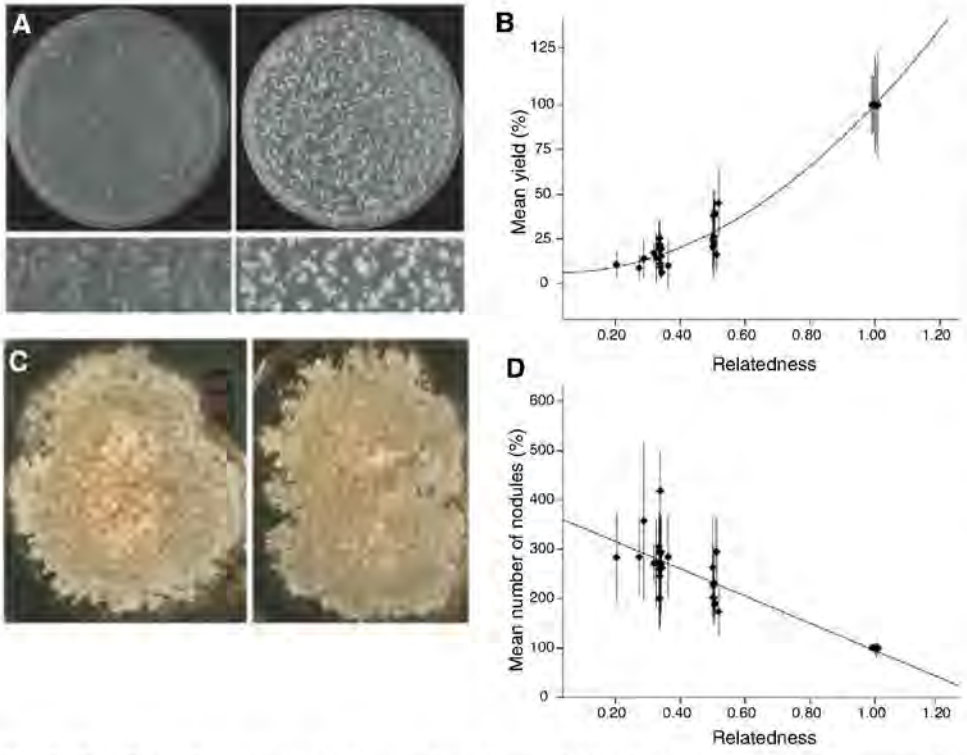


**Fig. 2.** The effects of symbiont relatedness on fungal spore yield and nodule number. (**A**) Representative examples of monoculture (right) and mixed culture of five strains (left) after we inoculated ~30,000 asexual spores per petri dish; (bottom) close-ups of plates. Normalized yield (**B**) and number of nodules (**D**) (relative to monocultures set at 100%) (*19*) against symbiont relatedness, the probability that two spores in a mixture are clonally related. Dots are averages of five replicates, bars are 95% confidence limits, and the lines are regressions (quadratic for yield, $R^2 = 0.956$, $P < 0.0001$; linear for nodule number, $R^2 = 0.735$, $P < 0.0001$) (*19*). (**C**) No direct mycelial antagonism was observed between two genetically different fungal strains inoculated on the same plate (left), relative to two strains of the same clone (right); the figure is a typical example of 21 strains tested in all 231 possible combinations) (*19*).

Our results imply that the *Termitomyces* farming symbiosis has both a very specific process for mediating partner choice and an extreme degree of partner fidelity. These two mechanisms have featured prominently in theoretical models to explain the evolutionary stability of mutualisms with horizontal, promiscuous partnership exchange (*2*, *3*, *31*), but as alternative pathways, rather than causally connected ones. Our study shows that a recurrent process of partner choice can enforce lifetime partner fidelity by direct positive reinforcement, a result that offers general insight into the mechanisms that stabilize promiscuous mutualisms. To appreciate this, it is important to realize that termite colonies with *Termitomyces* symbionts sequester their resource patches for symbiont growth inside the same insect society, so that they also control inoculation. It is the combination of these characteristics that allows positive frequency-dependence to enforce symbiont clonality, in spite of promiscuous acquisition and occasional recolonization by other strains. Lifetime partner fidelity is the inevitable consequence, and this eliminates evolutionary incentives for symbiont cheating (parasitic strains of *Termitomyces* are neither known nor expected).

This unique combination of characteristics is not found in other promiscuous mutualisms such as *Rhizobia* (*32*), arbuscular mycorrhizae (*33*), or corals (*34*). These hosts sequester their compartments for symbionts sequentially during growth and cannot directly control the colonization of new compartments, as the termite fungus farmers can. This lack of host control at the level of single compartments is the crucial difference that allows the persistence of cheating variants. Compartmentalization [reviewed in (*35*)] has repeatedly been suggested as a possible mechanism to reduce cheating in promiscuous mutualisms, because it induces high local relatedness (*1*, *17*, *18*), but our study experimentally confirms the necessity of a direct positive-reinforcement mechanism at the same single-compartment scale to ensure the monopoly of a single symbiont strain.

## References and Notes

1. S. A. Frank, *Proc. R. Soc. London B Biol. Sci.* **263**, 339 (1996).
2. E. A. Herre, N. Knowlton, U. G. Mueller, S. A. Rehner, *Trends Ecol. Evol.* **14**, 49 (1999).
3. J. L. Sachs, U. G. Mueller, T. P. Wilcox, J. J. Bull, *Q. Rev. Biol.* **79**, 135 (2004).
4. D. K. Aanen *et al.*, *Proc. Natl. Acad. Sci. U.S.A.* **99**, 14887 (2002).
5. J. P. E. C. Darlington, in *Nourishment and Evolution in Insect Societies*, J. H. Hunt, C. A. Nalepa, Eds. (Westview Press, Boulder, CO, 1994), pp. 105–130.
6. D. E. Bignell, in *Termites: Evolution, Sociality, Symbioses, Ecology*, T. Abe, D. E. Bignell, M. Higashi, Eds. (Kluwer Academic, Dordrecht, Netherlands, 2000), pp. 189–208.
7. C. Rouland-Lefevre, in *Termites: Evolution, Sociality, Symbioses, Ecology*, T. Abe, D. E. Bignell, M. Higashi, Eds. (Kluwer Academic, Dordrecht, Netherlands, 2000), pp. 289–306.
8. D. K. Aanen, P. Eggleton, *Curr. Biol.* **15**, 851 (2005).
9. R. Brandl *et al.*, *Mol. Phylogenet. Evol.* **45**, 239 (2007).
10. A. E. Emerson, *Field. Zool.* **37**, 465 (1955).
11. U. G. Mueller, N. M. Gerardo, D. K. Aanen, D. L. Six, T. R. Schultz, *Annu. Rev. Ecol. Evol. Syst.* **36**, 563 (2005).

12. S. Kambhampati, P. Eggleton, in *Termites: Evolution, Sociality, Symbioses, Ecology*, T. Abe, D. E. Bignell, M. Higashi, Eds. (Kluwer Academic, Dordrecht, Netherlands, 2000), pp. 1–24.
13. J. Korb, D. K. Aanen, *Behav. Ecol. Sociobiol.* **53**, 65 (2003).
14. H. H. de Fine Licht, A. Andersen, D. K. Aanen, *Mycol. Res.* **109**, 314 (2005).
15. D. K. Aanen *et al.*, *BMC Evol. Biol.* **7**, 115 (2007).
16. H. H. de Fine Licht, J. J. Boomsma, D. K. Aanen, *Mol. Ecol.* **15**, 3131 (2006).
17. K. R. Foster, T. Wenseleers, *J. Evol. Biol.* **19**, 1283 (2006).
18. S. A. Frank, *Am. Nat.* **150**, S80 (1997).
19. Materials and methods are available as supporting material on *Science* Online.
20. H. Katoh, T. Miura, K. Maekawa, N. Shinzato, T. Matsumoto, *Mol. Ecol.* **11**, 1565 (2002).
21. D. K. Aanen, *Biol. Lett.* **2**, 209 (2006).
22. R. H. Leuthold, S. Badertscher, H. Imboden, *Insect Soc.* **36**, 328 (1989).
23. J. J. Worrall, *Mycologia* **89**, 24 (1997).
24. M. Chamberlain, D. S. Ingram, in *Advances in Botanical Research Incorporating Advances in Plant Pathology* (Academic Press, London, 1997), vol. 24, pp. 71–87.
25. M. Poulsen, J. J. Boomsma, *Science* **307**, 741 (2005).
26. C. O. Micali, M. L. Smith, *Fungal Genet. Biol.* **38**, 209 (2003).
27. I. H. Chapela, S. A. Rehner, T. R. Schultz, U. G. Mueller, *Science* **266**, 1691 (1994).
28. U. G. Mueller, S. A. Rehner, T. R. Schultz, *Science* **281**, 2034 (1998).
29. T. R. Schultz, S. G. Brady, *Proc. Natl. Acad. Sci. U.S.A.* **105**, 5435 (2008).
30. T. G. Wood, R. J. Thomas, in *Insect-Fungus Interactions*, N. Wilding, N. M. Collins, P. M. Hammond, J. F. Webber, Eds. (Academic Press, London, 1989), pp. 69–92.
31. J. J. Bull, W. R. Rice, *J. Theor. Biol.* **149**, 63 (1991).
32. E. T. Kiers, R. A. Rousseau, S. A. West, R. F. Denison, *Nature* **425**, 78 (2003).
33. J. D. Bever, S. C. Richardson, B. M. Lawrence, J. Holmes, M. Watson, *Ecol. Lett.* **12**, 13 (2009).
34. N. Knowlton, F. Rohwer, *Am. Nat.* **162**, S51 (2003).
35. J. Maynard Smith, E. Szathmáry, *The Major Transitions in Evolution* (Oxford Univ. Press, Oxford, 1995).
36. We were supported by fellowships from the Netherlands Organization for Scientific Research—Vidi (D.K.A.); the C. T. de Wit Graduate School for Production Ecology and Resource Conservation, Wageningen University, Netherlands (D.K.A.); the Danish National Research Foundation (J.J.B.); and the Danish Natural Science Research Council—STENO (D.K.A.). We thank A. de Visser for help with statistical analyses and for comments on an earlier version of the manuscript, T. Nobre for comments, B. Nieuwenhuis for help with the figures, and the Forestry and Agricultural Biotechnology Institute (FABI) team led by M. Wingfield at the University of Pretoria for providing facilities during field and laboratory work.

**Supporting Online Material**

www.sciencemag.org/cgi/content/full/326/5956/1103/DC1
Materials and Methods
SOM Text
Figs. S1 to S4
Tables S1 to S4
References

12 March 2009; accepted 25 September 2009
10.1126/science.1173462

# Epicontinental Seas Versus Open-Ocean Settings: The Kinetics of Mass Extinction and Origination

**Arnold I. Miller[1]* and Michael Foote[2]**

Environmental perturbations during mass extinctions were likely manifested differently in epicontinental seas than in open-ocean–facing habitats of comparable depth. Here, we present a dissection of origination and extinction in epicontinental seas versus open-ocean–facing coastal regions in the Permian through Cretaceous periods, an interval through which both settings are well represented in the fossil record. Results demonstrate that extinction rates were significantly higher in open-ocean settings than in epicontinental seas during major mass extinctions but not at other times and that origination rates were significantly higher in open-ocean settings for a protracted interval from the Late Jurassic through the Late Cretaceous. These patterns are manifested even when other paleogeographic and environmental variables are held fixed, indicating that epicontinental seas and open-ocean–facing coastlines carry distinct macroevolutionary signatures.

Throughout the global history of Phanerozoic marine life, patterns of diversification and extinction varied substantially among different regions such as paleocontinents (*1*–*4*) and latitudinal belts (*5*). However, the primary geographic and environmental dichotomy recognized among ancient shallow-marine settings is the distinction between epicontinental seas, which covered broad regions of ancient continents during much of the Paleozoic era but began to wane thereafter, and open-ocean–facing coastlines, which became increasingly important through the Mesozoic and Cenozoic eras and rim present-day continents (*6*, *7*). Because they extended over unusually broad areas with water depths typically less than 100 m, epicontinental seas were likely characterized by sluggish circulation in comparison to coastal settings of comparable depths that faced the open ocean (*8*, *9*), and this may have had important ramifications for taxonomic origination and extinction (*6*, *10*). Potential mass extinction agents were probably manifested differently in the two settings. In epicontinental seas, for example, drops in sea level would have been more lethal because of the rapid subaerial exposure of unusually large expanses of shallow seafloor (*11*, *12*), and biotas there may also have been more susceptible to bottom-water anoxia because of relatively poor circulation and enhanced stratification (*13*). By contrast, shallow open-ocean–facing settings may have been affected more profoundly in cases where waterborne lethal effects emanated from point sources, such as impacts or volcanic events, the propagation of which may have been inhibited in epicontinental seas because of sluggish circulation.

Here, we contrast the kinetics of extinction and origination in epicontinental seas versus shallow ocean-facing settings during the Permian through the Cretaceous periods, an interval through which both settings are well represented in the fossil and sedimentary records. Global occurrences of marine genera were extracted from the Paleobiology Database [PaleoDB (*14*)] for a set of stage-level stratigraphic units that span the study interval. We used global paleogeographic maps (e.g., fig. S1) to demarcate the boundaries of epicontinental seas for each stage (*15*), and we mapped individual occurrences of marine genera in each stage with respect to these two settings on the basis of their paleogeographic locations. These, in turn, were used to parse the roster of 7868 genera into those with affinities for either epicontinental seas or ocean-facing settings in cases where a statistical preponderance of occurrences for a given genus was located in one regime or the other (*15*, *16*). In all, 3432 genera were assignable on this basis, and, of these, 3418 had first and last appearances that were stratigraphically resolvable to the stage level. Patterns of extinction and origination were then compared stage by stage through the study interval for genera with affinities for each of the two regimes, on the basis of their first and last appearances as depicted in the PaleoDB.

Comparative per capita extinction rates (*17*) through the study interval (Fig. 1A) document a striking pattern. Whereas there was virtually no difference in average extinction intensity between the two regimes, open-ocean–facing settings exhibited significantly higher extinction rates during the three most profound mass extinctions in the study interval: the end-Permian, end-Triassic, and end-Cretaceous events. This suggests that ocean-facing settings were more susceptible to the agents of extinction in these events.

In contrast, the penultimate stage of the Permian, the Guadalupian, exhibited a significantly higher extinction rate among genera in epicontinental seas than in open-ocean settings. This difference from the subsequent end-Permian event and the two other major extinctions does not demonstrate conclusively that it was caused by a mechanism unique to that interval. Nevertheless, sea-level regression has been implicated in the Guadalupian extinctions because of the loss of major shallow-water provinces (*12*), and its relation to the suite of catastrophic mechanisms

[1]Department of Geology, University of Cincinnati, Post Office Box 210013, Cincinnati, OH 45221, USA. [2]Department of the Geophysical Sciences, University of Chicago, 5734 South Ellis Avenue, Chicago, IL 60637, USA.

*To whom correspondence should be addressed. E-mail: arnold.miller@uc.edu

potentially implicated in the subsequent end-Permian event remains in question (*18*).

Per capita origination rate trajectories (Fig. 1B) generally exhibited more volatility than extinction rate trajectories, with numerous instances in which origination rates for a given stage were higher in one regime or the other and with no consistent pattern before the Kimmeridgian, the penultimate stage of the Jurassic. However, open-ocean settings thereafter exhibited significantly higher origination rates than epicontinental seas for nearly all of the remaining stages of the Mesozoic era.

Of potential relevance to this shift in origination rates, the mean geographic ranges of open-ocean–facing genera declined in the Late Jurassic (Fig. 1C) (*15*). Because reduced geographic range enhances the spatial isolation of taxa, such taxa may exhibit higher origination rates (*19*), and this may explain the increased origination rate among open-ocean–facing genera at that time. Despite the decline in geographic range, however, open-ocean genera maintained larger ranges through most of the Cretaceous than their epicontinental-sea counterparts. Furthermore, an increase in geographic

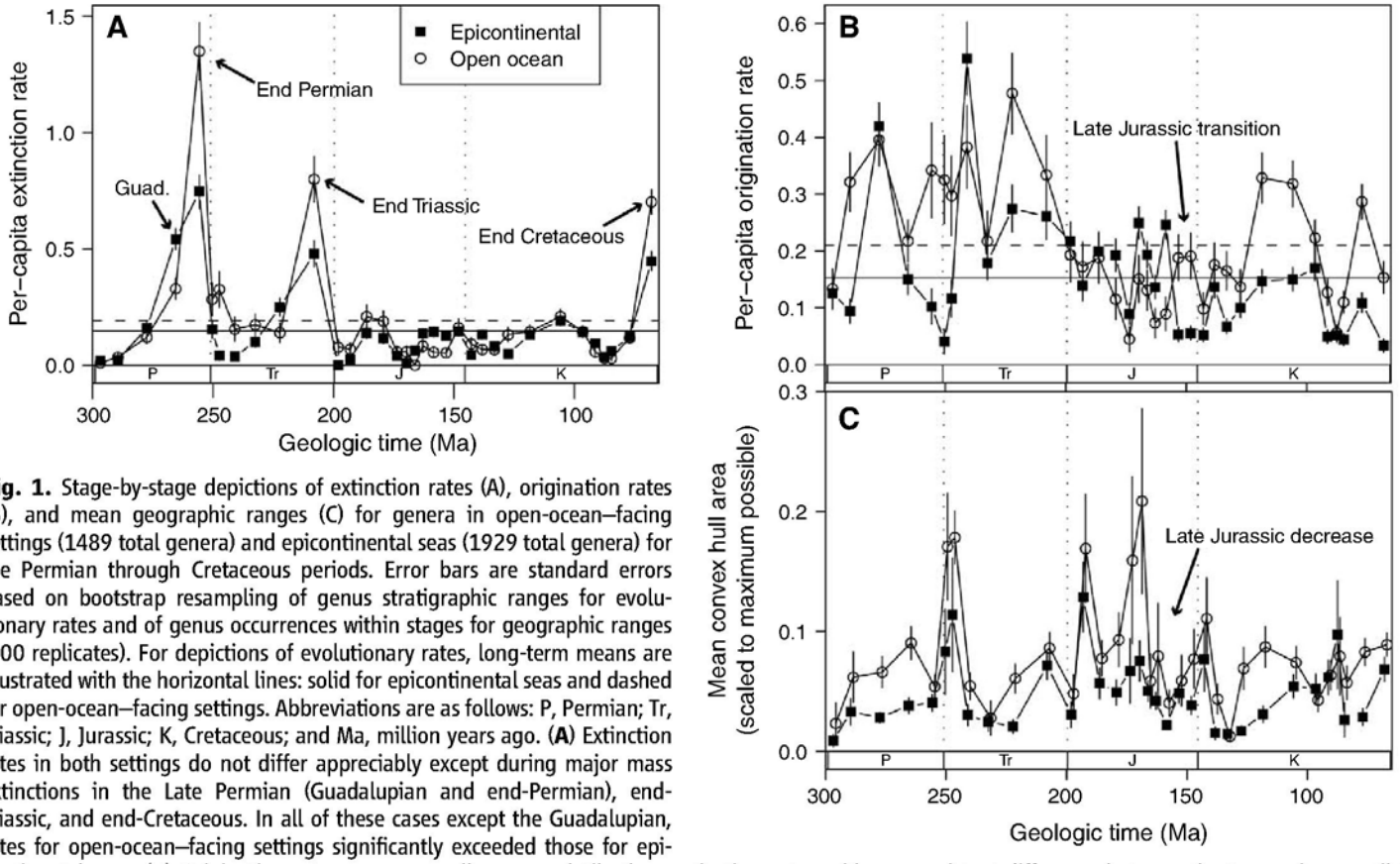


**Fig. 1.** Stage-by-stage depictions of extinction rates (**A**), origination rates (**B**), and mean geographic ranges (**C**) for genera in open-ocean–facing settings (1489 total genera) and epicontinental seas (1929 total genera) for the Permian through Cretaceous periods. Error bars are standard errors based on bootstrap resampling of genus stratigraphic ranges for evolutionary rates and of genus occurrences within stages for geographic ranges (500 replicates). For depictions of evolutionary rates, long-term means are illustrated with the horizontal lines: solid for epicontinental seas and dashed for open-ocean–facing settings. Abbreviations are as follows: P, Permian; Tr, Triassic; J, Jurassic; K, Cretaceous; and Ma, million years ago. (**A**) Extinction rates in both settings do not differ appreciably except during major mass extinctions in the Late Permian (Guadalupian and end-Permian), end-Triassic, and end-Cretaceous. In all of these cases except the Guadalupian, rates for open-ocean–facing settings significantly exceeded those for epicontinental seas. (**B**) Origination rates were generally more volatile than extinction rates, with no consistent difference between the two regimes until the Kimmeridgian; thereafter, open-ocean rates exceeded those for epicontinental seas in nearly every stage. (**C**) Mean geographic ranges of genera, which are based on convex-hull area scaled to the maximum possible (*15*), exhibit a volatile pattern through the study interval but nevertheless depict a significant downward trend for open-ocean–facing settings through the Late Jurassic.

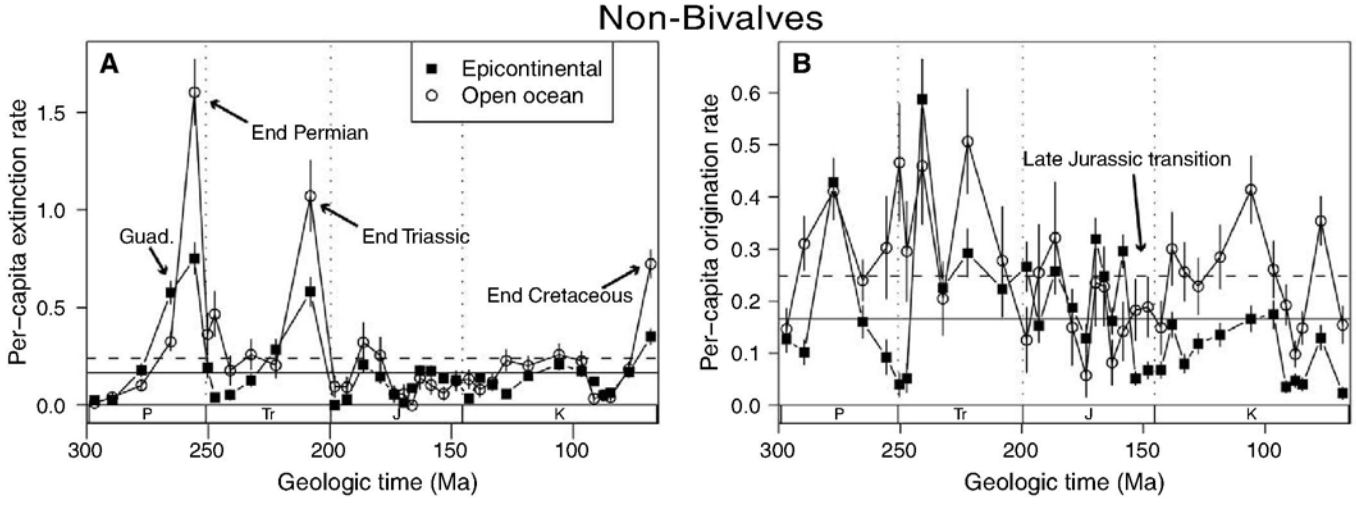


**Fig. 2.** Stage-by-stage depictions of extinction rates (**A**) and origination rates (**B**) for non-bivalve genera in open-ocean–facing settings (1088 total genera) and epicontinental seas (1617 total genera) for the Permian through Cretaceous periods. Salient features observed in Fig. 1, including elevated open-ocean extinction rates during major mass extinctions and higher open-ocean origination rates from the Kimmeridgian through the remainder of the study interval, are maintained, despite the exclusion of bivalves from the analysis.

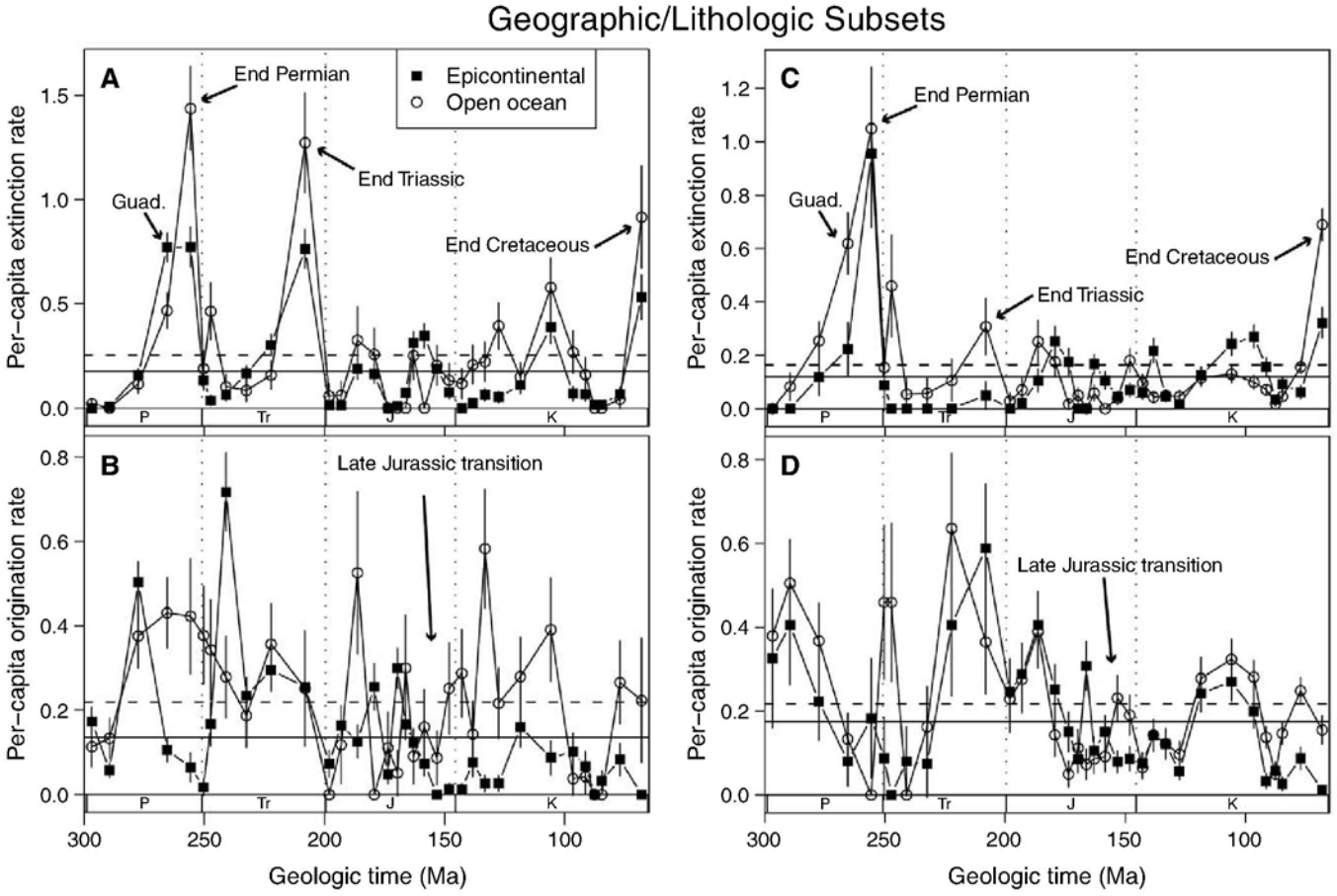


**Fig. 3.** Stage-by-stage depictions of extinction rates and origination rates for genera in open-ocean–facing settings and epicontinental seas for the Permian through Cretaceous periods for subsets of the data limited to tropical carbonate regimes (**A** and **B**) (822 total genera for epicontinental seas and 508 for open-ocean–facing settings), and nontropical clastic regimes (**C** and **D**) (513 total genera for epicontinental seas and 792 for open-ocean–facing settings) (*15*). As in Fig. 2, salient features observed in Fig. 1 are maintained for tropical carbonate regimes, but extinction characteristics for nontropical clastic regimes are altered for the Late Permian, perhaps reflecting the relative paucity of data from these regimes for the Permian. This exception notwithstanding, the general maintenance of the differences observed in Fig. 1 between epicontinental seas and open-ocean–facing settings indicates that it transcends paleolatitude and sedimentary regime.

range of open-ocean genera through the late Early Cretaceous appears to coincide with an increase, rather than a decrease, in origination rate.

Although a decline in geographic range does not explain the shift in origination rates among open-ocean genera, this decline is intriguing in its own right because an increase in region-to-region faunal differentiation among marine biotas has recently been documented through the Jurassic (*20*). As the northern Atlantic Ocean opened in the Jurassic (*21*), the distance between its western and eastern margins may have separated enough that ocean-facing biotas in these two coastal regions became effectively isolated.

Bivalve molluscs compose a large percentage of the genera contained in most Mesozoic stratigraphic bins when compared with other higher taxa, so we tested whether the patterns documented here were driven by properties inherent to bivalves or instead transcended higher taxonomic membership by using a data set from which all bivalves had been removed. The principal patterns illustrated in Fig. 1, A and B, remained unchanged (Fig. 2).

Most epicontinental seas throughout the Phanerozoic—particularly in the Paleozoic—were in tropical settings (i.e., less than 30° latitude) and dominated by carbonate sedimentation (*6*, *7*), whereas open-ocean–facing coasts—particularly in the Mesozoic and Cenozoic—predominated in nontropical settings characterized by terrigenous clastic sedimentation. Because latitude and the nature of sedimentation are known to have substantially affected Phanerozoic diversity (*16*, *22*, *23*), this raises the prospect that our results might reflect these other, correlated factors. We therefore analyzed data sets limited first to tropical, carbonate settings and then to nontropical, clastic settings. In both cases, most major features illustrated in Fig. 1 were preserved (Fig. 3) with a few exceptions: Most notably, nontropical clastic settings did not exhibit a significantly higher Guadalupian epicontinental-sea extinction rate, and they exhibited only a marginally higher open-ocean rate for the Lopingian (end-Permian; Fig. 3C). This likely relates to a paucity of available data, reflecting the sedimentary and fossil records for that interval: Nontropical clastic data for the Guadalupian and Lopingian included substantially fewer genera, with concomitantly higher uncertainties in rate estimates, than coeval data from tropical-carbonate milieus. This is especially true for epicontinental genera: In the Guadalupian, only 19 are sampled in nontropical clastic milieus, compared with 264 in tropical carbonates; in the Lopingian the corresponding numbers are 24 and 113. Overall, however, these results show that most of our findings were not affected or caused by overprints of paleolatitude or substrate type.

Our results therefore provide evidence of significant differences in the kinetics of mass extinction and origination in epicontinental seas versus shallow, open-ocean–facing settings during the Permian through Cretaceous periods. Because there was a secular transition through the Phanerozoic in the relative spatial extent of these two regimes, there may have been parallel transitions in the relative importance of causes of extinction and origination that acted preferentially in one regime or the other.

### References and Notes

1. D. Jablonski, *Science* **279**, 1327 (1998).
2. A. Z. Krug, M. E. Patzkowsky, *Paleobiology* **33**, 435 (2007).
3. A. I. Miller, *Paleobiology* **23**, 410 (1997).
4. A. I. Miller, *Geobios Mem. Spec.* **20**, 397 (1997).
5. A. Z. Krug, D. Jablonski, J. W. Valentine, K. Roy, *Astrobiology* **9**, 113 (2009).
6. S. E. Peters, *Nature* **454**, 626 (2008).
7. L. J. Walker, B. H. Wilkinson, L. C. Ivany, *J. Geol.* **110**, 75 (2002).

8. R. Slingerland, *Sedimentology* **33**, 487 (1986).
9. M. R. Wells *et al.*, *J. Sediment. Res.* **77**, 843 (2007).
10. P. A. Allison, M. R. Wells, *Palaios* **21**, 513 (2006).
11. P. M. Sheehan, *Annu. Rev. Earth Planet. Sci.* **29**, 331 (2001).
12. S. Z. Shen, G. R. Shi, *Paleobiology* **28**, 449 (2002).
13. S. E. Peters, *Paleobiology* **33**, 165 (2007).
14. http://paleodb.org/
15. Materials and methods are available as supporting material on *Science* Online.
16. M. Foote, *Paleobiology* **32**, 345 (2006).
17. M. Foote, *Paleobiology* **26** (suppl. 1), 74 (2000).
18. M. E. Clapham, S. Z. Shen, D. J. Bottjer, *Paleobiology* **35**, 32 (2009).
19. D. Jablonski, K. Roy, *Proc. R. Soc. London Ser. B* **270**, 401 (2003).
20. A. I. Miller *et al.*, *Paleobiology* **35**, 612 (2009).
21. K. O. Emery, E. Uchupi, *The Geology of the Atlantic Ocean* (Springer-Verlag, Berlin, 1984).
22. W. Kiessling, M. Aberhan, *Paleobiology* **33**, 414 (2007).
23. A. I. Miller, S. R. Connolly, *Paleobiology* **27**, 768 (2001).
24. We thank D. Buick, W. Kiessling, S. Kolbe, A. Lagomarcino, and J. Wittmer for discussions; two anonymous reviewers for helpful comments; A. Lagomarcino for assistance in drafting figures; and NASA (program in Exobiology) and NSF (programs in Biocomplexity and in Geology and Paleontology) for financial support. This is Paleobiology Database publication no. 102.

**Supporting Online Material**
www.sciencemag.org/cgi/content/full/326/5956/1106/DC1
Materials and Methods
Figs. S1 to S3
References

3 August 2009; accepted 16 September 2009
10.1126/science.1180061

# A Periplasmic Reducing System Protects Single Cysteine Residues from Oxidation

**Matthieu Depuydt,[1] Stephen E. Leonard,[2] Didier Vertommen,[1] Katleen Denoncin,[1] Pierre Morsomme,[3] Khadija Wahni,[4,5] Joris Messens,[4,5] Kate S. Carroll,[2] Jean-François Collet[1]***

The thiol group of the amino acid cysteine can be modified to regulate protein activity. The *Escherichia coli* periplasm is an oxidizing environment in which most cysteine residues are involved in disulfide bonds. However, many periplasmic proteins contain single cysteine residues, which are vulnerable to oxidation to sulfenic acids and then irreversibly modified to sulfinic and sulfonic acids. We discovered that DsbG and DsbC, two thioredoxin-related proteins, control the global sulfenic acid content of the periplasm and protect single cysteine residues from oxidation. DsbG interacts with the YbiS protein and, along with DsbC, regulates oxidation of its catalytic cysteine residue. Thus, a potentially widespread mechanism controls sulfenic acid modification in the cellular environment.

Many proteins secreted into the *Escherichia coli* periplasm contain even numbers of cysteines, most of which form disulfide bonds important for protein stability. These disulfides are introduced by the oxidoreductase enzyme DsbA (disulfide bond A), which is reoxidized by DsbB [reviewed in (*1*)]. When proteins require disulfides to be formed between nonconsecutive cysteines, DsbA can introduce incorrect disulfides. These non-native disulfides are corrected by the isomerase DsbC, a V-shaped dimeric protein. Each subunit of DsbC contains a CXXC motif, located within a thioredoxin fold, which is kept reduced by DsbD, a membrane protein that transfers electrons from the cytoplasmic thioredoxin system to the periplasm (*1*).

The periplasm contains another protein that could potentially serve as an isomerase, DsbG (*2*). DsbG shares 26% sequence identity with DsbC and is also a V-shaped dimeric protein, with a thioredoxin fold and a CXXC motif that is kept reduced by DsbD. The structure of DsbG resembles that of DsbC, but the dimensions of the DsbG cleft are larger and its surface is less hydrophobic (*3*). It has thus been predicted that DsbG preferentially interacts with proteins that are folded or partially folded (*3*). However, the substrates of DsbG are not known and its function has remained obscure.

We sought to clearly define the function of DsbG by identifying its substrates. We first used a global proteomics approach to compare the proteome of a *dsbG* mutant strain to that of a wild type but did not find a single protein that was affected by the absence of DsbG (table S1).

To trap DsbG bound to its substrates, we produced the $DsbG_{CXXA}$ mutant, in which an alanine replaces the second cysteine of the CXXC motif. This approach has been used to trap thioredoxin substrates (*4*). $DsbG_{CXXA}$ was purified under denaturing conditions. DsbG and slower migrating bands were present in the purified sample (Fig. 1A). Addition of the reducing agent dithiothreitol (DTT) led to the disappearance of most of these bands and the corresponding increase of DsbG, which suggests that the upper bands corresponded to DsbG bound to unknown proteins.

The complexes were separated by two-dimensional gel electrophoresis (Fig. 1B). Three periplasmic proteins, YbiS, ErfK, and YnhG, were potential substrates of DsbG. The cytosolic proteins Ef-Tu, DnaK, and Fur were also identified but probably represent false positives that react with DsbG during cell lysis. Indeed, Ef-Tu has highly reactive cysteines and has also been found in a complex with DsbA (*5*).

The three periplasmic proteins are homologous proteins belonging to the same family of L,D-transpeptidases, which catalyze the cross-linking of peptidoglycan for cell wall synthesis (fig. S1). Because they possess a sole cysteine, essential for activity (*6*), these proteins are not likely in need of a disulfide isomerase but rather of a reductase to rescue their cysteine from oxidation within the oxidizing periplasm. To investigate this further, we studied the interaction between

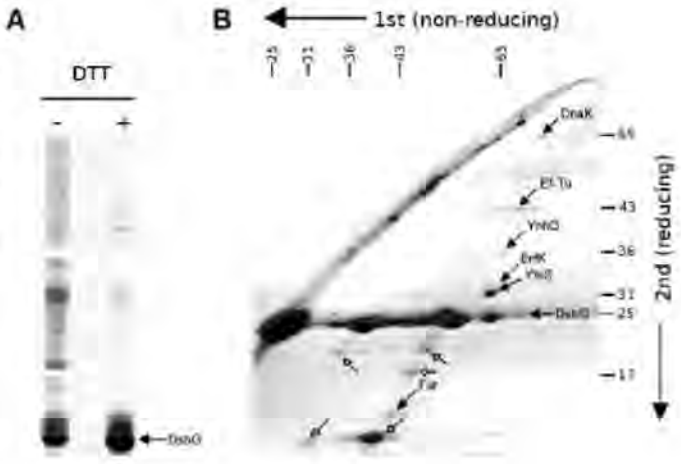


**Fig. 1.** Identification of DsbG substrates. **(A)** SDS-PAGE analysis of purified $DsbG_{CXXA}$. **(B)** Separation of the complexes in a second reducing dimension. Proteins were identified by mass spectrometry. Open arrows correspond to smaller versions of DsbG resulting from proteolysis.

[1]de Duve Institute, Université catholique de Louvain, B-1200 Brussels, Belgium. [2]Life Sciences Institute, University of Michigan, Ann Arbor, MI 48109–1048, USA. [3]Institut des Sciences de la Vie, Université catholique de Louvain, B-1348 Louvain-la-Neuve, Belgium. [4]Department of Molecular and Cellular Interactions, Vlaams Instituut voor Biotechnologie (VIB), Vrije Universiteit Brussel, B-1050 Brussels, Belgium. [5]Structural Biology Brussels, Vrije Universiteit Brussel, B-1050 Brussels, Belgium.

*To whom correspondence should be addressed. E-mail: jfcollet@uclouvain.be

DsbG and YbiS, the most active of the three L,D-transpeptidases (*7*).

We modified the cysteine of purified YbiS with 2-nitro-5-thiobenzoate (TNB) and monitored the reduction of this residue by following the release of the TNB anion (Fig. 2A) (*8*). The release of TNB was faster when YbiS-TNB was incubated with reduced DsbG than with DsbC (Fig. 2B), which suggests that DsbG catalyzes the reaction more efficiently. Thus, YbiS and, presumably by extension, the other homologous L,D-transpeptidases are substrates for DsbG.

We sought to confirm that DsbG interacts with YbiS in vivo. Expression of $DsbG_{CXXA}$ in a *dsbG* strain led to the appearance of a band of ~70 kD, detected by antibodies to both YbiS and DsbG (Fig. 2C). This band migrated with the size expected for a DsbG-YbiS complex and was sensitive to DTT. In contrast, no YbiS-DsbC complex was detected when a $DsbC_{CXXS}$ mutant was expressed in a *dsbC* strain. Thus, DsbG specifically interacts with YbiS in vivo.

The fact that we trapped YbiS in complex with DsbG implied that the cysteine of YbiS oxidizes in the periplasm and suggested that YbiS requires functional DsbG to maintain its reduced, catalytically active state. To test the oxidation state of YbiS, samples were taken from *dsbG*, *dsbC*, *dsbCdsbG*, and wild-type strains grown in stationary phase, a condition under which reactive oxygen species (ROS) accumulate. Reduced thiols were modified with methoxypolyethylene glycol (mPEG), a 5-kD molecule that covalently reacts with free thiols, leading to a shift on SDS–polyacrylamide gel electrophoresis (SDS-PAGE). More oxidized YbiS was observed in *dsbG* strains (~60%) than in wild-type (~40%) and *dsbC* (~40%) strains (Fig. 2D), indicating that YbiS can be oxidized in vivo and that it preferentially depends on DsbG for reduction. The accumulation of oxidized YbiS was somewhat greater in the *dsbCdsbG* mutant (~70%), which suggests that DsbC is able to partially replace DsbG.

Both DsbG and DsbC depend on electrons provided by DsbD to stay reduced in the periplasm (*9*). In the absence of DsbD, both proteins are found oxidized and are thus inactivated (*1*). To confirm that inactivation of DsbG and DsbC leads to increased oxidation of YbiS by ROS, we studied the effect of *dsbD* deletion on the oxidation state of YbiS in mutant strains in which ROS accumulate (*10*). Deletion of *dsbD* caused increased oxidation of YbiS in a strain lacking the catalase KatE and the alkyl hydroperoxidase system AhpCF (Fig. 2E). Thus, electrons flowing from the cytoplasm to DsbG and DsbC via DsbD keep the single cysteine of YbiS reduced.

We next asked how the single cysteine residues of DsbG substrates are oxidized. Oxidized glutathione (GSSG), which is present in the *E. coli* periplasm (*11*), could potentially react with the cysteine of the transpeptidases (RSH) to form a glutathionylated adduct (RSSG). We expressed $DsbG_{CXXA}$ in a strain lacking gamma-glutamylcysteine synthase (*gshA*), the first enzyme of the glutathione biosynthesis pathway. The formation of the YbiS-DsbG complex was still observed, even when bacteria were grown in minimal media (fig. S2). Thus, although we cannot rule out that a small fraction of YbiS may indeed be glutathionylated, S-glutathionylation is not the primary oxidation product in YbiS.

We next considered whether the cysteine of YbiS might be oxidized to a sulfenic acid (Cys-SOH) by oxidants present in the periplasm. Sulfenic acids are highly reactive groups that tend either to react rapidly with other cysteine residues present in the vicinity to form a disulfide bond or to be further oxidized to sulfinic or sulfonic acids (*12*). Sulfenic acids can also be stabilized by electrostatic interactions within the micro-environment of certain proteins when no other cysteine is present. YbiS reacts with a genetically encoded probe based on the redox-regulated domain of Yap1 (*13*), a yeast transcription factor that reacts with electrophilic cysteines such as sulfenic acids (*14*). Thus, the active site cysteine residue of YbiS may be prone to sulfenylation.

Because of their high reactivity, sulfenic acids are often difficult to identify. To determine whether the cysteine residue of YbiS could form a stable sulfenic acid, we used DAz-1, a probe that is chemically selective for sulfenic acids (*15*). In addition, DAz-1 contains an azide chemical handle that can be modified to append a biotin moiety, allowing detection of the labeled proteins by streptavidin-conjugated horseradish peroxidase (Strep-HRP). Purified YbiS was labeled by DAz-1, indicating that YbiS undergoes sulfenic acid formation in vitro (Fig. 3A). Moreover, incubation of YbiS with $H_2O_2$ led to an increase in protein labeling. The presence of the sulfenic acid modification was further verified by mass spectrometry (fig. S3). By contrast, no labeling was observed for $YbiS_{C186A}$, a mutant protein lacking the catalytic cysteine. Although in some proteins, such as the organic peroxide sensor OhrR (*16*), cysteine sulfenates condense with a backbone amide to generate a cyclic sulfenamide, this modification was not observed with YbiS.

We confirmed that YbiS forms a sulfenic acid in vivo by labeling the oxidized protein directly in living cells using DAz-2, an analog of DAz-1 with improved potency (*17*). After biotinylation of the probe, sulfenic acid–modified proteins were captured on streptavidin beads. Immunoblot analysis with antibody to YbiS shows that YbiS is present in the DAz-2–labeled protein fraction (Fig. 3B). Likewise, recombinant His-tagged YbiS could be modified in vivo by DAz-2. After enrichment on a $Ni^{2+}$ column,

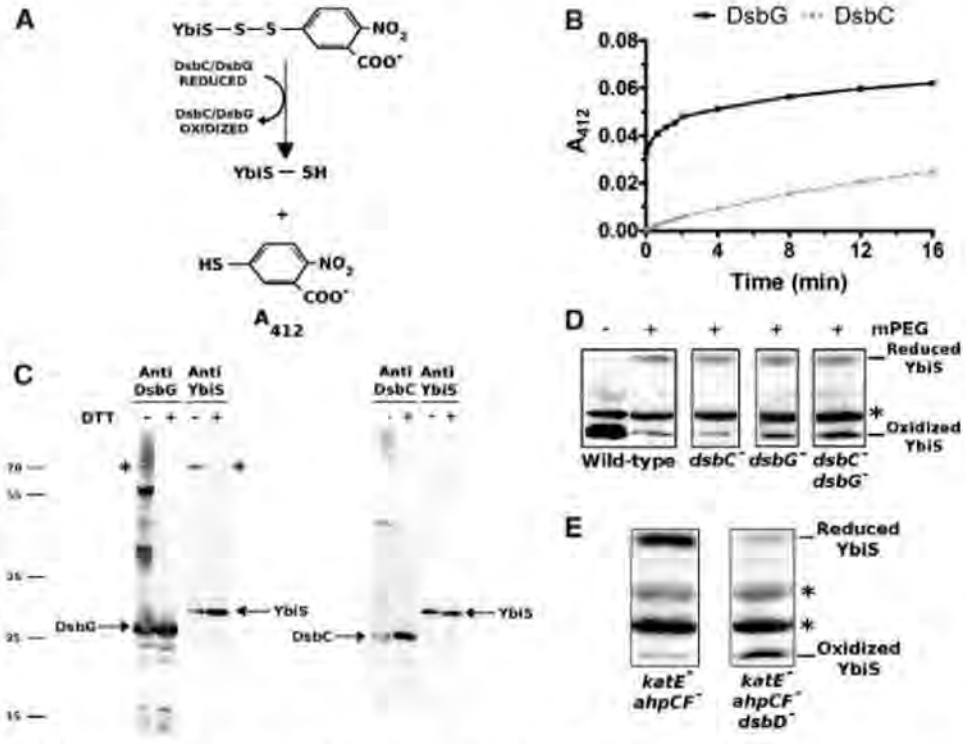


**Fig. 2.** DsbG interacts with YbiS in vitro and in vivo. (**A**) Reduction of YbiS-TNB leads to the release of the TNB anion, which can be monitored at 412 nm. (**B**) Spectrophotometric analysis of the reaction between YbiS-TNB and DsbC or DsbG. (**C**) Immunoblot of samples prepared from strains expressing $DsbG_{CXXA}$ or $DsbC_{CXXS}$. Asterisks denote the DsbG-YbiS complex. (**D**) Immunoblots of samples prepared from *dsbC*, *dsbG*, *dsbCdsbG*, and (**E**) *katE ahpCF dsbD* strains probed with antibody to YbiS. The asterisks denote an unknown protein recognized by the antiserum.

YbiS was biotinylated and detected by Strep-HRP (Fig. 3C). Control reactions carried out in the *ybiS* strain (Fig. 3B) or in the absence of DAz-2 (Fig. 3C) gave no detectable protein labeling, as expected.

To determine whether DsbG and DsbC control the level of sulfenylation in the periplasm, wild-type, *dsbG*, *dsbC*, and *dsbCdsbG* strains were grown in stationary phase, sulfenic acids were labeled in living cells, and periplasmic extracts were prepared. After biotinylation of DAz-2, samples were analyzed by immunoblot using both Strep-HRP and an antibody to YbiS. Several periplasmic proteins were labeled by DAz-2, including a band migrating at the same position as YbiS (Fig. 4). This in vivo snapshot of the global sulfenic acid content of a subcellular compartment reveals that sulfenic acid formation is a major posttranslational modification in the periplasm. Although the biotinylated bands were observed in periplasmic extracts prepared from all strains, the labeling was more intense in the samples prepared from *dsbCdsbG* mutants. This indicates that DsbG and DsbC are part of a periplasmic reducing system that controls the level of cysteine sulfenylation in the periplasm and provides reducing equivalents to rescue oxidatively damaged secreted proteins.

We propose the following model for the control of cysteine sulfenylation in the periplasm and the protection of single cysteines in this oxidizing compartment (fig. S4). In the periplasm, many proteins contain an even number of cysteines (*18*) that form disulfide bonds and are thus protected from further oxidation. However, some proteins, including YbiS, contain either a single cysteine or an odd number of cysteines (*18*). Because they are not involved in disulfides, these cysteines would, without protection, tend to be vulnerable to oxidation and form sulfenic acids. Sulfenic acids, unless they are stabilized within the micro-environment of the protein, are susceptible to reaction with small molecule thiols to form mixed disulfides, as in the organic peroxide sensor OhrR (*16*), or to further oxidation to sulfinic and sulfonic acids. Oxidizing a catalytically active thiol inactivates the protein, necessitating a system in the periplasm that could rescue single cysteine residues from oxidation. DsbG, whose negatively charged surface is better suited to interact with folded proteins, appears to be a key player in this reducing system. DsbC, whose inner surface is lined with hydrophobic residues, seems to be designed to interact with unfolded proteins to correct non-native disulfides. In parallel to this function, DsbC could also serve as a backup for DsbG. Both DsbC and DsbG are kept reduced by DsbD. Thus, the electron flux originating from the cytoplasmic pool of reduced nicotinamide adenine dinucleotide phosphate provides the reducing equivalents required for both the correction of incorrect disulfides and the rescue of sulfenylated orphan cysteines.

Sulfenic acid formation is pervasive in certain eukaryotic cells, both as unwanted products of cysteine oxidation by ROS and in enzyme catalysis and signal transduction (*14*, *19*). Proteins from the thioredoxin superfamily are widespread and have been identified in most genomes. Thus, some of these thioredoxin superfamily members may play similar roles in controlling the global sulfenic acid content of eukaryotic cellular compartments.

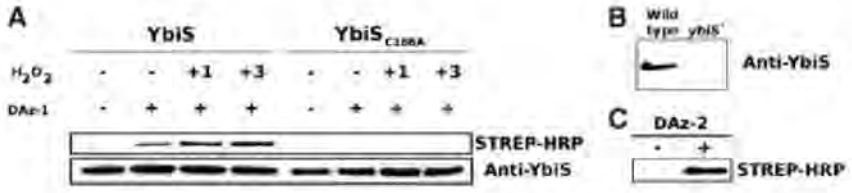


**Fig. 3.** YbiS forms a stable sulfenic acid in vitro and in vivo. (**A**) Sulfenic acid modification of YbiS or $YbiS_{C186A}$, untreated or exposed to one or three equivalents of $H_2O_2$. Sulfenylation was detected by immunoblot with Strep-HRP. Equal protein loading was verified by reprobing with antibody to YbiS. Detection of (**B**) endogenous and (**C**) recombinant YbiS labeled in vivo with DAz-2.

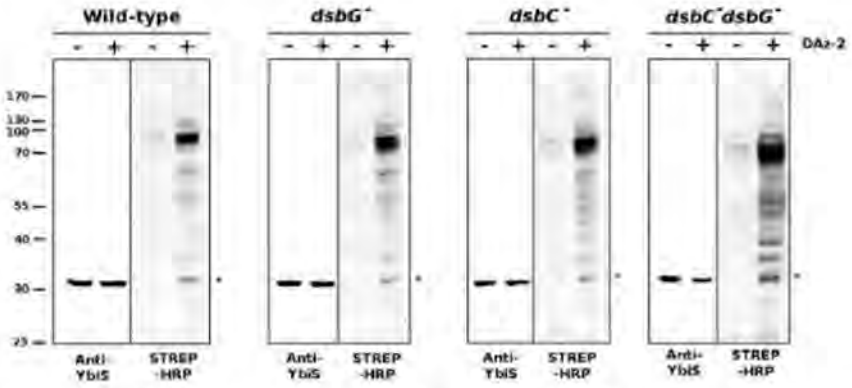


**Fig. 4.** Protein sulfenic acids accumulate in the periplasm of *dsbCdsbG* strains. The asterisks denote a band corresponding to YbiS.


**References and Notes**

1. J. Messens, J. F. Collet, *Int. J. Biochem. Cell Biol.* **38**, 1050 (2006).
2. P. H. Bessette, J. J. Cotto, H. F. Gilbert, G. Georgiou, *J. Biol. Chem.* **274**, 7784 (1999).
3. B. Heras, M. A. Edeling, H. J. Schirra, S. Raina, J. L. Martin, *Proc. Natl. Acad. Sci. U.S.A.* **101**, 8876 (2004).
4. Y. Balmer *et al.*, *Proc. Natl. Acad. Sci. U.S.A.* **101**, 2642 (2004).
5. H. Kadokura, H. Tian, T. Zander, J. C. Bardwell, J. Beckwith, *Science* **303**, 534 (2004).
6. J. L. Mainardi *et al.*, *J. Biol. Chem.* **282**, 30414 (2007).
7. S. Magnet *et al.*, *J. Bacteriol.* **189**, 3927 (2007).
8. J. Messens *et al.*, *J. Mol. Biol.* **339**, 527 (2004).
9. A. Rietsch, P. Bessette, G. Georgiou, J. Beckwith, *J. Bacteriol.* **179**, 6602 (1997).
10. L. C. Seaver, J. A. Imlay, *J. Bacteriol.* **183**, 7173 (2001).
11. M. Eser, L. Masip, H. Kadokura, G. Georgiou, J. Beckwith, *Proc. Natl. Acad. Sci. U.S.A.* **106**, 1572 (2009).
12. K. G. Reddie, K. S. Carroll, *Curr. Opin. Chem. Biol.* **12**, 746 (2008).
13. C. L. Takanishi, L. H. Ma, M. J. Wood, *Biochemistry* **46**, 14725 (2007).
14. C. E. Paulsen, K. S. Carroll, *Chem. Biol.* **16**, 217 (2009).
15. K. G. Reddie, Y. H. Seo, W. B. Muse III, S. E. Leonard, K. S. Carroll, *Mol. Biosyst.* **4**, 521 (2008).
16. J. W. Lee, S. Soonsanga, J. D. Helmann, *Proc. Natl. Acad. Sci. U.S.A.* **104**, 8743 (2007).
17. S. E. Leonard, K. G. Reddie, K. S. Carroll, *ACS Chem. Biol.* **4**, 783 (2009).
18. R. J. Dutton, D. Boyd, M. Berkmen, J. Beckwith, *Proc. Natl. Acad. Sci. U.S.A.* **105**, 11933 (2008).
19. L. B. Poole, K. J. Nelson, *Curr. Opin. Chem. Biol.* **12**, 18 (2008).


20. We thank G. Connerotte and H. Degand for technical help, and E. VanSchaftingen, M. VeigadaCunha, F. Swisser, P. Leverrier, A. Hiniker, J. Bardwell, and U. Jakob for discussions. J.F.C. and P.M. are Chercheur Qualifié and D.V. is Collaborateur Logistique of the Fonds de la Recherche Scientifique. M.D. is a research fellow of the Fonds pour la formation à la Recherche dans l'Industrie et dans l'Agriculture, and J.M. is a project leader of the VIB. This research was supported by grants from the FNRS to J.F.C. and from the Leukemia and Lymphoma Society (Special Fellows Award 3100-07) and the American Heart Association (Scientist Development Grant 0835419N) to K.S.C. Conflict of Interest Statement: Patent protection has been applied for for the DAz-1 and DAz-2 chemical probes. These compounds will soon be commercially available from Cayman Chemical (Ann Arbor, MI, USA). For inquiries regarding the DAz probes: katesc@umich.edu.


**Supporting Online Material**

www.sciencemag.org/cgi/content/full/326/5956/1109/DC1
Materials and Methods
Figs. S1 to S4
Tables S1 to S4
References

23 July 2009; accepted 28 September 2009
10.1126/science.1179557

# The B73 Maize Genome: Complexity, Diversity, and Dynamics

Patrick S. Schnable,[1,2,3,4]* Doreen Ware,[5,6]* Robert S. Fulton,[7]† Joshua C. Stein,[6]† Fusheng Wei,[8]† Shiran Pasternak,[6] Chengzhi Liang,[6] Jianwei Zhang,[8] Lucinda Fulton,[7] Tina A. Graves,[7] Patrick Minx,[7] Amy Denise Reily,[7] Laura Courtney,[7] Scott S. Kruchowski,[7] Chad Tomlinson,[7] Cindy Strong,[7] Kim Delehaunty,[7] Catrina Fronick,[7] Bill Courtney,[7] Susan M. Rock,[7] Eddie Belter,[7] Feiyu Du,[7] Kyung Kim,[7] Rachel M. Abbott,[7] Marc Cotton,[7] Andy Levy,[7] Pamela Marchetto,[7] Kerri Ochoa,[7] Stephanie M. Jackson,[7] Barbara Gillam,[7] Weizu Chen,[7] Le Yan,[7] Jamey Higginbotham,[7] Marco Cardenas,[7] Jason Waligorski,[7] Elizabeth Applebaum,[7] Lindsey Phelps,[7] Jason Falcone,[7] Krishna Kanchi,[7] Thynn Thane,[7] Adam Scimone,[7] Nay Thane,[7] Jessica Henke,[7] Tom Wang,[7] Jessica Ruppert,[7] Neha Shah,[7] Kelsi Rotter,[7] Jennifer Hodges,[7] Elizabeth Ingenthron,[7] Matt Cordes,[7] Sara Kohlberg,[7] Jennifer Sgro,[7] Brandon Delgado,[7] Kelly Mead,[7] Asif Chinwalla,[7] Shawn Leonard,[7] Kevin Crouse,[7] Kristi Collura,[8] Dave Kudrna,[8] Jennifer Currie,[8] Ruifeng He,[8] Angelina Angelova,[8] Shanmugam Rajasekar,[8] Teri Mueller,[8] Rene Lomeli,[8] Gabriel Scara,[8] Ara Ko,[8] Krista Delaney,[8] Marina Wissotski,[8] Georgina Lopez,[8] David Campos,[8] Michele Braidotti,[8] Elizabeth Ashley,[8] Wolfgang Golser,[8] HyeRan Kim,[8] Seunghee Lee,[8] Jinke Lin,[8] Zeljko Dujmic,[8] Woojin Kim,[8] Jayson Talag,[8] Andrea Zuccolo,[8] Chuanzhu Fan,[8] Aswathy Sebastian,[8] Melissa Kramer,[6] Lori Spiegel,[6] Lidia Nascimento,[6] Theresa Zutavern,[6] Beth Miller,[6] Claude Ambroise,[6] Stephanie Muller,[6] Will Spooner,[6] Apurva Narechania,[6] Liya Ren,[6] Sharon Wei,[6] Sunita Kumari,[6] Ben Faga,[6] Michael J. Levy,[6] Linda McMahan,[6] Peter Van Buren,[6] Matthew W. Vaughn,[6] Kai Ying,[3] Cheng-Ting Yeh,[1,2] Scott J. Emrich,[9,10] Yi Jia,[3] Ananth Kalyanaraman,[9,11] An-Ping Hsia,[1,2] W. Brad Barbazuk,[12] Regina S. Baucom,[13] Thomas P. Brutnell,[14] Nicholas C. Carpita,[15] Cristian Chaparro,[16] Jer-Ming Chia,[6] Jean-Marc Deragon,[16] James C. Estill,[13,17] Yan Fu,[2,4] Jeffrey A. Jeddeloh,[18] Yujun Han,[13,17] Hyeran Lee,[19] Pinghua Li,[14] Damon R. Lisch,[20] Sanzhen Liu,[3] Zhijie Liu,[6] Dawn Holligan Nagel,[13,17] Maureen C. McCann,[21] Phillip SanMiguel,[22] Alan M. Myers,[23] Dan Nettleton,[24] John Nguyen,[25] Bryan W. Penning,[15,21] Lalit Ponnala,[26] Kevin L. Schneider,[27] David C. Schwartz,[28] Anupma Sharma,[27] Carol Soderlund,[29] Nathan M. Springer,[30] Qi Sun,[26] Hao Wang,[13,17] Michael Waterman,[25] Richard Westerman,[22] Thomas K. Wolfgruber,[27] Lixing Yang,[13] Yeisoo Yu,[29] Lifang Zhang,[6] Shiguo Zhou,[28] Qihui Zhu,[13,17] Jeffrey L. Bennetzen,[13] R. Kelly Dawe,[13,17] Jiming Jiang,[19] Ning Jiang,[31] Gernot G. Presting,[27] Susan R. Wessler,[13,17] Srinivas Aluru,[1,9,32] Robert A. Martienssen,[6] Sandra W. Clifton,[7] W. Richard McCombie,[6] Rod A. Wing,[8] Richard K. Wilson[7,33]‡

We report an improved draft nucleotide sequence of the 2.3-gigabase genome of maize, an important crop plant and model for biological research. Over 32,000 genes were predicted, of which 99.8% were placed on reference chromosomes. Nearly 85% of the genome is composed of hundreds of families of transposable elements, dispersed nonuniformly across the genome. These were responsible for the capture and amplification of numerous gene fragments and affect the composition, sizes, and positions of centromeres. We also report on the correlation of methylation-poor regions with *Mu* transposon insertions and recombination, and copy number variants with insertions and/or deletions, as well as how uneven gene losses between duplicated regions were involved in returning an ancient allotetraploid to a genetically diploid state. These analyses inform and set the stage for further investigations to improve our understanding of the domestication and agricultural improvements of maize.

Maize (*Zea mays* ssp. *mays* L.) was domesticated over the past ~10,000 years from the grass teosinte in Central America (*1*) and has been subject to cultivation and selection ever since. Maize is an important model organism for fundamental research into the inheritance and functions of genes, the physical linkage of genes to chromosomes, the mechanistic relation between cytological crossovers and recombination, the origin of the nucleolus, the properties of telomeres, epigenetic silencing, imprinting, and transposition (*2*). Maize also is an important crop, yielding in the USA alone 12 billion (B = $10^9$) bushels of grain from ~86 million acres with a value of $47 B [2008 data from (*3*)]. Over the last century, breeders have increased grain yields eightfold (*4*), in part by harnessing heterosis (hybrid vigor), a universal, but poorly understood, phenomenon that can increase yields of hybrids by 15 to 60% relative to inbred parents (*5*).

The maize genome has undergone several rounds of genome duplication, including that of a paleopolyploid ancestor ~70 million years ago (mya) (*6*) and an additional whole-genome duplication event about 5 to 12 mya (*7*, *8*), which distinguishes maize from its close relative, *Sorghum bicolor* (*9*). The 10 chromosomes of the maize genome are structurally diverse and have undergone dynamic changes in chromatin composition. The size of the maize genome has expanded dramatically (to 2.3 gigabases) over the last ~3 million years via a proliferation of long terminal repeat retrotransposons (LTR retrotransposons) (*10*).

We sequenced the maize genome using a minimum tiling path of bacterial artificial chromosomes (BACs) ($n$ = 16,848) and fosmid ($n$ = 63) clones derived from an integrated physical and genetic map (*11*, *12*), augmented by comparisons with an optical map (*13*). Clones were shotgun sequenced (four- to sixfold coverage), followed by automated and manual sequence improvement (*14*) of the unique regions only, which resulted in the B73 reference genome version 1 (B73 RefGen_v1).

We identified the full complement of maize transposable elements (TEs) accessible from B73 RefGen_v1, which includes active class II DNA TEs and an abundance of class I RNA TEs (*15*).

[1]Center for Plant Genomics, Iowa State University, Ames, IA 50011, USA. [2]Department of Agronomy, Iowa State University, Ames, IA 50011, USA. [3]Department of Genetics, Development and Cell Biology, Iowa State University, Ames, IA 50011, USA. [4]Center for Carbon Capturing Crops, Iowa State University, Ames, IA 50011, USA. [5]U.S. Department of Agriculture (USDA), North Atlantic Area, Robert Holley Center for Agriculture and Health, Ithaca, NY 14853, USA. [6]Cold Spring Harbor Laboratory, Cold Spring Harbor, NY 11724, USA. [7]The Genome Center at Washington University, St. Louis, MO 63108, USA. [8]Arizona Genomics Institute, School of Plant Sciences and Department of Ecology and Evolutionary Biology, BIO5 Institute for Collaborative Research, University of Arizona, Tucson, AZ 85721, USA. [9]Department of Electrical and Computer Engineering, Iowa State University, Ames, IA 50011, USA. [10]Department of Computer Science and Engineering, University of Notre Dame, Notre Dame, IN 46556, USA. [11]School of Electrical Engineering and Computer Science, Washington State University, Pullman, WA 99164, USA. [12]Department of Botany, University of Florida, Gainesville, FL 32611, USA. [13]Department of Genetics, University of Georgia, Athens, GA 30602, USA. [14]Boyce Thompson Institute, Cornell University, Ithaca, NY 14853, USA. [15]Department of Botany and Plant Pathology, Purdue University, West Lafayette, IN 47907, USA. [16]Université de Perpignan Via Domitia, CNRS, Perpignan, France. [17]Department of Plant Biology, University of Georgia, Athens, GA 30602, USA. [18]NimbleGen, Madison, WI 53711, USA. [19]Department of Horticulture, University of Wisconsin–Madison, Madison, WI 53706, USA. [20]Department of Plant Biology, University of California, Berkeley, CA, 94720, USA. [21]Department of Biological Sciences, Purdue University, West Lafayette, IN 47907, USA. [22]Department of Horticulture and Landscape Architecture, Purdue University, West Lafayette, IN 47907, USA. [23]Department of Biochemistry, Biophysics, and Molecular Biology, Iowa State University, Ames, IA, 50011, USA. [24]Department of Statistics, Iowa State University, Ames, IA 50011, USA. [25]Departments of Mathematics, Biology, and Computer Science, University of Southern California, Los Angeles, CA 90089, USA. [26]Cornell University Computational Biology Service Unit, Cornell University, Ithaca, NY 14850, USA. [27]Molecular Biosciences and Bioengineering, University of Hawaii, Honolulu, HI 96822, USA. [28]Laboratory for Molecular and Computational Genomics, Department of Chemistry, Laboratory of Genetics, University of Wisconsin–Madison, Madison, WI 53706, USA. [29]BIO5 Institute for Collaborative Research, University of Arizona, Tucson, AZ 85721, USA. [30]Department of Plant Biology, University of Minnesota, St. Paul, MN 55108, USA. [31]Department of Horticulture, Michigan State University, East Lansing, MI 48824, USA. [32]Indian Institute of Technology, Bombay, India. [33]Department of Genetics, Washington University School of Medicine, St. Louis, MO 63110, USA.

*These authors contributed equally to this work.
†These authors contributed equally to data production and analysis.
‡To whom correspondence should be addressed. E-mail: rwilson@wustl.edu

Almost 85% of the B73 RefGen_v1 consists of TEs (table S2). Indeed, the existence of TEs (*16*), as well as the first members of the *CACTA* (*Spm/En*), *hAT* (*Ac*), *PIF/Harbinger* and *Mutator* superfamilies, and MITE family (*Tourist*), were all initially discovered in maize (*17*). Further, both the existence and unparalleled abundance of LTR retrotransposons in plants were originally discovered in maize (*18*).

The B73 RefGen_v1 contains 855 families of DNA TEs that make up 8.6% of the genome; most of these (82%) were identified in this study (table S2) (*14*). The most complex of these superfamilies is *Mutator*, with dramatic variation in element sequence and size, including 262 Pack-MULEs (*Mutator*-like elements that contain gene fragments) carrying fragments of 226 nuclear genes. About 40,000 nonredundant *Mu* insertion sites were amplified from *Mu*-active lines, sequenced, and mapped to B73 RefGen_v1. The nonuniformly distributed *Mu* insertion sites co-localize with gene-rich regions of the genome that have the highest rates of meiotic recombination per megabase (Fig. 1) (*19*). Like *Mu*, most maize DNA TEs (but not the *CACTA* elements) were enriched in the gene-rich, recombinationally active chromosome ends (Fig. 1 and fig. S1).

*Helitrons*, a class of DNA elements believed to transpose by a rolling-circle mechanism (*20*), are present in plants, animals, and fungi, but are particularly active, variable, and abundant in maize (*21*). Maize contains eight families of *Helitrons* with a combined copy number of ~20,000, which are particularly active in gene fragment acquisition (table S2). In maize, we observed that *Helitrons* are located predominantly within gene-rich regions, whereas, in all previously studied plant and animal genomes, they are enriched in gene-poor regions (*22*, *23*). LTR retrotransposons compose >75% of the B73 RefGen_v1 and are diverse. Most of the 406 families have fewer than 10 copies. LTR retrotransposons exhibited family-specific, nonuniform distributions along chromosomes, e.g., *Copia*-like elements are over-represented in gene-rich euchromatic regions, whereas *Gypsy*-like elements are overrepresented in gene-poor heterochromatic regions (fig. S1) (*24*, *25*). We observed more than 180 acquisitions of nuclear gene fragments inside LTR retrotransposons (table S2).

Protein-encoding and microRNA (miRNA) (*26*) genes were predicted from assembled or improved BAC contigs by a combination of evidence-based (*27*) and ab initio approaches, projected to B73 RefGen_v1, and subsequently filtered to a set of 32,540 protein-encoding and 150 miRNA genes (*14*) (fig. S2). Exon sizes of maize genes were similar to that of their orthologous genes in rice and sorghum, but maize genes contained more large introns because of insertion of repetitive elements (*11*, *28*) (figs. S3 and S4 and tables S5 and S6). A comparative analysis with rice, sorghum, and *Arabidopsis* revealed similar numbers of gene families (*14*) (Fig. 2), of which a core set of 8494 families is shared among all four species, and of the 11,892 maize families, all but 465 are conserved with at least one other species. Species- and lineage-specific families point out potential inconsistencies between annotation projects, but also reflect genuine biological differences in gene inventories.

Because of the stringent criteria used for including genes in the filtered gene set (*14*), we expected to miss some genes. About 95% of a collection of 63,851 full-length maize cDNAs (fl-cDNAs) (*29*, *30*) mapped to B73 RefGen_v1. On the basis of the ratio of fl-cDNA to supported genes in the filtered set, we estimated that this set accounts for at least 85% of all genes in the B73 RefGen_v1 (*14*).

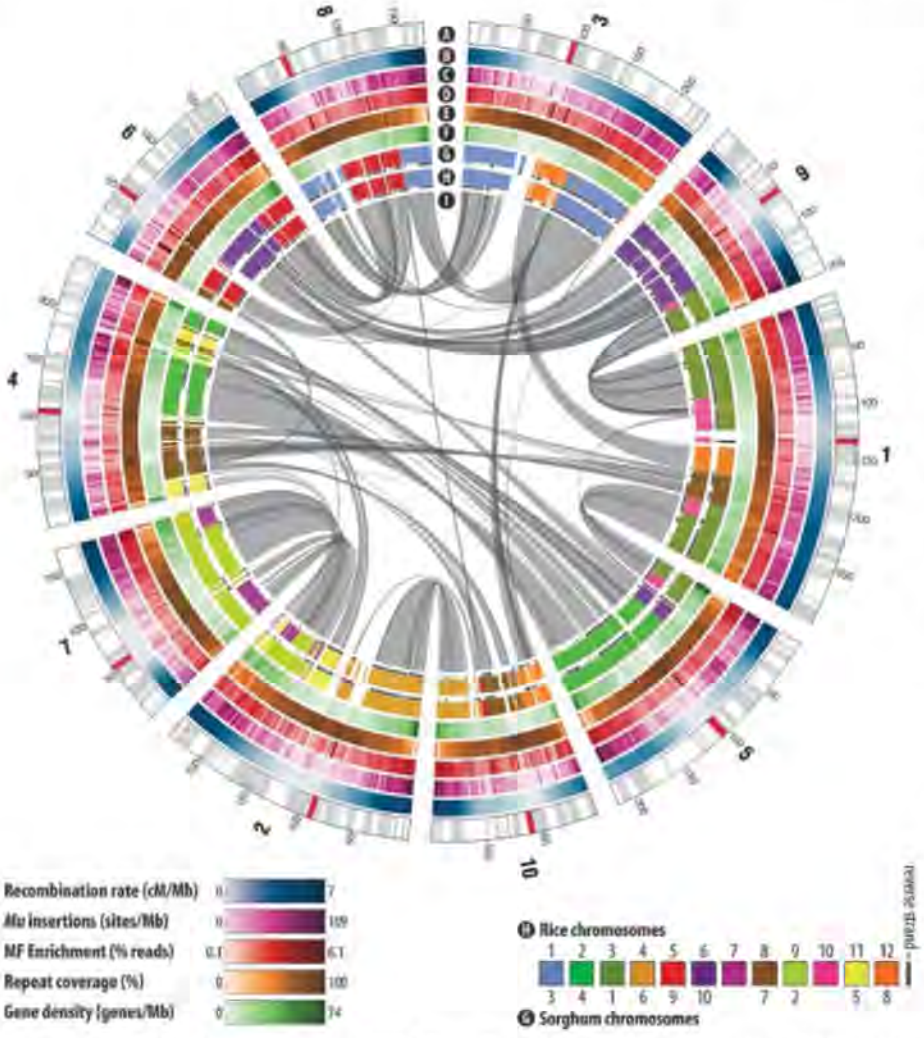


**Fig. 1.** The maize B73 reference genome (B73 RefGen_v1): Concentric circles show aspects of the genome. Chromosome structure (A). Reference chromosomes with physical fingerprint contigs (*11*) as alternating gray and white bands. Presumed centromeric positions are indicated by red bands (*31*); enlarged for emphasis. Genetic map (B). Genetic linkage across the genome, on the basis of 6363 genetically and physically mapped markers (*14*, *19*). *Mu* insertions (C). Genome mappings of nonredundant *Mu* insertion sites (*14*, *19*). Methyl-filtration reads (D). Enrichment and depletion of methyl filtration. For each nonoverlapping 1-Mb window, read counts were divided by the total number of mapped reads. Repeats (E). Sequence coverage of TEs with RepeatMasker with all identified intact elements in maize. Genes (F). Density of genes in the filtered gene set across the genome, from a gene count per 1-Mb sliding window at 200-kb intervals. Sorghum synteny (G) and rice synteny (H). Syntenic blocks between maize and related cereals on the basis of 27,550 gene orthologs. Underlined blocks indicate alignment in the reverse strand. Homoeology map (I). Oriented homoeologous sites of duplicated gene blocks within maize.

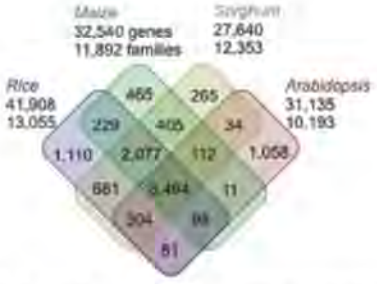


**Fig. 2.** Venn diagram showing unique and shared gene families between and among the three sequenced grasses (maize, rice, and sorghum) and the dicot, *Arabidopsis*.

The maximum rate of false-positive gene annotations was estimated by aligning ~112 million RNA-seq (transcriptome sequencing) reads from various tissues to the filtered gene set (*14*) (figs. S10 and S11). These experiments provided evidence for the transcription of ~91% of the genes in the filtered gene set (29,541 out of 32,540). Manual annotation of 200 randomly chosen genes from the filtered gene set indicated that only two are likely to be TE-derived. Additional manual annotation of smaller sets of selected genetically well-characterized genes (tables S8 to S10) indicated that the vast majority of genes and proteins predicted in the filtered gene set are mostly correct.

Maize centromeres were found to contain variable amounts of the tandem CentC satellite repeat and centromeric retrotransposon elements of maize (CRMs). On the basis of comparisons to B73 whole-genome shotgun data, we initially identified about half of the genome's CentC content (table S13). We captured additional CentC sequence by draft sequencing 101 centromeric repeat–containing BACs and anchoring them to the genetic and physical maps, thereby localizing all of the centromeres (*31*). We delineated the functional centromeres on the basis of their centromere-specific histone H3 (CENH3) (*32*) by using chromatin immunoprecipitation (ChIP) with an antibody against CENH3, followed by pyrosequencing. The centromere regions delineated in this way, although mostly incomplete, correlated with a high density of CentC and CRM1/CRM2/CRM3 repeats, but a number of these repeats also occurred outside of the functional centromeres (fig. S12). The CRM2 subfamily appears to be the centromeric repeat most closely associated with CENH3 in maize, as it is more enriched in the CENH3 chromatin fraction than CentC, CRM1, or CRM3 (table S13).

We traversed two centromeres (2 and 5) in their entirety and determined that they differ in size and CENH3 density (*31*). Because CRM elements have generated recombinants with distinct periods of activity (*33*, *34*), we were able to demonstrate that the regional centromeres of maize are dynamic loci and that the CENH3 domain shifts over time (*31*).

To protect genome integrity, TEs are usually transcriptionally silenced (*35*) in part via the RNA-directed DNA methylation (RdDM) pathway, which requires an RNA-dependent RNA polymerase 2 (RDR2). When the maize homolog of RDR2 (*36*) is mutated, it alters the accumulation of transcripts from many characterized transposons, but unexpectedly, some TEs are down-regulated by loss of RDR2 function (*37*). In most plant genomes, genes are less densely methylated than heterochromatic TEs and other repeats. Consequently, ~2× coverage of the maize genome by methylation-filtered (MF) reads includes portions of ~95% of maize genes (*38*). Mapping MF reads (*39*) of maize and sorghum onto their respective genomes revealed species-specific distributions of heterochromatic DNA methylation along the reference chromosomes (fig. S13, A and B). It is noteworthy that, in the sorghum genome, hypomethylated genes are largely excluded from the pericentromeric regions, whereas they are dispersed more widely in maize. Visual comparisons between sorghum and maize (*14*) revealed high levels of coalignment, including centromeres where centromeric repeats are undermethylated relative to the surrounding heterochromatin (*39*, *40*) (fig. S13C). Thus, the B73 RefGen_v1 yields evidence that heavily methylated regions are more condensed during interphase.

Anchoring the B73 RefGen_v1 to a newly developed genetic map (*19*) revealed that rates of meiotic recombination per megabase are highest at the ends of the reference chromosomes and very low in the middle half of each chromosome surrounding the centromeres (Fig. 1) (*19*, *41*). Although recombination occurs preferentially in genes (*2*) and gene density shows a similar distribution (Fig. 1), gene density does not fully explain the nonrandom distribution of recombination events, because a pronounced nonuniform distribution is still observed even when gene density is taken into consideration (*19*). Instead, epigenetic marks, including hypomethylation and histone modifications, are implicated in guiding both *Mu* insertion and meiotic recombination (*19*). Epigenetic processes have also been invoked to explain the observation that genomic imprinting contributes to the expression of thousands of genes in maize hybrids (*42*).

Maize exhibits extremely high levels of both phenotypic and genetic diversity. This genomic diversity was explored with both resequencing (*41*) and array-based comparative genomic hybridization between the B73 and Mo17 inbred lines (*43*). This revealed extensive structural variation, including hundreds of copy number variants (CNVs) and thousands of present-absent variants (PAVs). Many of the PAVs, including an ~2-Mb region on chromosome 6, contain intact, expressed single-copy genes that are present in one inbred genome but absent from the other. These haplotype-specific sequences may contribute to heterosis and the substantial degree of phenotypic variation among maize inbreds (*43*).

After a whole-genome duplication, the return to a genetically diploid state was associated with numerous chromosomal breakages and fusions, as shown by alignment to the genomes of sorghum and the more distantly related rice (Fig. 1 and fig. S14) (*12*). In contrast, sorghum has experienced relatively few interchromosomal rearrangements since its lineage split with rice (*8*); therefore, its chromosomal configuration closely resembles the ancestral state of maize's two subgenomes (*12*). Cosynteny of maize genes to common reference genes in rice or sorghum defined maize's duplicate regions (fig. S15). Although syntenic blocks cover 1832 Mb (~89% of the genome), individual gene losses were common and resulted in retention of only ~8110 genes as duplicate homoeologs (~25% of total genes; ~30% having orthologs in rice and/or sorghum). On the basis of an analysis of GO (gene ontology) terms (*14*, *44*) (table S15), retention of genes as duplicates is not random, e.g., retained duplicates are significantly enriched for transcription factors (>1.5-fold; $P$ value = $7.6 \times 10^{-22}$) (table S15), as is also the case in rice (*44*) and *Arabidopsis* (*45*). An example of biased retention is the CesA family, in which all 10 ancestral sites were retained as duplicates (fig. S16) (*46*). Using the sorghum genome to project extant maize regions to ancestral chromosomes (*14*) revealed a strong bias for gene loss (fractionation) between sister regions (table S16 and fig. S17). Fractionation bias has been observed in other plant lineages and species (*47*–*50*).

Sites containing proximately duplicated paralogs tend to exist as single copies, or not at all, at corresponding homoeologous positions (table S18). Of the 1454 proximately duplicated paralogs identified (making up 3614 genes), only 126 (~9%) could be found at homoeologous positions (*14*). Of the remainder, 279 (19%) had a single paralog at the corresponding homoeologous site, and 1049 (72%) had no homoeologs.

Nearly identical paralogs (NIPs) are genes with pairwise alignments of ≥500 bp, ≥98% identity, and ≥95% coverage with other genes (*51*). Of maize-filtered genes, 2.5% (828 out of 32,540) were NIPs from 386 families, most of which have only two members ($n$ = 349); the largest has nine members. Almost half (46%) of the NIP pairs had both members physically linked within 200 kb of each other, whereas in most of the remaining cases, the two members were distant from each other or on different chromosomes (fig. S18).

Just as cytogenetic and genetic maps (*52*) revolutionized research and crop improvement over the last century, the B73 maize reference sequence promises to advance basic research and to facilitate efforts to meet the world's growing needs for food, feed, energy, and industrial feed stocks in an era of global climate change. Findings derived from this genome sequence briefly summarized here are described in more detail in a series of companion papers (*11*, *13*, *19*, *22*, *24*–*26*, *30*, *31*, *37*, *41*–*43*, *46*). Annotation data and browser are available at www.maizegenome.org.

### References and Notes


1. J. F. Doebley, B. S. Gaut, B. D. Smith, *Cell* **127**, 1309 (2006).
2. J. L. Bennetzen, S. Hake, *Handbook of Maize: Genetics and Genomics* (Springer, New York, 2009).
3. C. P. National Corn Growers Association, Table showing corn harvested, yield, production, mya price, and value, 1991–2008; http://ncga.com/corn-production-trends.
4. A. F. Troyer, *Crop Sci.* **46**, 528 (2006).
5. D. N. Duvick, *Science* **286**, 418 (1999).
6. A. H. Paterson, J. E. Bowers, B. A. Chapman, *Proc. Natl. Acad. Sci. U.S.A.* **101**, 9903 (2004).
7. G. Blanc, K. H. Wolfe, *Plant Cell* **16**, 1667 (2004).
8. Z. Swigonova *et al.*, *Genome Res.* **14**, 1916 (2004).
9. A. H. Paterson *et al.*, *Nature* **457**, 551 (2009).
10. P. SanMiguel, B. S. Gaut, A. Tikhonov, Y. Nakajima, J. L. Bennetzen, *Nat. Genet.* **20**, 43 (1998).

11. F. Wei *et al.*, *PLoS Genet.*, 19 November 2009 (10.1371/journal.pgen.1000715).
12. F. Wei *et al.*, *PLoS Genet.* **3**, e123 (2007).
13. S. Zhou *et al.*, *PLoS Genet.*, 19 November 2009 (10.1371/journal.pgen.1000711).
14. Materials and methods are available as supporting material on *Science* Online.
15. P. SanMiguel *et al.*, *Science* **274**, 765 (1996).
16. B. McClintock, *Cold Spring Harbor Symp. Quant. Biol.* **16**, 13 (1951).
17. C. Feschotte, N. Jiang, S. R. Wessler, *Nat. Rev. Genet.* **3**, 329 (2002).
18. A. Kumar, J. L. Bennetzen, *Annu. Rev. Genet.* **33**, 479 (1999).
19. S. Liu *et al.*, *PLoS Genet.*, 19 November 2009 (10.1371/journal.pgen.1000733).
20. V. V. Kapitonov, J. Jurka, *Proc. Natl. Acad. Sci. U.S.A.* **98**, 8714 (2001).
21. S. Lal, N. Georgelis, L. Hannah, in *Handbook of Maize: Genetics and Genomics*, J. L. Bennetzen, S. Hake, Eds. (Springer, New York, 2008), pp. 329–339.
22. L. Yang, J. L. Bennetzen, *Proc. Natl. Acad. Sci. USA*, published online 19 November 2009 (10.1073/pnas.0908008106).
23. L. Yang, J. L. Bennetzen, *Proc. Natl. Acad. Sci. U.S.A.* **106**, 12832 (2009).
24. R. S. Baucom *et al.*, *PLoS Genet.*, 19 November 2009 (10.1371/journal.pgen.1000732).
25. F. Wei *et al.*, *PLoS Genet.*, 19 November 2009 (10.1371/journal.pgen.1000728).
26. L. Zhang, *PLoS Genet.*, 19 November 2009 (10.1371/journal.pgen.1000716).
27. H. Liang, W. H. Li, *Mol. Biol. Evol.* **26**, 1195 (2009).
28. G. Haberer *et al.*, *Plant Physiol.* **139**, 1612 (2005).
29. N. N. Alexandrov *et al.*, *Plant Mol. Biol.* **69**, 179 (2009).
30. C. Soderlund *et al.*, *PLoS Genet.*, 19 November 2009 (10.1371/journal.pgen.1000740).
31. T. K. Wolfgruber *et al.*, *PLoS Genet.*, 19 November 2009 (10.1371/journal.pgen.1000743).
32. C. X. Zhong *et al.*, *Plant Cell* **14**, 2825 (2002).
33. A. Sharma, G. G. Presting, *Mol. Genet. Genomics* **279**, 133 (2008).
34. A. Sharma, K. L. Schneider, G. G. Presting, *Proc. Natl. Acad. Sci. U.S.A.* **105**, 15470 (2008).
35. D. Lisch, *Annu. Rev. Plant Biol.* **60**, 43 (2009).
36. M. Alleman *et al.*, *Nature* **442**, 295 (2006).
37. Y. Jia *et al.*, *PLoS Genet.*, 19 November 2009 (10.1371/journal.pgen.1000737).
38. Y. Fu *et al.*, *Proc. Natl. Acad. Sci. U.S.A.* **102**, 12282 (2005).
39. L. E. Palmer *et al.*, *Science* **302**, 2115 (2003).
40. W. Zhang, H. R. Lee, D. H. Koo, J. Jiang, *Plant Cell* **20**, 25 (2008).
41. M. A. Gore *et al.*, *Science*, **326**, 1115 (2009).
42. R. A. Swanson-Wagner *et al.*, *Science* **326**, 1118 (2009).
43. N. M. Springer *et al.*, *PLoS Genet.*, 19 November 2009 (10.1371/journal.pgen.1000734).
44. C. G. Tian *et al.*, *Yi Chuan Xue Bao* **32**, 519 (2005).
45. C. Seoighe, C. Gehring, *Trends Genet.* **20**, 461 (2004).
46. B. W. Penning *et al.*, *Plant Physiol.*, published online 19 November 2009 (10.1104/pp.109.136804).
47. H. Shaked, K. Kashkush, H. Ozkan, M. Feldman, A. A. Levy, *Plant Cell* **13**, 1749 (2001).
48. K. Song, P. Lu, K. Tang, T. C. Osborn, *Proc. Natl. Acad. Sci. U.S.A.* **92**, 7719 (1995).
49. J. A. Tate, P. Joshi, K. A. Soltis, P. S. Soltis, D. E. Soltis, *BMC Plant Biol.* **9**, 80 (2009).
50. B. C. Thomas, B. Pedersen, M. Freeling, *Genome Res.* **16**, 934 (2006).
51. S. J. Emrich *et al.*, *Genetics* **175**, 429 (2007).
52. B. McClintock, *Science* **69**, 629 (1929).
53. The Maize Genome Sequencing Project supported by NSF award DBI-0527192 (R.K.W., S.W.C., R.S.F., R.A.W., P.S.S., S.A., L.S., D.W., W.R.M., R.A.M.). The Maize Transposable Element Consortium and the Maize Centromere Consortium supported by NSF awards DBI-0607123 (S.R.W., J.L.B., R.K.D., N.J., P.S.M.) and DBI-0421671 (R.K.D., J.J., G.G.P.). Also supported by NSF grants DBI-0321467 (D.W.), DBI-0321711 (P.S.S.), DBI-0333074 (D.W.), DBI-0501818 (D.C.S.), DBI-0501857 (Y.Y.), DBI-0701736 (T.P.B., Q.S.), DBI-0703273 (R.A.M.), and DBI-0703908 (D.W.), and by USDA National Research Initiative Grants 2005-35301-15715 and 2007-35301-18372 from the USDA Cooperative State Research, Education, and Extension Service (P.S.S.) and from the USDA-ARS (408934 and 413089) to D.W., and from the Office of Science (Biological and Environmental Research), U.S. Department of Energy, grant DE-FG02-08ER64702 to N.C.C. and M.C.M. Sequences of the reference chromosomes have been deposited in GenBank as accession numbers CM000777 to CM000786. RNA-sequence reads have been deposited in the Gene Expression Omnibus (GEO) database (www.ncbi.nlm.nih.gov/geo) as accession numbers GSE16136, GSE16868, and GSE16916. Centromeric sequences have been deposited in the National Center for Biotechnology Information, NIH, Trace Archive as accessions 1757396377 to 1757412600 and 2185189231 to 2185200942.


**Supporting Online Material**

www.sciencemag.org/cgi/content/full/326/5956/1112/DC1
Materials and Methods
SOM Text
Figs. S1 to S18
Tables S1 to S18
References

1 July 2009; accepted 13 October 2009
10.1126/science.1178534

# A First-Generation Haplotype Map of Maize

**Michael A. Gore,[1,2,3]*† Jer-Ming Chia,[4]* Robert J. Elshire,[3] Qi Sun,[5] Elhan S. Ersoz,[3] Bonnie L. Hurwitz,[4]‡ Jason A. Peiffer,[2] Michael D. McMullen,[1,6] George S. Grills,[7] Jeffrey Ross-Ibarra,[8] Doreen H. Ware,[1,4]§ Edward S. Buckler[1,2,3]§**

Maize is an important crop species of high genetic diversity. We identified and genotyped several million sequence polymorphisms among 27 diverse maize inbred lines and discovered that the genome was characterized by highly divergent haplotypes and showed 10- to 30-fold variation in recombination rates. Most chromosomes have pericentromeric regions with highly suppressed recombination that appear to have influenced the effectiveness of selection during maize inbred development and may be a major component of heterosis. We found hundreds of selective sweeps and highly differentiated regions that probably contain loci that are key to geographic adaptation. This survey of genetic diversity provides a foundation for uniting breeding efforts across the world and for dissecting complex traits through genome-wide association studies.

Maize (*Zea mays* L.) is both a model genetic system and an important crop species. Already a critical source of food, fuel, feed, and fiber, the addition of genomic information allows maize to be further improved through plant breeding that exploits its tremendous genetic diversity (*1*–*3*). Genome-wide association studies (GWAS) of diverse maize germplasm offer the potential to rapidly resolve complex traits to gene-level resolution, but these studies require a high density of genome-wide markers. To do this, we targeted the 20% of the maize genome that is low-copy (*4*, *5*) on a diverse panel of 27 inbred lines (representative of maize breeding efforts and worldwide diversity)—founders of the maize nested association mapping (NAM) population (*6*)—and used sequencing-by-synthesis (SBS) technology with three complementary restriction enzyme–anchored genomic libraries (figs. S1 and S2A) (*7*).

More than 1 billion SBS reads (>32 gigabases of sequence) were generated, covering ~38% of the total maize genome, albeit at mostly low-coverage levels. We focused on the ~93 million base pairs (Mbp) of low-copy sequence present in 13 or more lines in this study. Roughly 39% of the sequenced low-copy fraction was derived from introns and exons (*5*), covering 32% of the total genic fraction in the genome. We identified 3.3 million single-nucleotide polymorphisms (SNPs) and indels (table S1) and found that, overall, 1 in every 44 bp was polymorphic ($\pi = 0.0066$ per base pair). In a subset used for the population genetics analyses, the error rate was 1/2570 or 17-fold lower than $\pi$ (roughly half the errors are paralogy issues). The absolute level of diversity we examined, though high, may be slightly reduced because of difficulties aligning highly divergent sequences and our low power to call

[1]United States Department of Agriculture–Agriculture Research Service (USDA-ARS). [2]Department of Plant Breeding and Genetics, Cornell University, Ithaca, NY 14853, USA. [3]Institute for Genomic Diversity, Cornell University, Ithaca, NY 14853, USA. [4]Cold Spring Harbor Laboratory, Cold Spring Harbor, NY 11724, USA. [5]Computational Biology Service Unit, Cornell University, Ithaca, NY 14853, USA. [6]Division of Plant Sciences, University of Missouri, Columbia, MO 65211, USA. [7]Institute for Biotechnology and Life Science Technologies, Cornell University, Ithaca, NY 14853, USA. [8]Department of Plant Sciences, University of California, Davis, CA 95616–5294, USA.

*These authors contributed equally to this work.
†Present address: United States Arid-Land Agricultural Research Center, Maricopa, AZ 85138, USA.
‡Present address: Department of Ecology and Evolutionary Biology, University of Arizona, Tucson, AZ 85721, USA.
§To whom correspondence should be addressed. E-mail: ware@cshl.edu (D.H.W.); esb33@cornell.edu (E.S.B.)

singleton variants [60% of the expected rate on the basis of Sanger sequencing of candidate gene amplicons (*8*)].

Due to duplications of an ancestral genome, maize has many paralogous regions (*5*), and, as a result, 41% of the identified polymorphisms appear to be differences between paralogous sequences in these inbred lines. We thus defined two sets of SNPs: (i) the association set and (ii) the diversity set. Paralogous variants can be used effectively for GWAS and were retained in our association SNP data set, but they pose problems for analyses of diversity and were removed from our diversity SNP data set. The diversity set provides SNPs for characterizing genome-wide variation patterns, whereas the association set provides access to more regions of the genome. Comparisons between pairs of maize inbred lines identified structural variation for both retrotransposons and gene fragments (*9*, *10*). Similarly, our diverse lines averaged an excess of 7.8% of reads that were unique or unalignable to the reference genome (fig. S2B). On the basis of these data, the B73 genome may only capture ~70% of the alignable low-copy fraction represented by these 27 lines. Capturing the entire genome space for maize will be critical to evaluation of the functional importance of such divergent sequences.

In spite of the considerable molecular variation in the maize genome, the evolutionary potential of many variants is limited by linkage. Because this HapMap was built on the 27 founders of the NAM population, which captures ~135,000 meiotic crossovers (*6*), we could compare estimates of the recombination rate (*R*) with historical recombination patterns inferred on the basis of the SNP distribution (ρ). Overall, *R* and ρ were strongly correlated, indicating that recombination patterns tend to be stable over time [Spearman correlation $r^2_{sp}$ = 0.56 (Fig. 1B and fig. S3B)]. At the chromosomal scale, total genic bases were nearly perfectly correlated (probably the euchromatin fraction) with the total *R* on the basis of the NAM [$r^2_{sp}$ = 0.88 (Fig. 1A and fig. S3A)]. Recombination varied dramatically along

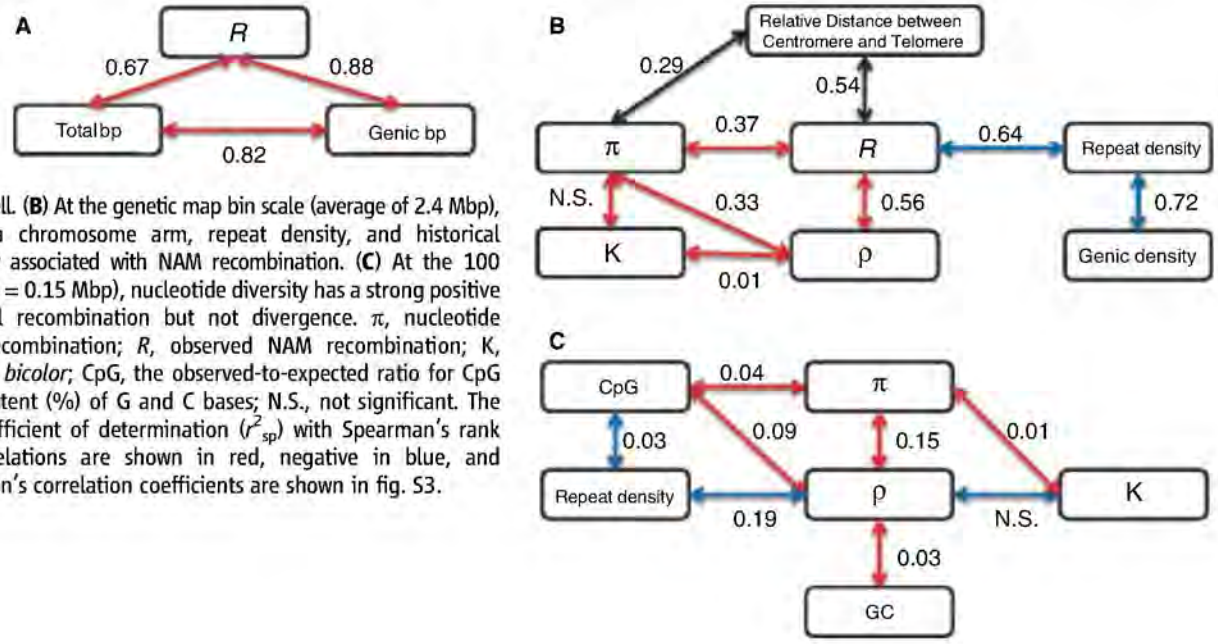


**Fig. 1.** Relation between sequence features, recombination, and diversity at three scales. **(A)** At the chromosomal scale (average of 200 Mbp), the total genic size of a chromosome predicts total recombination well. **(B)** At the genetic map bin scale (average of 2.4 Mbp), relative distance along a chromosome arm, repeat density, and historical recombination are strongly associated with NAM recombination. **(C)** At the 100 SNP bin scale (average size = 0.15 Mbp), nucleotide diversity has a strong positive correlation with historical recombination but not divergence. π, nucleotide diversity; ρ, historical recombination; *R*, observed NAM recombination; K, divergence from *Sorghum bicolor*; CpG, the observed-to-expected ratio for CpG dinucleotides; GC, the content (%) of G and C bases; N.S., not significant. The numbers indicate the coefficient of determination ($r^2_{sp}$) with Spearman's rank correlation. Positive correlations are shown in red, negative in blue, and symmetric in black. Pearson's correlation coefficients are shown in fig. S3.

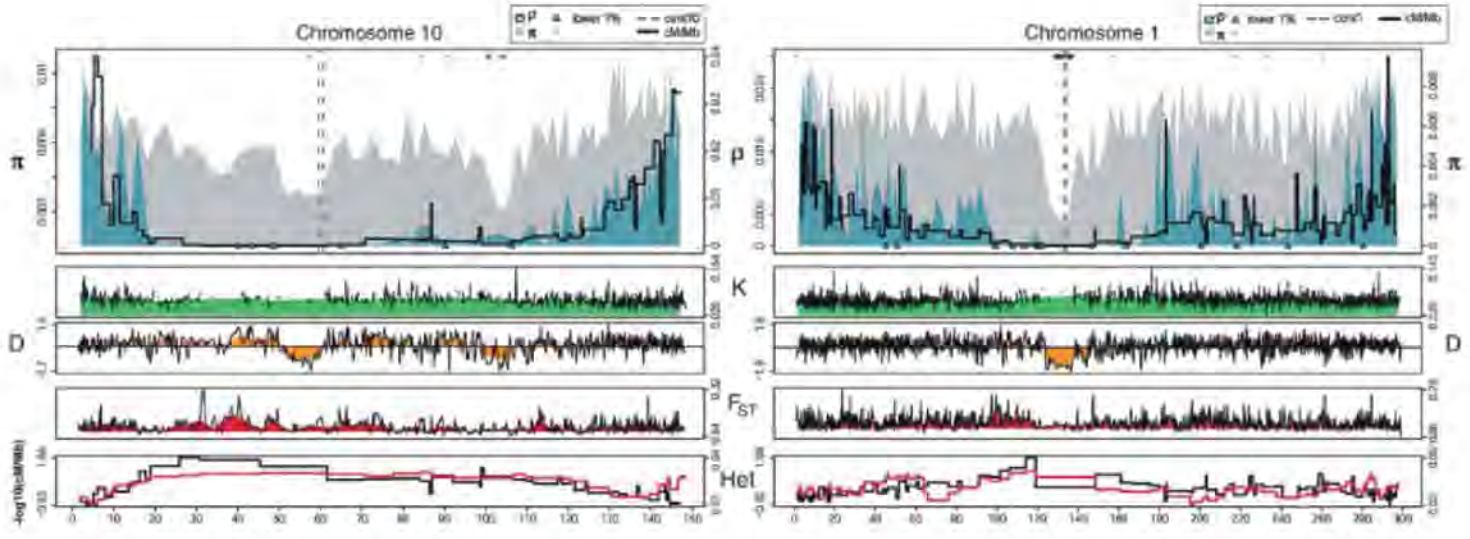


**Fig. 2.** Diversity along maize chromosomes 1 and 10. The horizontal axes are in units of million base pairs along the B73 reference genome; centromeres (*25*) are delineated by vertical dotted lines. Each chromosome shows (top panel) nucleotide diversity (π) and historical (ρ) and observed (cM/Mb, *R*) recombination (bottom panels) divergence from *Sorghum bicolor* (K), Tajima's measure of the site-frequency spectrum (D), population differentiation ($F_{ST}$), and a comparison of recombination [-log10(cM/Mb)] to residual heterozygosity (Het). Filled polygons represent the median of population genetic data from 10 100-SNP windows. Thin black lines denote data plotted for individual windows; thicker lines indicate data for residual heterozygosity and recombination represent estimates over NAM genetic map bins.

the chromosome (Fig. 2 and fig. S4), with 95% of total $R$ limited to slightly more than half of the genome. The 90th versus 10th percentiles varied 28-fold for $R$ and 12-fold for ρ. All chromosomes had a pericentromeric region of 60 to 113 Mbp with low recombination; these regions contain 21% of the total genic fraction. Similarly, sorghum has large pericentromeric regions that are recombinationally suppressed (*11*), but with fewer genes contained in these regions. We identified two correlated drivers of recombination: (i) the relative distance along a chromosome arm [$r^2_{sp} = 0.54$ (Fig. 1B and fig. S3B)] and (ii) repeat density [$r^2_{sp} = 0.64$ (Fig. 1B and fig. S3B)].

An earlier study on the NAM population identified considerable residual heterozygosity in pericentromeric regions of the maize genome and posited that this retention was probably a consequence of heterosis (*6*). We extended this finding by evaluating the relation of residual heterozygosity with recombination rates, genetic variation, and gene density. We found that regions of increased residual heterozygosity ($P < 0.01$) had 36% of all genes and nearly average diversity (91% of the genome average π). By anchoring recombination to the physical genome and controlling for a chromosome effect, residual heterozygosity and $R$ were inversely related [$r^2_{sp} = 0.35$ (Fig. 2)], whereas gene density ($r^2_{sp} = 0.18$) and diversity (π) ($r^2_{sp} = 0.16$) were less related. When we control for recombination, gene density and π have a statistically nonsignificant effect on residual heterozygosity. This result indicates that recombination is the major factor determining residual heterozygosity. This result indicates that a relatively low recombination rate is the major factor that contributes to the retention of residual heterozygosity. As a consequence, the tremendous genetic diversity at pericentromeric regions is constrained from being recombined into the most vigorous allelic combinations, thus lending further credence to pseudo-overdominance as the genetic basis for heterotic phenotypes in $F_1$ hybrids.

Examining nucleotide diversity, we found that chromosomes were punctuated by numerous million base pair–scale valleys of low nucleotide diversity and an excess of low-frequency variants (Fig. 2 and fig. S4). Most notably, 9 of the 10 maize centromeres are in or near such valleys. This observation is consistent with selection and rapid evolution at centromeric regions (*12*) and similar to observations in humans (*13*) and *Drosophila* (*14*), but contrasts with the high pericentromeric diversity in *Arabidopsis* (*15*, *16*). Although most regions of low diversity were associated with centromeres, a large number of low-diversity regions occur throughout the genome, many in regions with considerable recombination.

Genome-wide, nucleotide diversity was correlated with both ρ [$r^2_{sp} = 0.33$ (Fig. 1B)] and $R$ [$r^2_{sp} = 0.37$ (Fig. 1B)], but was nearly independent of divergence from *Sorghum* [$r^2_{sp} \leq 0.01$ (Fig. 1, B and C)], indicating that regions of reduced diversity have been the targets of selection. We tested 18 regions that have undergone a selective sweep (table S2), resulting in a median sweep in the 3.1% low tail of nucleotide diversity, suggesting that our HapMap has reasonable power to detect selected regions. In the high-recombination fraction of the genome, we identified 148 regions showing less diversity then the domestication gene *tb1* (*17*): 37 in high-recombination regions and 111 in low-recombination regions, including 1 of 11 megabases in size. A large region identified on the long arm of chromosome 10 has recently been associated with selection during domestication (*18*).

Given the recent divergence of lineages in *Zea* (*19*), selective sweeps may not be associated with domestication, but instead reflect selection in its ancestor, teosinte. Distinguishing between these possibilities and identifying their timing require sampling of diversity in both teosinte and early domesticated varieties (*2*, *20*). Additionally, demographic change has probably contributed to the observed variance in diversity (*2*, *21*), making it difficult to quantify what fraction of low-diversity regions may be due to neutral processes. Hence, investigation of the function and adaptive importance of regions defined here will be an important avenue of future research.

Maize has spread from the tropics into the northern and southern temperate zones and can clearly be differentiated with HapMap SNPs (fig. S5). However, $F_{ST}$ (a statistic that provides a measure of the extent of genetic differentiation between populations) had an average of only 3.8% between temperate and tropical germplasm, which suggests minimal differentiation. Although 43% of the genome has some $F_{ST}$ differentiation ($P < 0.05$), 183 regions showed a highly significant $F_{ST}$ ($P < 0.0001$), and may contain loci involved in the adaptation of maize to temperate versus tropical environments.

GWAS studies require markers in high LD with polymorphisms throughout the genome. This has been challenging, as in diverse maize LD generally decays ($r2 < 0.1$) within 2000 bp (fig. S6) (*22*). However, we also found evidence of longer haplotypes extending for thousands and millions of bases. Association studies in a genome with numerous small QTL effects (*23*) require high LD ($r^2 > 0.8$). We used a SNP hiding test (*24*), which revealed high LD ($r^2 > 0.8$) 55% of the time. When we conducted the same test on SNPs separated by at least 500 bp, high LD was found only 34% of the time. Thus, complete coverage for GWAS may require another order of magnitude of markers and the ability to anchor markers into the middle of retrotransposon domains.

With the maize HapMap and genome, we identified evidence for hundreds of regions that are probably involved in domestication and the geographic differentiation of maize. Remarkably, all of this selection has had to work against a genome with very strong recombinational suppression, which has effects that are embodied in modern-day heterosis and ancient, massive sweeps in centromeric regions. The future of maize improvement will not only depend on the ability to identify favorable alleles from the world's germplasm, but also the application of selection in a manner that effectively overcomes these recombinational constraints.

## References and Notes


1. M. I. Tenaillon *et al.*, *Proc. Natl. Acad. Sci. U.S.A.* **98**, 9161 (2001).
2. S. I. Wright *et al.*, *Science* **308**, 1310 (2005).
3. S. A. Flint-Garcia *et al.*, *Plant J.* **44**, 1054 (2005).
4. P. SanMiguel *et al.*, *Science* **274**, 765 (1996).
5. P. S. Schnable *et al.*, *Science* **326**, 1112 (2009).
6. M. D. McMullen *et al.*, *Science* **325**, 737 (2009).
7. Materials and methods are available as supporting material on *Science* Online.
8. www.panzea.org
9. H. Fu, H. K. Dooner, *Proc. Natl. Acad. Sci. U.S.A.* **99**, 9573 (2002).
10. M. Morgante *et al.*, *Nat. Genet.* **37**, 997 (2005).
11. A. Paterson *et al.*, *Nature* **457**, 551 (2009).
12. S. Henikoff, K. Ahmad, H. S. Malik, *Science* **293**, 1098 (2001).
13. I. Hellmann *et al.*, *Genome Res.* **18**, 1020 (2008).
14. D. J. Begun *et al.*, *PLoS Biol.* **5**, e310 (2007).
15. R. M. Clark *et al.*, *Science* **317**, 338 (2007).
16. A. Kawabe, A. Forrest, S. I. Wright, D. Charlesworth, *Genetics* **179**, 985 (2008).
17. R.-L. Wang, A. Stec, J. Hey, L. Lukens, J. Doebley, *Nature* **398**, 236 (1999).
18. F. Tian, N. M. Stevens, E. S. Buckler, *Proc. Natl. Acad. Sci. U.S.A.* **106**, 9979 (2009).
19. J. Ross-Ibarra, M. Tenaillon, B. S. Gaut, *Genetics* **181**, 1399 (2009).
20. M. Yamasaki *et al.*, *Plant Cell* **17**, 2859 (2005).
21. K. R. Thornton, J. D. Jensen, C. Becquet, P. Andolfatto, *Heredity* **98**, 340 (2007).
22. D. L. Remington *et al.*, *Proc. Natl. Acad. Sci. U.S.A.* **98**, 11479 (2001).
23. E. S. Buckler *et al.*, *Science* **325**, 714 (2009).
24. S. Kim *et al.*, *Nat. Genet.* **39**, 1151 (2007).
25. T. K. Wolfgruber *et al.*, *PLoS Genet.* **5**, e1000743 (2009).


26. We thank D. Costich and L. Rigamer Lirette for technical editing of the manuscript; researchers at the Lita Annenberg Hazen Genome Sequencing Center of Cold Spring Harbor Laboratory for discussion about sequencing and library construction; and T. Stelick, P. Schweitzer, and J. I. VanEe for assistance with the SBS data, all of which was generated at the Cornell University Life Sciences Core Laboratories Center. Mention of trade names or commercial products was solely to provide specific information and does not imply recommendation or endorsement by the USDA. This work was supported by NSF grants DBI-0321467, DBI-0638566, and DBI-0820619, and by the USDA-ARS. Sequences have been deposited at National Center for Biotechnology Information Short Read Archive with accession number SRP001145, and SNP calls are available at www.panzea.org.


## Supporting Online Material

www.sciencemag.org/cgi/content/full/326/5956/1115/DC1
Materials and Methods
Figs. S1 to S7
Tables S1 and S2
References

17 June 2009; accepted 20 October 2009
10.1126/science.1177837

# Paternal Dominance of Trans-eQTL Influences Gene Expression Patterns in Maize Hybrids

Ruth A. Swanson-Wagner, Rhonda DeCook,* Yi Jia, Tim Bancroft, Tieming Ji, Xuefeng Zhao, Dan Nettleton, Patrick S. Schnable†

Heterosis refers to the superior performance of hybrid progeny relative to their inbred parents, but the mechanisms responsible are unknown. Hybrids between the maize inbred lines B73 and Mo17 exhibit heterosis regardless of cross direction. These reciprocal hybrids differ from each other phenotypically, and 30 to 50% of their genes are differentially expressed. We identified ~4000 expression quantitative trait loci (eQTL) that allowed us to identify markers linked to variation in expression. We found that over three-quarters of these eQTL act in trans (78%) and that 86% of these differentially regulate transcript accumulation in a manner consistent with gene expression in the hybrid being regulated exclusively by the paternally transmitted allele. This result suggests that widespread imprinting contributes to the regulation of gene expression in maize hybrids.

Heterosis, the enhanced agronomic performance of a hybrid relative to its inbred parents (*1*), is widely exploited, but the underlying molecular mechanisms have not been deciphered (*2*). There are widespread differences in gene expression in the maize Mo17 × B73 hybrid relative to its inbred parents, B73 and Mo17 (*3*–*5*). Because maize is monoecious, with a physical separation between the male and female flowers on a single plant, any given plant can be used as both male and female parents of hybrids. Reciprocal B73 × Mo17 (female × male) and Mo17 × B73 hybrids are both highly heterotic but, despite having identical nuclear genomes, exhibit statistically significant differences in development (table S1). Reciprocal effects on phenotypes have been documented in plants (*6*) but have not been widely investigated at the molecular level (*7*, *8*).

Genome-wide transcript accumulation in the B73 × Mo17 and Mo17 × B73 hybrids was measured with a cDNA microarray (*9*), and the analysis identified 1515 (~11%) significantly differentially expressed genes with a 5% false discovery rate (FDR) cutoff (table S2). Similar results were obtained from an independent RNA-sequencing experiment (tables S2 and S3). Although the magnitude of these effects (expression fold changes) were modest (fig. S1), we estimated (*9*) that >50% ($N$ = 7325/14,118) of the genes on the array and ~33% ($N$ = 871/2640) of the highly expressed genes in the RNA sequencing experiment were differentially expressed. Smaller proportions of genes showing reciprocal expression effects have been previously reported in several species (*10*–*13*).

Expression QTL (eQTL) experiments (*14*) are typically conducted with recombinant inbred lines (RILs) or other inbred genotypes and thus are unable to determine the effects of heterozygosity on gene expression patterns (*10*). We examined eQTL in a set of 29 IBM (intermated B73 × Mo17) RILs derived from a cross between the maize B73 and Mo17 lines and hybrids generated by crossing each RIL onto B73 (B73 × RIL) and Mo17 (Mo17 × RIL). These hybrids provided a contrast between gene expression regulation at heterozygous and homozygous genotypes across all loci that are polymorphic between B73 and Mo17 (Fig. 1A).

Separate eQTL analyses were conducted within each cross type (B73 × RIL, Mo17 × RIL, and RIL) by scanning the genome with 1064 highly informative markers (*9*) and comparing the genetic map positions of differentially regulated genes relative to the genetic positions of the regulating eQTL. We defined an eQTL as acting in cis if a regulated gene and its corresponding eQTL were within 5 cM of each other. Trans-eQTL were defined as those located on different chromosomes than the genes they regulate.

*P* values and estimated FDRs (*9*) resulted in 1334 to 1904 significant eQTL associations within each cross type (table S4). About 25% of the significant genes were regulated in multiple cross types. In the majority of such cases, the same genomic region regulated the gene among multiple cross types (table S5 and figs. S2 and S3).

Only 10% of the detected eQTL acted in cis, which on average showed larger effects than the trans-eQTL (table S4 and fig. S4), consistent with previous reports for maize (*4*, *14*) and other species (*15*). Trans-eQTL with large effects may be rare because they can regulate many genes or entire pathways that, if substantially up- or down-regulated, could be detrimental (*16*, *17*). Many cis-regulated genes detected within the RIL cross type were previously (*5*) identified as differentially expressed between the B73 and Mo17 inbred lines (79/114) and exhibited consistent directions of effect in the current study. Because the RILs used for this study were mosaics of the B73 and Mo17 genomes, this validates the stability of these cis-eQTL across genetic backgrounds.

Nearly 80% of the eQTL acted in trans (table S4 and fig. S3), consistent with reports from other species (*15*, *18*–*23*) and of trans-regulation of diverse biological processes in maize (*24*–*28*). Previous studies may have overestimated the number or proportion of cis-regulated genes (*3*, *29*) due to ascertainment bias because they only analyzed genes containing single nucleotide polymorphisms between B73 and Mo17 and/or had limited statistical power to detect the more subtle effects of trans-eQTL (*15*).

Clustering of expression patterns of all genes regulated by eQTL distinguished cis- and trans-regulated genes (Fig. 1B). Most (93%) genes with additive gene action are cis-regulated and have similar amounts of expression in the two heterozygotes (Mo17 × $RIL_{BB}$ and B73 × $RIL_{MM}$; clusters 1 and 2, Fig. 1, A and B). Instead of showing additive gene action, most (86%) trans-eQTL exhibit a mode of gene action we term "paternal dominance" that is consistent with imprinting, wherein expression values in those heterozygotes with a $RIL_{BB}$ as the paternal parent matched expression values in lines that were homozygous for the B allele of the trans-eQTL; similarly, heterozygotes with a $RIL_{MM}$ as the paternal parent had expression values that matched the expression values in lines that were homozygous for the M allele of the trans-eQTL (i.e., MB was not equal to BM; clusters 3 and 4, Fig. 1B). Because our experimental design held the maternally contributed allele in hybrids constant, we could detect variation in paternally contributed alleles (Fig. 1A) while controlling for maternal or cytoplasmic effects. Hence, these results suggest that gene expression in the hybrids is regulated exclusively by the paternally transmitted allele of these trans-eQTL.

An eQTL marker (interval 377) associated with the differential regulation of more than 20 genes was back-crossed into the Mo17 inbred genetic background for multiple generations (fig. S5). Seedlings of the BM and MM genotypes generated at this interval in genetic backgrounds that were otherwise 87.5% homozygous for the Mo17 genotype showed significant differences in expression that were consistent with patterns observed in the eQTL analysis. Thus, this trans-eQTL is stable across generations and technologies (table S6).

Because no direct comparisons were performed between B73 × $RIL_{MM}$ and Mo17 × $RIL_{BB}$, we validated the unusual paternal dominance patterns of gene expression for five genes regulated in trans by interval 377 by using a combination of quantitative reverse transcription polymerase chain reaction and Sequenom (Sequenom, San Diego, CA) quantitative gene expression (QGE) assays (table S6).

It is not possible to conclude how widely distributed paternal dominance is across species because previous studies have most commonly been performed with only inbred genotypes; such

Iowa State University, Ames, IA 50011, USA.

*Present address: Department of Statistics and Actuarial Science, University of Iowa, Iowa City, IA 52242, USA.

†To whom correspondence should be addressed. E-mail: schnable@iastate.edu

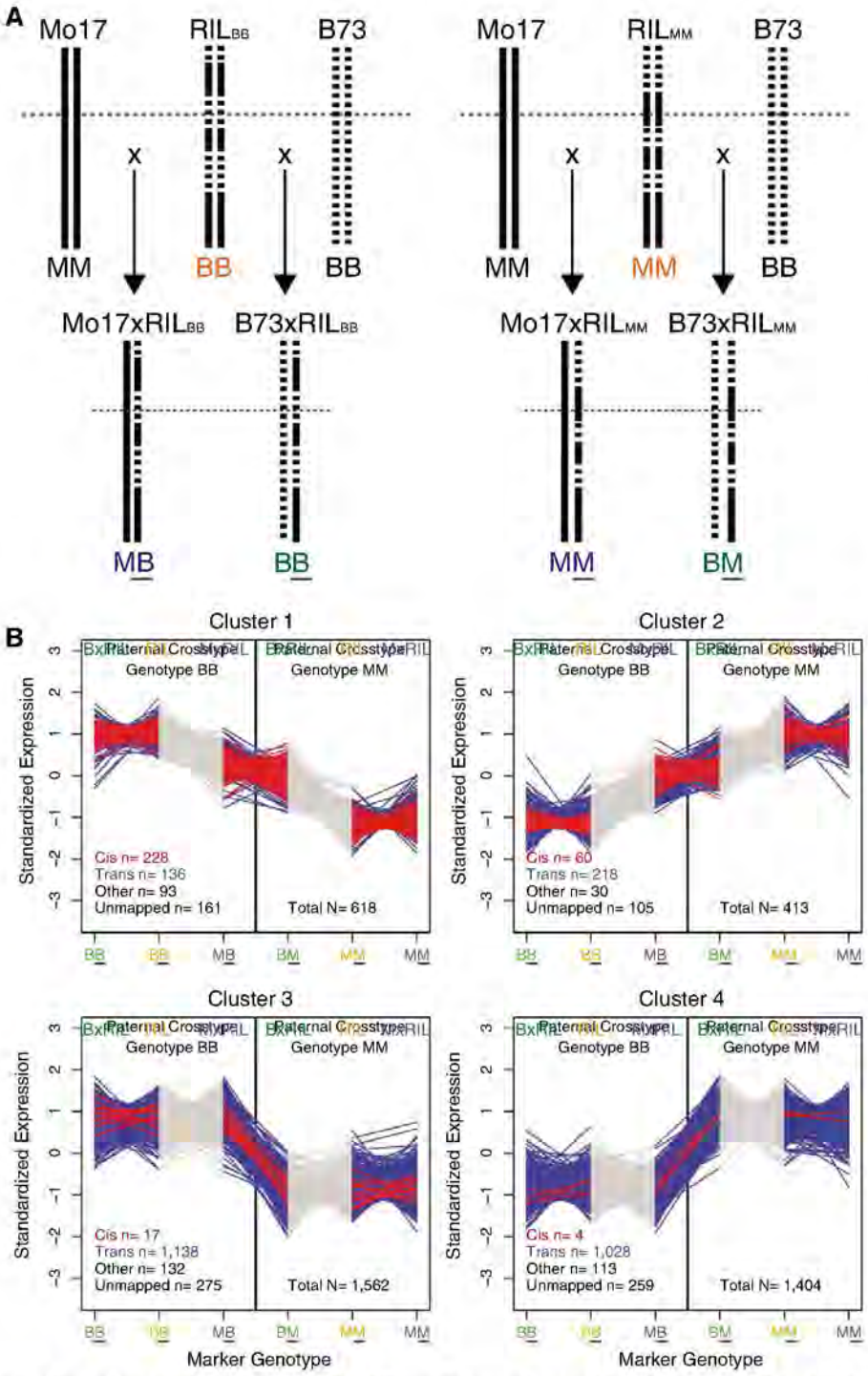


**Fig. 1.** Cis- and trans-regulated genes exhibit different patterns of expression. **(A)** Because the inbred IBM RILs are derived from a cross between B73 and Mo17, a given IBM RIL is homozygous for either the B (B73) or M (Mo17) allele of a given marker (denoted by a gray dashed line). We designate such RILs as $RIL_{BB}$ and $RIL_{MM}$, respectively. When crossed onto B73 (BB), $RIL_{BB}$ and $RIL_{MM}$ RILs will generate hybrids that are homozygous and heterozygous for the marker in question, respectively. Similarly, when crossed onto Mo17 (MM), $RIL_{BB}$ and $RIL_{MM}$ RILs will generate hybrids that are heterozygous and homozygous for the marker in question, respectively. Thus, each cross type provided mean expression values for each of two genotypic groups. The allele inherited from the paternal parent is underlined. **(B)** Standardized expression values (*y* axis) were clustered to group genes with similar expression patterns. For clustering purposes, each nonredundant gene-marker association ($N = 3997$) was represented by a vector of six expression means. The four resulting clusters were plotted according to the genotype of the associated regulating eQTL marker (*x* axis). Red lines denote cis-eQTL, and blue lines denote trans-eQTL. The cross type in which the expression was measured is indicated at the top of each plot (B73 × RIL, green; RIL, orange; and Mo17 × RIL, purple), and the allele inherited from the paternal genome is underlined in the *x*-axis labels. Clusters 1 and 2 both show additive gene action but differ as to whether lines homozygous for the B allele of an eQTL locus show higher expression than lines homozygous for the M allele or vice versa. Clusters 3 and 4 both show paternal dominance but have opposite modes of gene action as described for clusters 1 and 2.

experiments cannot define the mode of gene action and cannot detect genomic imprinting because the effects of heterozygosity and reciprocally generated genotypes are not typically investigated. If we had only examined one of the two hybrid cross types, the gene action of the paternally dominant trans-eQTL would have incorrectly been classified as Mendelian dominant. Lastly, sufficient statistical power is needed to detect the modest effects of trans-eQTL.

We hypothesize that at least some paternally dominant trans-eQTL are small RNAs, because small RNAs regulate gene expression in trans (*30*, *31*) and can be subject to parent-specific genomic imprinting (*32*, *33*). Because there are many paternally dominant trans-eQTL in maize, and many of these regulate multiple genes, their effects are broadly propagated throughout the transcriptome. Paternal dominance may, therefore, contribute to the observed phenotypic differences between reciprocal hybrids.

## References and Notes


1. G. H. Shull, *Am. Breeders Assoc.* **4**, 296 (1908).
2. P. S. Schnable, R. A. Swanson-Wagner, in *Handbook of Maize: Its Biology*, J. L. Bennetzen, S. C. Hake, Eds. (Springer, New York, 2009), pp. 457–467.
3. M. Guo *et al.*, *Plant Mol. Biol.* **66**, 551 (2008).
4. R. M. Stupar, N. M. Springer, *Genetics* **173**, 2199 (2006).
5. R. A. Swanson-Wagner *et al.*, *Proc. Natl. Acad. Sci. U.S.A.* **103**, 6805 (2006).
6. M. Gonzalo, T. J. Vyn, J. B. Holland, L. M. McIntyre, *Heredity* **99**, 14 (2007).
7. R. M. Stupar, P. J. Hermanson, N. M. Springer, *Plant Physiol.* **145**, 411 (2007).
8. N. Hoecker, B. Keller, H. P. Piepho, F. Hochholdinger, *Theor. Appl. Genet.* **112**, 421 (2006).
9. Materials and methods are available as supporting material on *Science* Online.
10. G. Gibson *et al.*, *Genetics* **167**, 1791 (2004).
11. M. Vuylsteke, F. van Eeuwijk, P. Van Hummelen, M. Kuiper, M. Zabeau, *Genetics* **171**, 1267 (2005).
12. X. Wang *et al.*, *PLoS One* **3**, e3839 (2008).
13. P. J. Wittkopp, B. K. Haerum, A. G. Clark, *Genetics* **173**, 1817 (2006).
14. E. E. Schadt *et al.*, *Nature* **422**, 297 (2003).
15. D. Kliebenstein, *Annu. Rev. Plant Biol.* **60**, 93 (2009).
16. J. M. Aury *et al.*, *Nature* **444**, 171 (2006).
17. B. G. Hansen, B. A. Halkier, D. J. Kliebenstein, *Trends Plant Sci.* **13**, 72 (2008).
18. R. B. Brem, G. Yvert, R. Clinton, L. Kruglyak, *Science* **296**, 752 (2002); published online 28 March 2002 (10.1126/science.1069516).
19. N. Hubner *et al.*, *Nat. Genet.* **37**, 243 (2005).
20. S. A. Monks *et al.*, *Am. J. Hum. Genet.* **75**, 1094 (2004).
21. M. Morley *et al.*, *Nature* **430**, 743 (2004).
22. M. A. West *et al.*, *Genetics* **175**, 1441 (2007).
23. G. Yvert *et al.*, *Nat. Genet.* **35**, 57 (2003).
24. X. Niu, T. Helentjaris, N. J. Bate, *Plant Cell* **14**, 2565 (2002).
25. F. T. Nogueira, A. K. Sarkar, D. H. Chitwood, M. C. Timmermans, *Cold Spring Harbor Symp. Quant. Biol.* **71**, 157 (2006).
26. N. Satoh-Nagasawa, N. Nagasawa, S. Malcomber, H. Sakai, D. Jackson, *Nature* **441**, 227 (2006).
27. C. Shi *et al.*, *BMC Genomics* **8**, 22 (2007).
28. M. D. Yandeau-Nelson, B. J. Nikolau, P. S. Schnable, *Genetics* **174**, 101 (2006).
29. N. M. Springer, R. M. Stupar, *Plant Cell* **19**, 2391 (2007).
30. G. Chuck, H. Candela, S. Hake, *Curr. Opin. Plant Biol.* **12**, 81 (2009).
31. J. A. Goodrich, J. F. Kugel, *Crit. Rev. Biochem. Mol. Biol.* **44**, 3 (2009).
32. J. Brennecke *et al.*, *Science* **322**, 1387 (2008).
33. R. K. Slotkin *et al.*, *Cell* **136**, 461 (2009).

34. We thank S. Hargreaves, M. Smith, M. Wilkening, T. Kemmerer, P. Lu, C.-T. Yeh, and L. Coffey for sample and data processing and the maize genome sequence project (NSF DBI-0527192) for sharing genome sequences before publication. Funding provided by Iowa State University's Plant Sciences Institute. Microarray and sequencing data are available at the National Center for Biotechnology Information GEO database in series GSE16136.

**Supporting Online Material**
www.sciencemag.org/cgi/content/full/326/5956/1118/DC1
Materials and Methods
Figs. S1 to S6
Tables S1 to S9
References

26 June 2009; accepted 15 October 2009
10.1126/science.1178294

# Symbiotic Nitrogen Fixation in the Fungus Gardens of Leaf-Cutter Ants

**Adrián A. Pinto-Tomás,[1,2,3] Mark A. Anderson,[4] Garret Suen,[1,5] David M. Stevenson,[6] Fiona S. T. Chu,[4] W. Wallace Cleland,[4] Paul J. Weimer,[6] Cameron R. Currie[1,5]***

**Bacteria-mediated acquisition of atmospheric $N_2$ serves as a critical source of nitrogen in terrestrial ecosystems. Here we reveal that symbiotic nitrogen fixation facilitates the cultivation of specialized fungal crops by leaf-cutter ants. By using acetylene reduction and stable isotope experiments, we demonstrated that $N_2$ fixation occurred in the fungus gardens of eight leaf-cutter ant species and, further, that this fixed nitrogen was incorporated into ant biomass. Symbiotic $N_2$-fixing bacteria were consistently isolated from the fungus gardens of 80 leaf-cutter ant colonies collected in Argentina, Costa Rica, and Panama. The discovery of $N_2$ fixation within the leaf-cutter ant–microbe symbiosis reveals a previously unrecognized nitrogen source in neotropical ecosystems.**

Ants play a critical role in shaping terrestrial ecosystems. They make up at least one-third of the global insect fauna biomass and 86% of the arthropod biomass in tropical forest canopies, and, in the Amazon forest, they represent four times more biomass than do all land vertebrates combined (*1*–*3*). Among ants, the leaf cutters (tribe Attini: genera *Atta* and *Acromyrmex*) play an important role as one of the most dominant herbivores in New World tropical ecosystems, stimulating new plant growth and facilitating nutrient cycling (*4*). Mature *Atta* colonies are among the largest of any social insect, consisting of up to 8 million workers and occupying an underground volume of more than 20 $m^3$ (Fig. 1, A and B) (*5*). These "superorganisms" harvest more than 240 kg dry weight of leaf material per year (*4*), which they use to cultivate a fungus for food (*6*). This ability to grow a specialized fungal crop using freshly cut plant material is a key factor in the ecological success of leaf-cutter ants (*7*). In addition to their relationship with fungal mutualists (family Lepiotaceae), the ants engage in a second mutualism with Actinobacteria (genus *Pseudonocardia*), which produce antibiotics to help defend the fungus garden from parasites (*8*, *9*). We explored the possibility that leaf-cutter ants engage in mutualistic associations with $N_2$-fixing symbionts to supplement the nitrogen budget of their fungus gardens.

Nitrogen is expected to be a growth-limiting resource in leaf-cutter ant agriculture: The primary nutrient input into their colonies is fresh leaves, which have a much lower nitrogen-to-carbon (N:C) ratio than is required by insects (*10*, *11*). In contrast to this expectation, several field studies have shown that the exhausted leaf substrate removed from the bottom of fungus gardens by ant workers contains higher proportions of N than either freshly harvested leaf material or surrounding leaf litter does, indicating that N enrichment occurs as the plant substrate is processed by the colony (*4*, *12*, *13*). Although these findings suggest the presence of $N_2$-fixing symbionts, potential additional sources are mineralized N from the soil and compensatory feeding by the ants (*13*, *14*). We analyzed the N content of laboratory-maintained colonies of *Atta cephalotes* in which we prevented N input from these alternate sources (*15*). We found an increase in N content as leaf substrate passes through the system: N content was lowest in fresh leaf cuttings, significantly higher in the fungus

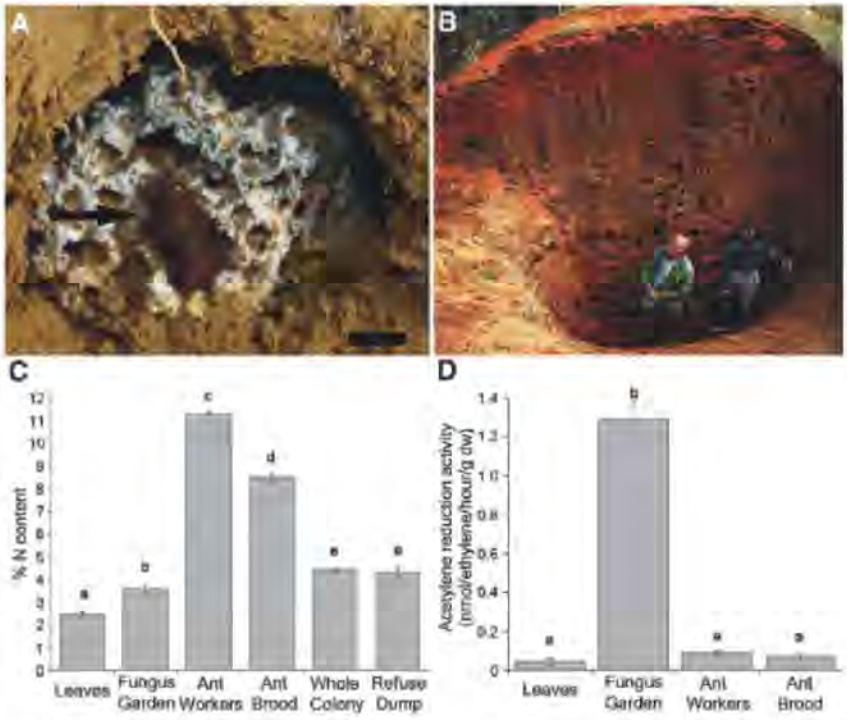


**Fig. 1.** Evidence for $N_2$ fixation in the fungus gardens of leaf-cutter ants. (**A** and **B**) The agricultural system of leaf-cutter ants is extremely efficient, allowing colonies to grow from a single fungus garden chamber [(A) incipient *At. cephalotes* colony with queen (black arrow) on top of fungus garden; scale bar = 1 cm] to a massive underground operation with hundreds of chambers, intricate tunnel systems, and millions of workers [(B) partially excavated nest of a mature *Atta* colony]. (**C**) Nitrogen content of the different components of five *At. cephalotes* colonies. (**D**) $N_2$-fixation activity measured by acetylene reduction for different components of 10 *Atta* spp. colonies. All results are shown as means ± SEM. Means labeled with different letters (a to e) are statistically different ($P < 0.05$). [Photo credits: (A) Graham D. Anderson, (B) M. Moffett/Minden Pictures]

[1]Department of Bacteriology, University of Wisconsin–Madison, 1550 Linden Drive, Madison, WI 53706, USA. [2]Departamento de Bioquímica, Facultad de Medicina, Universidad de Costa Rica, San Pedro de Montes de Oca, San José, Costa Rica. [3]Centro de Investigaciones en Estructuras Microscópicas, Universidad de Costa Rica, San Pedro de Montes de Oca, San José, Costa Rica. [4]Institute for Enzyme Research, Department of Biochemistry, University of Wisconsin–Madison, 1710 University Avenue, Madison, WI 53726, USA. [5]U.S. Department of Energy Great Lakes Bioenergy Research Center, University of Wisconsin–Madison, 1550 Linden Drive, Madison, WI 53706, USA. [6]U.S. Department of Agriculture–Agricultural Research Service, U.S. Dairy Forage Research Center, 1925 Linden Drive West, Madison, WI 53706, USA.

*To whom correspondence should be addressed. E-mail: currie@bact.wisc.edu

garden, and even higher in the ants' refuse dump, where the exhausted leaf substrate is placed by workers (Fig. 1C) ($F_{(5,24)} = 458.34$, $P < 0.0001$, $n = 5$ colonies). Our results confirm that N is enriched as substrate passes through leaf-cutter ant colonies, and because other sources of N input were prevented, it suggests that, like other insects with low-N diets (*11*, *16*, *17*), leaf-cutter ants acquire additional N from symbiotic $N_2$ fixers [see also supporting online material (SOM) text].

We conducted acetylene reduction (AR) assays to determine whether N enrichment within leaf-cutter ant colonies is occurring, at least in part, through $N_2$ fixation. AR is a functional test that demonstrates the presence of an active nitrogenase enzyme complex and has been widely used to provide evidence for biological $N_2$ fixation (*16*–*18*). We detected positive AR activity in the fungus gardens of all leaf-cutter ant colonies evaluated [mean = 1.03 ± 0.06 SEM nmol of ethylene per hour per g dry weight (dw)], including five species of *Acromyrmex* ($n = 14$ colonies) and three *Atta* species ($n = 21$ colonies; table S1). Overall, mean AR activity in the fungus garden was higher in *Atta* colonies (1.16 ± 0.07 SEM nmol of ethylene per hour per g dw) than in *Acromyrmex* colonies (0.81 ± 0.06 SEM nmol of ethylene per hour per g dw). Long-term monitoring of three *Atta* spp. colonies showed that $N_2$ fixation was both consistent and continuous over a 2-year period (SOM text and fig. S1). $N_2$-fixation rates were significantly higher in the middle of fungus gardens, where most feeding on the cultivated fungus occurs (fig. S2). In contrast to the fungus garden, only marginal AR activity (<0.1 nmol of ethylene per hour per g dw) was detected in ant workers, ant brood, and leaf material used by the ants to grow their fungus (Fig. 1D) ($F_{(3,36)} = 210.40$, $P < 0.0001$, $n = 10$ colonies; see also figs. S3 and S4). These results showed that $N_2$ fixation occurs in leaf-cutter ant fungus gardens and indicated the presence of $N_2$-fixing bacteria within the garden matrix.

To locate $N_2$ fixers, we used a culture-independent approach to detect *nifH*, a gene that encodes a subunit of the evolutionarily conserved nitrogenase enzyme complex, which is used by most $N_2$-fixing bacteria (*19*). *nifH* was detected in 50% of the fungus garden samples tested from seven different leaf-cutter ant species in the genera *Atta* and *Acromyrmex* (table S2). The presence of *nifH* was found in only 25% of the ant workers, and because the ants showed insignificant $N_2$-fixation activity as measured by AR, it is likely that these amplicons correspond to undigested fungus garden in their digestive systems. *nifH* was not detected in pure cultures of either *Pseudonocardia* or the fungal cultivar, the latter of which was tested because of the possible presence of endosymbiotic bacteria, because $N_2$ fixation is not known in any fungi. These findings, coupled with the results from the AR assays, reveal that $N_2$ fixation occurs in vivo within the fungus gardens of leaf-cutter ant colonies.

To determine whether fixed $N_2$ directly benefits leaf-cutter ants, we conducted enrichment experiments using the natural stable isotope of nitrogen $^{15}N_2$. Paired leaf-cutter ant subcolonies were placed in airtight containers (Fig. 2A), whose internal atmosphere was exchanged with either a mixture of 80% $^{15}N_2$ and 20% $O_2$ (treatment) or regular atmospheric air. Under these conditions, eight *At. cephalotes* subcolonies were assayed for 2 weeks (Fig. 2, B and C, and tables S3 and S4). After 1 week, significant $^{15}N$ enrichment was found in the fungus garden (paired $t$ test; $t = 7.45$, $P = 0.0001$), worker ants ($t = 5.28$, $P = 0.001$), and ant brood ($t = 2.47$, $P = 0.04$) (Fig. 2B). At the end of 2 weeks, significant enrichment was detected in the fungus garden ($t = 4.87$, $P = 0.002$) and in ant workers ($t = 3.08$, $P = 0.02$), but not in ant brood ($t = 1.28$, $P = 0.247$), because most immature individuals had developed into pupae, which do not feed (Fig. 2C). Using the $^{15}N$ natural abundance measurements for fungus gardens and leaves used to feed the leaf-cutter ant colonies in the laboratory, we estimate that *At. cephalotes* fungus gardens can obtain between 45 and 61% of their N supply through their symbiotic association with $N_2$-fixing bacteria (SOM text and figs. S5 and S6). These findings show that leaf-cutter ant workers obtain nitrogen from $N_2$-fixing bacteria, which appear to serve as a substantial source of N for the ants' fungal crop.

To further support our findings of $N_2$ fixation in the fungus gardens of leaf-cutter ants and to begin identifying the microbes responsible, we conducted extensive enrichment isolations using N-free media. Bacteria in the genus *Klebsiella* were isolated from the fungus gardens of 69% of leaf-cutter colonies from four different ant species collected across different ecosystems in Costa Rica and Panama ($n = 58$ colonies). These isolates fix $N_2$ at rates comparable to rates of known free-living diazotrophs, including *Azospirillum* sp. (Fig. 3A). We also re-isolated *Klebsiella* from leaf-cutter ant fungus gardens several months after field collection, which suggests that these $N_2$ fixers proliferate within the fungus garden. Phylogenetic analyses revealed that leaf-cutter–associated *Klebsiella* form a specific clade that includes the type strain for *K. variicola* (Fig. 3B). Bacteria in the genus *Pantoea* were also consistently isolated, but these isolates fix $N_2$ at a significantly lower rate than the *Klebsiella* isolates do and were obtained less frequently in the field (in 30% of leaf-cutter ant colonies collected in Costa Rica). Leaf-cutter–associated *Pantoea* also form a well-supported

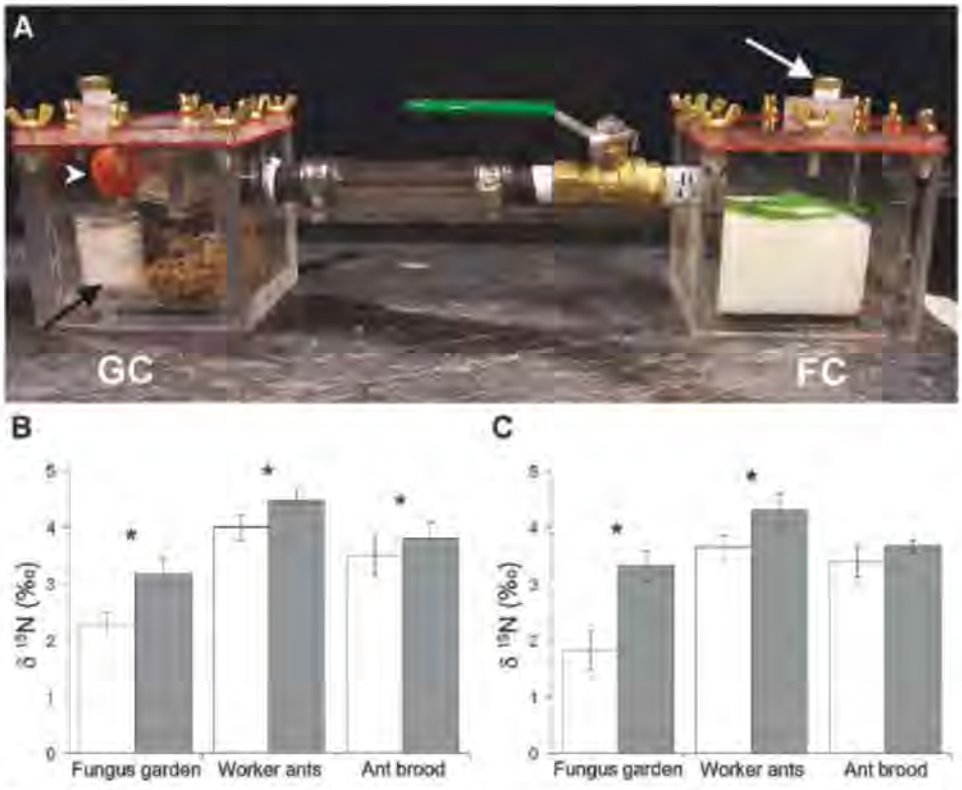


**Fig. 2.** $^{15}N_2$-enrichment experiments demonstrate that leaf-cutter ants obtain N from $N_2$-fixing symbionts. (**A**) The airtight apparatus used in the enrichment experiments consists of a fungus garden chamber (GC) and a feeding chamber (FC), joined by a foraging tube. It included injection ports for gas exchange (white arrow), a $CO_2$ trap (white arrowhead), and a moisture device (black arrow). (**B** and **C**) Results for $^{15}N_2$-enrichment experiments with eight *At. cephalotes* subcolonies, 1 week [(B) $n = 8$ subcolonies] and 2 weeks [(C) $n = 7$] after the initial treatment. The mean $\delta^{15}N$ value [N isotopic ratio, per mil (‰)] is provided for the different components of leaf-cutter ant subcolonies maintained in a control (white bars) and a $^{15}N_2$-enriched (gray bars) atmosphere. The asterisks indicate significant $^{15}N$ enrichment (two-tailed paired $t$ test, $P < 0.05$). Error bars represent SEM.

clade in our multilocus phylogeny (Fig. 3B). We sequenced the full *nif* cluster from leaf-cutter–associated *Klebsiella* and *Pantoea*, and we found that both contain intact clusters that use the canonical molybdenum-iron nitrogen-fixing pathway (*20*), and both are identical with respect to gene content and synteny (SOM text and table S6). The presence of these clusters in the fungus garden was further confirmed through real-time polymerase chain reaction (PCR); we detected leaf-cutter–associated *Klebsiella* and *Pantoea* *nifH* within the fungus gardens from all eight *Atta* colonies tested (SOM text and fig. S9). Given the high $N_2$-fixation rates measured for these *Klebsiella* isolates, the prevalence and apparent persistence in leaf-cutter fungus gardens, and the fact that they form a specialized monophyletic clade in our phylogenetic analyses, it is likely that *Klebsiella* is an important $N_2$-fixing symbiont of leaf-cutter ants (SOM text).

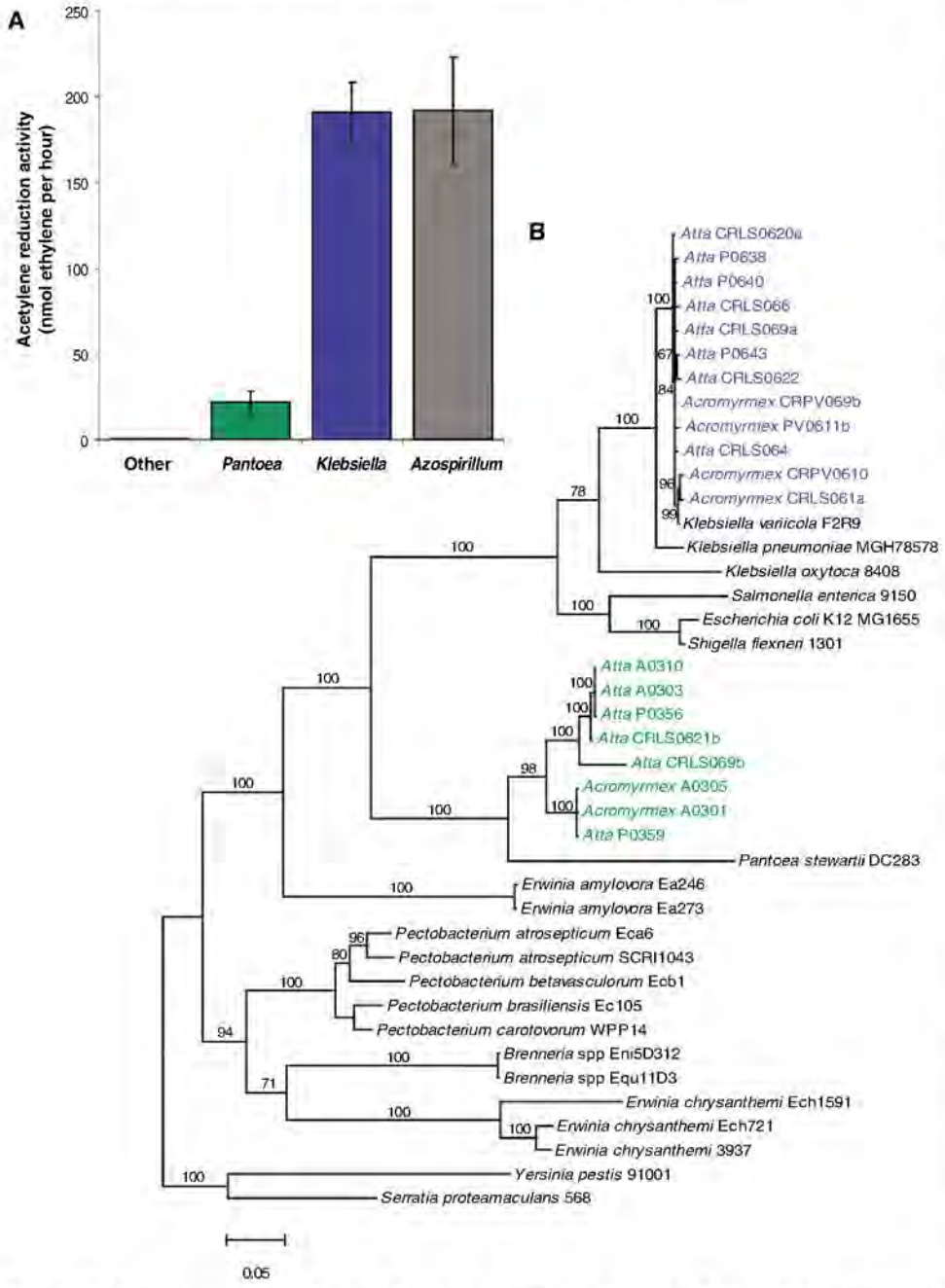


**Fig. 3.** $N_2$-fixing symbionts associated with leaf-cutter ant colonies. (**A**) $N_2$-fixing activity measured by acetylene reduction for bacterial isolates obtained from multiple leaf-cutter ant colonies. *Azospirillum* sp., a known free-living diazotroph, was used as a positive control. Results are shown as means ± SEM [*Pantoea*, $n = 23$; *Klebsiella*, $n = 44$; *Azospirillum*, $n = 4$; isolates from other genera were obtained in N-free media ($n = 27$)]. (**B**) Bayesian phylogeny of leaf-cutter ant–associated $N_2$-fixing symbionts. The phylogenetic tree was constructed using concatenated gene fragments from three housekeeping genes (*gapA*, *icdA*, and *mtlD*) of each isolate. Isolates of leaf-cutter ant–associated $N_2$ fixers are labeled with the host ant species and color-coded to indicate whether they belong in the genus *Klebsiella* (blue) or *Pantoea* (green). The numbers above the branches represent their Bayesian-calculated posterior probabilities.

The ecological success of leaf-cutter ants is derived, in large part, from the combined ability of the ants to break down plant antifungal barriers and of the fungus garden to neutralize plant anti-insect toxins (*21*). Consequently, the leaf-cutters are able to use a high diversity of plant families (*22*), in contrast to most herbivorous insects, which specialize in a few plant species (*14*). However, the reliance on leaf material means that leaf-cutter ant colonies are potentially N-limited. Our work shows that these ants can potentially overcome such limitation through symbiotic associations with $N_2$-fixing bacteria. Indeed, our estimates, using the natural abundance of the $^{15}N$ isotope, suggest that leaf-cutter colonies obtain a substantial proportion of their N requirements from symbiotic $N_2$ fixers, roughly equivalent to estimates calculated for termite species that are known to heavily rely on $N_2$-fixing symbionts for N acquisition (*22*). *Klebsiella* spp., the main leaf-cutter ant–associated $N_2$ fixer we identified in this study, is also known to engage in symbiotic associations with termites (*23*) and fruit flies (*17*). In these other insect/$N_2$-fixing bacteria mutualisms, symbiotic $N_2$ fixation occurs in the host's gut, whereas in leaf-cutter ants, $N_2$ fixation takes place in the fungus garden. This is consistent with the role of the fungus garden as the external digestive system of the leaf-cutter ant superorganism.

Herbivory by leaf-cutter ants has a major impact on the structure of neotropical plant communities (*5*), and through their collection of vast quantities of leaf biomass, these ants also play a critical role in nutrient cycling in the ecosystems in which they live (*24*). Nutrient enrichment by leaf-cutter ant colonies results in significant enhancement of fine root production and higher overall plant diversity near leaf-cutter refuse dumps (*4*, *25*, *26*). Nitrogen, an element that typically limits primary production across terrestrial ecosystems (*27*), is 26-fold more abundant in *At. colombica* refuse dumps than in the surrounding leaf litter (*4*). It is assumed that this N enrichment is achieved through the concentration of nutrients by the ants' extensive foraging activity, but here we show that additional N is acquired through symbiotic $N_2$-fixing bacteria that are present in the fungus gardens of leaf-cutter ant colonies. We estimate that a single mature leaf-cutter ant colony may contribute as much as 1.8 kg of fixed N per year into neotropical ecosystems (see SOM text for details). Associations with symbiotic $N_2$ fixers may be a widespread phenomenon in tropical ants: Davidson and collaborators (*28*) reported that many arboreal ant species obtain little N through predation and scavenging, indicating that these insects must obtain additional N through other means, such as microbial symbionts. Given the dominance of ants in general, and leaf-cutter species in particular, these discoveries identify a potential major source of fixed N in neotropical ecosystems.

### References and Notes

1. E. O. Wilson, *Success and Dominance in Ecosystems: The Case of the Social Insects. Excellence in Ecology, 2* (Ecology Institute, Oldendorf/Luhe, Germany, 1990).

2. D. W. Davidson, L. Patrel-Kim, in *Neotropical Biodiversity and Conservation*, A. C. Gibson, Ed. (Mildred E. Mathias, Botanical Garden, Los Angeles, 1996), pp. 127–140.
3. E. J. Fittkau, H. Klinge, *Biotropica* **5**, 2 (1973).
4. R. Wirth, H. Herz, R. J. Ryel, W. Beyschlag, B. Holldobler, *Herbivory of Leaf-Cutting Ants. A Case Study on* Atta colombica *in the Tropical Rain Forest of Panama* (Springer, Berlin, 2003).
5. B. Hölldobler, E. O. Wilson, *The Ants* (Harvard Univ. Press, Cambridge, MA, 1990).
6. N. A. Weber, *Gardening Ants, the Attines* (Memoirs of the American Philosophical Society, Philadelphia, 1972).
7. E. O. Wilson, in *Fire Ants and Leaf Cutting Ants. Biology and Management*, C. S. Lofgren, R. K. Vander Meer, Eds. (Westview Press, Boulder, CO, 1986), pp. 1–9.
8. C. R. Currie, J. A. Scott, R. C. Summerbell, D. Malloch, *Nature* **398**, 701 (1999).
9. T. R. Schultz, U. G. Mueller, C. R. Currie, S. A. Rehner, in *Ecological and Evolutionary Advances in Insect-Fungal Associations*, F. Vega, M. Blackwell, Eds. (Oxford Univ. Press, New York, 2005), pp. 149–190.
10. J. M. Scriber, P. Feeny, *Ecology* **60**, 829 (1979).
11. J. B. Nardi, R. I. Mackie, J. O. Dawson, *J. Insect Physiol.* **48**, 751 (2002).
12. B. L. Haines, *Biotropica* **10**, 270 (1978).
13. E. H. Bucher, V. Marchesini, A. Abril, *Biotropica* **36**, 327 (2004).
14. L. M. Schoonhoven, J. J. A. van Loon, M. Dicke, *Insect-Plant Biology* (Oxford Univ. Press, New York, 2005).
15. Materials and methods are available as supporting material on *Science* Online.
16. J. A. Breznak, W. J. Brill, J. W. Mertins, H. C. Coppel, *Nature* **244**, 577 (1973).
17. A. Behar, B. Yuval, E. Jurkevitch, *Mol. Ecol.* **14**, 2637 (2005).
18. R. H. Burris, *Methods Enzymol.* **24**, 415 (1972).
19. J. P. Zehr, B. D. Jenkins, S. M. Short, G. F. Steward, *Environ. Microbiol.* **5**, 539 (2003).
20. R. Dixon, D. Kahn, *Nat. Rev. Microbiol.* **2**, 621 (2004).
21. J. M. Cherrett, R. J. Powell, D. J. Stradling, in *Insect Fungus Interactions. 14th Symposia of the Royal Entomological Society of London*, N. Wilding, N. M. Collins, P. M. Hammond, J. F. Webber, Eds. (Academic Press, London, 1989), pp. 93–120.
22. I. Tayasu, A. Sugimoto, E. Wada, T. Abe, *Naturwissenschaften* **81**, 229 (1994).
23. M. Doolittle, A. Raina, A. Lax, R. Boopathy, *Bioresour. Technol.* **99**, 3297 (2008).
24. I. Perfecto, J. Vander Meer, *Biotropica* **25**, 316 (1993).
25. A. G. Farji Brener, C. A. Medina, *Biotropica* **32**, 120 (2000).
26. M. Garrettson *et al.*, *J. Trop. Ecol.* **14**, 17 (1998).
27. P. M. Vitousek *et al.*, *Biogeochemistry* **57**, 1 (2002).
28. D. W. Davidson, S. C. Cook, R. R. Snelling, T. H. Chua, *Science* **300**, 969 (2003).


29. We thank R. Steffensen, L. Schwab, L. Uribe, M. Mora, B. Matarrita, D. Brenes, R. Araya, H. Read, J. Mentzer, D. Maly, and G. Pine for technical assistance; Y. Zhang, E. Pohlmann, and G. Roberts for assistance with acetylene reduction assays; A. Little, S. Price, and U. Mueller for leaf-cutter ant colony collection; M. Rogel-Hernández and E. Martínez-Romero for providing isolate *K. variicola* F2R9; B. Ma, A. Charkowski, and N. Perna for assistance with phylogenetic analyses; E. Sánchez, R. Moreira, and T. Escalante for assistance with microscopic analyses; N. Keuler for statistical advice; the sequencing and production teams at the Joint Genome Institute; and S. Adams, F. Aylward, E. Caldera, N. Gerardo, H. Goodrich-Blair, K. Grubbs, S. Marsh, M. Poulsen, K. Raffa, G. Roberts, E. Ruby, T. Schultz, and J. Scott for comments on the manuscript. We acknowledge the Organization for Tropical Studies (OTS) and the Ministerio de Ambiente y Energía in Costa Rica, the Autoridad Nacional del Ambiente in Panama, and the Government of Argentina for facilitating the research and granting collecting permits. This work was funded by NSF grants MCB-0731822, MCB-0702025, and DEB-0747002 to C.R.C.; NIH grant GM 18938 to W.W.C., and an OTS research fellowship to A.A.P.-T. G.S. and C.R.C. were supported by the U.S. Department of Energy's Great Lakes Bioenergy Research Center under contract DE-FC02-07ER64494; D.M.S. and P.J.W. were supported by U.S. Department of Agriculture–Agricultural Research Service Current Research Information System project 3655-41000-005-00D. DNA sequence data were deposited in GenBank under accession numbers FJ593730 to FJ593840 and GQ342603 to GQ342604.


**Supporting Online Material**

www.sciencemag.org/cgi/content/full/326/5956/1120/DC1
Materials and Methods
SOM Text
Figs. S1 to S10
Tables S1 to S6
References and Notes

4 March 2009; accepted 27 August 2009
10.1126/science.1173036

# Structural Basis of Immune Evasion at the Site of CD4 Attachment on HIV-1 gp120

**Lei Chen,[1]* Young Do Kwon,[1]* Tongqing Zhou,[1]* Xueling Wu,[1] Sijy O'Dell,[1] Lisa Cavacini,[2] Ann J. Hessell,[3] Marie Pancera,[1] Min Tang,[1] Ling Xu,[1] Zhi-Yong Yang,[1] Mei-Yun Zhang,[4] James Arthos,[5] Dennis R. Burton,[3,6] Dimiter S. Dimitrov,[4] Gary J. Nabel,[1] Marshall R. Posner,[2] Joseph Sodroski,[7] Richard Wyatt,[1] John R. Mascola,[1] Peter D. Kwong[1]†**

The site on HIV-1 gp120 that binds to the CD4 receptor is vulnerable to antibodies. However, most antibodies that interact with this site cannot neutralize HIV-1. To understand the basis of this resistance, we determined co-crystal structures for two poorly neutralizing, CD4–binding site (CD4BS) antibodies, F105 and b13, in complexes with gp120. Both antibodies exhibited approach angles to gp120 similar to those of CD4 and a rare, broadly neutralizing CD4BS antibody, b12. Slight differences in recognition, however, resulted in substantial differences in F105- and b13-bound conformations relative to b12-bound gp120. Modeling and binding experiments revealed these conformations to be poorly compatible with the viral spike. This incompatibility, the consequence of slight differences in CD4BS recognition, renders HIV-1 resistant to all but the most accurately targeted antibodies.

More than 25 years after the discovery of HIV-1, an effective vaccine remains elusive. In this time, an estimated 60 million individuals have been infected by HIV-1, and ~20 million have died (*1*). Identification of a site on the HIV-1 gp120 envelope glycoprotein that is vulnerable to neutralizing antibodies (*2*), along with the discovery that a major subpopulation of individuals infected with HIV-1 develops broadly effective antibodies against this site (*3*–*7*), has provided both a vaccine target and evidence that it is possible to induce broadly neutralizing antibodies in humans. The site of vulnerability corresponds to the initial site of attachment between gp120 on the viral spike and the CD4 receptor on the host cell. However, most CD4–binding site (CD4BS) antibodies do not effectively neutralize HIV-1 (*8*–*10*).

The HIV-1 gp120 envelope glycoprotein contains a number of features that help evade humoral immunity, including variable loops (*11*), N-linked glycosylation (*12*, *13*), and conformational flexibility (*14*). How the initial site of CD4 attachment is protected, however, remains unclear. Of the variable loops, only one (V5, the least variable) is in close proximity, and the site itself is relatively conserved in sequence. N-linked glycosylation, meanwhile, surrounds half the site, though the site itself is free of glycosylation. In addition, though gp120 is conformationally flexible, the site of initial CD4 attachment is conformationally inert. In our experiment, we characterized neutralization breadth and potency for a panel of CD4BS antibodies, measured binding to gp120 variants with altered sites of CD4 binding, and determined co-crystal structures for two of these antibodies: (i) F105 (*15*) in complex with a YU2 gp120 core with V3 and (ii) b13 (*16*) in complex with an HXBc2 core stabilized to retain the CD4-bound conformation. The results show in atomic

[1]Vaccine Research Center, National Institute of Allergy and Infectious Diseases, National Institutes of Health, Bethesda, MD 20892, USA. [2]Head and Neck Oncology Program, Dana-Farber Cancer Institute, Harvard Medical School, Boston, MA 02115, USA. [3]Departments of Immunology and Microbial Science and International AIDS Vaccine Initiative Neutralizing Antibody Center, The Scripps Research Institute, La Jolla, CA 92037, USA. [4]Center for Cancer Research, National Cancer Institute, Frederick, MD 21702, USA. [5]Laboratory of Immunoregulation, National Institute of Allergy and Infectious Diseases, National Institutes of Health, Bethesda, MD 20892, USA. [6]Ragon Institute of Massachusetts General Hospital, Massachusetts Institute of Technology and Harvard University, Boston, MA 02114, USA. [7]Department of Cancer Immunology and AIDS, Dana-Farber Cancer Institute, Harvard Medical School, Boston, MA 02115, USA.

*These authors contributed equally to this work.
†To whom correspondence should be addressed. E-mail: pdkwong@nih.gov

detail how the conformational flexibility of gp120 facilitates a decoy strategy that misdirects the humoral immune response.

To guide vaccine development, panels of reference HIV-1 isolates have recently been defined (*17*, *18*). Tier 1 viruses are relatively easy to neutralize, whereas those in tier 2 are more difficult, and neutralization of tier 2 viruses is thought to be a necessary bar that an effective HIV-1 vaccine needs to surpass. To define the efficacy of CD4BS antibodies against these strains, we tested 10 CD4BS monoclonal antibodies, including the broadly neutralizing antibody b12 (*19*–*21*). Although CD4BS antibodies could neutralize diverse tier 1 viruses, except for antibody b12, they were largely ineffective against tier 2 isolates (table S1) (*22*).

To understand the inability of most CD4BS antibodies to neutralize tier 2 viruses, we employed robotic and variational techniques (*23*, *24*) to crystallize a CD4BS antibody in complex with gp120. We assessed more than 10,000 crystallizations of 11 CD4BS antibody–gp120 complexes, including four variants of gp120, five CD4BS antibodies, and two V3-directed antibodies (table S2). Diffraction data to 2.9 Å resolution were collected from an R32 crystal of the antigen-binding fragment (Fab) of antibody F105 in complex with a YU2 gp120 core containing an intact V3. Structure solution of the two complexes in the asymmetric unit was accomplished by molecular replacement (*25*), and refinement to $R_{cryst}$ 20.2% ($R_{free}$ 24.3%) defined the F105-gp120 structure, for all except gp120 residues 302 to 326 and 396 to 411, which correspond to the flexible V3 and V4 regions, respectively (Fig. 1A, fig. S1, and table S3).

Overall, F105 binding to gp120 occurred primarily through heavy-chain interactions, which were similar in many respects to those of CD4. Instances of precise mimicry were observed, for example, between $Arg^{100F}$ of F105 and $Arg^{59}$ of CD4, both of which make analogous hydrogen bonds to $Asp^{368}$ of gp120 (Fig. 1C) (*26*). The approach angle of F105 was also comparable to that of CD4 (fig. S2); the F105-heavy chain resided 18% more within the CD4 envelope of approach than that of b12 (*27*). Moreover, F105 recognized a conformation in gp120 similar to that induced by CD4 (Fig. 1B); superposition of the inner and outer domains of core gp120 in F105 and CD4-bound conformations showed a root mean square deviation (RMSD) in Cα-positions of 1.97 Å, only about twice the RMSD of 0.78 Å between HIV-1 gp120 cores from strains HXBc2 and YU2, when both are bound to CD4. One critical part of gp120, however, the four-stranded "bridging sheet" (Fig. 2), was considerably altered from the CD4-bound state. All four strands of the sheet were displaced to uncover a hydrophobic surface (Fig. 2A), which served as a focus of F105 binding.

To assess the necessity and generality of access to this hydrophobic surface for CD4BS antibodies, we mutationally tethered the loop between strands β20 and β21 of the bridging sheet to the α1 helix by creating a disulfide bond between residues 109 and 428 (*28*). A monomeric 109-428 disulfide variant was recognized at close to wild-type levels by CD4 and CD4-induced antibodies, 17b and m6. In contrast, binding was ablated to eight of the CD4BS antibodies, and only b12 and b13 were able to recognize the 109-428

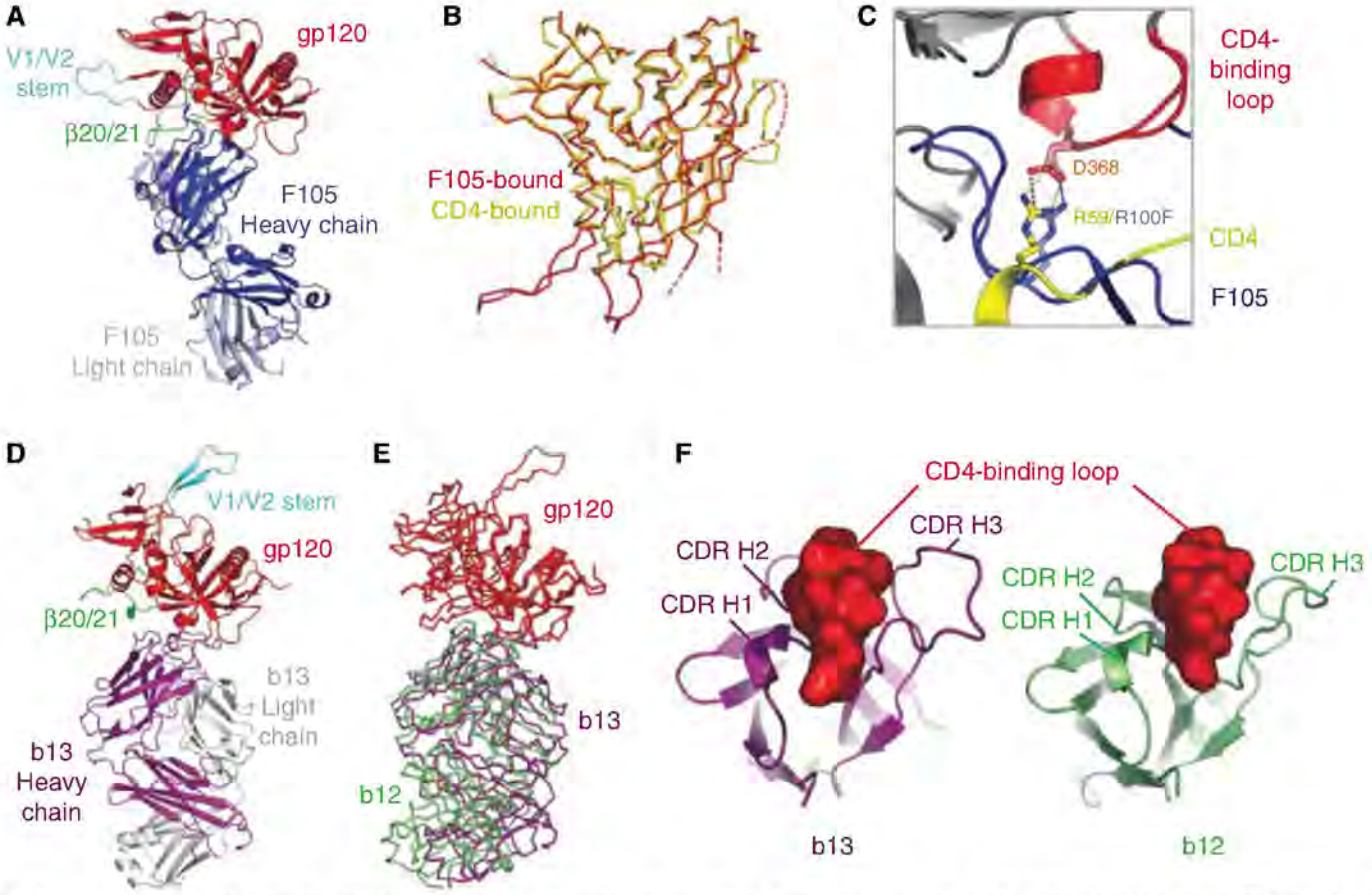


**Fig. 1.** Co-crystal structure of antibodies F105 and b13 in complex with HIV-1 gp120. (**A**) Fab F105 in complex with a YU2 gp120 core with intact V3. Polypeptide chains are depicted in ribbon representation, with F105 in dark and light blue for heavy and light chain, respectively, and gp120 in red (with β20/β21 and V1/V2 stem highlighted in green and cyan, respectively). (**B**) Cα-backbone traces for F105- and CD4-bound conformations of gp120. The F105-bound structure corresponds to the core with V3 determined here, whereas the YU2 structure corresponds to the original core, with V3 truncation (*46*). Dashed lines correspond to the disordered V3 (fig. S1) and V4 regions. (**C**) Similarities in recognition of $Asp^{368}$ of gp120 by $Arg^{100F}$ of F105 (blue) and $Arg^{59}$ of CD4 (yellow) (*47*). (**D**) Fab b13 in complex with an HXBc2 gp120 core restrained to be in the CD4-bound state. Polypeptide chains are depicted in ribbon representation with b13–heavy chain in purple, light chain in gray, and gp120 colored as in (A). (**E**) Cα-backbone traces for heavy chain of antibody b12 (green) and antibody b13 (purple) in complexes with gp120 (red) after gp120-outer domain superposition. (**F**) Heavy-chain complementarity-determining regions (CDRs) for b13 (purple) and b12 (green) binding the CD4-binding loop (red) of gp120.

variant (tables S4 and S5). The results suggest that most CD4BS antibodies rely on access to the hydrophobic surface under the bridging sheet (*29*). Such access necessitates movement of bridging-sheet strands β20 and β21, which abut the initial site of CD4 attachment, as well as of the neighboring strands, β2 and β3, from which the V1/V2 loops emanate. With F105 bound, the tip of the V1/V2 stem shifts up to 40 Å, with respect to the equivalent region in the CD4-bound state (fig. S3).

To model the consequences of the F105-recognized alteration of the bridging sheet in the context of the oligomeric viral spike, we used the cryo–electron microscopy (EM) tomograms of the viral spike from the BaL isolate of HIV-1 (Fig. 2C) (*30*). In the BaL spike tomograms of CD4- and b12-bound states, ligand positions were used to orient placement of gp120 atomic-level models. We used these atomic-level models as guides for placement of the F105-bound conformation of gp120. Major clashes between equivalent protomers around the trimer threefold were predicted for expected positions of V1/V2 stem (Fig. 2C) (*31*). Although the precise displacement of the bridging sheet probably depends on antibody particulars, because of the constrained location of this sheet and especially of the V1/V2 stem and its proximity to neighboring protomers at the trimer interface, displacement from the CD4-proximal face of gp120 probably results in a clash in the oligomeric context. Thus, CD4BS antibodies that access the hydrophobic region under the bridging sheet recognize or induce conformations in gp120 that are poorly compatible with the functional viral spike (*32*).

Unlike other CD4BS antibodies, antibody b13 showed substantial, though reduced, binding to the 109-428 variant. In addition, b13, like b12, was able to recognize an outer domain–only variant of gp120 (tables S4 and S5). To understand how b13 recognizes both 109-428 and outer domain–only variants of gp120 (yet still cannot effectively neutralize HIV-1), we again turned to crystallography. In light of our difficulty in obtaining CD4BS antibody–complex crystals with unconstrained versions of gp120, we crystallized the Fab of b13 with a 2-disulfide variant of gp120, which we had previously crystallized with b12 (crystals were also obtained with an outer domain–only variant, but these were not suitable for analysis) (*2*). The crystals formed in two space groups, C222 and $C222_1$, which diffracted to minimum Bragg spacings of 2.5 and 3.2 Å, respectively. We determined the structures of both by molecular replacement and refined to $R_{cryst}$ values of 17.8 and 19.6% ($R_{free}$ values of 23.9 and 23.7%), respectively (table S3). We describe the higher-resolution C222 structure, which is depicted in Fig. 1D.

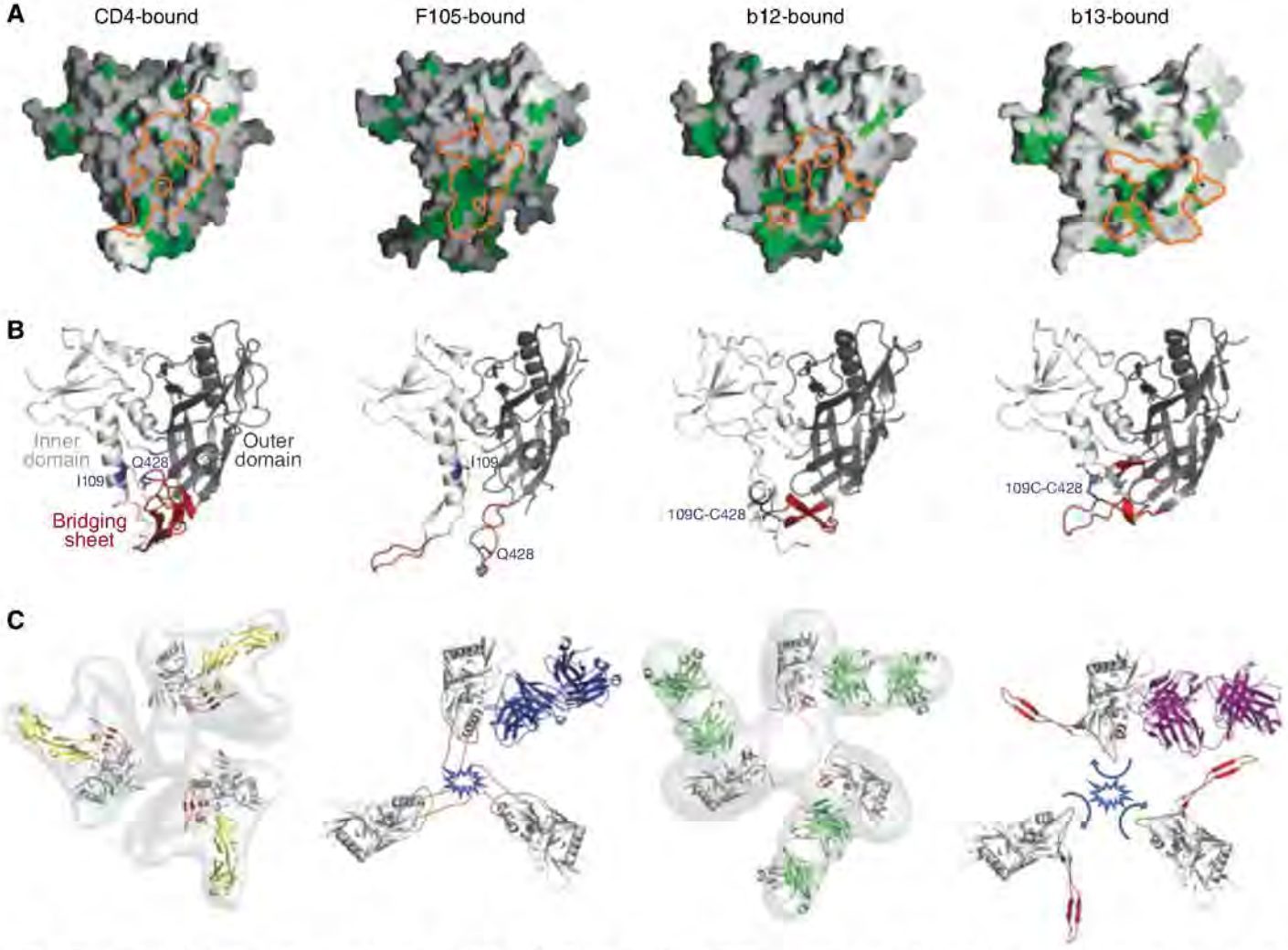


**Fig. 2.** Epitopes, bound conformations, and trimer modeling. (**A**) Epitope hydrophobicity. The surface of gp120 is shown in gray, with hydrophobic residues highlighted in green. Binding surfaces for CD4, F105, b12, and b13 are outlined in orange. (**B**) Ligand-bound conformation of gp120. Polypeptides of gp120 are depicted in ribbon representation with inner domains shown in light gray, outer domains in dark gray, and regions that in the CD4-bound state correspond to the bridging sheet shown in red. Residues 109 and 428 are highlighted in blue and shown in stick representation. (**C**) Viral spike compatibility. Density maps derived from the cryo–electron tomography of HIV-1 BaL isolate spike are shown in gray for CD4 and 17b- and b12-bound states (first and third from left, respectively), along with optimal fits of atomic-level models (*30*). To model F105- and b13-bound forms of gp120 into likely viral spike orientations, the invariant β-sandwich of the gp120 inner domain was superimposed. Likely clashes of V1/V2 in the superimposed conformation with neighboring protomers close to the trimer axis are highlighted in light blue.

Antibody b13 bound gp120 similarly to antibody b12 (Fig. 1E). A rotation of only 17° would superimpose the variable portions of these two antibodies precisely (table S6). With b13, as with b12, heavy chain–only recognition was employed, with the central focus of the b13–complementarity determining loops on the CD4-binding loop of gp120 (Fig. 1F) (*33*). Despite this overall similarity in antibody recognition, the 17° difference in recognition moved the b13 epitope 6 Å toward the bridging-sheet region. This lead to a 13 Å movement in strands β20 and β21 of gp120. The β20–β21 movement was amplified by a more dramatic alteration in the neighboring β2–β3 strands, which twisted 152° from the CD4-facing side to the "back"-side of gp120. As the connection between strands β2 and β3 extends into V1/V2, we would expect such a change to be even more pronounced in the context of a full-length V1/V2 loop. Modeling the consequences of the ligand-induced alteration on the EM tomograms of the HIV-1 BaL isolate revealed substantial clashes between equivalent protomers around the trimer threefold to achieve the expected positions of V1/V2 in the b13-bound conformation (Fig. 2C) (*34*). Because the precise conformation observed in the monomeric crystal structure containing the flexible V1/V2 stem may not reflect solution or oligomeric behavior, we tested binding for the panel of CD4BS antibodies to an uncleaved form of the ectodomain (gp140) appended to a trimerization domain to confirm clash predictions (*35*). We did this for two primary isolate-derived variants, though because of avidity effects, we only measured on-rates. CD4 and b12 showed on-rates that were reduced four- to sixfold from that of gp120, whereas all other CD4BS antibodies showed more substantially reduced on rates (tables S4 and S7). We also measured binding to cell-surface viral spikes from the primary HIV-1 isolate JR-FL, in cleaved and uncleaved states, as the cell-surface cleaved state more accurately mimics the functional viral spike (*36*). CD4 and antibody b12 recognized cleaved and uncleaved spikes with similar affinity, whereas all other CD4BS antibodies showed markedly reduced recognition of the cleaved state (fig. S4). Thus, despite similarities in epitopes recognized by F105 and b13 and those recognized by CD4 and b12 (Fig. 3 and fig. S3), small differences in recognition induced [or selected (*32*)] more substantial differences in gp120 conformation. In particular, both F105 and b13 recognized conformational shifts in the position of the V1/V2 stem, resulting in a V1/V2 orientation poorly compatible with the functional viral spike. As functional viral spikes, which contain the properly formed attachment site, are an immunogenic minority—with monomeric gp120 and viral debris in vast abundance—such conformational diversity begins to explain why CD4BS antibodies are frequently elicited but do not neutralize.

Our results reveal how induced conformation can modify the recognition of a site that is itself conformationally invariant. This mechanism represents a twist on that of conformational masking (*37*), whereby the virus uses quaternary constraints to resist conformational changes required for exposure or formation of a particular antibody epitope (and thereby resists binding of and neutralization by that particular antibody). Conformational masking was previously shown for epitopes like the CD4- and co-receptor–binding sites on HIV-1, neither of which is fully formed in the nascent viral spike, or the V3, which is not accessible on most primary isolates. With the initial site of CD4 attachment, however, the target site is fully formed, reasonably accessible, and conformationally inert. However, the bridging sheet and V1/V2 loops detect and amplify any recognition that strays outside the target site (Fig. 3 and fig. S3). Should an antibody stray, even by just a few angstroms, then gp120 conformational changes that are poorly compatible with the functional viral spike become a constraining factor for binding and neutralization.

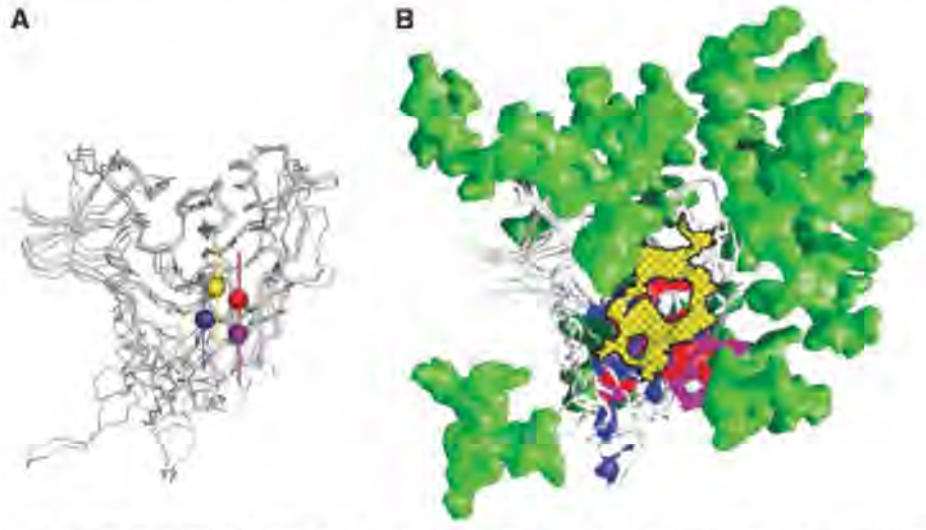


**Fig. 3.** Immune evasion at the site of initial CD4 attachment. **(A)** Recognition similarity. Centers of recognition for CD4, F105, b12, and b13. After superposition of gp120 outer domains, the centers of the recognition surface of each ligand on gp120 is denoted by balls for CD4 (yellow), F105 (blue), b12 (red), and b13 (purple). **(B)** Immune evasion. The initial site of CD4 attachment (cross-hatched yellow surface) is circumscribed by a combination of glycan (green) and conformational constraints. The surface on gp120 recognized by F105, b12, and b13 (that strays beyond the site of CD4 attachment) is shown in blue, red, and purple, respectively. Glycosylation sterically crowds the immune response toward the bridging-sheet region (blue surface that F105 recognizes) or toward the V3 region (purple surface that b13 recognizes) (*48*). In either case, recognition of these regions of gp120 results in antibody-bound conformations of gp120 that are poorly compatible with the functional spikes of HIV-1 virions from tier 2 primary isolates.

### References and Notes


1. UNAIDS, "2006 Report on the Global AIDS Epidemic" (Joint United Nations Programme on HIV/AIDS, 2006); www.unaids.org/en/knowledgeCentre/HIVData/GlobalReport/2006/.
2. T. Zhou *et al.*, *Nature* **445**, 732 (2007).
3. D. N. Sather *et al.*, *J. Virol.* **83**, 757 (2009).
4. J. M. Binley *et al.*, *J. Virol.* **82**, 11651 (2008).
5. Y. Li *et al.*, *Nat. Med.* **13**, 1032 (2007).
6. Y. Li *et al.*, *J. Virol.* **83**, 1045 (2009).
7. A. K. Dhillon *et al.*, *J. Virol.* **81**, 6548 (2007).
8. P. Roben *et al.*, *J. Virol.* **68**, 4821 (1994).
9. J. F. Scheid *et al.*, *Nature* **458**, 636 (2009).
10. R. Pantophlet *et al.*, *J. Virol.* **77**, 642 (2003).
11. B. R. Starcich *et al.*, *Cell* **45**, 637 (1986).
12. R. Wyatt *et al.*, *Nature* **393**, 705 (1998).
13. X. Wei *et al.*, *Nature* **422**, 307 (2003).
14. D. G. Myszka *et al.*, *Proc. Natl. Acad. Sci. U.S.A.* **97**, 9026 (2000).
15. M. R. Posner *et al.*, *J. Immunol.* **146**, 4325 (1991).
16. C. F. Barbas III *et al.*, *J. Mol. Biol.* **230**, 812 (1993).
17. J. R. Mascola *et al.*, *J. Virol.* **79**, 10103 (2005).
18. B. Schweighardt *et al.*, *J. Acquired Immune Defic. Syndr.* **46**, 1 (2007).
19. D. R. Burton *et al.*, *Science* **266**, 1024 (1994).
20. Two of the CD4BS antibodies were tested as full-length immunoglobulin Gs (IgGs), four as Fabs, and four in both IgG and Fab format. Neutralization by IgG and Fab for b12, b13, m18, and F105 showed similar breadths and potencies (table S1).
21. Materials and methods are available as supporting material on *Science* Online.
22. We also tested soluble versions of the CD4 receptor, including a monomeric four-domain version (sCD4, 1mer) (*38*), a dimeric immunoglobulin chimera (CD4-IgG, 2mer) (*39*), and a dodecameric version (CD4 dodecamer, 12mer) (*40*), the latter designed to mimic oligomeric membrane-associated CD4 at the cell surface (table S1). Certain HIV-1 isolates and primary viral swarms are ineffectively neutralized by monomeric versions of soluble CD4 (*37*, *41*). Nonetheless, against tier 2 viruses, monomeric sCD4 was quite effective [94% breadth, 7.6 μg/ml average median inhibitory concentration ($IC_{50}$)], though not quite as potent as oligomeric versions (0.9 μg/ml average $IC_{50}$ for the CD4 dodecamer) (table S1) (*42*).
23. D. W. Morris, C. Y. Kim, A. McPherson, *Biotechniques* **7**, 522 (1989).
24. P. D. Kwong *et al.*, *J. Biol. Chem.* **274**, 4115 (1999).
25. The F105-gp120 structure described here was solved before release of the coordinates for the unbound F105 structure (*43*); bound- and unbound-Fab structures, however, do closely resemble each other.
26. Residue positions for antibodies are referred by Kabat numbering (*44*); thus, residue "100F" corresponds to insertion "F" at position "100" in Kabat nomenclature.
27. "Envelopes of approach" were assessed by comparing occluded volumes of binding ligands.

28. In addition to covering the hydrophobic site under the bridging sheet, tethering residues 109 and 428 was previously shown to impair binding of CD4BS antibodies (*2*); however, this previous study was carried out in the context of other mutations (e.g., $Ser^{375} \rightarrow Trp^{375}$), which by themselves may ablate F105 binding, and so the effect of the 109-428 linkage on CD4BS antibodies had not been clearly assessed previously.
29. The percentage of gp120-hydrophobic side chains contacted in the epitopes for antibodies b12, b13, and F105 is 27.5, 23.4, and 39.2%, respectively.
30. J. Liu, A. Bartesaghi, M. J. Borgnia, G. Sapiro, S. Subramaniam, *Nature* **455**, 109 (2008).
31. Many tier 1 HIV-1 isolates, including the BaL isolate, are neutralized by CD4BS antibodies (table S1). So whereas the F105-bound conformation of gp120 may not be favored in the functional viral spike, in tier 1 isolates, there appears to be sufficient spike flexibility to permit binding.
32. CD4BS antibodies probably use a mixture of induced fit and conformational selection to bind gp120 (*45*). We use the term "induced" to describe the antibody-bound conformation of gp120, though "selected" might also be appropriate.
33. Antibodies b12 and b13 are phage display–derived constructs. The binding of these two antibodies by their heavy chains is likely to be a direct function of this derivation, and these antibodies may not represent the expressed B cell repertoire in humans.
34. A lattice interaction of convergent stems influences the position of the V1/V2 stem in the b13-gp120 crystal. Nonetheless, it is unlikely that these crystals could form, unless the structural alterations described here caused the V1/V2 stem to twist so drastically from the CD4-bound state. Also, though the particular gp120 conformation recognized by b13 is a consequence in part of the gp120 alterations used in the crystallization, such alterations constrain the conformation of gp120 to be in the CD4-bound state. So the extent that these alterations affect conformation is likely to be similar to the extent that they decrease the differences between b13- and CD4-bound states.
35. X. Yang *et al.*, *J. Virol.* **76**, 4634 (2002).
36. M. Pancera, R. Wyatt, *Virology* **332**, 145 (2005).
37. P. D. Kwong *et al.*, *Nature* **420**, 678 (2002).
38. K. C. Deen *et al.*, *Nature* **331**, 82 (1988).
39. A. Traunecker, J. Schneider, H. Kiefer, K. Karjalainen, *Nature* **339**, 68 (1989).
40. J. Arthos *et al.*, *J. Biol. Chem.* **277**, 11456 (2002).
41. J. P. Moore, J. A. McKeating, Y. X. Huang, A. Ashkenazi, D. D. Ho, *J. Virol.* **66**, 235 (1992).
42. Whereas CD4 effectiveness provides partial validation of the CD4BS as a vaccine target, additional validation can be found in patient sera. Here we demonstrate one patient serum to be effective against 30 of 31 tier 2 clade B and C viruses (table S1). Against a subset of these isolates, we further analyzed the effect of adsorption by gp120 and by a gp120 variant with an Asp-to-Arg substitution at position 368, a critical site in the CD4-binding loop. In two-thirds of the cases tested, the wild-type gp120 adsorption reduced neutralization by more than a factor of 2 over the $Asp^{368} \rightarrow Arg^{368}$ mutant (table S8). These results, along with others that have recently been published (*3*–*7*), suggest that naturally elicited CD4BS antibodies can occur at titers sufficient to neutralize tier 2 viruses.
43. R. A. Wilkinson *et al.*, *J. Virol.* **79**, 13060 (2005).
44. E. A. Kabat, T. T. Wu, H. M. Perry, K. S. Gottesman, C. Foeller, *Sequences of Proteins of Immunological Interest* (U.S. Department of Health and Human Services, National Institutes of Health, Bethesda, MD, ed. 5, 1991).
45. G. G. Hammes, Y. C. Chang, T. G. Oas, *Proc. Natl. Acad. Sci. U.S.A.* **106**, 13737 (2009).
46. P. D. Kwong *et al.*, *Structure* **8**, 1329 (2000).
47. Single-letter abbreviations for the amino acid residues are as follows: A, Ala; C, Cys; D, Asp; E, Glu; F, Phe; G, Gly; H, His; I, Ile; K, Lys; L, Leu; M, Met; N, Asn; P, Pro; Q, Gln; R, Arg; S, Ser; T, Thr; V, Val; W, Trp; and Y, Tyr.
48. Calculations of distances between gp120 glycans and binding surfaces of CD4 and antibodies (table S9) show that for distance cutoffs of 10 to 15 Å, the surfaces recognized by b12 and CD4 are closer to more glycans than surfaces recognized by b13 and F105.
49. L. Chen produced and assessed for crystallization CD4BS antibodies with unconstrained gp120, crystallized the F105-gp120 complex, assisted with F105-gp120 data collection and structure solution, and carried out mutagenesis and SPR binding experiments. Y.D.K. assisted with F105-gp120 crystallization, data collection, and structure solution and refined and analyzed the F105-gp120 structure. T.Z. purified, crystallized, solved, and analyzed the b13-gp120 complex. X.W., S.O.'D. and J.R.M. assessed neutralization potency and breadth of CD4, patient sera, and CD4BS antibodies. L. Chen and M.P. carried out cell-surface JR-FL binding experiments. M.T. and R.W. provided YU2 core gp120; L.X. and G.J.N. provided stabilized-core gp120; Z.-Y.Y. and G.J.N. converted b13 from Fab to IgG format and provided b13 IgG; L. Cavacini and M.R.P. provided F105; M.-Y.Z. and D.S.D. provided m6, m14, and m18; A.J.H. and D.R.B. provided b3, b6, b11, b12; and J.A. provided dodecameric CD4. J.A., D.R.B., D.S.D., G.J.N., M.R.P., J.S., R.W., and J.R.M. assisted with analysis and writing, and P.D.K. assisted with crystallography and experimental planning and wrote the first draft. Figures, tables, and supporting online material were produced by L. Chen, Y.D.K., M.P., T.Z. and X.W. We thank L. Shapiro and members of the Structural Biology Section, Vaccine Research Center (VRC), for discussions and comments on the manuscript, M. Connors for patient serum, M. Fung for antibodies G3-42 and G3-299, J. Robinson for antibodies 1.5e and F91, J. Stuckey for assistance with figures and tables, S. Subramaniam for EM tomograms, C. Winter and C. Huang for S2 production of core YU2 gp120, X. Yang for preparation of JR-FL gp120, and the Flow Cytometry Core, VRC, for assistance with antibody binding to cell-surface–expressed HIV-1 spikes. Support for this work was provided by the Intramural Research Program of NIH, the International AIDS Vaccine Initiative, a grant from the Bill and Melinda Gates Foundation Grand Challenges in Global Heath Initiative, and grants from NIH. The use of insertion device 22 (Southeast Region Collaborative Access Team) at the Advanced Photon Source was supported by the U.S. Department of Energy, Basic Energy Sciences, Office of Science, under contract number W-31-109-Eng-38. Coordinates and structure factors for the F105-gp120 complex (accession code 3HI1) and the b13-gp120 complexes (accession codes 3IDX and 3IDY for C222 and $C222_1$ forms, respectively) have been deposited with the Protein Data Bank.


**Supporting Online Material**

www.sciencemag.org/cgi/content/full/326/5956/1123/DC1
Materials and Methods
Figs. S1 to S4
Tables S1 to S9
References

5 May 2009; accepted 10 September 2009
10.1126/science.1175868

# The Schizophrenia Susceptibility Gene *dysbindin* Controls Synaptic Homeostasis

**Dion K. Dickman and Graeme W. Davis***

The molecular mechanisms that achieve homeostatic stabilization of neural function remain largely unknown. To better understand how neural function is stabilized during development and throughout life, we used an electrophysiology-based forward genetic screen and assessed the function of more than 250 neuronally expressed genes for a role in the homeostatic modulation of synaptic transmission in *Drosophila*. This screen ruled out the involvement of numerous synaptic proteins and identified a critical function for *dysbindin*, a gene linked to schizophrenia in humans. We found that dysbindin is required presynaptically for the retrograde, homeostatic modulation of neurotransmission, and functions in a dose-dependent manner downstream or independently of calcium influx. Thus, dysbindin is essential for adaptive neural plasticity and may link altered homeostatic signaling with a complex neurological disease.

At glutamatergic synapses of species as varied as *Drosophila* and humans, disruption of postsynaptic neurotransmitter receptor function can be precisely offset by an increase in presynaptic neurotransmitter release to homeostatically maintain normal postsynaptic excitation (*1*–*3*). The *Drosophila* neuromuscular junction (NMJ) is a glutamatergic synapse that is used as a model for this form of homeostatic signaling in the nervous system (*1*, *4*, *5*). Efficient homeostatic modulation of presynaptic release at the *Drosophila* NMJ can occur within 10 min after bath application of philanthotoxin-433 (PhTx), which persistently and specifically inhibits postsynaptic glutamate receptors (fig. S1) (*4*).

We systematically screened for mutations that block the rapid, PhTx-dependent induction of synaptic homeostasis (Fig. 1). Mutations in 276 genes were screened electrophysiologically (see supporting online text). For each mutant, we calculated an average value for the amplitude of both the spontaneous miniature excitatory junctional potential (mEJP) and evoked excitatory junctional potential (EJP) after treatment of the dissected neuromuscular preparation with PhTx for 10 min (*4*). We isolated 14 mutants with average EJP amplitudes more than two standard deviations smaller than the distribution mean (Fig. 1C, solid red bars). From these candidates we identified seven mutants that block synaptic homeostasis without an obvious effect on NMJ morphology or

Department of Biochemistry and Biophysics, University of California, San Francisco, CA 94158, USA.

*To whom correspondence should be addressed. E-mail: graeme.davis@ucsf.edu

baseline synaptic transmission. We conclude that the molecular mechanisms of synaptic homeostasis can be genetically separated from the mechanisms responsible for normal neuromuscular development and baseline synaptic transmission.

A fraction of the mutants we assayed (19.5%) are previously published genetic lesions. This allows us to rule out the involvement of numerous genes and associated biochemical processes. Mutations that disrupt RNA interference or microRNA processing, retrograde transsynaptic signaling, synaptic transmission, active zone assembly, synaptic vesicle endocytosis, and mitochondria all showed reliable homeostatic compensation (Fig. 1, D and E, and fig. S1). Therefore, synaptic homeostasis is a robust phenomenon unperturbed by a broad spectrum of synaptic mutations. In addition, significant homeostatic compensation in *synaptojanin* and *endophilin* mutants argues against the involvement of synaptic vesicle endocytosis and indicates that the size of the recycling synaptic vesicle pool is not a limiting factor for synaptic homeostasis. These data also underscore the importance and specificity of those mutations we identified that do block synaptic homeostasis. These include four ion channels, two of which are of unknown function, and two calcium-binding proteins of unknown function. Thus, homeostatic signaling at the NMJ may include previously unexplored mechanisms of synaptic modulation.

One mutation that was identified with a specific defect in homeostatic compensation is a transposon insertion that resides in the *Drosophila* homolog of *dysbindin* (CG6856; fig. S2). The *dysbindin* locus is linked with schizophrenia in humans (*6*–*11*). We identified a transposon insertion within *Drosophila dysbindin* ($pBac^{e01028}$, referred to as $dysb^{1}$; fig. S2) that showed a complete absence of homeostatic compensation after application of PhTx (Fig. 2, A and B). A similar effect was observed when $dysb^{1}$ was placed in trans to a deficiency that uncovers the *dysb* locus, indicating that the $dysb^{1}$ mutant was a strong loss-of-function or null mutation (Fig. 2, A and B). No significant change in baseline synaptic transmission in $dysb^{1}$ mutant larvae (0.5 mM extracellular calcium) was observed. Thus, under these recording conditions, this mutation disrupted synaptic homeostasis without altering baseline neurotransmission (Fig. 2B). As a control, synaptic homeostasis was normal in larvae in which the $pBac^{e01028}$ transposon was precisely excised (Fig. 2, C and D).

The *dysb* gene is ubiquitously expressed in *Drosophila* embryos (fig. S2), consistent with widespread expression in vertebrates (*12*, *13*). Therefore, we generated and expressed a *dysbindin* transgene in the $dysb^{1}$ mutant. Presynaptic expression of *dysb* fully restored homeostatic compensation in the $dysb^{1}$ mutant background, whereas muscle-specific expression of *dysb* did not (Fig. 2, C and D, and fig. S3). Thus, dysbindin is necessary presynaptically for the rapid induction of synaptic homeostasis.

We next asked whether dysbindin is also required for the sustained expression of synaptic homeostasis. We generated double-mutant flies harboring both the $dysb^{1}$ mutation and a mutation in a gene encoding a postsynaptic glutamate receptor (*GluRIIA*). *GluRIIA* mutant larvae normally show robust homeostatic compensation (*14*). However, homeostatic compensation was blocked in *GluRIIA;* $dysb^{1}$ double-mutant larvae (Fig. 2E). Thus, *dysbindin* was also necessary for the sustained expression of synaptic homeostasis over several days of larval development.

Next we demonstrated that synapse morphology was qualitatively normal in *dysb* mutants (Fig. 3A), taking into account the shape of the presynaptic nerve terminal as well as the levels, localization, and organization of synaptic markers including microtubules, synapsin, and synaptotagmin (fig. S4). Bouton number and active zone density are also normal in *dysb* mutants (Fig. 3, C to E) (*15*). Thus, the disruption of synaptic homeostasis in $dysb^{1}$ mutants is not a secondary consequence of altered or impaired NMJ development.

In the vertebrate nervous system, dysbindin is associated with synaptic vesicles (*16*). We examined the localization of a *Venus*-tagged *dysb* transgene (*ven-dysb*) that rescues the $dysb^{1}$ mutant (Fig. 2, C and D). Ven-Dysb showed extensive overlap with synaptic vesicle–associated proteins when expressed in neurons (Fig. 3B). Thus, dysbindin functions presynaptically, potentially at or near the synaptic vesicle pool.

To further define the function of dysbindin, we investigated baseline synaptic transmission in the *dysb* mutant in greater detail. At 0.5 mM extracellular calcium, synaptic transmission in $dysb^{1}$ mutant larvae was indistinguishable from the wild type (Fig. 2, A and B). However, when extracellular calcium was reduced (0.2 to 0.4 mM $Ca^{2+}$), baseline synaptic transmission was significantly impaired in *dysb* relative to the wild type (Fig. 4A), and this defect was rescued by presynaptic expression of *dysb* (fig. S5). Thus, there is an alteration of the calcium dependence of synaptic transmission in the *dysb* mutant. Indeed, at reduced extracellular calcium, both paired-pulse facilitation and facilitation that occurs during a prolonged stimulus train were increased in *dysb* mutants (Fig. 4B and fig. S6).

In vertebrates, levels of *dysb* expression correlate with parallel changes in extracellular glutamate concentration (*17*). Therefore, we tested whether *dysb* overexpression might increase presynaptic release. In wild-type larvae overexpressing *dysb* in neurons, synaptic transmission was normal at low extracellular calcium (0.2 and 0.3 mM $Ca^{2+}$) but was enhanced at relatively high extracellular calcium (0.5 mM $Ca^{2+}$; Fig. 4C and fig. S5). The complementary effects of *dysb* loss of

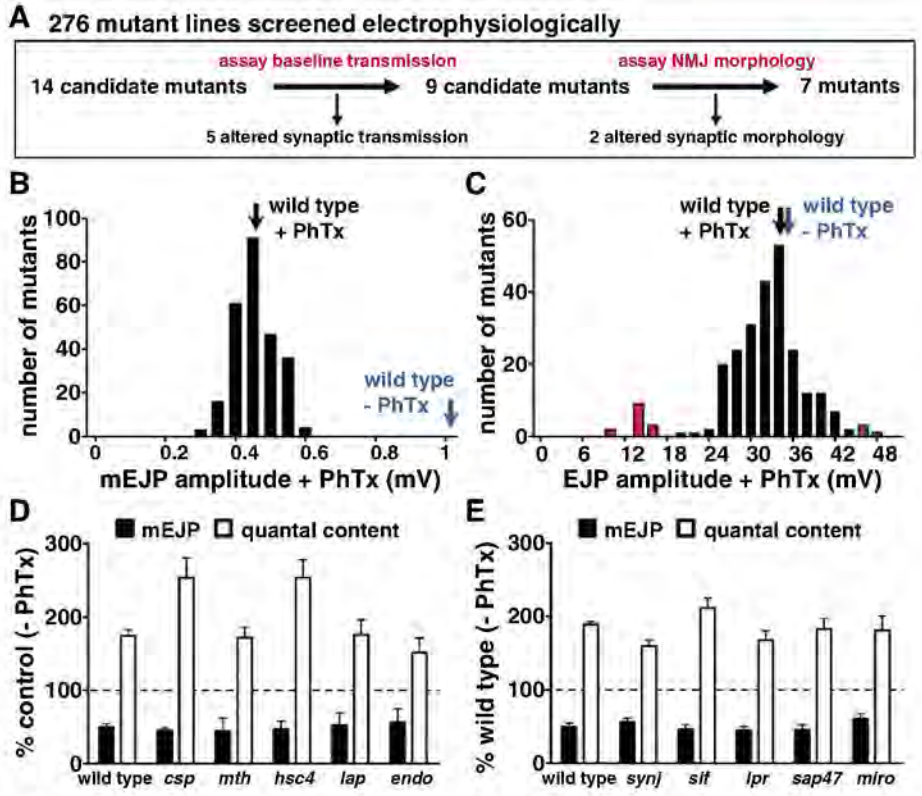


**Fig. 1.** Electrophysiology-based screen for homeostatic mutations. **(A)** Flow diagram of screen strategy and outcome. **(B)** Histogram of average mEJP amplitude per genotype after PhTx application. Wild-type average mEJP (blue arrow) and wild-type average mEJP after PhTx application (black arrow) are indicated. **(C)** Histogram of average EJP amplitudes per genotype after PhTx application [arrows as in (B)]. Red columns indicate values greater than two standard deviations from the mean. **(D** and **E)** Homeostatic increases in quantal content observed in published genetic mutations. Data are normalized to the same genotype without PhTx treatment in (D) and to wild-type values in (E). See tables S1 and S2 for full genotypes, *n* values, and references.

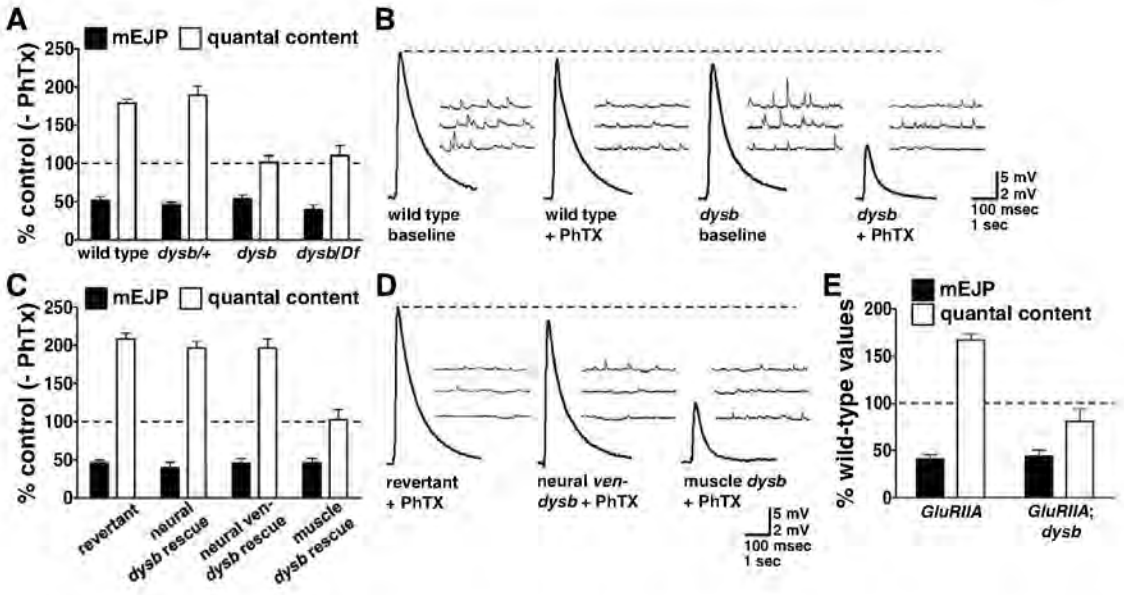


**Fig. 2.** Dysbindin is required presynaptically for synaptic homeostasis. (**A**) Mutations in *dysbindin* block the homeostatic increase in quantal content after PhTx application. Data are normalized to each genotype in the absence of PhTx. (**B**) Representative traces for data in (A). (**C**) Precise excision of the *e01028* transposon (revertant) restores compensation. Neuronal-specific expression of *dysb* (with or without a *venus* tag; *c155-GAL4/+; UAS-dysb/+; dysb*$^{1}$) restores compensation. Muscle-specific expression (*UAS-dysb/+; mhc-GAL4, dysb*$^{1}$*/dysb*$^{1}$) does not. (**D**) Representative traces for data in (C). (**E**) Sustained homeostatic compensation is blocked in *GluRIIA*$^{SP16}$*; dysb*$^{1}$ double mutants.

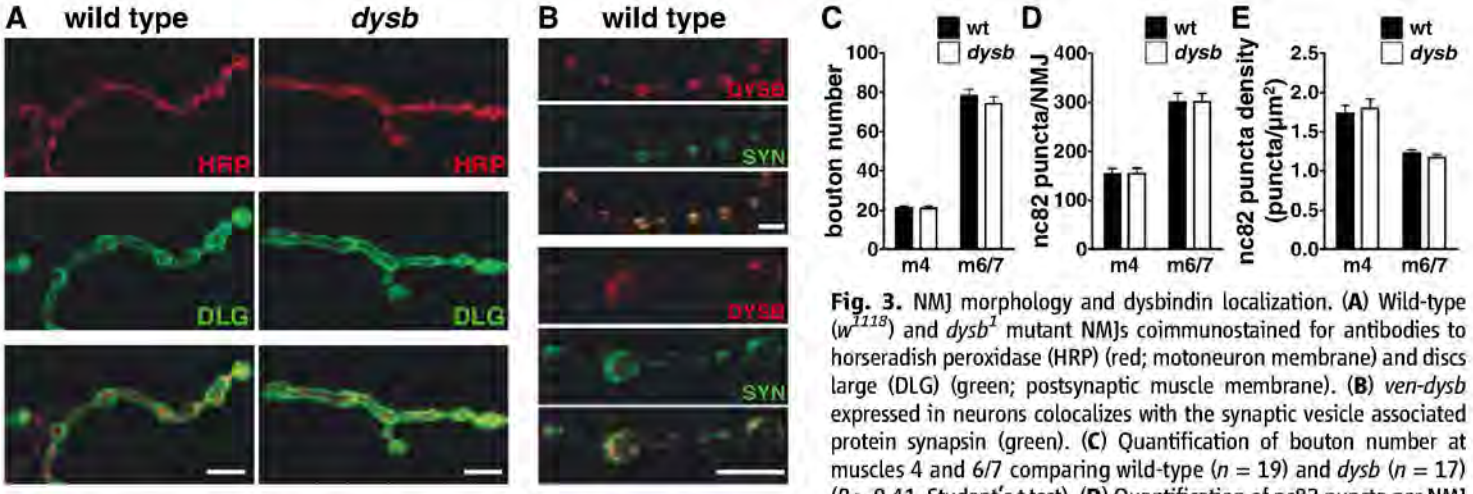


**Fig. 3.** NMJ morphology and dysbindin localization. (**A**) Wild-type ($w^{1118}$) and *dysb*$^{1}$ mutant NMJs coimmunostained for antibodies to horseradish peroxidase (HRP) (red; motoneuron membrane) and discs large (DLG) (green; postsynaptic muscle membrane). (**B**) *ven-dysb* expressed in neurons colocalizes with the synaptic vesicle associated protein synapsin (green). (**C**) Quantification of bouton number at muscles 4 and 6/7 comparing wild-type ($n = 19$) and *dysb* ($n = 17$) ($P > 0.41$, Student's *t* test). (**D**) Quantification of nc82 puncta per NMJ comparing wild-type ($n = 15$) and *dysb* ($n = 16$) ($P > 0.97$, Student's *t* test). (**E**) Density of nc82 puncta comparing wild-type ($n = 15$) and *dysb* ($n = 16$) ($P > 0.32$, Student's *t* test). Scale bars, 5 μm.

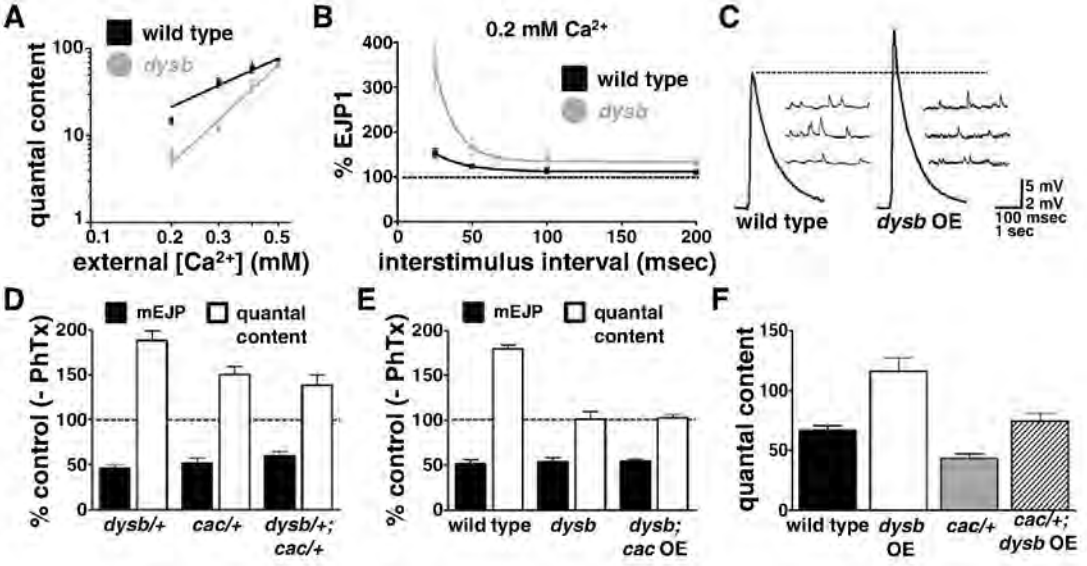


**Fig. 4.** Dysbindin modulates the calcium dependence of vesicle release. (**A**) Quantal content as a function of extracellular calcium concentration. (**B**) Enhanced paired-pulse facilitation in *dysb*$^{1}$ mutants. (**C**) Quantal content is increased by neuronal overexpression of *dysb* (*dysb OE; c155-GAL4/Y; UAS-dysb/+*). (**D**) Homeostatic compensation is calculated as in Fig. 1E. Compensation is suppressed in *cac*$^{S}$*/+* ($n = 15$) relative to the wild type ($n = 25$; $P < 0.001$, Student's *t* test) or *dysb*$^{1}$*/+* ($n = 17$; $P < 0.001$, Student's *t* test) but is not further suppressed in *cac*$^{S}$*/+; dysb*$^{1}$*/+* mutants ($n = 19$; $P > 0.27$, Student's *t* test). (**E**) Compensation remains blocked when *cac* is neuronally overexpressed in a *dysb*$^{1}$ mutant ($n = 9$, *dysb;cac OE; c155-GAL4/Y; UAS-cacGFP/+; dysb*$^{1}$). (**F**) Quantal content is increased by neuronal overexpression of *dysb* ($n = 17$, *dysb OE; c155-GAL4/Y; UAS-dysb/+*; $P < 0.0002$, Student's *t* test) and when *dysb* is overexpressed in a *cac*$^{S}$ mutant ($n = 19$, *cac*$^{S}$*/+; dysb OE; cac*$^{S}$*/c155-GAL4; UAS-dysb/+*; $P < 0.006$, Student's *t* test).

function and overexpression confirm that dysbindin has an important influence on calcium-dependent vesicle release.

The presynaptic $Ca_V2.1$ calcium channel, encoded by *cacophony* (*cac*), is required for synaptic vesicle release at the *Drosophila* NMJ (*18*). *cac* mutations decrease presynaptic calcium influx (*19*) and also block synaptic homeostasis (*4*). We therefore tested for a genetic interaction between *dysb* and *cac* during synaptic homeostasis. Because homozygous *cac* and *dysb* mutations individually block synaptic homeostasis, analysis of double-mutant combinations would not be informative. We resorted to an analysis of heterozygous mutant combinations and gene overexpression (*5*). Synaptic homeostasis was suppressed by a heterozygous mutation in *cac* (Fig. 4D). However, this suppression was not enhanced by the presence of a heterozygous mutation in *dysb* (Fig. 4 and fig. S7). In addition, neuronal overexpression of *cac* did not restore homeostatic compensation in *dysb* mutant larvae, and the enhancement of presynaptic release caused by neuronal *dysb* overexpression still occurred in a heterozygous *cac* mutant background (Fig. 4, E and F). Thus, dysbindin may function downstream or independently of Cac during synaptic homeostasis.

To further explore the relationship between dysbindin and Cac, we asked whether *dysb* mutations might directly influence presynaptic calcium influx. The spatially averaged calcium signal in $dysb^1$ was indistinguishable from the wild type, indicating no difference in presynaptic calcium influx (fig. S8). Thus, dysbindin appears to function downstream or independently of calcium influx to control synaptic homeostasis.

Through a systematic electrophysiological analysis of more than 250 mutants, we were able to rule out the involvement of numerous synaptic proteins and biochemical processes in the mechanisms of synaptic homeostasis and to show that this phenomenon is separable from the molecular mechanisms that specify structural and functional synapse development. We thus identify dysbindin as an essential presynaptic component within a homeostatic signaling system that regulates and stabilizes synaptic efficacy. Dysbindin functions downstream or independently of the presynaptic $Ca_V2.1$ calcium channel in the mechanisms of synaptic homeostasis.

Emerging lines of evidence suggest that glutamate hypofunction could be related to the etiology of schizophrenia (*20*–*24*). Likewise, reduced levels of *dysbindin* expression have been associated with schizophrenia (*25*, *26*). The *sandy* mouse, which lacks dysbindin, has a decreased rate of vesicle release (~30% decrease), a correlated decrease in vesicle pool size, and an increased thickness of the postsynaptic density (*27*). We confirm a modest, facilitatory function for dysbindin during baseline transmission. However, numerous mutations with similar or more severe defects in baseline transmission show normal synaptic homeostasis (Fig. 1, D and E). By contrast, loss of dysbindin completely blocks the adaptive, homeostatic modulation of vesicle release, which suggests that the potential contribution of *dysbindin* mutations to schizophrenia may derive from altered homeostatic plasticity as opposed to decreased baseline glutamatergic transmission.

## References and Notes


1. G. W. Davis, *Annu. Rev. Neurosci.* **29**, 307 (2006).
2. T. Branco, K. Staras, K. J. Darcy, Y. Goda, *Neuron* **59**, 475 (2008).
3. G. G. Turrigiano, S. B. Nelson, *Nat. Rev. Neurosci.* **5**, 97 (2004).
4. C. A. Frank, M. J. Kennedy, C. P. Goold, K. W. Marek, G. W. Davis, *Neuron* **52**, 663 (2006).
5. C. A. Frank, J. Pielage, G. W. Davis, *Neuron* **61**, 556 (2009).
6. C. A. Ross, R. L. Margolis, S. A. Reading, M. Pletnikov, J. T. Coyle, *Neuron* **52**, 139 (2006).
7. N. Norton, H. J. Williams, M. J. Owen, *Curr. Opin. Psychiatry* **19**, 158 (2006).
8. M. A. Benson, R. V. Sillitoe, D. J. Blake, *Trends Neurosci.* **27**, 516 (2004).
9. K. S. Kendler, *Am. J. Psychiatry* **161**, 1533 (2004).
10. M. J. Owen, N. M. Williams, M. C. O'Donovan, *J. Clin. Invest.* **113**, 1255 (2004).
11. N. M. Williams, M. C. O'Donovan, M. J. Owen, *Schizophr. Bull.* **31**, 800 (2005).
12. M. A. Benson, S. E. Newey, E. Martin-Rendon, R. Hawkes, D. J. Blake, *J. Biol. Chem.* **276**, 24232 (2001).
13. R. Nazarian, M. Starcevic, M. J. Spencer, E. C. Dell'Angelica, *Biochem. J.* **395**, 587 (2006).
14. S. A. Petersen, R. D. Fetter, J. N. Noordermeer, C. S. Goodman, A. DiAntonio, *Neuron* **19**, 1237 (1997).
15. D. A. Wagh *et al.*, *Neuron* **49**, 833 (2006).
16. K. Talbot *et al.*, *Hum. Mol. Genet.* **15**, 3041 (2006).
17. T. Numakawa *et al.*, *Hum. Mol. Genet.* **13**, 2699 (2004).
18. F. Kawasaki, R. Felling, R. W. Ordway, *J. Neurosci.* **20**, 4885 (2000).
19. G. T. Macleod *et al.*, *Eur. J. Neurosci.* **23**, 3230 (2006).
20. D. A. Collier, T. Li, *Eur. J. Pharmacol.* **480**, 177 (2003).
21. C. Konradi, S. Heckers, *Pharmacol. Ther.* **97**, 153 (2003).
22. J. T. Coyle, *Cell. Mol. Neurobiol.* **26**, 365 (2006).
23. M. Sodhi, K. H. Wood, J. Meador-Woodruff, *Expert Rev. Neurother.* **8**, 1389 (2008).
24. S. T. Patil *et al.*, *Nat. Med.* **13**, 1102 (2007).
25. C. S. Weickert, D. A. Rothmond, T. M. Hyde, J. E. Kleinman, R. E. Straub, *Schizophr. Res.* **98**, 105 (2008).
26. K. Talbot *et al.*, *J. Clin. Invest.* **113**, 1353 (2004).
27. X. W. Chen *et al.*, *J. Cell Biol.* **181**, 791 (2008).


28. We thank M. Muller for assistance with data analysis and members of the Davis laboratory for comments and discussion. Supported by postdoctoral fellowships from the A. P. Giannini Foundation and Jane Coffin Childs Memorial Fund (D.K.D.) and by NIH grant NS39313 (G.W.D.).


## Supporting Online Material

www.sciencemag.org/cgi/content/full/326/5956/1127/DC1
Materials and Methods
SOM Text
Tables S1 and S2
Figs. S1 to S8
References

27 July 2009; accepted 2 October 2009
10.1126/science.1179685

## Guide Tube

The MatriMix Guide Tube is designed to secure dispensers' flexible aspiration tubing in the MatriMix Spinner Flask. The reusable Guide Tube is made of high-grade polycarbonate and delrin. The MatriMix Spinner Flask is a disposable one-liter flask molded from virgin polycarbonate. A central magnetic stir paddle maximizes nutrient flow and minimizes dead volume. Its tear-drop shape breaks up laminar flow and allows for uninterrupted aspiration while spinning.

MatriCal Bioscience
For information 509-343-6225
www.matrical.com

## Proteomics Imaging and Analysis

The FluorChem Xplor is an imaging platform for proteomics imaging and analysis that can perform rapid and quantitative two-dimensional gel, chemiluminescent protein immunoblotting, and one-dimensional gel imaging. With this one instrument, a lab can address all its imaging needs relating to proteomics workflow, replacing the need for separate imaging stations or a darkroom and developing machine. The system provides fast, quantitative imaging of large gels. It includes integrated, protocol-driven software for image acquisition, enabling the easy imaging of multiple samples under reproducible lighting and exposure conditions. It also includes image analysis software that can detect spots, quickly normalize to a loading control, and automatically correct for background levels.

Alpha Innotech
For information 800-795-5556
www.alphainnotech.com

## Phosphotyrosine Signaling

The SH2 Domain Phosphotyrosine Capture Kits are fast and efficient tools for capturing specific tyrosine phosphorylated proteins from mammalian cell lysates. These kits enable researchers to monitor and profile specific tyrosine phosphorylation events and identify specific SH2 domain protein-protein interaction networks. The assay makes use of SH2 domain peptides tagged with glutathione S-transferase and glutathione agarose resin to capture and pull down the specific binding partners, providing an alternative to traditional immunoprecipitations using phospho-antibodies. The kits also offer an alternative to phosphoprotein enrichment resins that do not discriminate among proteins that are phosphorylated on serines, threonines, or tyrosines. Subsequent analysis of the SH2 domain interactions can be performed using protein immunoblots or mass spectrometry.

Thermo Fisher
For information 815-968-0747
www.thermo.com/pierce

## Sequencing Software

A Consolidation Tool has been added to the NextGENE software package that enhances the detection of low-frequency single nucleotide polymorphisms, such as mosaic/somatic mutations, from deep sequence data generated by second-generation sequencing systems such as the Illumina Genome Analyzer, Applied Biosytems' SOLiD System, and Roche Applied Science's Genome Sequencer. Identification of low-frequency variants is a valuable tool for developing personalized treatment for individuals with diseases such as human immunodeficiency virus and cancers in drug resistance and other studies.

SoftGenetics
For information 814-237-9340
www.softgenetics.com

## Wireless Barcode Scanner

Weighing only 225 g, the SampleScan Wireless Barcode Scanner combines the convenience of lightweight handheld operation with the versatility of being able to read coding symbologies, including a wide range of two-dimensional and linear barcodes. It can transmit information to a computer wirelessly using Bluetooth communication.

Micronic Europe
For information +31-(0)320-277070
www.micronic.com

## Histone Demethylase Screening Assay

The Universal Histone Demethylase Fluorescent Detection kit measures the activity of both LSD1-type and Jumonji-type histone demethylases. It allows calibration of activity across labs with its stable formaldehyde standard. Screening of inhibitor activity to any histone demethylase takes place in the supplied plates, followed by addition of the Formaldehyde Detection Reagent. After a short incubation, the amount of formaldehyde produced is measured in a plate reader with excitation at 450 nm and emission at 510 nm.

Luminos
For information 734-677-1774
www.LuminosAssays.com

## Mouse Monoclonal Isotyping

The Iso-Gold Rapid Mouse Monoclonal isotyping kits feature a rapid format that reduces the labor of the traditional enzyme-linked immunosorbent assay protocol from a day-and-a-half procedure to a 5-minute assay. The kit is a lateral flow assay that can be run on tissue culture supernatant or mouse ascites fluid. The kit requires a single step—adding diluted antibody sample into the loading well of a cassette—and in less than five minutes provides a color readout of the antibody subtype. The test is also available with kappa and lambda light chains determination.

AMS Biotechnology
For information +44-1235-828200
www.amsbio.com

Electronically submit your new product description or product literature information! Go to **www.sciencemag.org/products/newproducts.dtl** for more information.

Newly offered instrumentation, apparatus, and laboratory materials of interest to researchers in all disciplines in academic, industrial, and governmental organizations are featured in this space. Emphasis is given to purpose, chief characteristics, and availabilty of products and materials. Endorsement by *Science* or AAAS of any products or materials mentioned is not implied. Additional information may be obtained from the manufacturer or supplier.

## POSITIONS OPEN

### ASSISTANT OR ASSOCIATE PROFESSOR
**Cognitive Neuroscience (tenure track)**
**University of Washington Institute for Learning and Brain Sciences**

The University of Washington's Institute for Learning and Brain Sciences (I-LABS), an interdisciplinary brain research center, has a tenure-track faculty opening for an Assistant/Associate Professor in cognitive neuroscience with a focus on language. Departmental affiliation can be in Psychology, Speech and Hearing Sciences, Linguistics, or Biology, depending on the applicant's background and training. Ph.D. required. Appointment at the Associate Professor level will be considered for candidates who have an outstanding research record. I-LABS faculty study life-long learning and specialize in human cognitive development and learning. We have a growing developmental group at the Institute. The Institute will open its own Magnetoencephalography Brain Imaging Center in April 2010. The successful candidate will be one who brings expertise in human cognitive neuroscience with a focus in the domain of language, development, and/or research using MEG/event-related potentials. Faculty responsibilities will begin September 16, 2010.

Applicants should send a statement of teaching and research interests, curriculum vitae, up to five publication reprints, and three letters of recommendation to: **Patricia Kuhl, Co-Director, Institute for Learning and Brain Sciences, Mailstop 357988, University of Washington, Seattle, WA 98195. E-mail: pkkuhl@u.washington.edu**. Review of applications will begin in January 15, 2010, and will continue until the position is filled.

*The University of Washington is an Affirmative Action, Equal Opportunity Employer, and is building a culturally diverse faculty and staff and strongly encourages applications from women, minorities, individuals with disabilities, and covered veterans. UW faculty engage in teaching, research, and service. The University of Washington, a recipient of the 2006 Alfred P. Sloan award for Faculty Career Flexibility, is committed to supporting the work-life balance of its faculty.*

---

### TENURE-TRACK FACULTY POSITIONS
**Physiology**

The Department of Physiology at Wayne State University (WSU) School of Medicine invites applications for two tenure-track **ASSISTANT/ASSOCIATE PROFESSOR** positions. We seek well-trained individuals with research interests in the areas of molecular, cellular, systems, translational physiology and/or biophysics to strengthen and complement ongoing programs in the Department (**website: http://physiology.med.wayne.edu**). The Department is currently under major expansion and integrative development with the Cardiovascular Research Institute (**website: http://cvri.med.wayne.edu/index.php**) and C.S. Mott Center for Human Growth and Development (**website: http://mott.med.wayne.edu/**).

Startup packages and salaries are highly competitive. Candidates are expected to establish active, extramurally funded research programs and to participate in teaching medical/graduate students. Candidates must hold Ph.D., M.D., or equivalent and apply electronically with curriculum vitae, detailed research plan, and names/contact information of three references to **e-mail: wsuphysiologyfacultysearch@med.wayne.edu**. Review of applications will begin after December 15, 2009, and continue until positions are filled.

WSU offers 350 academic programs through 14 schools and colleges to over 31,000 students in metropolitan Detroit. The Detroit metro area combines cosmopolitan attractions with lovely suburban communities as part of a national technology hub. WSU School of Medicine is a state-of-the-art research environment, and is rated in the top third of all U.S. research institutions. *WSU is an Equal Opportunity/Affirmative Action Employer.*

## POSITIONS OPEN

The Mind RESEARCH NETWORK
For Neurodiagnostic Discovery

### SENIOR FACULTY/RESEARCH SCIENTIST
**University of New Mexico**
**and The Mind Research Network**

Up to three senior faculty positions available to lead the research at The Mind Research Network (MRN), Albuquerque, New Mexico, an independent research organization (**website: http://www.mrn.org**), with a joint appointment as a tenure-track faculty member either at the University of New Mexico or another institution in the United States. Significant startup fund and highly competitive salary from MRN. Strong external funding is prerequisite. Successful candidate should have expertise in one or more of the following areas: human brain development, schizophrenia, addiction, health psychology, and neuroinformatics, based on one or more of the following technologies: magnetic resonance imaging, magnetoencephalography, electroencephalography, neuropsychology, and genetics. To apply, please send curriculum vitae, a description of research and teaching interests, and three letters of recommendation to: **MRN, Attn: Human Resources/Chair of MRN/UNM Search Committee, 1101 Yale Boulevard N.E., Albuquerque, NM 87106-4188.** To send application materials electronically, use **e-mail: hr@mrn.org** with the subject Senior Faculty/Research Scientist. For questions, please contact the chair, **Dr. Kent Hutchison, e-mail: khutchison@mrn.org**. The committee will begin reviewing applications as they are received focused on a deadline. *Equal Opportunity Employer. Minorities/Females/Persons with Disabilities/Veterans.*

---

### ORGANISMAL BIOLOGIST, ASSISTANT PROFESSOR
**Tenure Track, Academic Year 100 Percent**

The Department of Biology in the College of Science and Health at the University of Wisconsin–La Crosse is expanding and invites applications for a new academic year, tenure-track position at the level of Assistant Professor. We seek an Organismal Biologist who will participate in teaching our biology core curriculum including organismal biology, and courses in her/his area of expertise. Training in invertebrate zoology, or seedless plants/algae, is preferred, but individuals with other organismal biology specialties are encouraged to apply. Our Department values diversity in its faculty, staff, and students. We seek a colleague who shares our Department's commitment to diversity and who will be a dedicated teacher, active scholar, and effective mentor for students with diverse backgrounds, preparation, and career goals. UW-L is nationally renowned as a comprehensive university with demonstrated excellence in undergraduate and graduate education and research. Coupled with the beautiful surroundings of the region, UW-L offers a stellar environment for professional and personal achievement. A Ph.D. in a biological science is required, and previous teaching experience is desirable. Successful candidates will be expected to develop an externally funded research program and to direct undergraduate and graduate (M.S.) research. Academic year salary is competitive and commensurate with experience. Start date is August 30, 2010. All applications must be submitted electronically at **website: https://employment.uwlax.edu**.

Applications must include a cover letter, curriculum vitae, statements of teaching philosophy and research interests, graduate and undergraduate transcripts, and the names and contact information of three references. Applications completed by January 15, 2010, will be given first priority, but the review process will continue until the position is filled. *The University of Wisconsin–La Crosse is an Affirmative Action/Equal Opportunity Employer. If you have a special need/accommodation to aid your participation in our hiring process, please contact **David Howard, e-mail: howard.davi@uwlax.edu** to make appropriate arrangements. Employment will require a criminal background check. A pending criminal charge or conviction will not necessarily disqualify an applicant. In compliance with the Wisconsin Fair Employment Act, UW-La Crosse does not discriminate on the basis of arrest or conviction record.*

WWW.NIH.GOV
Positions @ NIH
THE NATIONAL INSTITUTES OF HEALTH

**Genomics and Next Generation Sequencing**

**Post doctoral Fellow**

The Oncogenomics Section of the Pediatric Oncology Branch, at the Center for Cancer Research, National Cancer Institute has a postdoctoral position available immediately. Ongoing research efforts involve genomic approaches to the investigation of Pediatric Solid Tumors using next generation sequencing techniques. The candidate will work on identifying genomic alterations that are associated with disease progression and poor prognosis using sequence based analysis as well as the identification of biologically and clinically relevant Single Nucleotide Variants or mutations.

Candidate should be a US citizen or a Permanent Resident, hold a Ph.D. or M.D. and have an interest in Oncology as well as experience in Genomics or next generation sequencing methods. Candidates should have less than 3 year post-doctoral experience. **URL: http://home.ccr.cancer.gov/oncology/oncogenomics/**

If interested please contact **Dr. Javed Khan, khanjav@mail.nih.gov or telephone 301-435-2937**.

## Medical Oncology Branch
## Postdoctoral Positions Available

The Medical Oncology Branch (MOB) in the Center for Cancer Research (CCR), National Cancer Institute (NCI), National Institutes of Health (NIH) is currently seeking three postdoctoral fellows. The position is located in the Thoracic Oncology Section, under the direction of Dr. Giuseppe Giaccone. Accepted candidate will work on molecular and cellular biology of lung carcinomas.

For further information about the MOB, NIH, or NCI programs, faculty, and training please visit our respective websites: http://ccr.cancer.gov/labs/lab.asp?labid=753, http://ccr.nci.nih.gov, http://www.cancer.gov, http://www.nih.gov.

Applicants must have a Ph.D. or M.D. degree and less than five years' postdoctoral experience. Candidates should have basic research experience in biochemistry, molecular/cellular biology, and an interest in developing novel treatments and strategies for lung carcinomas. Preferred candidates will have expertise in lung cancer/stem cell research, genomics, or molecular pharmacology.

Interested candidates should send curriculum vitae including publications in peer review journals; a cover letter indicating interest in the position; and the names and contact information of three references. Mail applications to: Yisong Wang, Ph.D., NIH/NCI, 10 Center Drive, Room 8N258, Bethesda, MD 20892; E-mail application to: Lisa Eiben, lisaje@mail.nih.gov Phone: 301-435-4036.

## The NIH Director's Wednesday Afternoon Lecture Series

Biomedical scientists around the world are invited to join us online to hear leading investigators present their latest results to the NIH Intramural Research community. Lectures may be viewed live at 3:00 p.m., EST (20:00 GMT) on Wednesdays, from September through June. Live webcasts can be viewed under "Today's Events" at: <http://videocast.nih.gov/>

The current schedule of lectures is available at: <http://wals.od.nih.gov

Upcoming Lectures:

December 2: Tobias Meyer, Stanford University Medical School, "Shotgun siRNA Perturbation to Dissect Growth Factor Triggered Proliferation and Migration Signaling Systems"

December 9: Gerard Karsenty, Columbia University Medical Center, "The Novel Physiology of Bone"

December 16: Rebecca Richards-Kortum, University of Texas, "From Cell Phones to Cell Biology: High Tech, Low Cost Solutions for Global Health"

January 6: John Rich, Drexel University, "Wrong Place, Wrong Time: Understanding Trauma and Violence in the Lives of Young Black Men"

NIEHS
National Institute of Environmental Health Sciences
National Institutes of Health

## Stem Cell Biology
### Research Triangle Park, NC

A postdoctoral position is immediately available in the Stem Cell Biology Group of the National Institute of Environmental Health Sciences (NIEHS), Research Triangle Park, North Carolina, to investigate the molecular basis of embryonic stem cell self-renewal and differentiation. The group is part of the Laboratory (i.e., department) of Molecular Carcinogenesis (LMC) in NIEHS. We have recently identified a list of novel candidate genes that are important for ES cell self-renewal in large-scale RNAi screens, and we are going to investigate and characterize their function in ES cells, mouse development, and the reprogramming of somatic cells. In addition, we will also use functional genetic approaches to study lineage-specification during ES cell differentiation and adult stem cell self-renewal and differentiation.

Applicants must have a doctoral level degree with less than five years of postdoctoral research. Experience in gene regulation, stem cell biology, or embryology are highly encouraged but not required. Competitive stipends are determined by educational degree(s) and number of years of relevant postdoctoral experience.

Dr. Guang Hu
Stem Cell Biology Group • Laboratory of Molecular Carcinogenesis
National Institute of Environmental Health and Sciences
Mail Drop D4-03
111 Alexander Drive
Research Triangle Park, NC 27709
E-mail: hug4@niehs.nih.gov
http://niehs.nih.gov

U.S. DEPARTMENT OF HEALTH AND HUMAN SERVICES
National Institutes of Health

*DHHS and NIH are Equal Opportunity Employers.*

## Molecular and Cellular Biology Postdoctoral Opportunities at Dartmouth

The Molecular and Cellular Biology Graduate Program at Dartmouth is seeking outstanding and highly motivated candidates for a number of POST-DOCTORAL positions. Availability for on campus interviews desirable. Applications, assembled in a single PDF file, should be sent to **MCB@DARTMOUTH.EDU** (please indicate position/s of interest; see below) and should contain CV, cover letter describing research interests and goals, and names/contact information for three references. More detailed information on faculty and their research is available on our website **http://dms.dartmouth.edu/mcb/faculty/**.

Faculty/research areas with available positions: **Constance Brinckerhoff, PhD** - Novel functions of matrix metalloproteinases in arthritis and cancer; **David Bzik, PhD** - Genetic dissection of pathogen:host interactions in *Toxoplasma gondii* infection; **TY Chang, PhD** - Biochemistry and structural biology of enzymes in cholesterol metabolism; **Ambrose Cheung, PhD** - *Staphylococcus aureus* pathogenesis and mechanism of drug resistance; **Duane Compton, PhD** - Determination of the mechanisms causing chromosomal instability in human tumors; **Jose Conejo-Garcia, MD, PhD** - Use of nanomaterials to boost therapeutic immunity against ovarian cancer; **Barbara Conradt, PhD** - Developmental control of apoptosis and mitochondrial dynamics; **Jay Duulap, PhD** - Epigenetic control of light responses and circadian rhythms via next-generation sequencing; **James Gorham, MD, PhD** - T cell tolerance and autoimmunity in the liver; **William Green, PhD** - T Cell Immune Responses to Retroviral Diseases; **Henry Higgs, PhD** - Linking the biochemistry of actin dynamics to cellular function; **Mark Israel, MD** - The interface of CNS differentiation and tumorigenesis; **Thomas Jack, PhD** - Molecular genetics of flower development in the plant *Arabidopsis thaliana*; **David Leib, PhD** - Herpes simplex virus pathogenesis and immune evasion; **Jennifer Loros, PhD** - Genetics and circadian molecular biology of Neurospora and mammalian cells in culture; **Dean Madden, PhD** - Biophysical studies of ion channel activation, desensitization and trafficking; **Richard Saito, PhD** - Developmental regulation of cell cycle; **G. Eric Schaller, PhD** - Signaling by the plant hormones ethylene and cytokinin; **Elizabeth Smith, PhD** - Calcium control of dynein activity and regulation of ciliary motility; **Paula Sundstrom, PhD** - Virulence gene regulation and microbe host interactions in candidiasis; **Ronald Taylor, PhD** - Bacterial pathogenesis; colonization; virulence gene regulation; vaccines; antimicrobials; **Michael Whitfield, PhD** - Scleroderma diagnostics; cell cycle control; post-transcriptional regulation.

*Dartmouth College and Dartmouth Medical School are Affirmative Action/Equal Opportunity Employers and encourage applications from women and members of minority groups.*

## Nagaoka University of Technology

### Cultivation Center for Young Investigators through University-Industry Joint Research Program

### A few Associate Professor, Lecturers and/or Assistant Professor

**Applications are invited for a few tenure-track positions at the ranks of Associate Professor, Lecturer and Assistant Professor in the areas specified below for a 5-year term, from April 2010 and ending in March 2015.**
**Appointees will be provided with independent laboratories, startup budgets and research funds (altogether JPY 10,000,000 in the first year), as well as support staffs (post-doctoral fellows and RA's). Annual salary is over JPY 6,500,000 (US$ 72,200-94,400) and is fixed during the period of employment. Their promotion to tenured positions (employment guaranteed by the age of 65) with a minimum guaranteed annual salary will be determined through two reviews after appointment.**

**The research areas of interest are as followed fields; 1) Mechanical Engineering, 2)Electrical Electronics and Information Engineering, 3) Materials Science and Technology, 4) Environmental and Civil Engineering, 5) Bioengineering, 6) Management and Information Systems Science, and 7) of System Safety. Details in research areas are found following URL;**

**http://www.nagaokaut.ac.jp/j/annai/NUT-toprun/E.html**

**For inquiry, please contact Prof. Keizo Uematsu, a secretariat for the Committee of Selection of Young Investigators, e-mail: toprun@vos.nagaokaut.ac.jp**

## University of Nebraska Lincoln

### DIRECTOR
### School of Biological Sciences

We are seeking an extraordinary individual to serve as Director of the School of Biological Sciences at the University of Nebraska-Lincoln (UNL), an AAU and Land Grant University with a total enrollment of over 24,000 students. The School of Biological Sciences (SBS) is part of the College of Arts and Sciences, and plays a central role in undergraduate and graduate education and research at UNL. SBS has 640 undergraduate majors and high enrollments in our service and pre-professional courses. The forty-six SBS faculty pursue research across the full spectrum of areas in biology; the school's strategic plan **http://biosci.unl.edu/DOWNLOADS/SBS_STRAT_PLAN_2009.pdf** is based upon a commitment to understanding biological systems at multiple organizational levels, from genes, cells, and physiology through organisms to populations, communities, and ecosystems. SBS faculty currently mentor 93 MS and PhD students, and have $33 million in competitive extramural research support, primarily from NIH and NSF.

UNL is committed, as an institution, to achieving very high levels of academic excellence, as detailed in its "2020 Report" (see **http://www.unl.edu/svcaa/documents/2020report.pdf**), and to the continued growth and development of its Life Sciences programs. The successful candidate for Director will be a dynamic individual with outstanding scientific credentials, a commitment to quality education and the desire, ability and vision to lead the School. Candidates for this position must have a PhD degree, an outstanding record of extramural research funding, and demonstrated commitment to excellence; candidates must qualify for the rank of Professor with tenure. Candidates with research interests in any recognized biological discipline will be considered. The successful candidate will receive a competitive salary and start-up package.

Additional information about the department can be found at **http://www.biosci.unl.edu**. For consideration, applicants must complete the online Faculty/Administrative form and submit application materials at **http://employment.unl.edu**, requisition **#090659**. Application materials should include a cover letter, a curriculum vitae with a full list of publications, a summary of past, current, and pending research support, the names of three references, and a brief statement of research, educational, service, and administrative interests. Inquiries regarding the position or the application process should be directed to: **BioSciDirectorSearch@unl.edu**, or **SBS Search Committee Chair, College of Arts and Sciences, University of Nebraska-Lincoln, 1223 Oldfather Hall, Lincoln, NE 68588-0312 (Fax: 402-472-1123)**.

Review of applications will begin **January 15, 2010** and continue until the position is filled.

*The University of Nebraska has an active National Science Foundation ADVANCE gender equity program, and is committed to a pluralistic campus community through affirmative action, equal opportunity, work-life balance, and dual careers.*

# THE WISTAR INSTITUTE

TODAY'S DISCOVERIES – TOMORROW'S CURES

## DIRECTOR, CANCER CENTER AND CHIEF SCIENTIFIC OFFICER

The Wistar Institute, an NCI-designated cancer center, is seeking applications and nominations for the position of **Director, Cancer Center *and* Chief Scientific Officer**.

The Wistar Institute was founded in 1892 as the first institution of its kind devoted to medical research and training. In recognition of its increased focus on cancer research, the National Cancer Institute named Wistar as one of the first federally designated Cancer Centers; a distinction it has held continuously since 1972. Today, Wistar is one of only seven NCI-designated Cancer Centers devoted solely to basic research. The Wistar Institute Cancer Center has 31 laboratories, grouped into three research programs: Gene Expression and Regulation; Immunology; and Molecular and Cellular Oncogenesis. The Institute has nine shared facilities and four other centers, each of which is also a resource for the Cancer Center: The Vaccine Center; the Center for Systems and Computational Biology; the Brain Tumor Research Center; and its newest center, the Center for Chemical Biology and Translational Medicine. The annual Institute operating budget is $59M.

The Director/CSO will serve as second in command of The Wistar Institute and will play an important role in the planning and implementation of facility expansion currently under consideration. He/she will also serve as the Institute's external representative in scientific matters, working closely with CSO's from the University of Pennsylvania and the Children's Hospital of Philadelphia, organizations with whom Wistar shares a campus. He/she is expected to achieve significant growth in sponsored research funding and further increase the level of research productivity through mentoring and team building. The faculty of the Institute is projected to increase significantly over the next 3-5 years and recruitment will be an important element of the Director's role.

Candidates will have an M.D., Ph.D., or both, with a sustained record of peer reviewed funding by NIH, and have national and/or international recognition for their program in the field of cancer research. Candidates are expected to meet the requirements for appointment to the senior faculty ranks. Korn/Ferry International is assisting The Wistar Institute with this important search. Please forward, as soon as possible, nominations of appropriate candidates to:

**Warren E. Ross, M.D.**
**c/o Betsy Messina (betsy.messina@kornferry.com)**
**Korn/Ferry International**
**1835 Market Street, Suite 2000**
**Philadelphia, PA 19103**

*The Wistar Institute is an Equal Opportunity/Affirmative Action Employer and Educator.*

# The University of Edinburgh

**The University of Edinburgh is an exciting, vibrant, research led academic community offering opportunities to work with leading international academics whose visions are shaping tomorrow's world.**

## Readership in Computational Neuroscience

**£46,278 - £52,086**

The School of Informatics is expanding its activity in computational neuroscience and seeks to make a new appointment at the Readership level (roughly equivalent to US Associate Professor) in this area.

You will have an international research profile in computational neuroscience as applied to any aspect of the development and functioning of the nervous system. We are particularly interested in those who can develop collaborations within the broad spectrum of basic and clinical neuroscientists at Edinburgh, and/or develop links with other related fields represented at Edinburgh such as bioinformatics, systems biology and machine learning.

You will join the existing computational neuroscience group which includes five core academic staff and five postdoctoral researchers. The group has extensive research collaborations within the university, the UK and overseas, with considerable grant support. You will have the opportunity to be involved with the recently renewed multimillion pound EPSRC/MRC/BBSRC funded Doctoral Training Centre (DTC) in Neuroinformatics and Computational Neuroscience. The DTC offers 12 funded 4-year PhD studentships annually, with over 50 PhD projects currently running in this area.

This post forms part of Edinburgh's expansion within the Scottish Informatics and Computer Science Alliance (SICSA) initiative, see http://www.sicsa.ac.uk

**Apply online, view further details or browse more jobs at our website. Alternatively, telephone the recruitment line on 0131 650 2511.**
**Ref: 3011971S. Closing date: 15th January 2010.**

Committed to Equality and Diversity.

The University of Edinburgh is a charitable body, registered in Scotland, with registration number SC005336.

**One of the World's top 20 Universities**

**www.jobs.ed.ac.uk**

# Tulane University

## FACULTY POSITIONS in INFECTIOUS DISEASES
## Tulane National Primate Research Center

The Tulane National Primate Research Center (TNPRC) wishes to expand its infectious disease research programs involving molecular virology, bacteriology, and parasitology by reaching into areas covered by the NIH/NIAID National Biodefense Program, as well as vaccinology and vector-borne and emerging diseases. Agent-specific interests for the expansion include but are not limited to HIV/AIDS, brucellosis, and malaria.

Four positions are available at the rank of Assistant, Associate, or Full Professor. Designations may be either in the Tenure Track or within the Research Professor Series, depending on qualifications. Academic appointments will be in appropriate Departments of either the Tulane University School of Medicine or the Department of Tropical Medicine of the Tulane School of Public Health and Tropical Medicine. The research portfolio and infrastructure of the TNPRC, which is undergoing a vigorous expansion, currently includes NIH-funded research programs on AIDS, Lyme disease, tuberculosis, varicella, malaria, and Category A-C Select Agents, using chiefly nonhuman primates but also other animal models. The successful candidate will be expected to contribute to existing research programs and to build or bring his/her own independent research agenda. All necessary resources to assure that the candidate is successful will be provided including ample laboratory and office space.

The TNPRC has excellent infrastructure to support collaborative and independent research using nonhuman primates. In addition to holding one of the largest colonies of nonhuman primates in the country, the TNPRC is the only National Primate Research Center that houses a Regional Biosafety Laboratory, to support research under the NIH/NIAID National Biodefense Program. Research resources include extensive BSL2/ABSL2 and BSL3/ABSL3 facilities and highly integrated clinical and laboratory support for infectious disease studies using nonhuman primates. This includes a full time staff of clinical veterinarians and technicians and core services commonly used for infectious disease research including: (1) Diagnostic Parasitology (2) Vector-Borne Diseases (maintains arthropod vectors such as anopheline mosquitoes for malaria research, and tick-borne disease vectors), (3) DNA Microarray and Gene Expression, (4) Anatomic Pathology, (5) Clinical Pathology, (6) Molecular Pathology, (7) Confocal Microscopy and Image Analysis, (8) Flow Cytometry, (9) Cellular Immunology (10) Virus Characterization, Isolation and Production, (11) Pathogen Detection and Quantification, and (12) Infectious Disease Aerobiology. More information is available at the following link: **http://www.tnprc.tulane.edu/research_resou.html**.

To apply, send a letter indicating your research interests and experience, a curriculum vitae, and the names of three individuals who may be contacted for references to: **Ms. Rita Haynes, Coordinator, TNPRC Search Committee, Tulane National Primate Research Center, 18703 Three Rivers Road, Covington, LA 70433**; E-mail: **rita@tulane.edu**.

*Tulane University is an Affirmative Action and Equal Opportunity Educator and Employer. Women and minorities are strongly encouraged to apply.*

MRC Medical Research Council

UNIVERSITY OF OXFORD

# Director, MRC Human Immunology Unit

We invite applications from leading international scientists to succeed Professor Sir Andrew McMichael, as Director of the MRC Human Immunology Unit (HIU) when he stands down in 2010. The Unit has a long-standing reputation for excellence in science, particularly in the immunological bases of infectious diseases, cancer and autoimmunity. Its success has been underpinned by links with the Department of Medicine at the University of Oxford, enabling interactions that provide a blend of basic and clinical science and offer the opportunity to translate findings at a genetic/cellular level to *in vivo* investigations relevant to clinical medicine. Examples include the development of novel vaccines for influenza and HIV and new approaches to the treatment of cancer, multiple sclerosis, arthritis and eczema.

Housed in the Weatherall Institute of Molecular Medicine (WIMM) in Oxford University, the Unit will be one of the first MRC University Units from April 2010. Members of the Unit have excellent opportunities for interaction with other world-class medical scientists from a broad spectrum of disciplines and for sharing facilities e.g. for flow cytometry, structural biology, proteomics. The HIU currently has 11 research groups – each led by a clinical or non-clinical Principal Investigator – employing more than 100 staff and has an annual core funding from MRC of around £4m and an external grant income of £5.5m.

The new Directoral appointment is part of a strategic investment from MRC to support further development of translational activities within the WIMM and follows a strategic review of Human Immunology Research conducted across the UK. The review highlighted areas for new scientific development and it is envisaged that the MRC Unit and the broader environment at the WIMM will be at the forefront of such innovation.

The Director will be responsible for the over-arching research strategy in the MRC Unit, for providing an interactive and enabling environment for scientists at all levels of seniority, and for the core funding provided to the Unit by the MRC, which is subject to quinquennial review. He/she will also be expected to maintain a high level of additional, extramural funding. The Unit has provided training in immunology research for many clinical and non-clinical fellows and the Director would be expected to continue this.

You should:

- Be qualified to MD PhD or PhD level
- Already be, or on track to become a Fellow of the Royal Society, Fellow of the Academy of Medical Sciences or a national or international equivalent
- Possess a strong publication record in high impact journals, in a scientific field or fields related to human immunology
- Possess a broad knowledge of fundamental basic science and experience in bridging this with clinical medicine, understanding the implications of research for human disease and encouraging translational approaches where these are appropriate.

The Director will be employed at Professorial level by the University on terms and conditions commensurate with experience, and including a University pension. He/she will be expected to continue a personal programme of research in Human Immunology.

To discuss your interest in strict confidence, please contact Dr Kevin Young or Dr Marc Lambert quoting reference 09359 (Tel: +44 (0)1707 259333, email 09359@theRSAgroup.com).

**RSA**, The Melon Ground, Hatfield Park, Hatfield, Herts AL9 5NB
Tel +44 (0)1707 259333

RSA Executive Search

## Infectious Disease & International Health Section Chief

Dartmouth Medical School and Dartmouth-Hitchcock Medical Center (DMS/DHMC) invite applications for the position of Chief, Section of Infectious Disease & International Health within the Department of Medicine. This individual will lead the clinical, educational, and research missions of a comprehensive academic program. DHMC is a 400-bed tertiary care hospital in New Hampshire, with 500 medical and graduate students, and, along with its affiliate VA Medical Center, is a major teaching hospital for DMS. The successful candidate will be BC in Internal Medicine and Infectious Disease with active clinical responsibilities and have an outstanding record of scholarly achievement and original research and sustained extramural research funding. The candidate should also possess excellent interpersonal and mentoring skills as well as administrative acumen and experience. Applicants must qualify for a senior academic appointment as Associate or full Professor of Medicine at DMS. Additional research/academic opportunities include participation in: programs in international infectious diseases, such as the potential for involvement in the DarDar Programs in Tanzania on HIV and M. tuberculosis, and the Dartmouth-Boston University Fogarty AIDS International Training and Research Program. Other opportunities include extensive interactions with the faculty of Microbiology & Immunology, including a secondary academic appointment and collaborative participation in the research programs of faculty members; the NIH-funded Center of Biomedical Research Excellence in Molecular, Cellular, and Translational Immunological Research; The Dartmouth Institute; and Dartmouth College's Dickey Center of International Understanding. Additionally, the recent arrival of Dr. Jim Yong Kim, M.D., Ph.D. and leader of international health care initiatives, as the 17th President of Dartmouth College, provides an extraordinary opportunity for the new Chief of IDIH to interactively address health and infectious disease issues of global importance.

Candidates should submit a curriculum vitae along with a letter of application and the names of three references preferably using email to:

**Ronald Taylor, Ph.D., Chair, Search Committee**
**c/o Laurel Denison, Dept. of Medicine**
**Dartmouth-Hitchcock Medical Center**
**One Medical Center Drive, Lebanon, NH 03756**
**Ronald.K.Taylor@Dartmouth.edu**

Dartmouth-Hitchcock
MEDICAL CENTER

Dartmouth-Hitchcock Clinic is an Equal Opportunity/Affirmative Action employer and encourages applications from women and members of minority groups.

**www.dhmc.org**

---

MAYO CLINIC

*Heal the sick, advance the science, share the knowledge*

## Postdoctoral Fellowships in Cancer

### Mayo Clinic Cancer Center and College of Medicine

**Mayo Clinic in Rochester, Minnesota** announces new postdoctoral positions in cancer genetics/cancer genetic epidemiology. Positions will be funded by the Mayo Cancer Genetic Epidemiology Training Program, which is supported by a grant from the National Cancer Institute, and are 3 years in duration. Mentoring will be provided by experienced faculty, including cancer genetic epidemiologists, statistical geneticists, cancer geneticists, bioinformaticians and clinical mentors. The goal of this training program is to develop a new cadre of scientists capable of combining laboratory-based genetics and observational epidemiologic methods for developing independent careers that address cancer-related health issues, including prevention, detection, therapy and control. In addition to a stipend, the trainee will receive $15,000 per year for supplies. U.S. citizens or permanent residents only.

Located 80 miles southeast of the Minneapolis-St. Paul metro area, the Mayo Clinic is well regarded for its cancer research, which includes established resources such as the Rochester Epidemiology Project, and SPOREs in Prostate, Ovarian, Breast and Pancreatic cancers, Brain tumors, Lymphoma and Myeloma. The NCI-designated comprehensive Mayo Clinic Cancer Center (MCCC) provides extensive infrastructure support for patient-oriented research, including biostatistical support and shared analytical resources supporting population science, and well-equipped laboratories and cores. Please visit **http://mayoresearch.mayo.edu/mayo/research/cancercenter/** and **http://www.mayo.edu/** for more information.

Mayo offers an attractive benefit package. Salary is competitive, and will be determined by experience. Please send statement of interest and accomplishments, CV and the names of three references to:

**Gloria M. Petersen, Ph.D.**
**Director, Cancer Genetic Epidemiology Training Program**
***Mayo Clinic***
**200 First Street SW • Rochester, MN 55905**
**Phone: (507) 284-2896 • Fax: (507) 266-2478**
**E-mail: schuh.melissa@mayo.edu**

*Mayo Foundation is an affirmative action and equal opportunity employer and educator. Post-offer/pre-employment drug screening is required.*

---

# EVMS

**Eastern Virginia Medical School**

## ASSOCIATE PROFESSOR
### Cancer Biology

The newly established ***Cancer Biology and Infectious Disease Research Center*** at Eastern Virginia Medical School invites applications for the position of Associate Professor. We seek outstanding candidates with demonstrated excellence in cancer research as evidenced through peer-reviewed publication and external funding. The CBIDRC has existing strength in cancer translational research and capitalizes upon excellent clinical and basic science infrastructure. The CBIDRC also houses the George L. Wright Center for Biomedical Proteomics, which provides extensive expertise and resources for proteomics-based research. Candidates with expertise in cancer biology, cancer metastasis, treatment, molecular signaling or biomarker discovery using either proteomics and/or animal models are sought. However, all outstanding candidates in cancer research are encouraged to apply. EVMS will provide a competitive start-up package to the successful candidate.

Interested individuals should send a complete curriculum vitae, a statement of current and future research interests, and the contact information for three references to: **O. John Semmes, Ph.D., Director, Cancer Biology and Infectious Disease Center, Eastern Virginia Medical School, Lewis Hall 3110, 700 West Olney Road, Norfolk, VA 23507** or via e-mail: **brassidn@evms.edu**. Review of applications will begin **December 1, 2009**, and will continue until the position is filled.

EVMS was founded to improve health through teaching, discovering and caring. A collaborative culture at EVMS draws like-minded students, physicians and scientists from all over the country and encourages a multidisciplinary research approach with an emphasis on translational research.

*EVMS is an Affirmative Action/Equal Opportunity Employer and a drug-free/tobacco-free workplace.*

---

# DES MOINES UNIVERSITY

## FACULTY POSITION IN PHYSIOLOGY AND PHARMACOLOGY

The Department of Physiology and Pharmacology at Des Moines University seeks to fill a tenure track faculty position. Successful candidates must have demonstrated a commitment to and expertise in the discipline of physiology or pharmacology. Additionally, it is expected that the individual develop an innovative and extramurally funded research program utilizing contemporary approaches. Highly desirable applicants will have preparation and expertise in system-based physiology or pharmacology with experience and an interest in teaching cardiovascular, respiratory, renal or neuroscience topics for the medical, podiatric, and allied health curricula. Applicants must have an earned Ph.D. or equivalent and relevant postdoctoral experience.

For full consideration, candidates are invited to submit a letter of application stating their interest along with their curriculum vitae, a concise statement of teaching and research interests, educational philosophy and contact information for three references using the online applicant tracking system at **www.dmu.edu/employment**. Review of applications will begin on January 2, 2010 and continue until a successful candidate is identified and hired.

Candidates with questions specific to this position may contact the Search Committee Chair, **Dr. Matt Henry** at **515-271-1434** or **matthew.henry@dmu.edu**.

For complete job description, Faculty benefit summary and/or information on Des Moines University, please visit **www.dmu.edu/employment**.

*DMU is an EOE Employer.*

# TENURE-TRACK FACULTY POSITIONS

## Department of Biological Sciences

### Population Genetics, Assistant Professor

The Department of Biological Sciences at The University of Alabama invites applicants for a tenure-track faculty position at the rank of ASSISTANT PROFESSOR in POPULATION GENETICS (broadly-defined) to begin August 2010. All areas of empirical and/or theoretical population genetics will be considered. Candidates that integrate theoretical, mathematical approaches with empirical studies of natural populations are especially encouraged to apply. We seek a colleague with an exceptional research record in population genetics, quantitative genetics, ecological or evolutionary genetics, or similar evolutionary subfield.

Candidates must have a Ph.D. and post-doctoral research experience. The successful applicant will be expected to establish an active, externally-funded research program that includes graduate and undergraduate student mentoring. Teaching responsibilities will likely include an undergraduate core course in Genetics and a graduate course in the successful applicant's area of expertise. The successful applicant will interact with a wide variety of biologists across the department's two sections: Ecology, Evolution, and Systematics, and Molecular and Cellular Biology.

A complete application includes 1) an application letter with a list of at least three references (including contact information), 2) CV, 3) statement of research interests and goals, and 4) statement of teaching interests and philosophy. To apply, go **to https://facultyjobs.ua.edu,** complete the online application (Job # 0802695), and upload your CV. Send all of the materials (including CV) as .pdf attachments to **bsc-search@ua.edu** using "Population Genetics" in the subject line. Potential candidates may contact the chairperson of the search committee, Dr. Leslie J. Rissler at **Rissler@bama.ua.edu** or 205-348-4052, if additional information is required. Consideration of applications will begin 15 December 2009, and continue until the position is filled.

### Natural Resources Management/Wildlife Biology, Assistant/Associate Professor

The Department of Biological Sciences at the University of Alabama invites applications for a tenure-track faculty position in WILDLIFE BIOLOGY/NATURAL RESOURCES MANAGEMENT at either the rank of ASSISTANT or ASSOCIATE PROFESSOR to start August 2010. The successful candidate will serve as Director of the Natural Resource Management Minor (**http://www.as.ua.edu/naturalresource/index.html**) and oversee the development of the Tanglewood Outdoor Classroom/J. Nicholene Bishop Biological Field Station. The candidate will be expected to establish an active, externally-funded research program with a focus on natural or managed forest ecosystems and/or the conservation of species or ecosystems. In addition to teaching courses for the Natural Resource Management Minor and contributing to the departmental teaching mission, the candidate will also direct internships and undergraduate and graduate research. The successful candidate will interact with the department's faculty and other faculty in the College of Arts and Sciences and in the Culverhouse College of Commerce and Business Administration.

Candidates must have a Ph.D. in biology, fisheries, wildlife, forestry, or related fields and postdoctoral or relevant practical experience in natural resources management at the local, state, and/or federal level.

A complete application includes 1) an application letter with a list of references, 2) CV, 3) statement of research interests and goals, 4) statement of teaching interests and philosophy. To apply, go to **https://facultyjobs.ua.edu**, complete the online application (Job # 0802694), and upload your CV. Send all of the materials (including CV) as pdf attachments to **bsc-search@ua.edu** using "Wildlife Biology" in the subject line. Potential candidates may contact the chairperson of the search committee, Dr. Stephen Secor at **ssecor@biology.as.ua.edu** or 205-348-1809, if additional information is required. Consideration of applications will begin 15 December 2009, and continue until the position is filled.

### Genomics, Assistant Professor

The Department of Biological Sciences at the University of Alabama invites applications for a tenure-track position at the ASSISTANT PROFESSOR level in GENOMICS to begin August 2010. We seek a person who employs whole-genome, proteomic and/or metabolomic approaches to study fundamental problems in cell biology, developmental biology, genetics, microbiology, organismal biology and/or evolution. The successful candidate will be expected to establish a research program of high quality and impact and contribute to the teaching mission of the department.

A complete application includes 1) an application letter with a list of at least three references (including contact information), 2) CV, 3) statement of research interests and goals, and 4) statement of teaching interests and philosophy. To apply, go to **https://facultyjobs.ua.edu**, complete the online application (Job # 0802696), and upload your CV. Send all of the materials (including CV) as pdf attachments to **bsc-search@ua.edu** using "Genomics" in the subject line. Potential candidates may contact the chairperson of the search committee, Dr. Edwin Stephenson at **estephen@bama.ua.edu** or 205-348-1828, if additional information is required. Consideration of applications will begin 15 December 2009, and continue until the position is filled.

For information about the department visit our website at **http://www.as.ua.edu/biology/**

The University of Alabama is an Equal Opportunity/Affirmative Action Employer. Women and minorities are encouraged to apply.

touching lives
THE UNIVERSITY OF ALABAMA

## NYU School of Medicine

The Department of Surgery at NYU Langone Medical Center is seeking to recruit a Basic Scientist, for The Helen and Martin Kimmel Division of Wound Healing & Regenerative Medicine under the direction and leadership of **Harold Brem, MD**.

The Division of Wound Healing is seeking to fill several faculty positions at the rank of Assistant, Associate or Full Professor for scientists that use cellular and/or molecular-genetic approaches to address fundamental aspects of Wound Healing and Regenerative Medicine. The research laboratory is extremely collaborative with numerous resources in place. The program is purely translational and literal bridge to the operating room exists. Candidates with a background in wound healing, angiogenesis, pathology, stem cell biology, and regenerative cardiovascular medicine using mammalian systems or genetic approaches are especially encouraged to apply. Competitive salary, laboratory space and start-up funds are available. Candidates are expected to have a track record from the NIH. A PhD, MD, PhD/MD (or equivalent) is essential.

**Website: www.nyuwound.org**

Interested individuals should send their resume to the **Helen and Martin Kimmel Program Manager, Tracy Henry** via email to **tracy.henry@nyumc.org**.

---

## NYU School of Medicine

**Bioinformatics:**
Applications are sought in Bioinformatics for NIH funded researcher to work with **Dr. Harold Brem**, Division Chief of the Helen and Martin Kimmel Wound Center at New York University School of Medicine Department of Surgery- Division of Wound Healing and Regenerative Medicine.

**Responsibilities and Duties:**
- Data Analysis
- Develop algorithms and software tools in support of project research objectives
- Participating in writing project updates, reports, proposals and scientific articles
- Correlate Wound Electronic Medical Record (WEMR) data to clinical outcomes
- Collaborating with investigators within and outside the program, in furtherance of project objectives

**Requirements:**
Applicants must hold a MD or PhD degree in Bioinformatics, Biology, Engineering, Physics, Computer Science, Mathematics or a related scientific discipline pertinent to the position. Experience with bioinformatics methods, tools, websites and data resources highly desired. Track record from NIH preferred.

Qualified candidates should send your CV to the **Helen and Martin Kimmel Program Manager Tracy Henry** via email to **tracy.henry@nyumc.org**.

---

## CSH

### Cold Spring Harbor Laboratory
### Center for Quantitative Biology

# PROGRAM CHAIR

Cold Spring Harbor Laboratory (CSHL) has recently initiated a new Center for Quantitative Biology (CQB). CQB faculty are applying mathematical, statistical and computational methods to problems in biology ranging from genomics to neurobiology, and from single molecule to single cell to systems analysis. Members of the CQB will interact closely with other CSHL researchers.

We are currently seeking a senior scientist with strong training and experience in applied quantitative methods to take a leadership role in the Center and serve as Program Chair. Candidates should possess outstanding communication skills as well as broad biological interests that will enable them to facilitate interactions between biologists and quantitative scientists. Their research interests should be compatible with the existing CSHL research programs, which include, but are not limited to, cancer, neuroscience, plant biology, and population genetics. Candidates with expertise in genomic approaches to these areas are especially encouraged to apply.

This is a unique opportunity to help guide and build this new effort at CSHL. The Program Chair will be provided with the resources and support necessary to develop a world-class program that will contribute to and enhance the interactions between biology and mathematical and physical sciences.

*To apply for this position:*

Please send a letter of interest, CV, statement of research interests and contact information for three references via email with the subject line QB PROGRAM CHAIR SEARCH to the following address: **QBjobs09@cshl.edu**

CSHL is an Equal Opportunity/Affirmative Action Employer

**For more information: www.cshl.edu**

---

# Assistant Professor
# Neurobiology and Behavior

Stony Brook University's Department of Neurobiology and Behavior is continuing a major initiative in neuroscience with recruitment of a tenure-track faculty member at the assistant professor level in 2010. Outstanding scientists who study any aspect of systems neuroscience, with a particular emphasis on computational and theoretical approaches, will be considered.

Successful candidates will join an active and diverse group of neuroscientists at Stony Brook University and its affiliated institutions and will participate in the Department's research mission and in undergraduate, graduate, or medical school teaching. Exceptional packages include state-funded salary and benefits; newly renovated lab space; and generous start-up funding supported in part by a New Faculty Recruitment Award from NINDS, NIH as part of the American Recovery and Reinvestment Act (ARRA).

Applicants must have a Ph.D. or equivalent degree and postdoctoral experience. Review of applications starts immediately and will continue until the position is filled.

**For a full position description, application procedures, or to apply online, visit**: *www.stonybrook.edu/jobs* (JOBS Reference #: F-6116-09-11) or send a curriculum vitae, statement of research interests, and contact information for three references to: Faculty Search Committee, Department of Neurobiology and Behavior, Life Sciences Building Room 573, Stony Brook University, Stony Brook, NY 11794-5230

Fax: (631) 632-6661

Equal Opportunity/Affirmative Action Employer. Women, people of color, individuals with disabilities, and veterans are encouraged to apply.

STONY BROOK

---

## UNIVERSITY *of* CALIFORNIA, SAN DIEGO
## SCHOOL OF MEDICINE

The Division of Biological Sciences at UCSD and the Neurosciences Department in the UCSD School of Medicine invite applications for two open faculty positions in the area of

**NEURAL CIRCUITS AND BEHAVIOR**

We are seeking outstanding candidates interested in the development, organization, and function of neural circuits, and how they may be affected in nervous system disorders. Applicants must have an excellent record of research productivity and demonstrate the ability to develop a rigorous research program. We are particularly interested in applicants employing new technologies to explore the organization of neural circuits in rodent models. All applicants must have a Ph.D. or equivalent degree and a commitment to teaching at the undergraduate and graduate levels. Appointments will be at the Assistant Professor level with salary based on the published UC pay scale. Successful applicants will be provided with generous startup packages and laboratory space.

Applications received by **November 30, 2009** will be assured of consideration. Applications should comprise of a single .pdf file containing a CV, a statement of current and proposed research and teaching (not to exceed 4 pages), copies of up to 3 recent publications, and the names and addresses of three references, and should be submitted via email to: **nsearchc@ucsd.edu** with "Neural Circuits-candidate name" as the subject line. Please arrange for three letters of reference to be sent to: **nsearchz@ucsd.edu** with the "Reference-candidate name" on the subject line.

These positions are supported in part by a New Faculty Recruitment (P30) award from the National Institute of Neurological Diseases and Stroke, NIH, as part of the American Recovery and Reinvestment Act (ARRA)

*UCSD is an Equal Opportunity-Affirmative Action Employer with a strong institutional commitment to the achievement of diversity among its faculty and staff; applicants are also invited to summarize their own contributions to diversity.*

# Effective Lab Skills WEBINAR

## MANAGING PEOPLE, PROJECTS, AND MONEY

**December 2, 2009**
**12 noon Eastern Time**
**(9 a.m. Pacific, 5 p.m. GMT)**

Academic scientists face many challenges when it comes to running their own lab. Beyond doing good research, lab heads need to consider many practicalities, including managing staff (hiring, retaining, motivating), developing reasonable timelines for projects and keeping them on schedule, and tracking grant budgets.

Watch this *Science* Careers live webinar to gain insight from experts related to effective laboratory management skills. Don't miss this opportunity to pick the brains of experienced and practiced academic managers.

Questions can be submitted live to the panel during the webinar or in advance via e-mail provided with registration. To register, visit **www.sciencecareers.org/webinar**

**Participating Experts:**

**Karen M. Hill, Ph.D.**
*Assistant Professor*
Howard University
Washington, DC

**Klaus Nüsslein, Ph.D.**
*Associate Professor*
University of Massachusetts at Amherst
Amherst, MA

**Kelly Suter, Ph.D.**
*Associate Professor*
University of Texas at San Antonio
San Antonio, TX
*ScienceCareers.org Forum adviser*

Produced by the
*Science*/AAAS Business Office.

Science Careers
From the journal *Science* AAAS

DUKE NUS
GRADUATE MEDICAL SCHOOL SINGAPORE

**Faculty Positions in Neuroscience and Behavioral Disorders (Open Rank)**

The Duke-National University of Singapore Graduate Medical School (Duke-NUS GMS) invites applicants for positions in its new Neuroscience and Behavioral Disorders Program. In partnership with Duke University, the National University of Singapore and the Singapore Agency for Science, Technology and Research (A*STAR), we are seeking especially qualified researchers working on a range of topics in neuroscience and cognitive neuroscience. Duke-NUS is located on a modern campus that includes Singapore's largest hospital and several national research centers. In addition, the A*STAR-Duke-NUS Neuroscience Research Partnership links on the Duke-NUS Program with the resources at the nearby Biopolis research campus. Depending on their research interests, the faculty can be located on either campus. Opportunities exist for translational studies in collaboration with faculty at the Singapore General Hospital, the National Neuroscience Institute and the Institute of Mental Health. The overall mission is to conduct high-level basic and translational research, and to train graduate students, postdoctoral fellows, and physician-scientists in neuroscience. Further information about the strength of the neuroscience environment in Singapore can be found at **www.duke-nus.edu.sg.**

Applicants should have a PhD, MD or equivalent and a record of outstanding promise and achievement. Positions include full salary as well as generous start-up and ongoing research funding to assure a stable base of support to be supplemented by competitive grant awards. Candidates should submit, by March 1, 2010, a cover letter, curriculum vitae, summary of research accomplishments and an outline of future plans to:

**Dale Purves MD,**
**Director, Program in Neuroscience and Behavioral Disorders**
**Executive Director, A*STAR Partnership in Neuroscience**
**Duke-NUS Graduate Medical School Singapore**
**8 College Road, Singapore, 169857**
**email: NBD.Recruit@duke-nus.edu.sg**

MBL Biological Discovery in Woods Hole

ASSISTANT/ASSOCIATE AND SENIOR SCIENTISTS

## Regenerative Biology

The Marine Biological Laboratory (MBL) in Woods Hole, Massachusetts, is seeking outstanding, highly innovative candidates for Assistant, Associate, and Senior Scientist positions in a newly established Regenerative Biology program. The MBL is a leading international, independent, nonprofit institution dedicated to biological discovery and to improving the human condition through creative research and education in the biological, biomedical and environmental sciences.

Successful candidates are expected to develop independent research programs in the areas of regenerative biology, tissue regeneration, aging, and related fields, focusing in particular on marine and aquatic models. Areas of emphasis include, but are not limited to gene regulatory and systems analysis, genomics, comparative evolutionary biology, advanced imaging, and computational approaches. Exploration of collaborative opportunities and synergies with other research programs at the MBL is expected.

Applicants must have a Doctorate in biology or a related field, a strong record of scientific research and publication, and the potential to attract extramural funding to support an independent research program.

More information about the MBL is available at **www.mbl.edu.** Complete position announcement and application information is available at **https://mbl.simplehire.com.**

*The MBL is an Equal Opportunity/Affirmative Action Employer.*

UMEÅ UNIVERSITET

## Umeå University announces...

At Umeå University, Sweden, world-leading research is conducted within several areas. We offer an attractive range of courses and programmes taught in a quality study environment. The Umeå University campus is a creative and exciting place of work and study for our 4,000 employees and 33,000 students.

## Assistant professor in the field of printed organic electronic devices

**The Department of Physics** is now accepting applications for a position as assistant professor in the field of printed organic electronic devices. The new research program has received funding for the salary costs of the successful applicant and two PhD students for five years. The opportunities for additional start-up funding in the range €500,000 – 1,000,000 are considered good.

The application can be submitted either electronically or in paper form and should contain the following items: (i) A curriculum vitae, (ii) A publication list, (iii) A list of persons (with contact details) willing to provide oral or written recommendations, (iv) A statement of previous research achievements and teaching merits, (v) A research plan (maximum 4 pages), (vi) Copies of degree certificates, (vii) Reprints/copies of selected publications, numbered according to the publication list.

For more information, contact Professor Ludvig Edman, e-mail: ludvig.edman@physics.umu.se.

Your complete application, marked with **reference number 312-1019-09**, should be sent to jobb@umu.se or to the Registrar, Umeå University, SE-901 87 Umeå, Sweden to arrive **December 15, 2009** at the latest.

We look forward to receiving your application!

For further information: **www.phys.umu.se/opeg/ad.pdf**

City of Hope

**Assistant/Associate Professor**

The Division of Translational Vaccine Research invites applications for a tenure-track faculty position in any area of cancer vaccine research. Applicants with proven accomplishments in vaccine development or immunologic studies applicable to solid tumors in mouse models or humans are especially encouraged to apply. Applicants must be qualified for Cancer Center membership, while effectively developing an extramurally funded translational research program. Interaction among other members of the division is facilitated by an open floor-plan laboratory with dedicated space for the successful candidate. City of Hope offers a competitive start-up package including faculty salary and research support, commensurate with experience. A start date in the 2010 academic year is anticipated.

A Ph.D. or M.D. is required for this position as well as a fluency in spoken and written English. Qualified applicants should submit a statement of research interests, experience, current curriculum vitae, and names/addresses of three references to:

**Vaccine Research Faculty Search Committee**
**c/o Ms. Kim Lu**
**Research Operations**
**City of Hope**
**1500 E Duarte Road**
**Duarte, CA 91010.**
**E-mail: facultyrecruit@coh.org**

*City of Hope, a non-profit research and educational institution, and an NCI-designated Comprehensive Cancer Center, is located 25 miles northeast of Los Angeles. City of Hope offers a competitive salary and benefits package. City of Hope is an Affirmative Action/Equal Opportunity Employer.*

# FACULTY OF MEDICINE AND HEALTH SCIENCES
# UNITED ARAB EMIRATES UNIVERSITY
## Professor & Research Team
## CLINICAL EPIDEMIOLOGY

**The Faculty of Medicine & Health Sciences (FMHS)** at the United Arab Emirates University is seeking to appoint a top academic in Clinical Epidemiology for developing research efforts to enhance research productivity and strengthen the research ranking of the University. Eligible candidates should be leaders of high standing in their field, and must have a strong track record of successful research funding, and publications in peer-reviewed high impact factor journals. The successful applicant will establish a team of 2-3 researchers to initiate new research portfolios, and to work with academic staff of the Faculty of Medicine.

**The post** is based at the FMHS, United Arab Emirates University premises in the oasis city of Al-Ain (Abu Dhabi emirate). The UAE is an open and tolerant society and one of the most attractive places to live and work in the Middle East. Faculty academic staff receive a tax-free salary and allowances, generous leave, free housing with support for furnishings, family health insurance, annual airfares, educational assistance for up to three children, and support for attendance at international conferences. The final package will be open to negotiations.

**The Candidate:** An expert with at least 10 years of practical and research experience in the field of clinical epidemiology is required. Consultant status at the local hospitals will be sought for successful medical applicants. The priority task for the appointee will be to contribute to the research strategy of the FMHS. The epidemiological component of current research initiatives includes the leading causes of morbidity and mortality in the UAE e.g. genetic and congenital disorders, trauma, cancer, mental disorders and stress, maternal and child health, chronic and infectious diseases, occupational and environmental health. Non-medical applicants with relevant experience and qualifications will also be considered.

**Informal enquires** may be made to:
**Professor Tar-Ching Aw,** Chair of the Department of Community Medicine, FMHS. **(Email: Tcaw@uaeu.ac.ae)**

**Further details** about the position may be obtained by accessing the FMHS website **http://www.fmhs.uaeu.ac.ae/vacancy.asp**

**The FMHS operates an on-line recruitment system and all applications must be submitted electronically**

**Equal Opportunity Employer**

---

DANA-FARBER CANCER INSTITUTE

**DANA-FARBER CANCER INSTITUTE**
**Dedicated to Discovery...Committed to Care.**

### ASSISTANT PROFESSOR

The Department of Medical Oncology's Division of Molecular and Cellular Oncology is inviting applications for a full-time appointment at the Assistant Professor level. This individual will develop an independent disease-based laboratory research program focused on solid tumors and will interface with the relevant clinical research program within the Division of Solid Tumor Oncology. Candidates with an interest in gastrointestinal malignancies are especially encouraged to apply.

The candidate must have an MD and/or PhD and a proven track record of outstanding laboratory research. Interested applicants should direct their curriculum vitae, a research plan and 3 letters of reference to: **Myles Brown, MD, Chief, Division of Molecular and Cellular Oncology, Dana-Farber Cancer Institute, 44 Binney St. Boston, MA 02115.** Please send submissions via email to: **MCO_SEARCH@DFCI.HARVARD.EDU**

*DFCI is an Affirmative Action/Equal Opportunity Employer, appreciates a diverse work force and encourages all qualified applicants to apply.*

HARVARD MEDICAL SCHOOL

---

WILDLIFE TRUST

### Wildlife Trust announces 11 New Positions in Emerging Disease Ecology

Wildlife Trust is expanding its research programs in emerging disease ecology and seeks outstanding candidates for eleven positions. Full position descriptions available at **www.wildlifetrust.org/jobs**.

#### SEVEN SCIENCE AND RESEARCH POSITIONS

- **Senior Disease Ecologist, Conservation Biologist or Veterinarian** with a Ph.D or DVM/Ph.D and substantial experience managing international conservation and disease ecology research and field programs. Duties include management of field teams and building an independent research program on infectious disease ecology and conservation biology in emerging disease hotspots (S. America, S. Asia, SE. Asia).
- **Four positions: Post Doctoral Field Ecologist/Epidemiologist/Veterinarian** to conduct research on emerging diseases and run field programs in S. America, S. Asia, and SE. Asia surveying wildlife for our new USAID PREDICT program. Must have experience working in developing countries. Experience with free-ranging wildlife is preferred.
- **Post Doctoral Modeler/Epidemiologist/Ecologist** to study the dynamics of pathogens in wildlife, humans and domestic animals. Excellent spatial statistical and dynamic modeling skills required.
- **Modeling Research Assistant (graduate-level)** to analyze dynamics of pathogen spillover from wildlife and livestock to people. Strong statistical or dynamic modeling background required. Epidemiological skills an advantage.

#### TWO MOLECULAR BIOLOGY POSITIONS IN PATHOGEN DISCOVERY

Based at the Center for Infection and Immunity, Columbia University, in Prof. W. Ian Lipkin's laboratory, jointly supervised by Dr. Peter Daszak, Wildlife Trust.

- **Post Doctoral Molecular Biologist** to employ cutting edge technology to discover novel viral pathogens in wildlife samples. Ph.D. in Biological or Molecular Sciences and strong laboratory background are required.
- **Laboratory Technician** to employ cutting edge technology to discover novel viral pathogens in wildlife samples. MS in Biological or Molecular Sciences and strong laboratory experience are required.

#### TWO ADMIN. POSITIONS AT WILDLIFE TRUST NEW YORK CITY HEADQUARTERS

- **International Grant and Program Manager**, responsible for federal grant administration, logistical operations for research programs, and international project coordination. International travel is required. B.S. or M.S. degree in a suitable field.
- **Program Assistant**, to manage office functions in New York. Candidate must have excellent organizational and communication skills. Experience in financial management and IT is an advantage.

Further details can be found at **www.wildlifetrust.org/jobs**. All positions are based in New York and require some international travel. Review of applications will begin **November 15, 2009**. Candidates should submit, in one attached document, a full *CV*, names and email addresses of 2 academic references, and a 2-page cover letter by email to **jobs@wildlifetrust.org** stating clearly the position of interest and career goals.

## POSITIONS OPEN

# Yale

### YALE UNIVERSITY
### MICROBIAL DIVERSITY INSTITUTE

To further the development of its West Campus research enterprise, Yale University is seeking tenure-track **ASSISTANT PROFESSORS** for a new Microbial Diversity Institute. Faculty associated with this Institute will have primary appointments in any of several life science and physical science departments within the Faculty of Arts and Sciences, the School of Engineering and Applied Sciences, the School of Forestry and Environmental Studies, and the School of Medicine. Candidates must have a Ph.D. or equivalent degree in a relevant discipline and a record of research that demonstrates originality in addressing significant questions in the study of microbial interactions in the environment or with other organisms. Relevant research areas include, among others, functional and comparative genomics, environmental microbiology, geomicrobiology, and microbial physiology or pathogenesis, and may focus on any group of microorganisms, including viruses, bacteria, archaea, or eukaryotes. To apply, please submit a statement of research interests, complete curriculum vitae, and up to five reprints of published work, and arrange for three letters of recommendation to be sent to: **The Microbial Diversity Search Committee, c/o Michael Donoghue, Vice President for West Campus Planning and Program Development, 1 Hillhouse Avenue, New Haven, CT 06520.** Application materials may also be sent electronically to **e-mail: kelly.locke@yale.edu** with the subject heading Microbial Diversity Search. The review of applications will begin on January 15, 2010. *Yale University is an Affirmative Action, Equal Opportunity Employer. Yale values diversity among its faculty, students, and staff and strongly encourages applications from women and underrepresented minorities.*

### ASSISTANT PROFESSOR
### Massachusetts Institute of Technology
### Department of Chemical Engineering

The MIT Department of Chemical Engineering (**website: http://web.mit.edu/cheme/**) invites applicants to apply for a tenure-track faculty position at the Assistant Professor level, to begin July 2010 or thereafter. Applicants should hold a Ph.D. in chemical engineering or a related field by the beginning of the appointment period. In special cases, a more senior faculty appointment may be possible. The Department is particularly interested in candidates with energy and systems engineering interests. The candidate should have demonstrated excellence in original research. Faculty duties include teaching at the graduate and undergraduate levels.

Interested candidates should submit application materials electronically at **website: https://chemefacsrch.mit.edu**. Each application should include: curriculum vitae, the names and addresses of three or more references, a strategic statement of research interests, and a statement of teaching interests. We request that each candidate arrange for reference letters to be uploaded at **website: https://chemefacsrch.mit.edu/letters/**. Questions should be addressed to **e-mail: cheme-searchmaster@chemefacsrch.mit.edu**. Responses received by December 1, 2009, will be given priority.

*We especially encourage minorities and women to apply because of MIT's strong commitment to diversity in engineering education, research, and practice.*

University of North Carolina–Chapel Hill **POSTDOCTORAL ASSOCIATE** position available immediately to study immune evasion by *F. tularensis*. Prefer recent Ph.D. in either cellular immunology interested in learning about bacterial pathogenesis, or in bacterial pathogenesis interested in immunology. *Select Agent research requires U.S. citizenship.*

Please submit curriculum vitae and references to **e-mail: jfrelin@med.unc.edu.**

*UNC is Equal Opportunity Employer.*

## POSITIONS OPEN

BARROW Neurological Institute

### NEUROSCIENCE RESEARCH

The Barrow Neurological Institute is seeking accomplished investigators to complement the preclinical neuroscience research enterprise at a unique and dynamic institution. Qualified applicants holding an M.D., Ph.D., or equivalent degree will be considered as appropriate for appointment at the **ASSISTANT, ASSOCIATE,** or **FULL PROFESSOR** levels. Successful candidates will be expected to orchestrate a program of extramurally funded, independent research and to assume educational and administrative responsibilities. The specific area of investigation is open, although institutional strategic interests include translational research in neurostimulation and in neurotrauma. Please send either an initial letter of inquiry in confidence or a full application including vita, names and addresses of three references, and brief statements of research experience, interests, and career objectives to: **R.J. Lukas, Ph.D., Vice President of Research, Barrow Neurological Institute and St. Joseph's Hospital and Medical Center, 350 W. Thomas Road, Phoenix, AZ 85013. E-mail: bnisearch@chw.edu.** *Affirmative Action/Equal Opportunity Employer.*

### RESEARCH ASSISTANT PROFESSOR OF MEDICINE
### (Experimental Therapeutics)

The Division of Experimental Therapeutics in the Department of Medicine at the University of Pennsylvania School of Medicine seeks candidates for an Assistant Professor position in the nontenure research track. Applicants must have an M.D. or M.D.-Ph.D. degree and have demonstrated excellent qualifications in research.

The successful applicant will have experience in the field of experimental therapeutics. Responsibilities include conducting complex studies on the clinical pharmacology of lipid peroxidation and cyclooxygenase-2 inhibition with particular interest in how isoprostanes are modulated by omega-3 polyunsaturated fatty acids (fish oil) and ethanol, and how the cardiovascular risk profile of cyclooxygenase-2 inhibitors might be attenuated by coincidental inhibition of carbonic anhydrase. The successful candidate will conduct mechanistic studies in human and animal models and in cell culture. Knowledge of drug development on both sides of the translational divide between basic and clinical research is crucial. The successful candidate must have the ability to obtain and maintain extramural funding.

Apply for this position online at **website: http://www.med.upenn.edu/apps/faculty_ad/index.php/g323/d2144**.

*The University of Pennsylvania is an Equal Opportunity, Affirmative Action Employer. Women and minority candidates are strongly encouraged to apply.*

### SCIENCE TEACHER EDUCATION FACULTY POSITIONS

The University of Nebraska–Lincoln seeks to fill up to three tenured/tenure-track positions to support a major commitment to enhancing science teacher education. Individuals with a Ph.D. or Ed.D. in a field of science (physical, earth, life, agricultural, or natural resources sciences) and/or education and a demonstrated record of scholarly achievement are urged to submit their applications. Visit **website: http://nuteach.unl.edu** for complete job description.

To apply, go to **website: http://employment.unl.edu (requisition 090148)** and complete the faculty academic administrative information form. Attach a letter of application; curriculum vitae; and a personal statement describing your research and teaching interests and experience. Arrange for three letters of reference to be submitted electronically to **e-mail: bwest1@unl.edu**. Review of applications will begin December 15, 2009, and continue until all positions have been filled or the search is closed.

*The University of Nebraska has an active National Science Foundation ADVANCE Gender Equity program, and is committed to a pluralistic campus community through Affirmative Action, Equal Opportunity, work-life balance, and dual careers.*

## POSITIONS OPEN

Sea Grant California

### CALIFORNIA SEA GRANT DIRECTOR

The University of California (UC) System through its San Diego campus invites applications for the full-time position of Director of the California Sea Grant College Program. The program is the largest of the 32 Sea Grant programs throughout the nation and is supported by the National Oceanic and Atmospheric Administration, State of California, and University of California.

Salary and benefits are competitive and commensurate with experience and qualifications and are based on the UC San Diego pay scales.

Application procedure: Nominations and applications are invited. Applicants should provide a letter of application, curriculum vitae, immigration status, and the names, addresses, telephone numbers, and e-mail addresses of no fewer than four references to:

**Chair of Sea Grant Search Committee**
**Scripps Institution of Oceanography**
**9500 Gilman Drive, Department 0232**
**University of California, San Diego**
**La Jolla, CA 92093-0232**

Electronic applications are welcome and may be sent to **e-mail: csgdirrecruit@ucsd.edu**.

The search committee will begin reviewing applications on January 15, 2010.

Please see **website: http://www.csgc.ucsd.edu/ABOUTUS/DirectorRecruitment.html** for more information.

### OPEN-RANK FACULTY
### Department of Biological Sciences
### University of Delaware

The Department of Biological Sciences at the University of Delaware is seeking to fill an open-rank Faculty Position. The University, as a member of the Delaware Health Science Alliance (**website: http://www.delawarehsa.org/**), has established research initiatives in cardiovascular biology, rehabilitation medicine, neuroscience, and cancer biology for which the Department of Biological Sciences plays a central role. Priority will be given to those applicants whose area of research focus is translational biology in cardiovascular or rehabilitation medicine.

Requirements for the position include a Ph.D. or equivalent degree, a minimum two years of postdoctoral experience, and a strong commitment to both research and education at the graduate and undergraduate levels. A successful candidate is expected to develop or continue an active research program, pursue extramural funding, and participate in undergraduate and graduate education.

This position will occupy recently renovated laboratory space, receive a competitive salary and startup package, and have access to state-of-the-art core facilities within the Department (**website: http://www.bio.udel.edu/**), the Center for Translational Cancer Research (**website: http://www.udel.edu/ctcr/**), and the Delaware Biotechnology Institute (**website: http://www.dbi.udel.edu/**). The Department of Biological Sciences consists of 35 faculty and currently has 90 students in its M.S./Ph.D. program.

Please submit complete curriculum vitae, a two- to three-page description of research interests and plans as well as one to two pages of teaching plans, and the names of three references with contact information either to: **Dr. Ulhas P. Naik, Chair, Search Committee, Department of Biological Sciences, University of Delaware, Newark, DE 19716-1590** or to our **website: http://www.udel.edu/bio/news/facultysearch/**. Review of applications will begin upon receipt, but the application deadline is December 31, 2009. The starting date for this position is September 1, 2010.

*The University of Delaware is an Equal Opportunity Employer which encourages application from minority group members and women.*

# UNIVERSITY OF KONSTANZ

The University of Konstanz is one of the nine Universities of Excellence in the Federal Republic of Germany.

The Department of Biology in the Faculty of Science offers *two* vacancies for professorships to be filled **as soon as possible:**

## Professor (W3) for Chemical Ecology

This professorship is expected to cover teaching and research in the area of molecular communication at the intra- and interspecies level. We are looking for an internationally recognized researcher working, e.g., on the recognition of chemical signal compounds or the integration of the coded information into physiological reactions or the behaviour of organisms.

## Professor (W3) for Ecology

This position is supposed to cover teaching and research in the area of organismic interactions, using modern experimental methods. Research is expected to center around plant ecology, phytopathology, mycology, limnology or terrestrial ecology.

Further information is available on the Homepage of the University. **http://www.uni-konstanz.de/stellen .**

Applications including a completed submission form (URL), CV, list of publications, teaching experience, copies of degree certificates, a research plan for the next five years and reference to **Position 2009/164** must reach the Faculty of Science, University of Konstanz, 78457 Konstanz, Germany, **by December 31st, 2009** in electronic form (e.g. pdf.file).
E-mail: **prof-2009-164@uni-konstanz.de** .

### Cancer Research Center of Hawaii
### TENURE-TRACK CANCER EPIDEMIOLOGIST

The Epidemiology Program, Cancer Research Center of Hawaii (**www.crch.org**), University of Hawaii, is seeking a senior epidemiologist for appointment at the level of Full or Associate Professor. The Program emphasizes the ethnic and cultural diversity of Hawaii which provides a unique focus to the research, particularly the role of nutritional factors that may influence the risk of cancer. Interactions between lifestyle and external factors, such as infectious agents, or host susceptibility factors, such as genetic polymorphisms, are other established areas of activity. The Program has a strong molecular component that provides investigators with the capability to include in their studies state-of-the-art laboratory assays for nutritional exposures, biochemical markers, genetic variants, infectious agents, and hormones. Consistent with the interests and activities of the faculty, the Program includes particular expertise in molecular and infectious disease epidemiology, molecular genetics, nutrition, biostatistics and bioinformatics. Established resources with extensive biorepositories, including the Multiethnic Cohort, two Human Papillomavirus Cohorts, the Hawaii Colorectal Cancer Family Registry, and the Hawaii Tumor Registry, offer excellent research opportunities for new faculty members.

Candidates should have an outstanding record of accomplishment for their current rank, and will be expected to have transferable nationally peer-reviewed funding. Expertise in molecular and/or translational aspects of cancer epidemiology will be given highest priority. Applicants must have a doctoral degree in Epidemiology, Medicine, or a related field. The position is tenurable and includes an attractive start-up package; salary is negotiable.

Applicants should send a curriculum vitae and a statement of current and future research interests to **facultyjobs@crch.hawaii.edu** or **Search Committee, Cancer Research Center of Hawai'i, 1236 Lauhala Street, Suite 510, Honolulu, HI 96813.**

*An Equal Opportunity/Affirmative Action Employer.*

### THE PEDIATRIC DENGUE VACCINE INITIATIVE
### INTERNATIONAL VACCINE INSTITUTE

### POSITION ANNOUNCEMENT
### DIRECTOR

The Pediatric Dengue Vaccine Initiative (PDVI), a program hosted by the International Vaccine Institute (IVI), Seoul, Korea, is seeking a Director to oversee its development and operations. The PDVI has as its objective, to facilitate and accelerate the development and introduction of safe and effective dengue vaccines in developing countries. The PDVI has several programmatic components: 1) supportive research to facilitate the clinical testing of dengue vaccines by developing and improving immunological and diagnostic assays; 2) evaluation research focusing on development of field sites in dengue-endemic countries where clinical testing of dengue vaccines can take place and on field evaluations of dengue diagnostics and assays; 3) vaccine product development partnerships to achieve products designed for and affordable to dengue-endemic countries; and 4) activities to assure access to dengue vaccines, including research to better define the global dengue disease burden and disease costs, to model the potential cost-effectiveness of dengue vaccines, and to estimate the market for dengue vaccines, as well as collaborative activities with national and international partners, including the World Health Organization, to communicate this evidence and to plan for vaccine introduction into developing countries. The host organization, the IVI, is an international non-profit organization focused primarily on accelerating the research, development and introduction of new and improved vaccines for use primarily in developing countries. The PDVI headquarters are located at the IVI in Seoul, Korea.

The incumbent will be a recognized leader in one of the fields encompassed by the PDVI program, including virology, epidemiology, immunology, and vaccine development. A broad knowledge of dengue would be an advantage, as would experience working in the vaccine industry. The incumbent should have experience in program-building, resource mobilization, and in staff development.

Minimum qualifications include a doctorate degree in a relevant discipline, and significant experience in leading a multi-disciplinary field/ laboratory research program.

Salary will be internationally competitive. The Institute provides appropriate fringe benefits including a housing allowance, home leave, and income tax reimbursement.

The International Vaccine Institute is an independent international organization established under the Vienna Convention of 1969. It is governed by a Board of Trustees the majority of whom are elected based on their personal capacity.

Applications should be sent to:

**Ms. Eunsuk Kim**
**Human Resources Officer**
**International Vaccine Institute**
**San 4-8 Nakseongdae-dong**
**Gwanak-gu, Seoul, Korea**
**Tel: 82-2-872-2801 Fax: 82-2-872-2803**
**Email: eskim@ivi.int**

From whom further particulars can be obtained. Absolute confidentiality will be respected.

## POSITIONS OPEN

UC San Diego

*Local Impact, National Influence, Global Reach*

### ASSISTANT, ASSOCIATE, FULL PROFESSOR
**in Biology, Medicine, Engineering, Physical, Marine, or Social Sciences, or Any Other Pertinent Field for a Faculty Position in Stem Cell Science or Stem Cell Medicine**

The UCSD Stem Cell Program at the University of California, San Diego is seeking to recruit an Assistant, Associate, or Full Professor who conducts strongly interdisciplinary research in stem cell science or stem cell medicine. This faculty position is available in fall 2010.

The Program seeks candidates who will establish independent and vigorous, extramurally funded research programs in stem cell biology, biochemistry, medicine, engineering, or other fields related to stem cell science, with innovative approaches and expertise in more than one discipline. Candidates should have a track record of publications in internationally recognized journals, and a willingness to participate in graduate and undergraduate teaching. Applicants must possess a Ph.D. or M.D. degree.

The UCSD Stem Cell Program is an interdisciplinary and collaborative research and teaching program focused on using stem cells to understand basic biology and the causes and treatment of human disease. The Program seeks to improve human health by fostering innovation and collaboration and by providing mentoring and frequent opportunities for cross-disciplinary interaction among faculty. The successful applicant will have appointments in one or more home departments on the UCSD general campus, health sciences, or Scripps Institute of Oceanography.

For more information on our program, and to apply, please go to **website: http://stemcells.ucsd.edu/**.

You may also send your curriculum vitae, a statement of research experience and interests, and the names and e-mail addresses of three references to **e-mail: jbraswell@ucsd.edu**.

Review of applications will begin December 9, 2009, and the search will continue until position is filled.

*Equal Opportunity/Affirmative Action Employer.*

---

### TENURE-TRACK FACULTY POSITION
**Department of Molecular Medicine**
**Cornell University**

The Department of Molecular Medicine at Cornell University invites applications for a tenure-track faculty position at the rank of **ASSISTANT PROFESSOR.** Applications from individuals at a more advanced rank will also be considered. We seek candidates committed to a mechanistic understanding of intracellular and intercellular communication. Of particular interest are applicants using molecular, cellular, and physical approaches to address questions in cell signaling and biomembranes. The successful candidate is expected to develop a strong and independent research program and contribute to the teaching activities of the Department, located in the College of Veterinary Medicine.

Qualifications: Candidates should have a Ph.D., D.V.M., M.D, or equivalent degree, have a track record of excellence in research, and have the potential to develop an outstanding research program.

Applications should be addressed to **Dr. Maurine Linder, Chair, Department of Molecular Medicine.** Please submit electronically a single Adobe PDF with cover letter, curriculum vitae, and a two- to three-page research plan and have three letters of reference sent to **e-mail: mmsearch@cornell.edu**. Review of applicants begins December 1, 2009, and will continue until the position is filled.

*Cornell University is an Affirmative Action/Equal Opportunity Employer and Educator. Women and minority candidates are strongly encouraged to apply.*

## POSITIONS OPEN

UNIVERSITY OF WYOMING

### DEVELOPMENTAL BIOLOGIST
**University of Wyoming**

The Department of Zoology and Physiology at the University of Wyoming invites applications for a full-time, tenure-track faculty position, endowed by Hank Gardner and Marilyn Fiske, to start August 2010. The appointment is at the **ASSISTANT PROFESSOR** rank, although applications from individuals at the **ASSOCIATE** level, with an outstanding record of research accomplishments, will also be considered. We are seeking candidates with a Ph.D., or equivalent, and strong evidence of productivity conducting basic, biomedically relevant research into vertebrate development. Developmental biologists using physiological and/or molecular techniques to address integrative, systems-oriented questions that complement current departmental strengths in neuroscience, endocrinology, sensory, cellular and comparative physiology are especially encouraged to apply. The successful candidate will be expected to develop an NIH-funded research program and contribute to departmental teaching. A competitive startup package and excellent microscopy, analytical and animal core facilities, as well as an annual endowed research stipend, are associated with this position.

Interested applicants should electronically send curriculum vitae, a statement of research and teaching interests, three publications, and three letters of recommendation as PDF files to **e-mail: zprequest@uwyo.edu for the attention of The Gardner-Fiske Search Committee. Website: http://uwyo.edu/Zoology.** Review of applications will begin on 15 January 2010. The University of Wyoming is a Carnegie Foundation Research/Doctoral Extensive Institution. *It is committed to increasing the diversity of its faculty, staff, and students. We welcome applications from individuals of all backgrounds and perspectives.*

---

**COMMUNITY OR LANDSCAPE ECOLOGIST.** The Department of Biological Sciences at Old Dominion University invites applications for a tenure-track position in community or landscape ecology at the **ASSISTANT** or **ASSOCIATE PROFESSOR** level. Preference will be given to applicants with expertise in vertebrate ecology (specializing in mammals or birds) and those who utilize quantitative, molecular, or geographic information systems skills in their research. Candidates for Associate Professor must have a strong research program with publications and current, peer-reviewed extramural funding and must demonstrate a strong teaching record. Candidates at the Assistant Professor level must demonstrate strong potential for building independent research programs and performing quality teaching. Minimum requirements include a Ph.D. in ecology or related fields and excellent communication skills. Postdoctoral experience is preferred. The Department offers competitive salaries and startup packages and receives substantial support from state funds and from research grants from federal and other agencies. The Department has strong graduate programs, which currently have over 100 students, including a Ph.D. program in ecological sciences and a Ph.D. program in biomedical sciences. To apply, submit curriculum vitae, statement of research and teaching interests, and the names, telephone numbers, and addresses (postal and e-mail) of three references. Send applications electronically to **Ecology Search Committee, e-mail: ecol@odu.edu**. Review of applicants will begin immediately and continue until the position is filled.

Located in Norfolk, Virginia, Old Dominion University (**website: http://www.odu.edu**) is a state-supported, research intensive institution enrolling more than 24,000 students, of which 6,000 are graduate students. Norfolk is a culturally rich, historic city and a major international maritime center in a metropolitan area of over 1.5 million people. Within the area there are numerous cultural activities including a symphony orchestra, an opera company, and a ballet company as well as numerous museums. Norfolk is one of the seven cities comprising Hampton Roads, located on the Chesapeake Bay. *Old Dominion University is an Equal Opportunity, Affirmative Action Institution and requires compliance with the Immigration Reform and Control Act of 1986.*

## POSITIONS OPEN

Yale

The Section of Cardiovascular Medicine seeks exceptional candidates to establish research programs in cardiovascular developmental biology and genetics. Successful individuals will have Ph.D. and/or M.D. degrees and will have a proven record of originality and productivity. The Section is undergoing a major expansion and houses a newly formed Yale Cardiovascular Research Center. Yale University School of Medicine has established a close affiliation with University College London, United Kingdom, that among other benefits provides access to extensive clinical and translational genetics resources at UCL. Although all extraordinary candidates will be considered, we are especially interested in **DEVELOPMENTAL BIOLOGISTS** utilizing zebrafish as their model, who will be able to establish and operate a zebrafish research facility, and in **GENETICISTS** involved in translational genetics research, who will be able to run or participate in a clinical cardiovascular genetics program in addition to basic research efforts.

Please electronically send your curriculum vitae with a list of publications, a summary of research (two pages), and a research plan (three pages) along with the names of three references by December 1, 2009, to **e-mail: michael.simons@yale.edu.**

---

UNIVERSITY of LOUISVILLE

*Health Sciences Center*

### POSTDOCTORAL ASSOCIATE POSITION
**in Cellular Microbiology**

A Postdoctoral position is available immediately for highly motivated and talented individuals to join an interactive group studying molecular pathogenesis and cellular microbiology of the intracellular bacterium *Legionella pneumophila*. Priorities are given to individuals with expertise in molecular bases of bacterial pathogenesis and/or cell biology. Send curriculum vitae and the names of three references electronically to: **Dr. Yousef Abu Kwaik, Department of Microbiology and Immunology, University of Louisville Health Sciences Center, Room 412A, Louisville, KY 40292. E-mail: abukwaik@louisville.edu**. *University of Louisville is an Equal Opportunity Employer.*

## MARKETPLACE

# Call for Papers

# *Science Signaling*

***Science Signaling***, from the publisher of ***Science***, AAAS, features top-notch, peer-reviewed, original research weekly. Submit your manuscripts in the following areas of cellular regulation:

- Biochemistry
- Bioinformatics
- Cell Biology
- Development
- Immunology
- Microbiology
- Molecular Biology
- Neuroscience
- Pharmacology
- Physiology and Medicine
- Systems Biology

***Science Signaling*** is indexed in CrossRef and MEDLINE.




**Submit your research at:**
**www.sciencesignaling.org/about/help/research.dtl**

Subscribing to the weekly ***Science Signaling*** ensures that you and your lab have the latest cell signaling resources. For more information visit **www.ScienceSignaling.org**

Science Signaling

AAAS

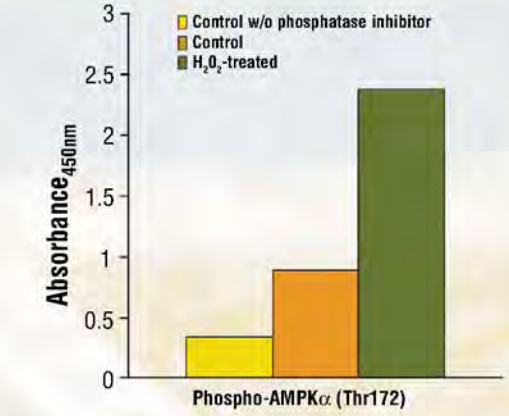


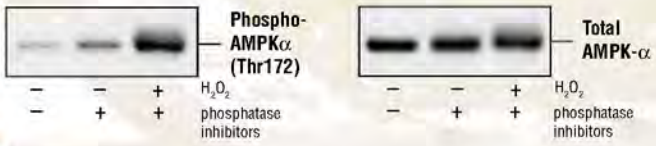




# PathScan® Sandwich ELISA Kits & Antibody Pairs

*from Cell Signaling Technology®*

***Above:*** *Treatment of C2C12 cells with $H_2O_2$ stimulates phosphorylation of AMPKα at Thr172, detected by the* ***PathScan® Phospho-AMPKα (Thr172) Sandwich ELISA Kit #7959****. The absorbance readings at 450 nm are shown in the top figure, while the corresponding western blots using Phospho-AMPKα (Thr172) (D79.5E) XP™ Rabbit mAb #4188 (left panel) or AMPKα (23A3) Rabbit mAb #2603 (right panel) are shown in the bottom figure.*

## Unparalleled product quality, validation and technical support

- Over 140 PathScan® ELISA Kits covering a broad spectrum of signaling pathways
- In-house development, production and validation ensures the highest product quality
- Technical support provided by the same scientists that develop and produce the products
- Matched modification state and total ELISA kits and Antibody Pairs available
- Custom 96- and 384-well formatting available upon request

**New PathScan® Chemiluminescent Kits offer the broadest dynamic range and assay sensitivity while requiring half the sample size due to the use of low volume microplates.**

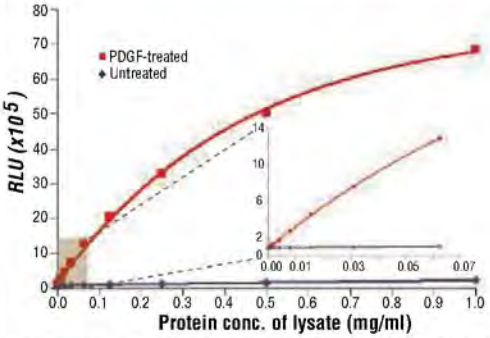


**PathScan® Phospho-Akt1 (Ser473) Chemiluminescent Sandwich ELISA Kit #7134**

for quality products you can trust...

www.cellsignal.com

Cell Signaling TECHNOLOGY®